



**UNIVERSITI TEKNOLOGI MARA**

**CHARACTERIZATION OF TMED-COPPER  
(I) IODIDE (CuI) THIN FILM AND  
PERFORMANCE FOR SOLID STATE DYE  
SENSITIZED SOLAR CELL  
APPLICATIONS**



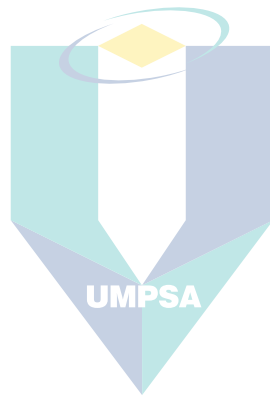
**AYIB ROSDI ZAINUN**

اونيورسيتي مليسيا قهغ السلطان عبد الله  
**UNIVERSITI MALAYSIA PAHANG  
AL-SULTAN ABDULLAH**

Thesis submitted in fulfillment  
of the requirements for the degree of  
**Doctor of Philosophy in Engineering**

**Faculty of Electrical Engineering**

October 2012



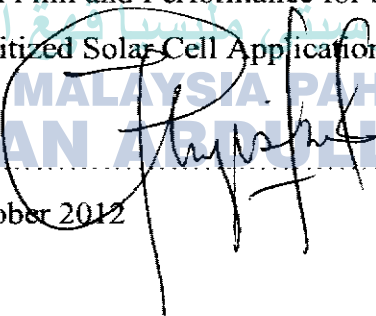
اونيورسيتي مليسيا قهغ السلطان عبد الله  
**UNIVERSITI MALAYSIA PAHANG**  
**AL-SULTAN ABDULLAH**

PERPUSTAKAAN UNIVERSITI MALAYSIA PAHANG	
No. Perolehan <b>089961</b> Tarikh	No. Panggilan IV 215 250
<b>18 AUG 2014</b>	

## AUTHOR'S DECLARATION

I declare that the work in this thesis/dissertation was carried out in accordance with the regulations of Universiti Teknologi MARA. It is original and is the result of my own work, unless otherwise indicated or acknowledged as referenced work. This thesis has not been submitted to any other academic institution or non-academic institution for any other degree or qualification.

I, hereby, acknowledge that I have been supplied with the Academic Rules and Regulations for Post Graduate, Universiti Teknologi MARA, regulating the conduct of my study and research.

Name of Student : Ayib Rosdi Bin Zainun  
Student ID No. : 2008536547  
Programme : Doctor of Philosophy in Electrical Engineering  
Faculty : Faculty of Electrical Engineering  
Thesis/Dissertation : Characterization of TMED - Copper (I) Iodide (CuI)  
Title : Thin Film and Performance for Solid State Dye sensitized Solar Cell Applications.  
Signature of Student :   
Date : October 2012

## ABSTRACT

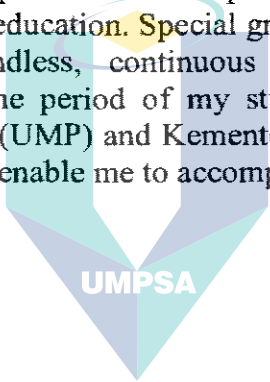
This thesis investigates the use of eco-friendly copper (I) iodide or cuprous iodide (CuI), a p-type semiconductor material, with the incorporation of a chelating agent or organic ligand, called tetramethylethylenediamine (TMED@TMEDA) in the preparation for solid-state dye-sensitized solar cells (DSSC). The CuI solution incorporated with the ligand was dispersed in acetonitrile solvent and deposited on glass and indium-doped tin oxide (ITO) substrates. The thin film is characterized to study its suitability for applications in dye sensitized solar cell (DSSC), a low cost solar cell but having high energy conversion efficiency. From the characterization, compared to that of pure CuI film, its optical properties show improved band-gap energy, while its electrical properties show improved conductivity. An efficient solid-state dye-sensitized solar cell (n-TiO<sub>2</sub>/dye/p-CuI) with improved stability was fabricated. The TMED-capped CuI crystals not only controls pore-filling of the dyed TiO<sub>2</sub> layer but also improves the electrical contacts between the TiO<sub>2</sub> particles, which in general improves the efficiency of the DSSCs. Current-voltage characteristics of the cell showed a larger energy conversion, achieving higher energy conversion efficiency and improved stability.



اونيورسيتي مليسيا قهغ السلطان عبد الله  
UNIVERSITI MALAYSIA PAHANG  
AL-SULTAN ABDULLAH

## ACKNOWLEDGEMENTS

In the name of Allah, the Most Gracious and the Most Merciful. Alhamdulillah, May all of my works are blessing and the knowledge about this research and all the matters related to it can be use in the futures. I would like to express my special appreciation to my research supervisor Prof. Madya Dr. Mohamad Rusop Mahmood for his continuous support, help, generous guidance, patience, encouragement and invaluable suggestions from the beginning of this works until its completion. I also wish to extend my appreciation to Encik Uzer Mohd Noor for his comments, advice and discussion. His ideas and suggestions have helped and supported me to improve and guide the directions of my research. A million thanks also to Prof. Dr. Ichimura Masaya of Nagoya Institute of Technology, Nagoya, Japan for his continuous advice as well as his permission to use his labs and equipments. In particular, my thanks to all the members of solar cell laboratory of faculty electric UiTM for their friendship, useful discussions and technical assistant especially at the beginning of this works. My endless gratitude to my parents for their pray of my successful and attention and encouragement towards my education. Special gratitude and thanks to my lovely wife, my children for their endless, continuous and strong support, patient and understanding throughout the period of my study. My sincerely to my employer Universiti Malaysia Pahang (UMP) and Kementerian Pengajian Tinggi (KPT) for the scholarship and support that enable me to accomplish this work.

The logo of Universiti Malaysia Pahang (UMP) is a stylized shield shape composed of several overlapping triangles in shades of blue, green, and yellow. The acronym 'UMPSA' is written in white capital letters across the center of the shield.

UMPSA

اونيورسيتي مليسيا قهغ السلطان عبد الله  
UNIVERSITI MALAYSIA PAHANG  
AL-SULTAN ABDULLAH

## TABLE OF CONTENTS

	<b>Page</b>
<b>AUTHOR'S DECLARATION</b>	ii
<b>ABSTRACT</b>	iii
<b>ACKNOWLEDGEMENT</b>	iv
<b>TABLE OF CONTENTS</b>	v
<b>LIST OF TABLES</b>	ix
<b>LIST OF FIGURES</b>	x
<b>LIST OF ABBREVIATIONS</b>	xiv
	
<b>CHAPTER ONE: INTRODUCTION</b>	
1.1 Development of CuI as Hole Conductor for DSSC	1
1.2 Objectives of The Research	4
1.3 Scope of Research	5
1.4 Thesis Organization	6
<b>CHAPTER TWO: LITERATURE REVIEW</b>	
2.1 Introduction	8
2.2 History of PEC	9
2.3 Overview of Solid State DSSC	13
2.4 Fabrication of Solid State DSSC	17
2.5 Problems in Solid State DSSC	18
2.5.1 Contact of Dye Molecule and Hole Conductor	18
2.5.2 Electron-Hole Recombination	20
2.5.3 Interfacial Blocking Layers	21
2.5.4 Device Operational Stability	24
2.5.5 Chelating Agent	26
2.6 Summary	27

## CHAPTER THREE: METHODOLOGY

3.1	Introduction	29
3.2	Cleaning of Substrates	29
3.3	Preparation of Copper (I) Iodide (CuI) Thin Films	31
3.3.1	Preparations of CuI Thin Films at Different Molar Concentration	32
3.3.2	Effect of Annealing Temperature on CuI Thin Films at Different Molar Concentration	34
3.3.3	Preparation of CuI Thin Films Incorporation of TMED	35
3.3.4	Effect of Annealing Temperature on CuI Thin Films That Incorporated TMED	36
3.4	Deposition of TiO <sub>2</sub> /dye/CuI Solid State DSSC	37
3.5	Characterization Method	40
3.5.1	Measurement of pH and Conductivity	41
3.5.2	Particles Size Measurement	42
3.5.3	Surface Morphology	42
3.5.4	Crystalline Properties	43
3.5.5	Characterization of Optical Properties	44
3.5.6	Luminescence properties	46
3.5.7	Current-Voltage Measurement	46
3.6	Summary	48

## CHAPTER FOUR: CHARACTERIZATION OF NANOPARTICLES COPPER (I) IODIDE (CuI) THIN FILMS

4.1	Introduction	49
4.2	Characterization at Different Molar Concentration of CuI Solution	50
4.2.1	Conductivity and pH	50
4.2.2	Particles Size Measurement	51
4.2.3	Surface Morphology of CuI Thin Film	53
4.2.4	XRD Spectra	55
4.2.5	UV-Vis-NIR Spectra	57
4.2.6	Photoluminescence (PL) Spectra	60
4.2.7	Electrical Properties of CuI Thin Films	61

4.3	Effect of Annealing Temperature on CuI Thin Films	64
4.3.1	Surface Morphology of Annealed Thin Films	65
4.3.2	XRD Spectra	66
4.3.3	UV-Vis-NIR Spectra	68
4.3.4	Photoluminescence (PL) Spectra	71
4.3.5	Electrical properties of Annealed Thin Films	73
4.4	Summary	75

**CHAPTER FIVE: CHARACTERIZATION OF NANOPARTICLES  
COPPER (I) IODIDE (CuI) THIN FILM THAT  
INCORPORATES TMED AS CHELATING AGENT**

5.1	Introduction	77
5.2	Study on Different Volumes of Chelating Agent into TMED-chelate CuI Solution	77
5.2.1	Conductivity and pH	78
5.2.2	Particle Size Measurement	79
5.2.3	Surface Morphology of TMED-chelate CuI Thin Films	81
5.2.4	XRD Spectra	84
5.2.5	UV-Vis-NIR Spectra	85
5.2.6	Photoluminescence (PL) Spectra	90
5.2.7	Electrical Properties of TMED-chelate CuI Thin Films	92
5.3	Effect of Annealing Temperature on TMED-chelate CuI Thin Films	95
5.3.1	Surface Morphology of Annealed Thin Films	95
5.3.2	XRD Spectra	96
5.3.3	UV-Vis-NIR Spectra	98
5.3.4	Photoluminescence (PL) Sepctra	102
5.3.5	Electrical properties of Annealed Thin Films	103
5.4	Summary	105

**CHAPTER SIX: PERFORMANCE OF n-TiO<sub>2</sub>/dye/p-CuI INCORPORATED  
WITH NEW CHELATING AGENT FOR SOLID STATE  
DYE SENSITIZED SOLAR CELL**

6.1	Introduction	108
6.2	Experimental Procedure	109
6.3	Results and Discussion	
6.3.1	Surface Morphology of n-TiO <sub>2</sub> /dye/p-CuI	109
6.3.2	Electrical Properties of n-TiO <sub>2</sub> /dye/p-CuI	115
6.4	Conclusion	118

**CHAPTER SEVEN: CONCLUSION**

7.1	Conclusion	120
7.2	Future Works	123

<b>REFERENCES</b>	125
-------------------	-----

<b>APPENDICES</b>	146
-------------------	-----



اونيورسيتي مليسيا قهغ السلطان عبد الله  
**UNIVERSITI MALAYSIA PAHANG  
AL-SULTAN ABDULLAH**

## LIST OF TABLES

Tables	Titles	Page
Table 2.1	Performance parameter results of solid-state DSSC based On $\text{TiO}_2$ and $\text{Al}_2\text{O}_3$ coated $\text{TiO}_2$ films under various intensities of simulated sunlight.	23
Table 3.1	Preparation and characterization of CuI thin films at Different molar concentrations.	33
Table 3.2	Preparation and characterizations of annealed CuI thin films.	34
Table 3.3	Preparation and characterizations of CuI thin films that incorporate TMED.	36
Table 3.4	Preparation and characterization of annealed CuI thin films that incorporate TMED.	37
Table 4.1	Conductivity and Acidity (pH) results of CuI solution at different molar concentration.	51
Table 5.1	Acidity (pH) and conductivity of CuI solution incorporated with different volumes of TMED.	78

اونيورسيتي مليسيا قهغ السلطان عبد الله  
UNIVERSITI MALAYSIA PAHANG  
AL-SULTAN ABDULLAH

## LIST OF FIGURES

Figures	Titles	Page
Figure 1.1	Schematic diagram of conventional silicon based solar cell.	2
Figure 2.1	Scematic diagram of electrolyte based DSSC.	10
Figure 2.2	Operational principle of Gratzel cell.	12
Figure 2.3	Schematic diagram of CuI based solid state DSSC.	14
Figure 2.4	Operational principle of solid state DSSC.	15
Figure 2.5	Structure hypothesis using CuI as p-type material in solid state DSSC.	18
Figure 2.6	Introduce of insulating layer as blocking layer in solid state DSSC.	22
Figure 2.7	(left) Ethylenediamine ligand of a chelate complex, (right) TMED chemical compound.	27
Figure 3.1	Process flow of substrates cleaning process.	30
Figure 3.2	Process flow of preparation and characterization of CuI thin film	31
Figure 3.3	Preparation and deposition process flow of TiO <sub>2</sub> thin films.	38
Figure 3.4	Apparatus used to blend the TiO <sub>2</sub> powder in (a) and process used to deposit TiO <sub>2</sub> thin films in (b).	39
Figure 3.5	Preparation and deposition process flow of CuI thin films.	40
Figure 3.6	Schematic diagram for I-V measurement of CuI thin films.	47
Figure 4.1	Particles size of CuI solution in different molar concentration.	52
Figure 4.2	FESEM images of CuI thin films at different molar concentrations (a)1.0M CuI, (b) 0.5M CuI, (c) 0.1M CuI and (d) 0.05M CuI.	54
Figure 4.3	EDX analysis of CuI thin film.	55
Figure 4.4	XRD spectra of CuI thin films at different molar concentrations.	56
Figure 4.5	Optical transmittance of CuI thin films at different molar concentrations.	57
Figure 4.6	Absorption coefficient of CuI thin films prepared with	58

	different molar concentrations.	
Figure 4.7	Optical band-gap energy estimation of CuI thin films at different molar concentrations using Tauc's plot.	59
Figure 4.8	Photoluminescence (PL) spectra of CuI thin films at Different molar concentrations (excitation wavelength at 325 nm).	61
Figure 4.9	Current-Voltage (I-V) measurement of CuI thin films at different molar concentrations.	62
Figure 4.10	Resistivity of CuI thin films at different molar concentrations.	63
Figure 4.11	FESEM images of 1.0M CuI thin films at different Annealed temperatures (a) as deposited, (b) 50°C, (c) 80°C, and (d) 110°C.	65
Figure 4.12	XRD spectra of 1.0M CuI thin films at different annealing temperatures.	67
Figure 4.13	Optical transmittance of 1.0M CuI thin films at different annealing temperatures.	69
Figure 4.14	Absorption coefficient of 1.0M CuI thin films at different annealed temperatures.	70
Figure 4.15	Optical band-gap energy estimation of 1.0M CuI thin films at different annealing temperatures using Tauc's plot.	71
Figure 4.16	Photoluminescence (PL) spectra of 1.0M CuI thin films at different annealing temperatures.	72
Figure 4.17	Current-Voltage (I-V) measurement of 1.0M CuI thin films at different annealing temperatures.	74
Figure 4.18	Resistivity of 1.0M CuI thin films at different annealed temperatures.	75
Figure 5.1	Particles size of CuI solution at different molar Concentrations without and with TMED as chelating agent (a) 1.0M CuI, (b) 0.5M CuI, (c) 0.1M CuI, and (d) 1:1 of CuI:TMED ratio.	80
Figure 5.2	FESEM images of CuI thin film at 1.0M CuI Concentration without and with TMED as chelating agent.	82

	(a) CuI without TMED, (b) CuI with 50 v% TMED, (c) CuI with 100 v% TMED, and (d) CuI with 150 v% TMED.	
Figure 5.3	EDX analysis of 1.0M CuI thin film incorporated with TMED.	83
Figure 5.4	XRD spectra and peak list table of 1.0M CuI thin film and 1.0M CuI thin film incorporated with TMED as chelating agent at different volume percentage.	85
Figure 5.5	Optical transmittance of TMED-chelate CuI thin films at different volume of TMED.	86
Figure 5.6	Absorption coefficient of TMED-chelate CuI thin films at different volume of TMED.	87
Figure 5.7	Optical band-gap energy estimation of TMED-chelate CuI thin films at different volume of TMED using Tauc's plot.	89
Figure 5.8	Photoluminescence (PL) spectra of TMED-chelate 1.0M CuI thin films at different volumes of TMED.	91
Figure 5.9	Current-Voltage (I-V) measurement of TMED-chelate 1.0M CuI thin films at different volumes of TMED.	93
Figure 5.10	Resistivity of TMED-chelate 1.0M CuI thin films at Different volumes of TMED.	94
Figure 5.11	FESEM images of 1:1 volume ratio of TMED-chelate CuI thin films at different annealed temperatures (a) 0°C, (b) 50°C, (c) 80°C, and (d) higher magnification of 80°C image.	96
Figure 5.12	XRD spectra and peak list table of 1:1 volume ratio of TMED-chelate CuI thin film at different annealing temperatures.	97
Figure 5.13	Optical transmittance of 1:1 volume ratio of TMED-chelate CuI thin films at different annealing temperatures.	99
Figure 5.14	Absorption coefficient of 1:1 volume ratio of TMED-chelate CuI thin films at different annealing temperatures.	100
Figure 5.15	Optical band-gap energy estimation of 1:1 volume ratio of TMED-chelate CuI thin films at different annealing temperatures using Tauc's plot.	101
Figure 5.16	Photoluminescence (PL) spectra of 1:1 volume ratio of TMED-chelate CuI thin films at different annealing temperatures.	102

Figure 5.17	Current-Voltage (I-V) measurement of 1:1 volume ratio of TMED-chelate CuI thin films at different annealing temperatures.	104
Figure 5.18	Resistivity of 1:1 volume ratio of TMED-chelate CuI thin Films at different annealing temperatures.	105
Figure 6.1	The morphology of fabricated DSSC cells (A) TiO <sub>2</sub> film, (B) CuI film without TMED, (C) CuI film with TMED, (D) TiO <sub>2</sub> /dye/CuI (TMED) film.	111
Figure 6.2	EDX measurements on top of TiO <sub>2</sub> /dye/CuI(TMED) film surface.	112
Figure 6.3	EDX measurements on the cross-section of TiO <sub>2</sub> /dye/CuI (TMED) film.	113
Figure 6.4	X-ray diffraction (XRD) spectra of the FTO substrate, TiO <sub>2</sub> /dye/CuI (TMED) film, TMED-chelate CuI film, and TiO <sub>2</sub> film.	114
Figure 6.5	An array of electrodes for the I-V measurement.	115
Figure 6.6	I-V characteristic of TiO <sub>2</sub> /dye/CuI film without TMED.	117
Figure 6.7	I-V characteristic of TiO <sub>2</sub> /dye/CuI film with TMED.	118

## LIST OF ABBREVIATIONS

### Abbreviations

DSSC	dye sensitized solar cell
TiO <sub>2</sub>	titanium dioxide
h $\nu$	photon
I	iodine
I <sub>3</sub> <sup>-</sup>	iodide
SSDSSC	solid-state dye sensitized solar cell
D	dye
SiC	silicon carbide
GaN	gallium nitrate
CuI	copper (I) iodide
CuBr	copper (I) bromide
CuSCN	copper (I) thiocyanate
UV	ultra violet
MgO	magnesium oxide
MEISCN	1-methyl-3-ethylimidazolium thiocyanate
THT	triethylamine hydrothiocyanate
TMED @ TMEDA	tetramethylethylenediamine
SEM	scanning electron microscopy
FESEM	field emission scanning electron microscopy
AFM	atomic force microscopy
EDX	energy dispersive x-ray spectroscopy
XRD	x-ray diffractometer
UV-Vis-NIR	ultra violet- visible- near infra red
PL	photoluminescence
I-V	current-voltage
DSPEC	dye-sensitized photo-electrochemical cell
ZnO	zinc oxide
Pt	platinum
LUMO	lowest unoccupied molecular orbital
HOMO	highest occupied molecular orbital

<i>spiro</i> -OMeTAD	spirobisfluorene-connected aryl amine
SnO <sub>2</sub> :F	fluoride-doped tin dioxide
FTO	florin-doped tin oxide
iodide/triiodide	redox couple
V <sub>oc</sub>	photovoltage
J <sub>sc</sub>	photocurrent
Al <sub>2</sub> O <sub>3</sub>	aluminium oxide
HfO <sub>2</sub>	hafnium oxide
XPS	x-ray photoelectron spectroscopy
ITO	indium doped tin oxide
DI	de-ionised water
Xe	xenon
In	indium
SCE	saturated calomel electrode
CuSO <sub>4</sub>	copper (II) sulfate
ECD	electrochemical deposition
S/cm <sup>-1</sup>	siemen per centimeter
H <sup>+</sup>	hydrogen
OH <sup>-</sup>	hydroxyl
eV	electron volt
rf-dc	radio frequency/direct current
PLD	pulsed laser deposition
PSD	particles size distribution
FWHM	full width at half maximum
ZnS	zinc sulphide
Sn	tin
O	oxygen
ZnGa <sub>2</sub> O <sub>4</sub> : Cr	zinc gallium oxide: chromium
fcc	face-centered-cubic
LMCT	ligand-to-metal charge transfer process
PEG	polyethylene glycol
Al	aluminum
ETA	extremely thin absorber

QD	quantum dot
ALCVD	chemical vapour deposition method
$\text{Cu}_2\text{O}$	cuprous oxide
KOH	potassium hydroxide
PbS	lead (II) sulphide



اونيورسيتي مليسيا قهغ السلطان عبد الله  
**UNIVERSITI MALAYSIA PAHANG**  
**AL-SULTAN ABDULLAH**

# CHAPTER ONE

## INTRODUCTION

### 1.1 DEVELOPMENT OF CuI AS HOLE CONDUCTOR FOR DSSC

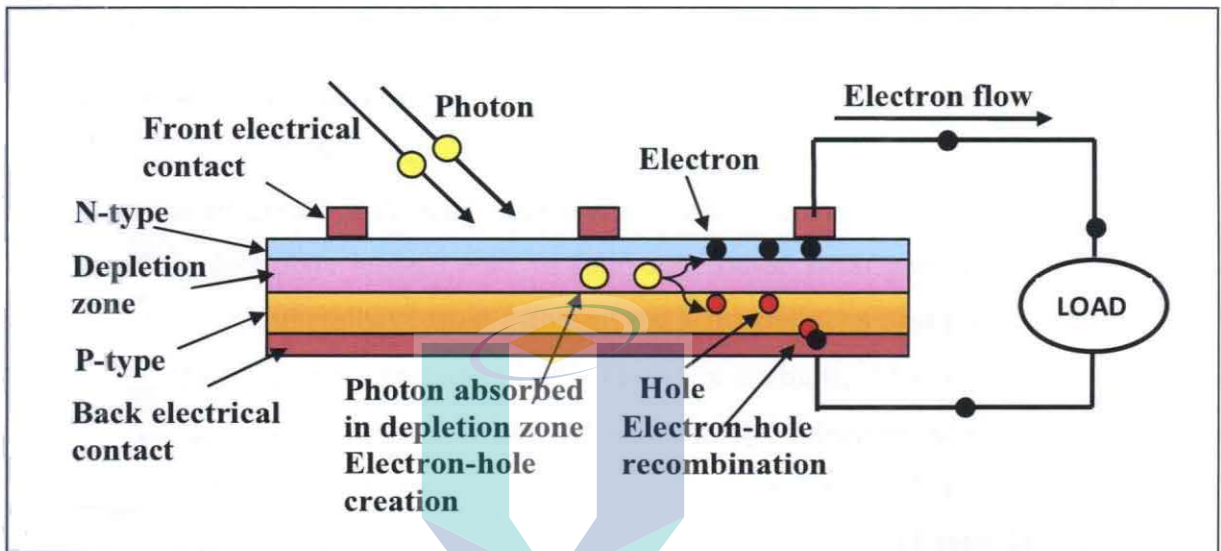
The property of a p-n junction plays an essential role in all semiconductor devices, such as in solar cells, diodes and transistors. In terms of electrical properties, electric field is created when p-type and n-type semiconductors are joined together creating a junction at the interface. The junction is formed through the flow of electrons from n-type and holes from p-type in opposite direction within the two types of semiconductor [1-2].

When a photon of light passes through the window of the solar cell, as illustrated in Figure 1.1, it will be absorbed by the atoms in the n-type silicon which will cause an electron to be freed, creating a negative charge (electron) and positive charge (hole) within the junction. By absorbing more photons, the electrons will gain sufficient energy to overcome the material's band gap energy and will be released into the depletion zone. By connecting the cathode to the anode with a conductor, the negative charges from the cathode will flow to positive charges at the anode, creating an electric current when the charges flow through an external load. On the other hand, the holes that are separated from the free electrons will travel to the positive charges of p-type material and gathers at the anode at the back of the electrical contact. When the negatively charged electrons approach the p-type semiconductor, it will combine with the positively charged hole and regenerate the neutrally charged photon [2-3]. The general concept of solar cells is that electric energy is produced through conversion of solar radiation. The production of electrical energy through conversion of solar radiation using silicon solar cells, with an efficiency of 6%, was first discovered by staffs of Bell Telephone Laboratories [3-4]. With recent advancement and modernisation in technology, where solar cells have become a source of alternative energy for human use, studies have shown that a common solar device could achieve a conversion efficiency of 15 to 20% [5-6].

However, the use of toxic chemicals have affected its reputation as a source of clean energy, and its high manufacturing cost has hindered it from being widely used.

Such factors have stimulated this study to find alternative solar cells that is low in cost and uses materials that is safe to human beings and the environment.

**FIGURE 1.1**  
Schematic Diagram Of Conventional Silicon Based Solar Cell.



Recently, researchers had found other alternative to the silicon based solar cells. Gratzel, et al. (1991) reported that they have created an environmental friendly solar cell called dye sensitized solar cells (DSSCs), which is based on photo electrochemical reaction, and its main function works on fast regenerative mechanism [7]. Under laboratory testing, DSSCs have achieved efficiency in the range of 7.1% - 7.9%, which is similar to that of conventional solar cell [8]. The difference between DSSC and the conventional solar cell is that a type of dye is used as the light absorber and charge carrier in DSSC while silicon is used in the conventional solar cell. The inexpensive organic dye together with the low cost processes made it possible to commercially produce solar cells that exhibit energy conversion efficiency that is similar to silicon-based cells. Furthermore, of utmost importance, the materials used in the fabrication of DSSCs are environment friendly.

Although liquid electrolytes based DSSCs under Air Mass (AM) 1.5 ( $1000\text{W}/\text{m}^2$ ) simulated light have obtained 10% efficiency [9], but evaporations of liquid cause by heat,

especially when the cell is improperly sealed, remain the major problem to the liquid electrolytes device stability. More specifically, performance of liquid cell may decline when the reaction between the water molecules or oxygen molecules with the electrolyte occur within the cell. Moreover, since the cell must be electrically wired with other cell to build a module or unit, it is quite difficult to get connected when chemically separated [10-11].

Consequently, the main objective among researchers is to improve the problems encountered with DSSC cells, and most researchers would prefer to replace the electrolyte-based DSSC with solid-state based DSSC. Several attempts have been made in converting electrolyte-based DSSC to solid-state based DSSC, such as utilizing ionic liquid electrolyte. Others have tried using p-type semiconductor and polymer electrolyte instead of iodine-based electrolyte [12-13]. From the attempts, it has been found that the stability and efficiency of the cell is good when p-type semiconductors is used, hence making it the best option in the fabrication of solid-state DSSCs. Some factors must be considered when using p-type semiconductor for fabricating solid-state DSSC [14-15] that has been illustrated in sub-chapter 2.2 of chapter 2.

A number of p-type semiconductors have been identified and tested but most of the materials only fulfil some of the conditions; the materials include well-used materials in p-type semiconductors such as silicon carbide (SiC) and gallium nitrate (GaN), both having a large band-gap. However, both SiC and GaN require high temperatures during deposition, and such deposition method is unsuitable as it will certainly worsen the dye in DSSC. From the extensive studies conducted by researchers, it has been found that a group of p-type semiconductor can fulfil all the conditions stated above. This group of materials are based on copper compounds, such as copper (I) iodide (CuI), copper (I) bromide (CuBr), or copper (I) thiocyanate (CuSCN) [12, 16-17]. Among all copper based materials tested, CuI and CuSCN shows good characteristic and their conductivity are more than  $10^{-2} \text{ Scm}^{-1}$ . These materials can also be deposited using solution or vacuum deposition method to form a layer that has the ability to conduct holes [17]. CuI was first successfully tested for solid-state DSSC in 1995 by Tennakone, et al. [18]. Under simulated sunlight at about  $800\text{Wm}^{-2}$ , around  $1.5 \sim 2.0 \text{ mA/cm}^2$  output of current density

was produced. It is likely the most impressive current density produced to date. Further studies conducted by Tennakone, et al. on solid-state DSSC using CuI, around 2.4% improvement in efficiency has been reported when they replaced cyanidin dye with a Ru-bipyridyl complex [19-20]. From the operations point of view, efficiency and stability are two important aspects that must be taken into account in a photovoltaic device.

## 1.2 OBJECTIVES OF THE RESEARCH

The problems and some of the solutions mentioned in Section 1.1 are the current progress in dye sensitized solar cells (DSSCs) where CuI is used as p-type material or as holes conductor. Hence, using CuI as the main precursor, this research proposes to provide an alternative approach to overcome the weakness and disadvantage of solid-state DSSCs by introducing a new chelating agent or stabilizer that functions as a ligand in synthesizing CuI solution for DSSC. The contribution of this new chelating agent is to suppress the growth of the CuI crystal with respect to their function as an electron bridge. The function of the chelating agent is similar to THT used by Tennakone, et al. in CuI solution, but the agent will not require complicated chromatography process. The chelating agent to be used in this research is called tetramethylethylenediamine (TMED @ TMEDA). Also, with the use of this new solution, the nanostructure CuI thin film properties, including optical and electrical properties, will be studied. The main objectives of this research are:

- i. To investigate the effect of introducing TMED as chelating agent in the process of fabrication nanostructure CuI thin film toward the structural, optical and electrical properties of the thin film.
- ii. To demonstrate the effect of introducing TMED as chelating agent in the process of fabrication nanostructure CuI thin film toward the performance of n-TiO<sub>2</sub>/dye/p-CuI solid-state DSSC device.

### 1.3 SCOPE OF RESEARCH

The aim of this research is to produce simple, low cost and high quality CuI thin films. The preparation of CuI thin film using sol-gel method is one of the ways that fulfils the requirement. In one case, the solution of CuI precursor is prepared using ecetonitrile as solvent, and in another case TMED is added to the CuI solution. The deposition of CuI thin films were achieved using drop and spin coating technique. Several parameters were taken into consideration for optimizing the CuI thin films to the desired characteristic. Such parameters are different molarities of CuI, different volumes of TMED that is added to CuI solution, the effect of annealing temperature, and the comparison of different deposition methods.

Before the deposition of CuI thin films take place, while the solution of CuI precursor still in the form of liquid, particle size measurement was conducted. This measurement is conducted to analyze the change (if any) in particle size of the main precursor before and after being deposited as thin films. After the CuI thin films were deposited with different parameters at every time of preparation, several measurements of its structural properties had been carried out using various instruments, such as scanning electron microscopy (SEM) or field emission scanning electron microscopy (FESEM) and atomic force microscopy (AFM). Furthermore, energy dispersive x-ray spectroscopy (EDX) has been used to identify the element in the sample such as the presence of contaminants in the specific region. Other measurements are X-ray diffractometer (XRD) for determining the crystal structure and orientation of CuI thin films, UV-Vis-NIR spectrophotometer and photoluminescence spectroscopy (PL) measuring optical properties and finally, two probes current-voltage (I-V) measurement system for electrical properties.

Performance of dye sensitized solar cell (n-TiO<sub>2</sub> / dye / p-CuI) was also considered as part of this research. CuI parameters used for fabricate DSSC is based on the characteristic of optimized CuI thin films. The TiO<sub>2</sub> thin film for this cell was prepared using squeegee method with constant thickness and rhodamine B, and ruthenium dye was used as photon absorber. The process started by soaking the TiO<sub>2</sub> thin

film into dye solution for 24 hours. The film is dried for some time before the deposition of CuI solution on top of the TiO<sub>2</sub>/dye films took place. CuI was deposited on TiO<sub>2</sub>/dye films using spin coating method and also drop and dry method; the methods are used to determine which of the two methods produce a better outcome. After the CuI deposition is completed, the films were annealed at a certain temperature for some time. Finally, the fabricated cell is measured for its efficiency.

#### **1.4 THESIS ORGANIZATION**

This thesis is arranged as follows:

Chapter 1 discusses the overview of the DSSC, including how the device operates, its development and current status, and the related problems. This chapter also discusses in general the history and progress of DSSC based on CuI as p-type material and as holes conductor. The objectives of the research are also included in this chapter.

In Chapter 2, literatures on DSSC are reviewed, from the history and development of electrolyte-based DSSC to the development of solid-state DSSC.

Chapter 3 discusses the methodology or experimental technique used in this research. CuI with and without chelating agent TMED thin film preparation using sol-gel spin-coating method and drop and dry method is discussed. All samples preparation, synthesis and characterization details including their parameter and theory are discussed in this chapter.

Chapter 4 presents the details of the characterization results and discussion of prepared p-type CuI thin film by drop and spin-coating method onto glass and ITO/FTO substrates. The study includes thin film surface morphology, optical and electrical properties at different molar concentration of CuI and annealing effect.

Chapter 5 described the characterization of TMED-chelate CuI thin film using the method and measurement properties that used in chapter 4.

Chapter 6 details the study on fabrication and the performance of the n-TiO<sub>2</sub>/dye/p-CuI and n-TiO<sub>2</sub>/dye/p-CuI (TMED) heterojunction solar cells.

Chapter 7 concludes the research conducted in this study while outlining related future works that can be carried out.



اونيورسيتي مليسيا قهغ السلطان عبد الله  
**UNIVERSITI MALAYSIA PAHANG  
AL-SULTAN ABDULLAH**

## CHAPTER TWO

### LITERATURE REVIEW

#### 2.1 INTRODUCTION

In the last 15 years, in the venture to develop new and environment friendly solar cells, solid-state dye-sensitized solar cell (DSSC) has become of great interest to researchers of solar cells [1-3]. The interest in this field of research first developed with the study on dye-sensitized photo-electrochemical cell (DSPEC). The operational principle of this solid-state is similar to the conventional silicon solar cells except that the liquid electrolyte is replaced with either a p-type solid-state semiconductor or organic materials that act as holes conductor [21-31]. Furthermore, DSPEC is better than silicon solar cells in terms of electron-hole separation for transporting charges to different types of semiconductors as the quality of the electrodes used in DSPEC is based on the purity and the crystalline structure of either the n-type or p-type semiconductor [32]. Unlike DSPEC, good electron-hole mobility in silicon solar cell is dependent on the purity and crystalline structure of the material to exploit the inner photovoltaic effect within the same compound. However, being a solid-state device, silicon solar cells could be easily produced and lower in cost than that of PECs, since problems such as leakage, corrosion and packaging which appear in liquid electrolyte could be prevented [33-38].

Even though solid-state devices have more advantages than electrolyte-based cells, the current development of solid-state DSSC is still not good enough to make it into device level. So far, the best reported efficiency of solid-state DSSC is less than 4% as compared to about 10%-11% for DSPEC solar cells [8, 39-42]. In fact, the latest development in solid-state DSSC is still not able to compete with DSPEC.

In principle, the difference between DSPEC and solid-state DSSC is that the former is a molecular electronic device based on chemical reaction on molecular scale, while the later works like p-n heterojunction whose behaviour can be described in terms of semiconductor physics [2]. Hence, one of the factors that might have contributed to the

unsatisfactory development of solid-state DSSC is that the knowledge of solid-state DSSC is based mainly on the knowledge already developed for DSPECs.

## 2.2 HISTORY OF PEC

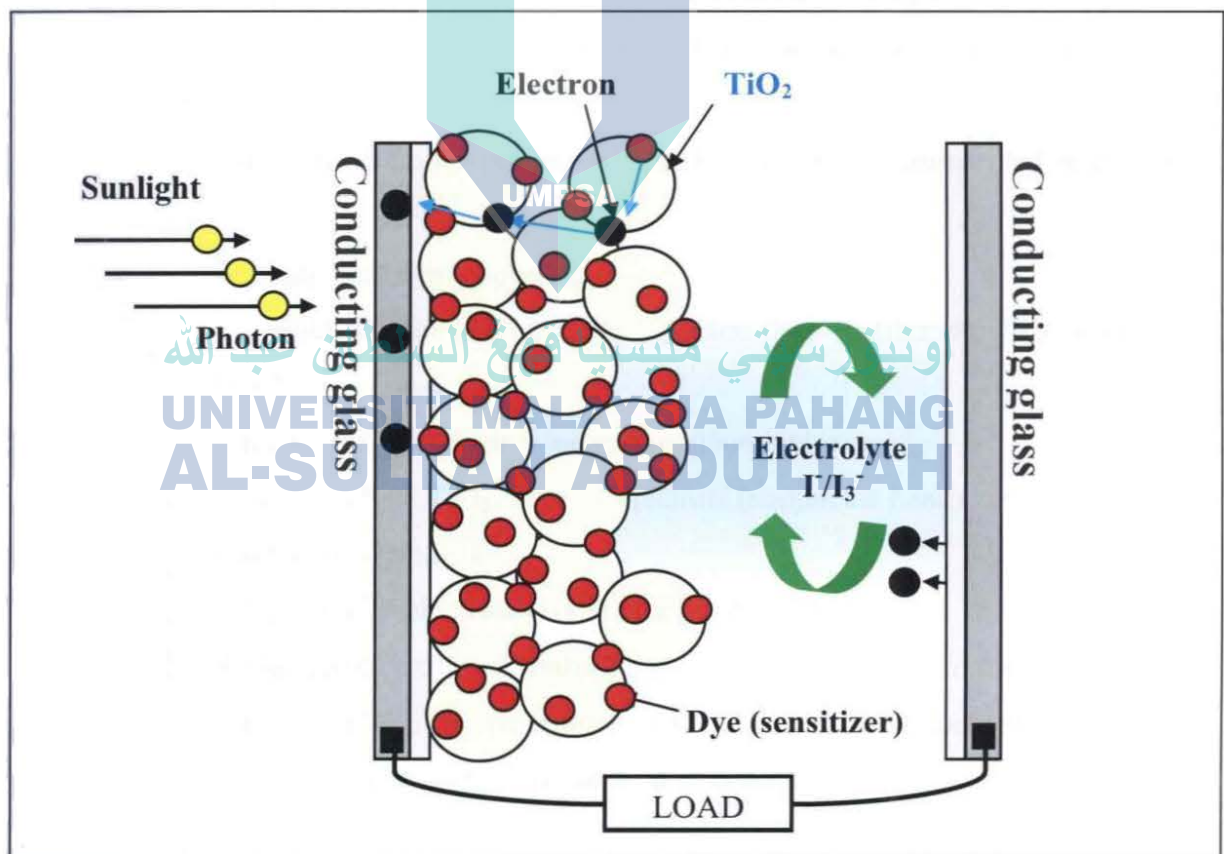
Research on PECs began when silicon-based solar cell has already reached  $3 \times 10^{24}$  Joules per year of solar energy in the late 60s, after world economy was facing the oil embargo in 1973. The supply of solar energy that was produced then seemed to be able to meet the energy needs of the people in the world. It was also recognized that solar energy was a clean energy source which could relieve the environment problems arising from the use of fossil fuels [8].

The invention of the rutile form single crystal titanium dioxide ( $\text{TiO}_2$ ) in the late 1960s by Akira Fujimura was a very valuable discovery in the history of photo electrochemistry. It was the beginning of photo-splitting of water through the process of PEC as it showed the possibility of solar energy conversion into clean fuel of  $\text{H}_2$  [43]. Unfortunately,  $\text{TiO}_2$  show a very low efficiency of solar energy conversion since it only absorbs the blue part, ultraviolet, of the solar spectrum. In the meantime, the theory and concept of DSPEC was used as references when Tributsch et al. [44] found the photocurrents in semiconducting electrode via dye sensitization in 1972. The photon absorbed by sensitized dye on semiconductor electrode generated photoelectric power via electrochemical cells. Moreover, DSPEC concept was more convincing when such a cell could function under red spectrum (visible light) and demonstrate good efficiency of solar energy conversion. In 1976, nearly 1.5% spectrum of solar efficiency is measured through incident photon of zinc oxide ( $\text{ZnO}$ ) ceramic electrodes sensitized by Rose Bengal dye was reported by Tsubomura et al. [45]. On further research, through incident photon within the dye spectrum, the same group reported an energy efficiency conversion of 2.5% (Matsumura et al., 1980) [46]. The only alteration made in the experiment is by maximising the specific surface area of  $\text{ZnO}$  electrodes.

A major breakthrough in DSPEC is in 1991 when Gratzel, O'Regan, et al. [7] produced 7% energy conversion efficiency using electrolyte based DSSC using similar

concept as that of DSPEC. They used mesoporous  $\text{TiO}_2$  in their experiments to deposit the film electrodes which could produce very large surface area, and used ruthenium bipyridyl complex as the sensitized dye that could sufficiently attached to the surface of  $\text{TiO}_2$  electrodes while exhibiting a wide absorption band in the visible spectrum. Since then, the cell created by Gratzel, came to be known as Gratzel cell, has become the standard model for DSPECs and has received worldwide attention on DSPECs. In 2003, Gratzel et al. [47] has reported 10.6% of solar energy efficiency when the cell was examined under full sunlight, and this value is very close to that the conventional solar cell.

FIGURE 2.1  
Schematic Diagram Of Electrolyte Based DSSC.



The schematic diagram in Figure 2.1 and 2.2 shows the structure and operational principal of the electrolyte based DSSC developed by Gratzel respectively. In general, the

cell consists of three main materials: n-type semiconductor, dye and electrolyte. The operation of the cell is as follows. Titanium dioxide (TiO<sub>2</sub>) is used as an n-type semiconductor and is sensitized with ruthenium, a kind of dye, to absorb the visible light photons. When the dye absorb sufficient energy from sunlight, the electron in the dye will be excited and will then be transferred to TiO<sub>2</sub>, which acts as an electron bridge, and it will flow to the conducting glass. Dye excitation and transferring of electrons to TiO<sub>2</sub> is called an injection process, after which the dye is positively charged due to holes. The charges will then be transferred to the electrolyte containing a redox mediator, one that works as an electrochemical reductor and oxidiser. After losing the charges, the dye then return to its reduction state and this process is called an interception process. The oxidised sensitizer is then reduced by the donor electron in the electrolyte, and the reduction process spreads till the positive counter electrode. The charges in the mediator will be regenerated when the electrons flow out of the cathode to the anode through the external circuit.

The actual electrochemical process within the cell can be summarized as in Figure 2.2:

- I. Excitation of dye by photon  

$$\text{Titanium dioxide (TiO}_2\text{) / Dye} + \text{photon (}h\nu\text{)} \rightarrow \text{Titanium dioxide (TiO}_2\text{) / Dye}^*$$
- II. Injection of electron into n-type semiconductor  

$$\text{TiO}_2 / \text{Dye}^* \rightarrow \text{TiO}_2 / \text{Dye}^+ + \text{electron}^- \text{ (conductor band)}$$
- III. Interception process  

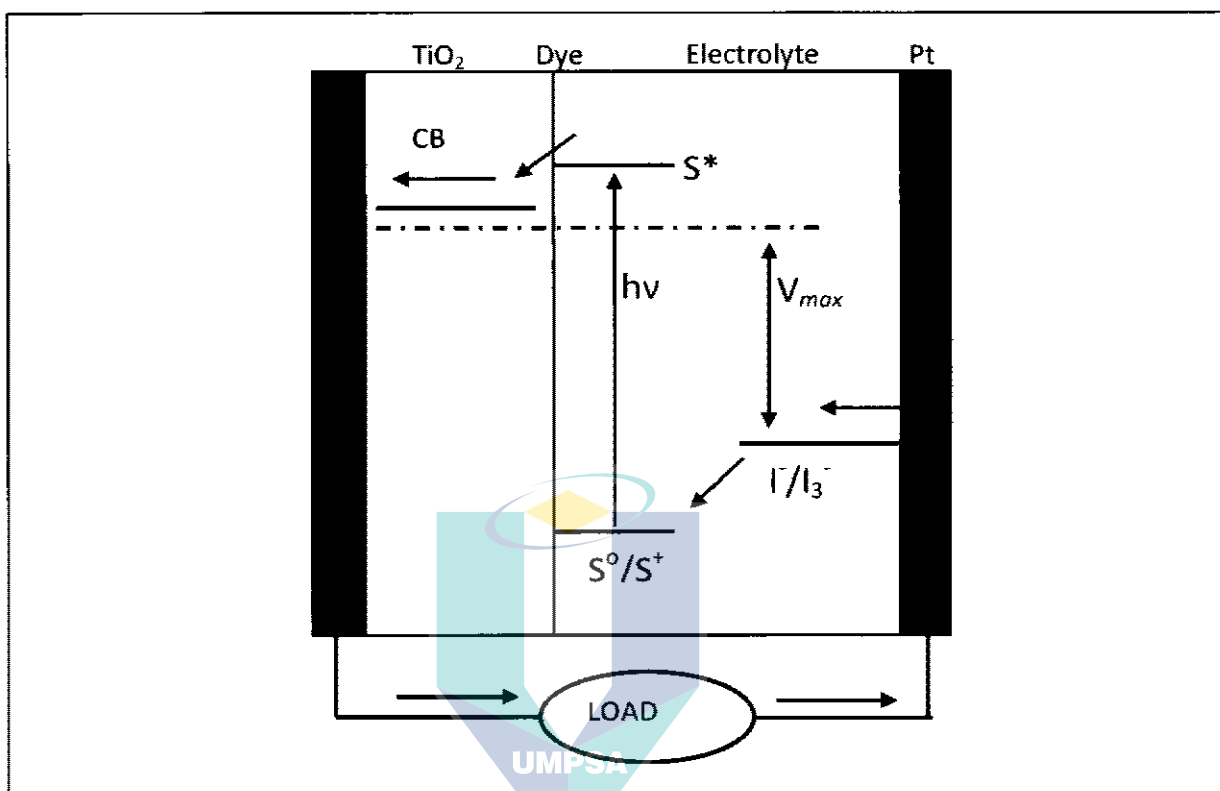
$$\text{TiO}_2 / \text{Dye}^+ + \text{electron}^- \text{ (conductor band)} \rightarrow \text{TiO}_2 / \text{Dye}$$
- IV. Reduction of oxidized sensitizer by the donor electron of the electrolyte  

$$\text{TiO}_2 / \text{Dye}^+ + 3/2 \text{ I (iodine)} \rightarrow \text{TiO}_2 / \text{Dye} + 1/2 \text{ I}_3^- \text{ (iodide)}$$
- V. Re-charge of mediator by electron at counter electrode  

$$1/2 \text{ I}_3 + \text{e}^- \text{ (conducting glass)} \rightarrow 3/2 \text{ I}$$
- VI. Reaction in the electrolyte between injected electron with electron acceptor  

$$\text{I}_3 + 2 \text{e}^- \text{ (conductor band)} \rightarrow 3\text{I}$$

**FIGURE 2.2**  
Operational Principle of Gratzel Cell.



The  $\text{TiO}_2$  solar cell, founded by Akira Fujimura, has become the semiconductor of choice for the mesoporous electrode in the Gratzel cell. Even though Fujimura et al. originally used the  $\text{TiO}_2$  in his experiments as a photo-function in the photo-electrochemical water splitting, but other researchers have shown that this material has many advantages in the case of sensitized photochemistry and photo-electrochemistry [43, 48]. It is also an inexpensive in cost, is abundantly available and a non-toxic material. It is reported as highly stable in electrolytic solution and it has almost an ideal energy band positions for the PEC. Furthermore,  $\text{TiO}_2$  has become the dominant material for environmental photo catalysis. In the case of Gratzel cell, it is quite an efficient solar energy convertor. Under normal sunlight, the ruthenium dye can maintain  $10^8$  redox cycles without perceptible suffer of performance, assuming that it can stand up to 20 years of continuous operation [47, 49].

However, the Gratzel cells that contain organic solvent and liquid iodine cause the

cell some problems like dye desorption, leakage and packaging [12]. These reasons will cause incomplete regeneration of reduction and oxidation process during cell operation, which could also affect the cell performance on the long term operational stability. Researchers have made some effort to overcome such problems by introducing methods which include utilizing electrolyte gel and high boiling point molten salt electrolyte [50], and these methods has shown some progress. However, replacing liquid electrolyte with a solid-state holes conductor is considered as the best alternative path, and it might provide a complete solution to overcome the problems of DSPECs.

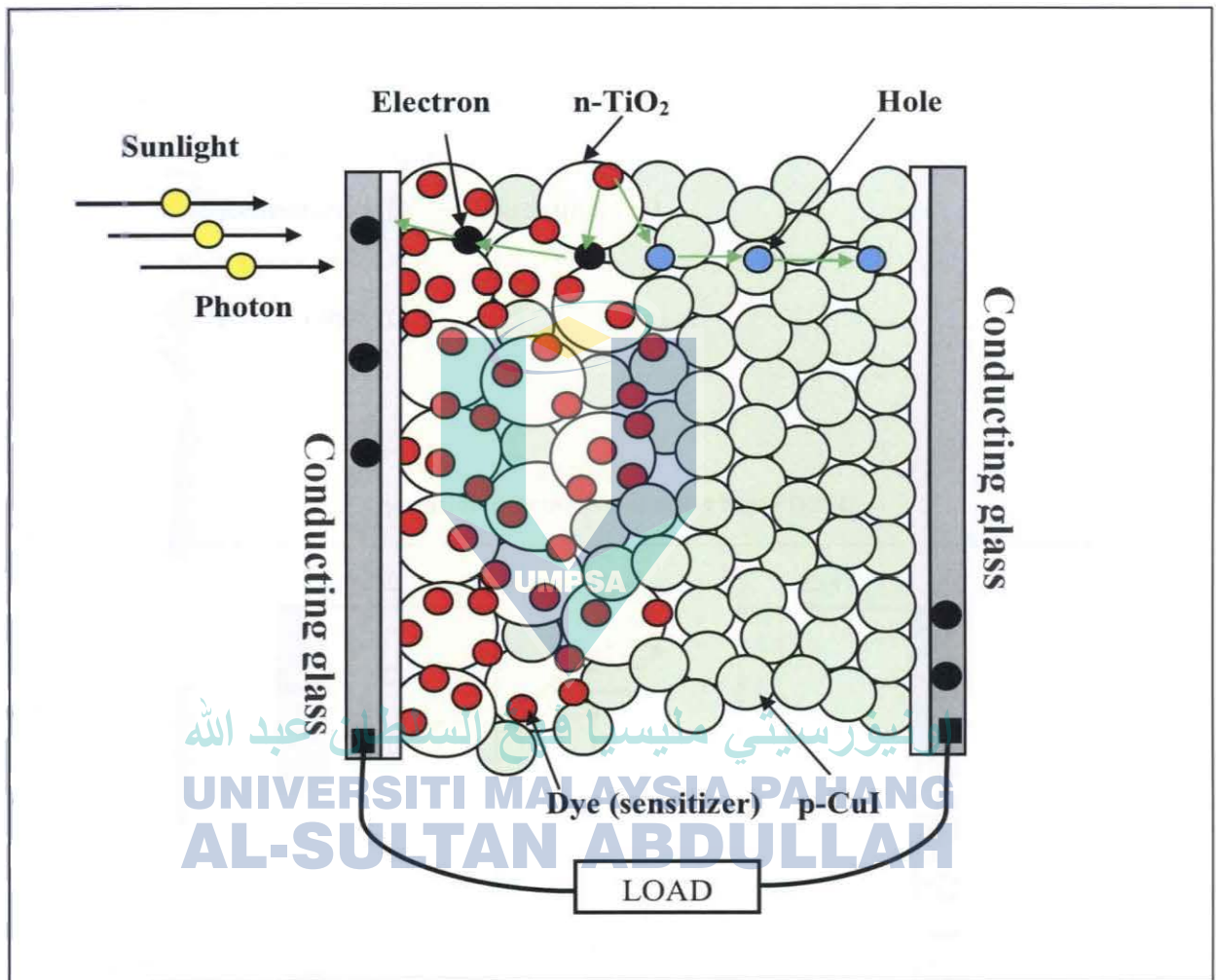
### 2.3 OVERVIEW OF SOLID STATE DSSC

Replacing electrolyte-based DSSC with p-type semiconductor as holes conductor in solid-state DSSC was first announced by Tennakone et al. and his research group in 1995 [14]. They had conducted experiments by attaching together the solid-state solar cell from a flower pigment cyaniding-sensitized  $\text{TiO}_2$  nanoporous electrode as n-type semiconductor and a p-type CuI (copper (I) iodide) semiconductor. Using spin coating deposition technique, the CuI solution prepared through sol-gel process was filled into the voids of the cyaniding-sensitized  $\text{TiO}_2$  film. About 0.8% of energy conversion efficiency was produced from the cell under direct sunlight. Although the efficiency obtained is low, the result created the possibility of fabricating solid-state DSSC devices from inexpensive and low quality materials.

The diagram illustrated in Figure 2.3 and Figure 2.4 shows structure and operational principal of solid-state dye sensitized solar cell (SSDSSC). The operating principle of solid-state DSSC is as follows. The dye, used as sensitizer, will inject an electron into the conduction band of  $\text{TiO}_2$  when the electron has absorbed enough energy from photons of light to exceed the band gap energy. Dye excitation and transferring of electron to  $\text{TiO}_2$  is called injection process. After the injection process, the dye itself will become positively charged by holes. At this moment, the positive charge is transferred to the p-type material as holes conductor. After the process, the dye reverts to its original state when it receives donor electrons from the p-type semiconductor. This process is

called the regeneration of the sensitizer. Through this process, the recapture of electrons from conduction band by the oxidized dye can be stopped.

**FIGURE 2.3**  
Schematic Diagram of CuI Based Solid State DSSC.



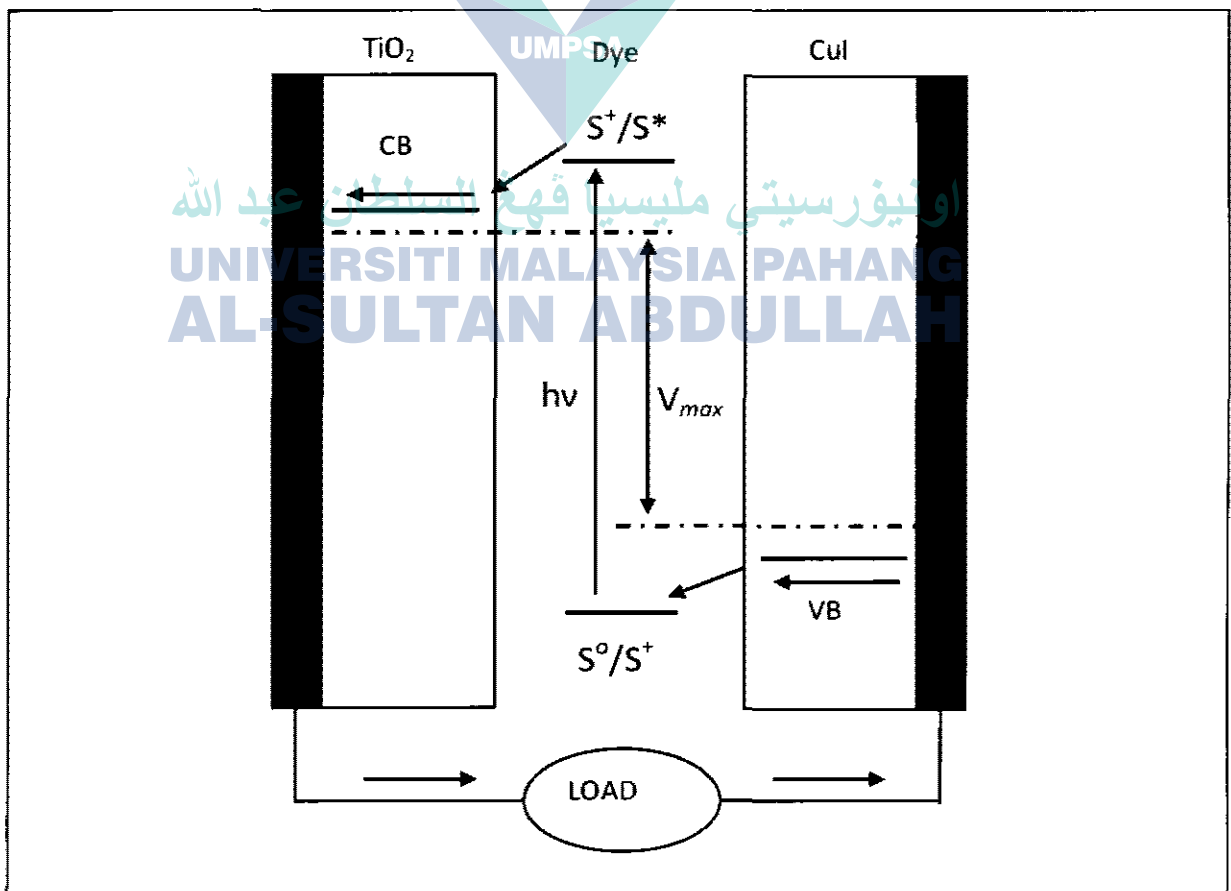
On the other hand, the electrons in p-type semiconductor will be regenerated by electrons that flow out from cathode and completing the circuit via electron motion through the external load.

The electrochemical operation of solid-state DSSC can be summarized as in Figure 2.4:

- I. Photo excitation through dye

- I.  $\text{Dye (D)} + \text{photon (} h\nu) \rightarrow \text{D}^*$
- II. Electron injection from dye  
 $\text{D}^* \rightarrow \text{D}^+ + \text{e}^- (\text{conductor band})$
- III. Electron transport  
 $\text{e}^- (\text{electrode}) \rightarrow \text{e}^- (\text{counter electrode})^+$
- IV. Reductor regeneration  
 $\text{Ox} + \text{e}^- \rightarrow \text{Reduction}$
- V. Dye regeneration  
 $\text{Reduction} + \text{D}^+ \rightarrow \text{Oxidation} + \text{D}$
- VI. Outcome  
 $H\nu \rightarrow \text{electricity}$

FIGURE 2.4  
Operational Principle of Solid State DSSC.



In terms of operational stability and manufacturing processes, almost all related researchers agreed on the advantages of a solid-state dye-sensitized photovoltaic device. However, the p-type semiconductor used in such devices and the dye used for sensitizing the TiO<sub>2</sub> need to have special properties. The requirements that the elements need to fulfill was summarized by Tennakone et al. [14, 51]:

- (1) The p-type material chosen should have a large band gap so that it is transparent to the visible spectrum so that the photons can be absorbed by the dye.
- (2) Availability of deposition method to deposit the p-type materials without decomposing or worsening the dye layer on the TiO<sub>2</sub> nanocrystallines.
- (3) The dye LUMO's (lowest unoccupied molecular orbital) level must be positioned over the bottom of TiO<sub>2</sub> conduction band and its HOMO (highest occupied molecular orbital) level is located below the top edge of p-type materials valence band.

So far, CuI is the best candidate to be used in the solid-state DSSC because it can be easily dissolved in organic solvents for deposition and its wide band gap (3.1 eV) covers the visible spectrum. It also fitted the HOMO level of the ruthenium bipyridyl used in the Gratzel cell where the valence band edge of CuI (-5.3 eV vs. the vacuum level) [52-53]. In 1998, Tennakone et al. reported 3.8% of energy conversion efficiency by assembling the cell from ruthenium dye-sensitized TiO<sub>2</sub> porous film and CuI [19].

Besides CuI, other p-type semiconducting materials have been tested for use in solid-state DSSCs. One such material is CuSCN (copper thiocyanate) which contains a stable Cu (I) p-type semiconductor. CuSCN has a band gap of 3.6eV and a valence band edge of -5.1eV with respect to the vacuum scale, thus fulfilling the requirements of solid-state dye-sensitized devices [16-17], but its solubility in organic solvents is not very good. So far, dipropyl sulfide which is an odorous and toxic chemical is the best solvent for CuSCN. Energy conversion efficiency over 2% has been reported recently for a cell assembled from ruthenium dye-sensitized TiO<sub>2</sub> mesoporous film and CuSCN [54].

Another usable p-type material for solid-state DSSCs is spirobisfluorene-connected aryl amine (*spiro-OMeTAD*). This material was first used in

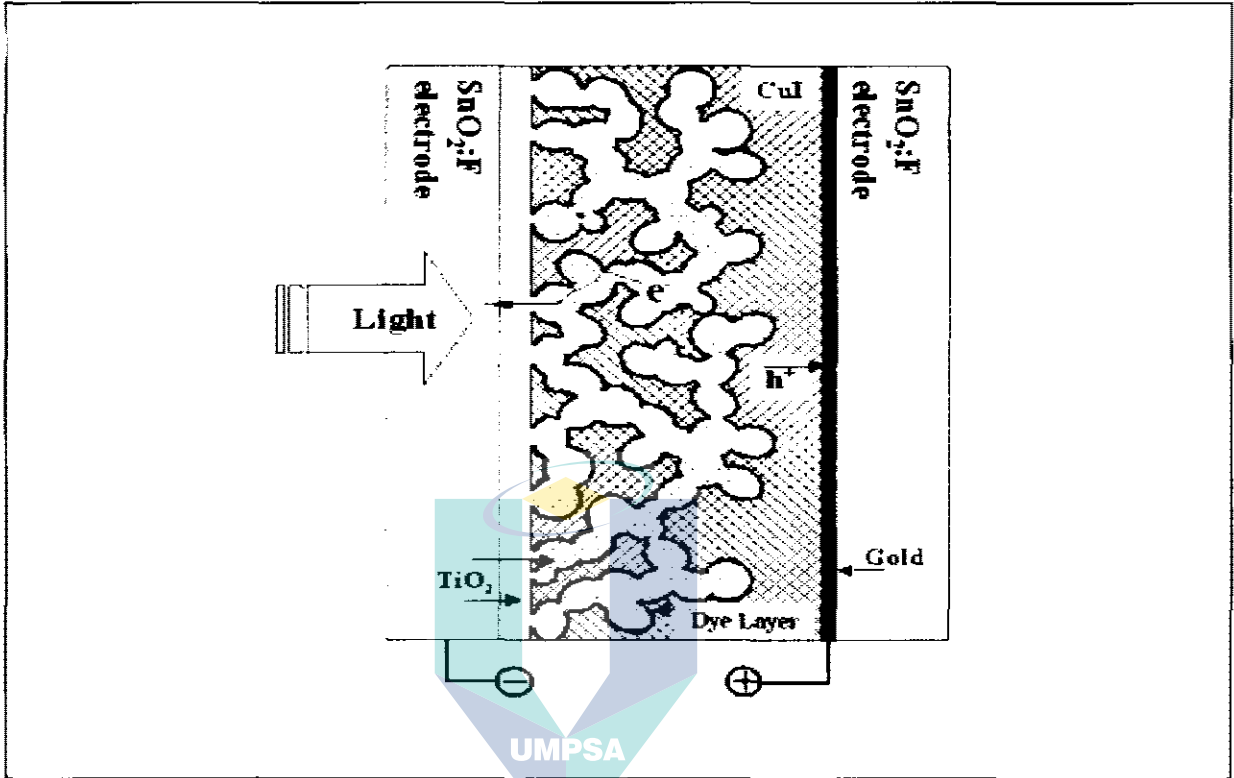
electroluminescent devices as a holes transmitter. The Gratzel group reported the application of this material is amorphous, resulting in a good contact with the dye monolayer is good [24, 55-58]. Transient spectroscopic data showed that spiro-OMeTAD reduced the oxidized ruthenium dye on the nanosecond scale [59]. Energy conversion efficiency over 3% has been reported recently for a cell using spiro-OMeTAD as hole conductor [60].

## 2.4 FABRICATION OF SOLID STATE DSSC

Figure 2.3 shows a model image of a solid-state DSSC using p-CuI as holes conductor [61]. The cell is made up of a conductive glass electrode-like  $\text{SnO}_2\text{:F}$  (fluoride-doped tin dioxide), a compact  $\text{TiO}_2$  thin film, a dye layer cover nanoporous  $\text{TiO}_2$  film, a CuI layer interpenetrated with  $\text{TiO}_2$  porous film and a gold-coated conducting glass electrode. First, a thick compact  $\text{TiO}_2$  thin layer is deposited on top of fluorin-doped tin oxide (FTO) to avoid the direct contact between CuI and conducting glass electrode, which would short circuit the cell. CuI is deposited into the dye-coated  $\text{TiO}_2$  nanoporous films by repeatedly applying the droplets of the CuI solution. Gold film is attached on top of CuI layer as the anode for solid-state DSSCs, but other conducting materials such as platinum, graphite and carbon materials are also give good conductivity [62-67].

In any kind of solid-state DSSCs, the common cell structure is as shown in Figure 2.5. The use of a mesoporous  $\text{TiO}_2$  to enhance photon absorption by the dye monolayer serves the same function as that of DSPECs. As solid-state DSSC device, it works by majority carriers where electron flow in n-type  $\text{TiO}_2$  while holes flow in p-type materials. This point is very crucial since it is the key to ensure the low cost and environment friendly materials is used for fabrication of solid-state DSSCs. In contrast, the classical p-n junction solar cells which work by minority carriers must use very high purity semiconductor materials and adopt high-cost manufacturing technology.

**FIGURE 2.5**  
**Structure Hypothesis Using CuI as P-Type Material in Solid-State DSSC**



Note: X.-t. Zhang, I. Sutanto, T. Taguchi, K. Tokuhira, Q.-b. Meng, T. N. Rao, A. Fujishima, H. Watanabe, T. Nakamori and M. Uragami, *Solar Energy Materials and Solar Cells* **80** (3), 315-326 (2003)

اونيورسيتي مليسيا قهغ السلطان عبد الله

UNIVERSITI MALAYSIA PAHANG  
 AL-SULTAN ABDULLAH

## 2.5 PROBLEMS IN SOLID STATE DSSC

### 2.5.1 Contact of Dye Molecule and Hole Conductor

To generate the oxidized dye molecules in solid-state DSSC, the function of redox couple (iodide/triiodide) in DSPEC is replaced by p-type materials. For efficient regeneration of oxidized dye molecules, intimate contact between p-type materials and the dye is essential. To deposit p-type materials on nanoporous  $\text{TiO}_2$  and to make the particles of p-type get close contact with the dye monolayer covering the nanoporous  $\text{TiO}_2$  electrode could be a trifling and very difficult process. The CuI and CuSCN that are used as holes conductor tend to crystallize

inside the mesoporous TiO<sub>2</sub> film and the possibility of ruining their contact to the dye molecules is high. Fortunately, a promising result has been reported for the ruthenium dye-based solid-state DSSCs, probably due to the firm bonding between the ruthenium dye and the cuprous ion, which may affect the growth and nucleation of CuI or CuSCN microcrystal inside the TiO<sub>2</sub> porous film [53]. In the case of organic holes conductor like spiro-OMeTAD, close contact with dye monolayer can be created due to its special molecular structure where it forms an amorphous solid inside the TiO<sub>2</sub> porous film [60].

However, the problem of contact in solid-state DSSC between the dye monolayer molecules and holes conductor is not fully solved. O'Regan et al. announced similar result could be produced in a cell that uses liquid electrolyte with mesoporous TiO<sub>2</sub> thin film that is less than 2μm, while the Gratzel-type solid-state cell worked poorly when the film thickness is more than 2μm [16]. This is due to the fact that the particles size of p-type materials is not sufficiently small to fill into the void volume of the mesoporous TiO<sub>2</sub> film, and the situation becomes worse when a thicker film is used. This is a drawback of the solution deposition method. Unfortunately, the development of deposition method has not progressed enough to replace the solution deposition method introduced some years ago. Another type of nanoporous TiO<sub>2</sub> film was developed by Tennakone et al. for solid-state DSSCs [11]. In this case, few layers of TiO<sub>2</sub> film is repeated deposited on heated conductive glass electrode using colloidal TiO<sub>2</sub> solution while vigorously stirring the solution during preparation. Due to the vigorous stirring of the solvent during the preparation, the TiO<sub>2</sub> film produced large pores from the surface down to the conductive glass substrate. The film produced using this method is suitable to be used with the solution deposition method since thicker film (~10μm) is used to fabricate the solar cell. However, this preparation method is time consuming and is unsuitable for large-scale manufacturing. Furthermore, taking surface roughness into consideration for effective absorption of incident light, the roughness of the ~10μm thick film prepared by Tennakone was about 300 nm is small compared to the more than 1000nm surface roughness

of mesoporous  $\text{TiO}_2$  film used in DSPEC. This factor is another reason that could affect the energy efficiency of solid-state DSSC [68].

### 2.5.2 Electron-Hole Recombination

Recombination of electrons and holes at the interface, called interfacial recombination of both semiconductors, is another serious problem currently encountered with solid-state DSSC, especially when using materials like  $\text{CuI}$  and  $\text{CuSCN}$ . Interfacial recombination in solid-state DSSC is almost similar to an internal short-circuit. This problem could be better understood by recalling the structure and the principle of operation of solid-state DSSCs, and depicting the cell as a dye-sensitized heterojunction. In general, this type of heterojunction has two elements with a large surface area and fragile interfacial electric field due to its interpenetrating structure [69-70]. Theoretically, the important condition to have good quality of heterojunction, it is important to have a substantial built-in electric field. Also, unlike the interpenetrating structure with large surface area, the physical heterojunction device is composed of a planar structure [71-74]. However, in the case of solid-state DSSC, the interfacial recombination between electron in the  $\text{TiO}_2$  and hole in p-type semiconductor after the initial charge generation cannot be avoided. In contrast, a serious recombination problem does not happen in DSPEC since it is a molecular device, where its charge mediator is electrolyte based that used iodide/triiodide as for redox mediator. In the case of DSPEC, the charge transfer kinetics in the iodide/triiodide redox couple is irreversible and the reduction of triiodide to iodide in the electrolyte between surface of  $\text{TiO}_2$  and conducting glass electrode is very slow [75].

Despite the serious interfacial recombination that lowers the performance of solid-state DSSC, researchers are making good progress with the outcome of the cell output. One of the solutions is the existence of a ruthenium dye monolayer that covers  $\text{TiO}_2$  surface structure. According to Tennakone et al., the dye monolayer with about 1 nm thick act as a physical barrier layer at the

interface and blocks the interfacial recombination [19, 76]. The recombination between the electrons in TiO<sub>2</sub> and holes in p-type materials could be completely suppressed if the dye monolayer is perfectly compact. However, it is quite difficult to form such a compact dye monolayer due to the electrostatic repulsion between the molecules and large size of the dye molecules [77-78]. Thus, direct contact between TiO<sub>2</sub> and the holes conductor is nearly unavoidable for solid-state DSSCs.

The recombination rate in a solid-state DSSC using CuI have not been available until now but O'Regan et al. have measured the recombination rate in a solid-state DSSC using CuSCN as the holes conductor [54, 75, 79] where they observed that the cell produced ~600mV photovoltage ( $V_{oc}$ ) and ~8mA/cm<sub>2</sub> of photocurrent ( $J_{sc}$ ). Compared to that of DSPEC, this result shows that the recombination in the solid-state DSSC is 10 times faster at the open circuit potential  $V_{oc}$  ( $t_{1/2} \sim 150\mu s$ ) and 100 times at short circuit ( $t_{1/2} \sim 450\mu s$ ). In the case of using CuI as holes conductor, the cell always exhibited a  $V_{oc}$  of 400-500mV, much lower than the theoretical  $V_{oc}$  (~ 1V). However, both kinds of cells exhibited similar charge transport rate ( $t_{1/2} \sim 200\mu s$ ). The similarity in the charge transport and recombination rates in both holes conductor results in acceptable photocurrent losses and low fill factor, both factors limits the efficiency of the solid-state DSSC. Thus, one key factor in producing higher efficiency performance in solid-state DSSCs is to overcome the problems of electron-hole recombination.

### 2.5.3 Interfacial Blocking Layers

Interfacial recombination problems in CuI based solid-state DSSC can be controlled by introducing a blocking layer as shown in Figure 2.4.3 [28]. An insulating thin layer deposited throughout the TiO<sub>2</sub> nanocrystalline film surface acts as a physical barrier, avoiding direct contact between TiO<sub>2</sub> and CuI. This layer should be less than 1 nm thickness so that it can maintain the tunnelling

efficiency of electrons from the dye molecules to  $\text{TiO}_2$ , and suppress the recombination at interface that cause degraded performance of the cells. Zhang et al. has conducted measurements of transient photo voltage by depositing the aluminium oxide ( $\text{Al}_2\text{O}_3$ ) layer on the surface of  $\text{TiO}_2$  [61]. Using solution deposition method, an ultrathin  $\text{Al}_2\text{O}_3$  layer was coated on the surface of  $\text{TiO}_2$  nanoporous film and assembled the solar cell with  $\text{CuI}$  as holes conductor. This experiment gives an analysis of interfacial recombination that occurred at p-n interface under open circuit condition when light generate the charges in the cell. With a slight alteration on  $\text{TiO}_2$ , the results of the studies revealed that the amount of dye absorption is enhanced, while reducing trap sites on  $\text{TiO}_2$  and controlling the problem of electron-hole recombination. Coating  $\text{Al}_2\text{O}_3$  for 4 minutes on  $5\mu\text{m}$  thick  $\text{TiO}_2$  improves the cell efficiency to 5.91% from 3.93%. [80-81].

**FIGURE 2.6**  
**Introduce Of Insulating Layer As Blocking Layer In Solid State DSSC.**

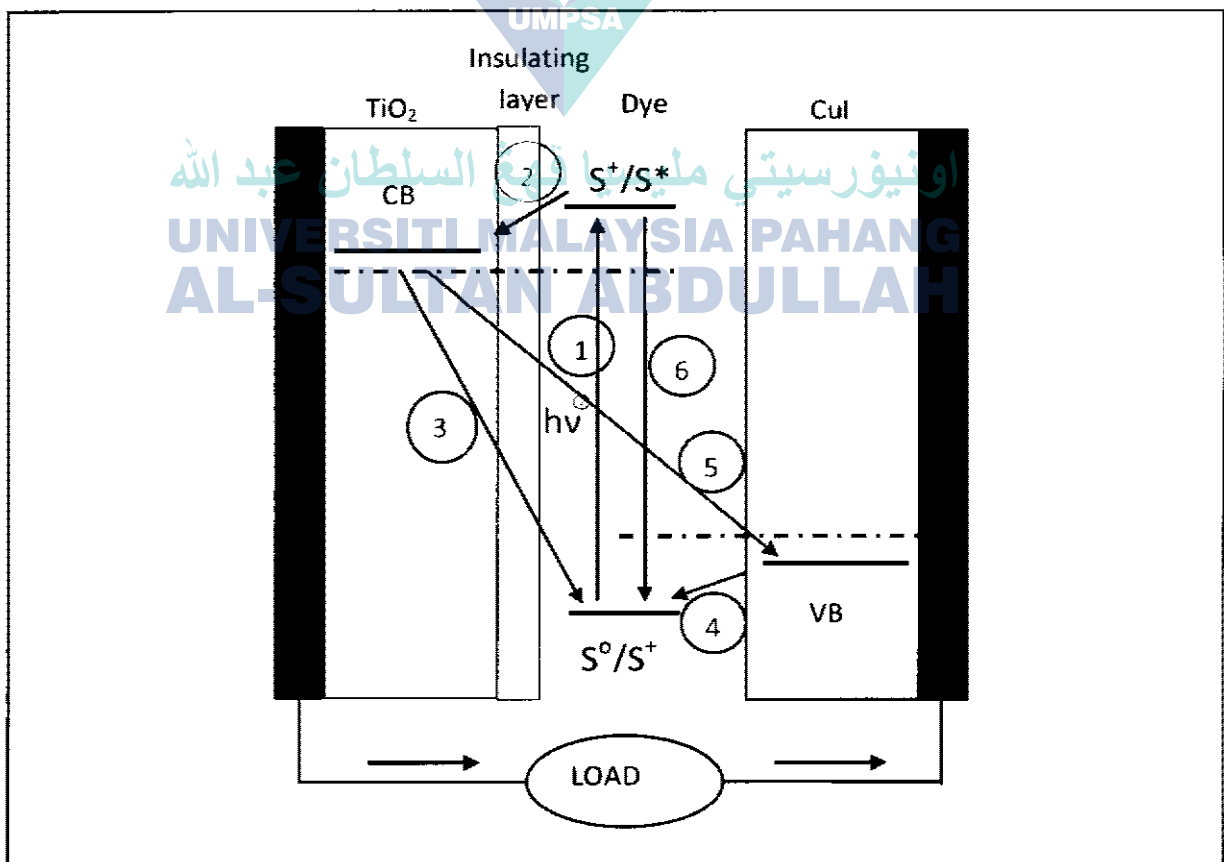


**Table 2.1**  
**Performance Parameters of Solid-State DSSC Based On TiO<sub>2</sub> and Al<sub>2</sub>O<sub>3</sub>**  
**Coated TiO<sub>2</sub> Films Under Various Intensities of Simulated Sunlight.**

	Light intensity (mW/cm <sup>2</sup> )	V <sub>oc</sub> (V)	J <sub>sc</sub> (mA/cm <sup>2</sup> )	FF	Efficiency (%)
TiO <sub>2</sub>	4.1	0.29	0.40	0.51	1.45
	17.6	0.35	1.97	0.58	2.27
	31.4	0.37	3.62	0.56	2.38
	89.0	0.40	9.10	0.48	1.94
TiO <sub>2</sub> /Al <sub>2</sub> O <sub>3</sub>	4.1	0.35	0.40	0.56	1.92
	17.6	0.42	2.08	0.57	2.86
	31.4	0.45	3.77	0.57	3.03
	89.0	0.47	9.46	0.52	2.59

The improvement in the cell performance due to the Al<sub>2</sub>O<sub>3</sub> layer is as shown in Table 2.1 [82]. With the existence of a thin blocking layer attached to the TiO<sub>2</sub> film, better overall efficiency of the cell is achieved, which include parameters such as open circuit voltage V<sub>oc</sub>, short circuit current J<sub>sc</sub>, and the fill factor. The improvements in these parameters proved that the suppression of electron-hole recombination in the cell has occurred. Also, the two cells resulted in low short circuit current J<sub>sc</sub> under very weak illumination (4mW/cm<sup>2</sup>), however, J<sub>sc</sub> increased gradually with the higher light intensity is used. This indicated that the function of Al<sub>2</sub>O<sub>3</sub> as a blocking layer improved the cell charge collection. Under illumination intensity in the range of 4.1 ~ 31.4mW/cm<sup>2</sup>, J<sub>sc</sub> of both cells increased linearly but varies under higher light intensity. Thus, this indicated that the quality of the 0.19 nm thick Al<sub>2</sub>O<sub>3</sub> layer was not sufficient to resolve the recombination problem.

Taguchi et al. had introduced magnesium oxide (MgO) as a blocking layer in solid-state DSSCs [12]. Other insulating materials, such as hafnium oxide (HfO<sub>2</sub>) [83], might also work well as the recombination blocking layer. The blocking function should depend on the thickness and the density of the layer, instead of the materials used. However, some wide band-gap semiconductors, such as ZnO, also showed a blocking function similar to that of an insulating layer

[84-85]. One possible reason is the high packing density of dye molecules on the ZnO covered TiO<sub>2</sub> film.

A discussion on the effect of insulating layer on the photocurrent is beneficial at this stage. A cell containing a 0.33nm thick Al<sub>2</sub>O<sub>3</sub> layer exhibited a higher fill factor and V<sub>oc</sub> than one with 0.19nm thick Al<sub>2</sub>O<sub>3</sub> layer, but its J<sub>sc</sub> is lower as the electron injection is exponentially dependent on the thickness of the insulating layer [61]. In an extreme condition, a very thick MgO layer improved the V<sub>oc</sub> of a CuI based cell up to 800mV but its J<sub>sc</sub> is negligible [86-87]. This shows that in principle the insulating layer can increase the V<sub>oc</sub> of the cell greatly through suppressing recombination, but the problem is how to prevent the J<sub>sc</sub> from decreasing at the same time. Note that the currently used preparation method, the surface sol-gel method, is not an optimal method for preparing insulating blocking layers. It depends on the hydrolysis and condensation of metal alkoxide on the surface of the TiO<sub>2</sub> film, through the reaction with adsorbed water. It is possible to prepare an ultrathin insulating layer on the TiO<sub>2</sub> film using this method, but it is impossible to prepare a dense insulating layer since the cleavage of bulky alkoxy groups will leave pores in the surface of TiO<sub>2</sub>.

If a better for preparing dense insulating layers on the TiO<sub>2</sub> surface can be found, it will be possible to resolve the interfacial recombination problem discussed above. A physical method, for example atomic layer chemical vapour deposition, might be a good choice for the preparation. In addition, post treating a dyed TiO<sub>2</sub> nanoporous film with the precursor of insulating materials is also a promising method to resolve the recombination problem. Since the dye molecules are adsorbed on the TiO<sub>2</sub> film, the insulating material will not hinder the electron injection.

#### **2.5.4 Device Operational Stability**

Operational stability is one of the most important factors that a photovoltaic device should have, and it should be measured at the maximum

output of the device. Previous studies on DSPECs always emphasized the stability under open circuit conditions, which could not provide a meaningful and accurate evaluation of the operational stability of the device [88]. In this study, the discussion will be on the operational stability of the CuI based solar cell under maximum output.

The operational stability is a controversial issue for solid-state DSSCs. Stability data for the CuSCN and *spiro*-OMeTAD based solar cells are not available. Previous studies have suggested that the CuI based solar cell was not stable for long term operation or even for long term storage, possibly due to the growth of CuI microcrystal inside the cell [14, 18]. The CuI based cell exhibited very fast degradation under simulated sunlight, and the output became almost zero after 72 hours of continuous illumination [12]. The illumination area turned from red (the color of the ruthenium dye) to black after the stability test, which is evidence of the existence of cupric oxide. However, when the stability test was carried out under the UV-free illumination ( $\lambda > 435\text{nm}$ ), the cell exhibited good operational stability. The cell retained more than 90% of the initial conversion efficiency after continuous illumination over 500 hours. X-ray photoelectron spectroscopy (XPS) studies confirmed the oxidation of CuI by  $\text{TiO}_2$  to cupric compound under ultraviolet light. The oxidation may involve  $\text{TiO}_2$  ultraviolet light and residual water in the cell. Water is oxidized to form  $\text{OH}^\cdot$  radicals which react with CuI to form the cupric compound. Since the reaction happened at the interface, the oxidation of CuI might degrade the heterojunction directly and finally degrade the cell. This mechanism suggests that, in order to fabricate highly stable CuI-based DSSCs, the photo catalytic activity of  $\text{TiO}_2$  should be purposefully suppressed and the residual water should be kept to a very low level. Also, the insulating blocking layer has been found to improve the operational stability of the cell under simulated sunlight possibly by blocking the photo oxidative function of  $\text{TiO}_2$  [12].

The results of the operational stability of the CuI based DSSC are rather promising. It is expected that the CuSCN based DSSC should exhibit even better

operational stability than that of CuI-based DSSC, since CuSCN in itself exhibit is more stable than CuI against oxidation.

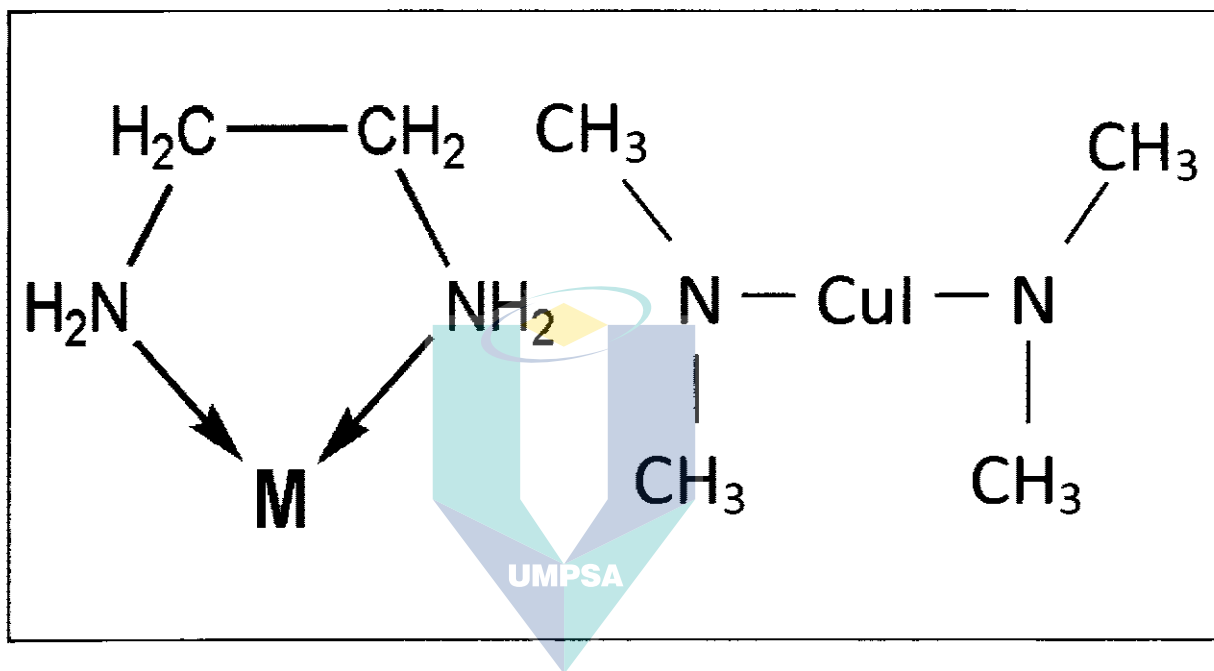
### 2.5.5 Chelating Agent

The stability of the DSSC using CuI with holes as conductor can be improved by adding a small portion of molten salt, such as ( $10^3$  M) of 1-methyl-3-ethylimidazolium thiocyanate (MEISCN), into the CuI solution [89]. Tennakone et al. stated that MEISCN act as a suppressor to CuI crystal growth but it will not alter the properties of CuI, such as the interface between CuI grain boundaries and the dyed  $\text{TiO}_2$  remains the same. Meng, et al. has put MEISCN under simulated continuous illumination for approximately two weeks and manage to improve the cell's efficiency to 3.8% while getting better stability [84]. However, purification of MEISCN requires compound separation by chromatographic process and it is quite expensive in cost. Further study conducted by Tennakone et al. found another substance, called triethylamine hydrothiocyanate (THT), which is much simpler than MEISCN but was equally or more effective to be used in CuI solution as hole conductor for fabrication of solid-state DSSC [90]. The compound stabilized the surfaces of CuI microcrystal by the strong interaction of the thiocyanate anion and the surface cuprous cation. Other thiocyanate salts also exhibited a similar effect [90].

The propose chelating agent for this research is called tetramethylethylenediamine (TMED or TMEDA or TEMED), a chemical compound with the formula  $(\text{CH}_3)_2\text{NCH}_2\text{CH}_2\text{N}(\text{CH}_3)_2$ , is derived from ethylenediamine by replacing the four N-H groups with four N-methyl ( $\text{CH}_3$ ) groups as shown in Figure 5.1 [91]. TMED, normally an organic compound, is widely used as a ligand for metal ions giving complexes that are soluble in organic solvents. It serves as a bidentate ligand and is known as chelating agents. A ligand or chelating agent is an ion or molecule that binds to a central metal

atom to form a coordination complex, and the bonding generally involves formal donation of one or more of the ligand's electron pairs [91-92].

FIGURE 2.7  
(Left) Ethylenediamine Ligand Of A Chelate Complex, (Right) TMED Chemical Compound.



## 2.6 SUMMARY

Recent studies in solid-state DSSC have encountered two problems that restrict the performance of the cell efficiency. The first problem is the incomplete pore-filling of the nanoporous TiO<sub>2</sub> layer by the holes transporter, and this affects the determination of the final efficiency of the cell. This problem will lead to the lack of surface area inside the TiO<sub>2</sub> film which results in poor absorption of light. The second problem that causes the degradation of the cell is interfacial recombination due to the lack of a strong interfacial electric field. However, the operational stability of the CuI-based DSSC has been found to be good for a 500 hours continuous test when crystal growth inhibitor is added to the CuI solution.

The interfacial recombination in the solid-state DSSC can be suppressed using a thin layer of insulating material, but the current preparation methods for this insulating layer are not satisfactory. A recent study on the ETA solar cell has suggested that the ALCVD method is a possible candidate for the preparation of a thin, dense insulating layer on a porous structure [93-94]. It can be predicted that a breakthrough in the energy conversion efficiency will occur for the solid-state DSSC when a preparation method for a high quality insulating blocking layer is developed. Furthermore, the high quality insulating will improve the operation stability of the solid-state DSSC.

The problem of insufficient light absorption may be overcome by replacing the ruthenium dye with another organic dye with a greater extinction coefficient [95-99]. Another suggestion to increase the spectral response near IR region is to use multilayer dye so that optical absorption in solar energy spectrum can be broadened [100-101]. The semiconductor quantum dot is also a possible option for panchromatic sensitizers. The absorption spectra of the quantum dots II-VI and III-V semiconductor nanoparticles can be adjusted to cover the visible and near IR region by changing the particle size. Optical design can also improve the light collection in the solid-state DSSC and thus improve its solar energy conversion efficiency.

The morphology of the porous film electrode is also very important for the solid-state DSSC. In solid-state DSSC, a desirable morphology for the porous film would have mesoporous structure [102-104] or vertically aligned TiO<sub>2</sub> nanorods in parallel to each other with respect to the conducting glass substrate [105-107]. Such morphology would help to improve pore-filling with p-type materials, allow the formation of a higher quality heterojunction, and exhibit faster charge transport in the film, compared to the random mesoporous morphology. Future studies should also be carried out to developing the fabrication technology for the solid-state DSSC. While recent progress in solution deposition [54, 108] is encouraging, more efforts are required for the reproducible production of the solid-state DSSC.

## CHAPTER THREE

### METHODOLOGY

#### 3.1 INTRODUCTION

This chapter discusses the details of the methodology used in the preparations of the CuI thin films and its characterization techniques. The preparation procedures include substrates cleaning, the synthesis of CuI thin films with and without incorporation of chelating agent TMED, the fabrication of DSSC cell, and the characterization technique employed. This chapter is divided into 5 main parts.

1. Cleaning of substrates, such as glass and Indium doped Tin Oxide (ITO) glass.
2. Preparation and deposition of CuI thin film, with and without incorporation of chelating agent TMED.
3. Characterization of deposited CuI thin film, with and without incorporation of chelating agent TMED.
4. Fabrication of CuI-based (n-TiO<sub>2</sub>/dye/p-CuI) solid-state dye sensitized solar cells (SSDSSC).
5. Characterizations of the fabricated thin films.

The details of the parts will be discussed in subsequent chapters.

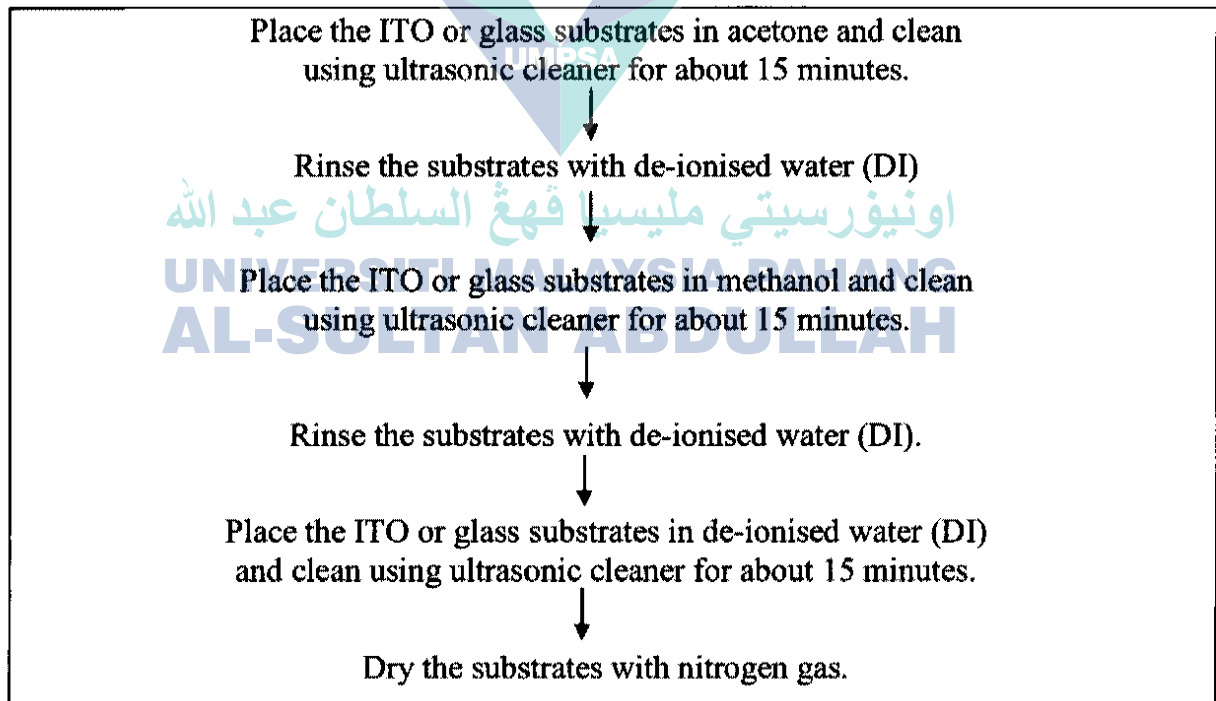
#### 3.2 CLEANING OF SUBSTRATES

In order to produce high quality CuI materials, the substrate needs to be cleaned to remove organic and inorganic contamination. Contamination on the substrate will affect the development of the material, thus changing its properties. In this research, two kinds of substrate were used, namely, Indium doped Tin Oxide (ITO) substrate and glass substrate. In most of the experiments, the ITO substrates are used to investigate CuI materials surface morphology, and this is conducted using scanning electron microscopy (SEM) or field emission scanning electron microscopy (FESEM) as the substrates are

electrically conductive. However, both the glass and ITO substrates are used when measuring electrical and optical properties.

The process of substrate cleaning could be explained as follows; the glass substrates were cut in 2cm x 2cm in size while ITO also in the same size of glass was obtained from suppliers. Both kinds of substrates were placed into different beakers which contain acetone as cleaning material in each beaker. The beakers were then placed into ultrasonic device which contain half of water in it and clean by the device for about 15 minutes. After reached 15 minutes, the substrate was then rinsed with de-ionised (DI) water. The above step was repeated using methanol and DI water as cleaning material until finally the substrate was dry using nitrogen gas. The whole process of cleaning is summarized as in Figure 3.1.

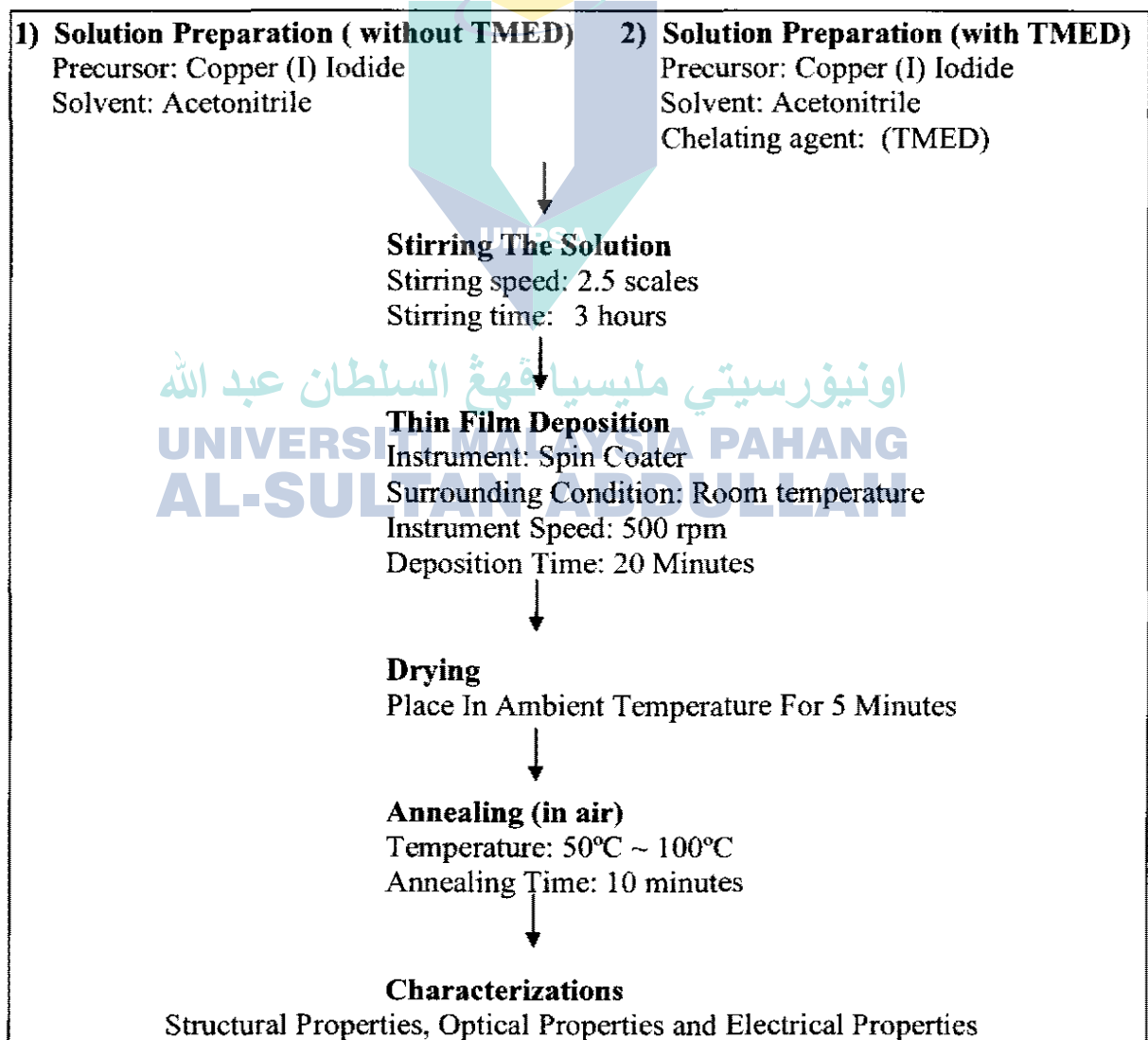
**FIGURE 3.1**  
**Process Flow Of Substrates Cleaning Process.**



### 3.3 PREPARATION OF COPPER (I) IODIDE (CuI) THIN FILMS

In this research, CuI thin films and TMED chelate CuI thin films have been prepared and studied. In the preparation, CuI is used as precursor materials, acetonitrile as solvent and tetra-methyl-ethylene-diamine (TMED@TMEDA) as stabilizer, also known as a chelating agent. The solutions were prepared in two parts using sol-gel method, one without TMED and the other with TMED, and the thin films were deposited using drop and spin-coating deposition technique.

FIGURE 3.2  
Process Flow of Preparation and Characterization of CuI Thin Film.



Drop and spin coating method is a technique that uses an instrument called spin coater. It is a device which is able to produce uniform thin films on the substrates at a constant spin speed in a given time. The spin coater has a sample holder, which is in a vacuum, used to hold the substrate during deposition process. The deposition process was done by dropping the solution onto the substrate, letting it dry in air of room temperature for a certain time, and then accelerated again using the spin coater at a certain speed for a certain time. The complete deposited samples then anneal between  $50^{\circ}\text{C} \sim 100^{\circ}\text{C}$  in 10 minutes and ready to be characterized.

In general, the overall process of thin film preparation is illustrated in the process flow diagram shown in Figure 3.2.

### 3.3.1 Preparation of CuI Thin Films at Different Molar Concentration

All the chemicals used in this research were as obtained from the suppliers and no further purification was carried out. Copper (I) iodide (CuI) (ALDRICH 99%) precursor is prepared in molar concentrations ranging from 0.05 M to 1.0 M, and each concentrate is dissolved in 50 ml of acetonitrile. A clear and homogeneous solution can be observed after the solution was stirred at 2.5 scales for 3 hours, after which the solution is ready for thin film deposition process.

CuI thin films were deposited on glass and ITO substrates by drop and spin coating technique. The speed of spin coater was set at 100 rpm for 10 seconds. During the process, two drips of CuI solution were dropped onto the substrates. The solution was left to dry at room temperature for five minutes inside the spin coater with nitrogen flowing in the spin coater. Then, the coater was spanned for another 20 seconds at 500rpm for the substrate to be coated with the film, after which the film was heated at  $50^{\circ}\text{C}$  for five minutes. This process ends after 5 to 10 times of repeated operations, depending on the required thickness of the film.

The crystal structure and orientation of CuI thin films are investigated

using X-ray diffractometer (XRD, Rigaku ULTIMA IV) with Cu K $\alpha$  radiation, and the morphology of the film is characterized using SEM (JEOL JSM6360LA). The optical properties of CuI thin films were measured in the 300 nm to 800 nm wavelength range using UV-Vis-NIR spectrophotometer (Cary 5000) and photoluminescence (PL) spectrofluorometer (Jobin Yvon Horiba FluoroMax 3).

**TABLE 3.1**  
**Preparation and Characterization of CuI Thin Films at Different Molar Concentrations.**

Preparation of precursor solution (sol-gel method)		
CuI solution molarities (M)	0.05 M, 0.1 M, 0.5 M and 1.0 M	
Substrate	Microscope slide glass (Sail brand) and ITO	
Material	Precursor	Copper (I) Iodide
	Solvent	Acetonitrile (50mL)
Stirring	Stir speed	2.5 scale
	Time	3 hours
Deposition of thin film using drop and spin coating method		
Spin coater	Speed	100rpm/500 rpm
	Time	10sec/20 sec
Deposition repetitions	10 times	
Drying	Temperature	Room temperature
	Time	5 min
Heating in air	Temperature	50°C
	Time	5 min
Characterization of CuI thin films		
Structural properties	1) XRD (Rigaku D/MAX-2000 system) 2) SEM @ FESEM	
Optical properties	1) UV-Vis-NIR spectrophotometer 2) PL spectroscopy (Jobin Yvon Horiba Fluoro-Max 3)	
Electrical properties	Two probe current-voltage (I-V) measurement system (solar simulator)	

The PL instrument uses Xenon (Xe) lamp as photon source that excites at a wavelength of 325 nm. The electrical properties of the thin films were characterized using solar simulator (BUNKOKEIKI). Indium (In), used as the

electrode for current-voltage (I-V) measurements, has been deposited on the thin films using thermal evaporator (ULVAC KIKO, VPC-1100). The preparation parameters and characterization methods of CuI thin films at different molar concentration are summarized in Table 3.1.

### 3.3.2 Effect of Annealing Temperature on CuI Thin Films at Different Molar Concentration

For the purpose of studying the effects of annealing on the properties of CuI films, samples are similarly prepared as described in Section 3.2.1, except that the samples were annealed in air at different temperatures for ten minutes after the heating process. The preparation parameters and characterization procedure of CuI thin films at different annealing temperature are summarized in Table 3.2.

**TABLE 3.2**  
Preparation and Characterizations of Annealed CuI Thin Films.

Preparation of precursor solution (sol-gel method)		
CuI solution molarities (M)	0.05 M, 0.1 M, 0.5 M and 1.0 M	
Substrate	Microscope slide glass (Sail brand) and ITO	
Material	Precursor	Copper (I) Iodide
	Solvent	Acetonitrile (50mL)
Stirring	Stir speed	2.5 scale
	Time	3 hours
Deposition of thin film using drop and spin coating method		
Spin coater	Speed	100rpm/500 rpm
	Time	10sec/20 sec
Deposition repetitions	10 times	
Drying	Temperature	Room temperature
	Time	5 min
Heating in air	Temperature	50°C
	Time	5 min
Annealing in air	Temperature	As deposited, 50°C, 80°C and 110°C
	Time	10 min

Characterization of CuI thin films	
Structural properties	1) XRD (Rigaku D/MAX-2000 system) 2) SEM @ FESEM
Optical properties	1) UV-Vis-NIR spectrophotometer 2) PL spectroscopy (Jobin Yvon Horiba Fluoro-Max 3)
Electrical properties	Two probe current-voltage (I-V) measurement system (solar simulator)

### 3.3.3 Preparation of CuI Thin Films Incorporation of TMED

Incorporating TMED as chelating agent onto CuI thin film was prepared using sol-gel method. All the chemicals used in this research were as obtained from the suppliers and no further purification was carried out. The TMED obtained from the suppliers is in the form of liquid. The TMED chelate CuI solution is first prepared using the same process as described in Section 3.2.1. Different volumes of TMED chelating agent was added to the CuI solution with various volume ratios. The solution is then stirred using magnetic stirrer at room temperature for 3 hours.

CuI thin films that incorporate TMED were deposited using drop and spin coating method. A few drips of the solution are dropped onto the substrate and left to dry for five minutes inside the spin coater under a flow of nitrogen. Then it was spanned at 500 rpm for 20 seconds for the solution to coat the substrate. The film was then heated at 50°C for 5 minutes and the process was repeated to obtain the required thickness.

The characteristics of these films are then examined using the same characterization procedures as conducted in Section 3.3.1. The preparation of the CuI thin films that incorporate TMED is summarized in Table 3.3.

**TABLE 3.3**  
**Preparation and Characterizations of CuI Thin Films That Incorporate TMED.**

Preparation of precursor solution (sol-gel method)		
CuI solution molarities (M)	0.05M, 0.1M, 0.5M, 1.0 M	
CuI:TMED ratio	1 : 0, 1 : 0.5, 1 : 1.0, 1 : 1.5	
Substrate	Microscope slide glass (Sail brand) and ITO	
Material	Precursor	Copper (I) Iodide
	Solvent	Acetonitrile (50mL)
	Chelating agent	Tetramethylethelinediamine (TMED)
Stirring	Stir speed	2.5 scales
	Time	3 hours
Deposition of thin film using drop and spin coating method		
Spin coater	Speed	100rpm/500rpm
	Time	10sec/20sec
Deposition repetition	10 Times	
Drying	Temperature	Room temperature
	Time	5 min
Heating in air	Temperature	50 <sup>o</sup> C
	Time	5 min
Characterization of CuI thin films		
Structural properties	1) XRD (Rigaku D/MAX-2000 system) 2) SEM @ FESEM	
Optical properties	1) UV-Vis-NIR spectrophotometer 2) PL spectroscopy (Jobin Yvon Horiba Fluoro-Max 3)	
Electrical properties	Two probe current-voltage (I-V) measurement system (solar simulator)	

### 3.3.4 Effect of Annealing Temperature on CuI Thin Films That Incorporate TMED

For the purpose of studying the effects of annealing on the properties of CuI films that incorporate TMED, samples were similarly prepared as described in Section 3.2.3. However the samples were annealed at different temperatures for ten minutes after the heating process. The preparation process and

characterization procedures of CuI thin films that incorporate TMED at different annealing temperature are summarized in Table 3.4.

**TABLE 3.4**  
**Preparation and Characterization of Annealed CuI Thin Films That Incorporate TMED.**

Preparation of precursor solution (sol-gel method)		
CuI solution molarities (M)	0.05M, 0.1M, 0.5M, 1.0 M	
CuI:TMED ratio	1 : 0, 1 : 0.5, 1 : 1.0, 1 : 1.5	
Substrate	Microscope slide glass (Sail brand) and ITO	
Material	Precursor	Copper (I) Iodide
	Solvent	Acetonitrile (50mL)
	Chelating agent	Tetramethylethelinediamine (TMED)
Stirring	Stir speed	2.5 scales
	Time	3 hours
Deposition of thin film using drop and spin coating method		
Spin coater	Speed	100rpm/500 rpm
	Time	10sec/20 sec
Deposition repetitions	10 times	
Drying	Temperature	Room temperature
	Time	5 min
Heating in air	Temperature	50°C
	Time	5 min
Annealing in air	Temperature	As deposited, 50°C, 80°C and 110°C
	Time	10 min
Characterization of CuI thin films		
Structural properties	1) XRD (Rigaku D/MAX-2000 system) 2) SEM @ FESEM	
Optical properties	1) UV-Vis-NIR spectrophotometer 2) PL spectroscopy (Jobin Yvon Horiba Fluoro-Max 3)	
Electrical properties	Two probe current-voltage (I-V) measurement system (solar simulator)	

### 3.4 DEPOSITION OF TiO<sub>2</sub>/DYE/CuI SOLID STATE DSSC

All the chemicals used in this research are as obtained from the suppliers and no further purification was carried out. The F-doped SnO<sub>2</sub> (FTO) coated glass and Indium

doped SnO<sub>2</sub> (ITO) substrates were used to study the characteristics of fabricated TiO<sub>2</sub>/dye/CuI cells. The substrates were cleaned with methanol and rinsed with deionizer water. In all stages of the preparation, the glass and substrates were placed in dip ultra sonic water for 15 minutes where then they were dried with nitrogen gas.

TiO<sub>2</sub> films with a thickness of approximately 15 μm were prepared by the squeegee method using a 0.8 g/mL paste of TiO<sub>2</sub> powder (P25, Aerosol Japan) with 0.5 mL of acetyl acetone. 5mL of water was divided into two parts which is 2mL + 3 mL and was added to paste and stirred again by hand in 5 minutes of time for each step. The paste was mixed and blended with 0.4 g of polyethylene glycol and 2.5 mL of triton X for about five minutes. Then, the TiO<sub>2</sub> films were heated and annealed at 100°C and 400°C for 30 minutes at room temperature. The apparatus and the process of depositing the thin films are shown in Figure 3.4. The preparation and deposition of the TiO<sub>2</sub> thin film is summarised in the following process flow diagram.

**FIGURE 3.3**  
**Preparation and Deposition Process Flow of TiO<sub>2</sub> Thin Films.**

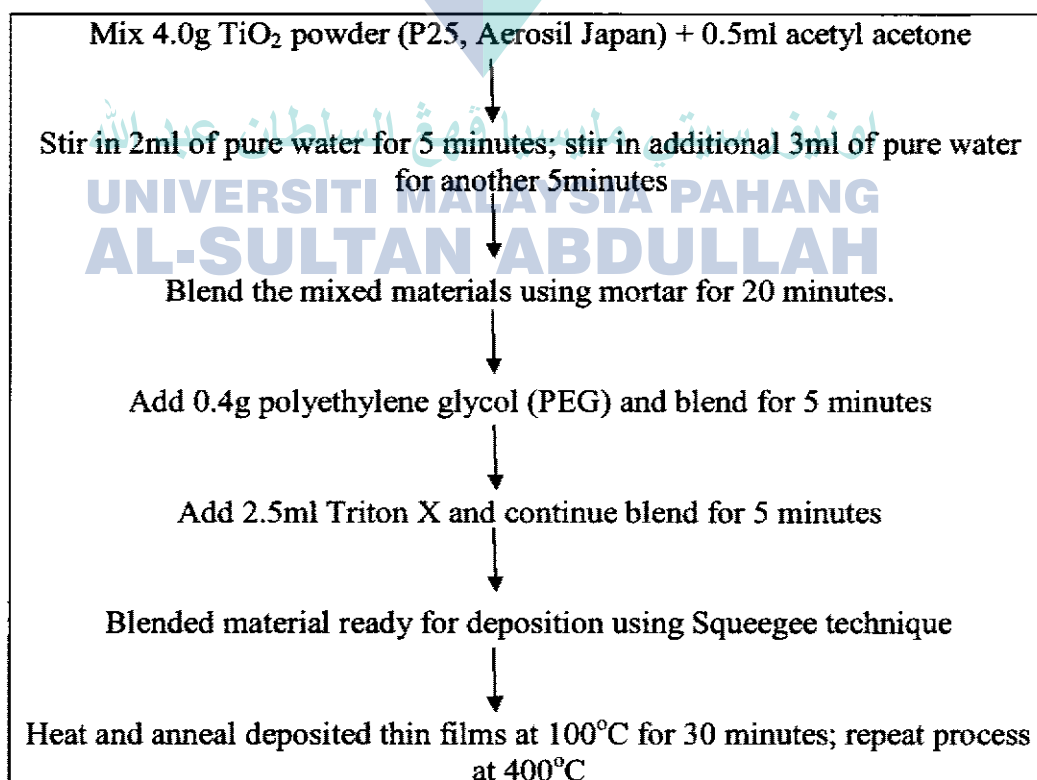
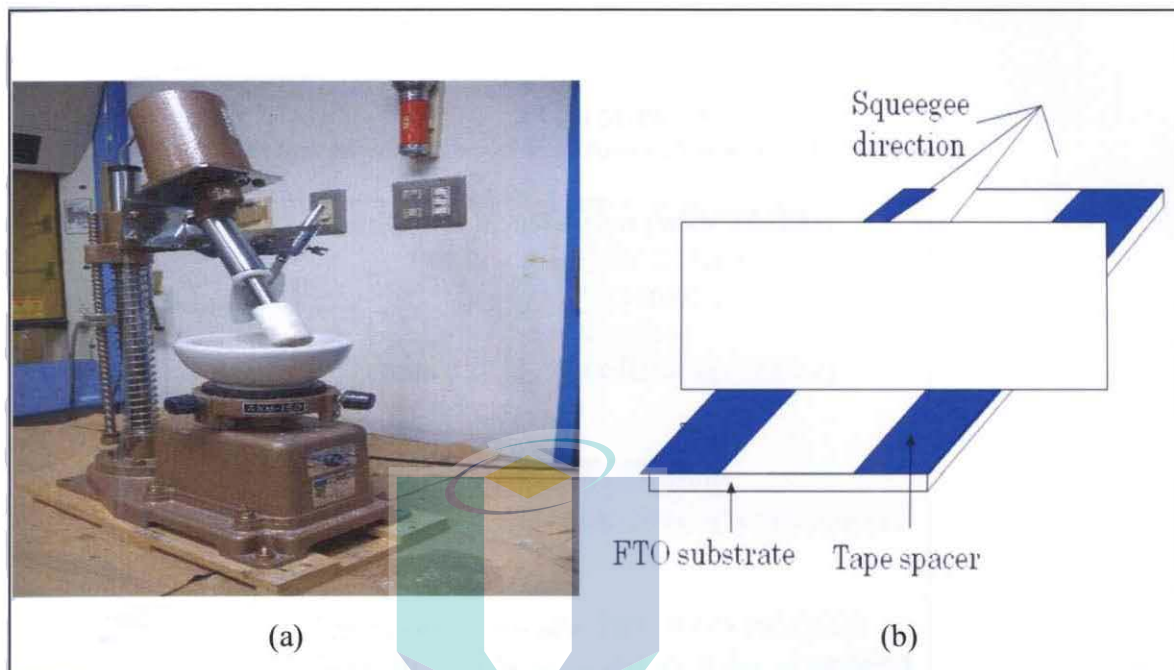


**FIGURE 3.4**  
**Apparatus Used To Blend the TiO<sub>2</sub> Powder in (a) and Process Used To Deposit TiO<sub>2</sub> Thin Films in (b).**



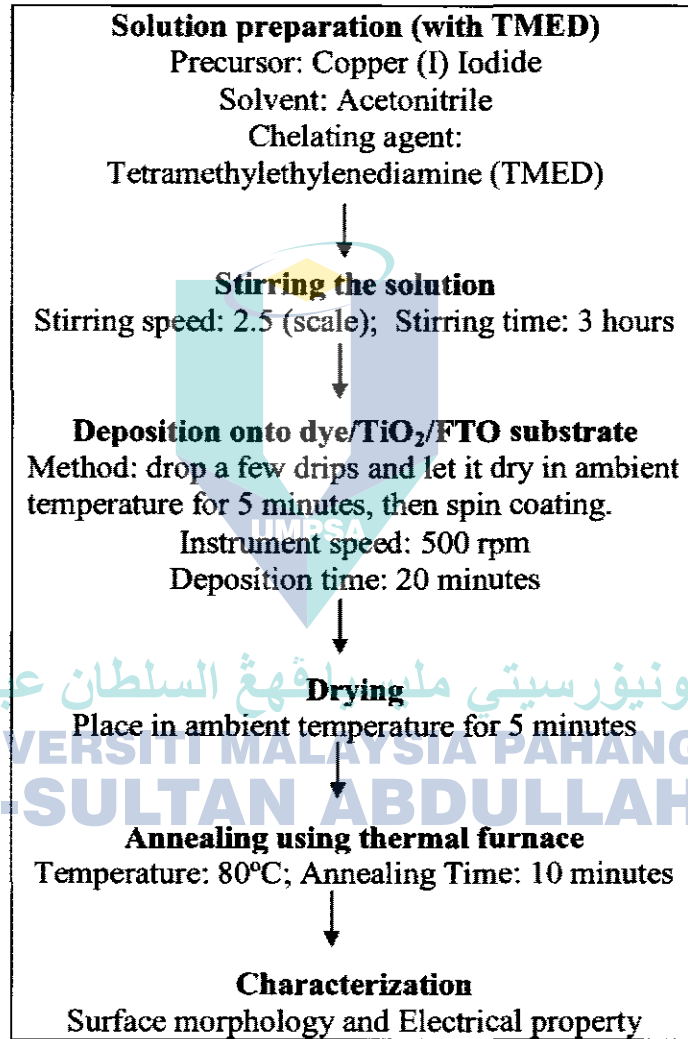
After completing the preparation of TiO<sub>2</sub> films, the films are soaked for 24 hours in a dye, Rhodamine B, which is prepared by dissolving 50 mM of Rhodamine B into pure water and stirred for about one hour.

For the deposition of CuI and TMED-chelate CuI solution onto dye/TiO<sub>2</sub> thin film, a saturated CuI coating solution with and without TMED were prepared by dissolving 1.0 M of CuI powder (ALDRICH 99%) into acetonitrile at room temperature. Approximately 3.725 mL of TMED (Sigma-Aldrich 99%) was added to the CuI solution to produce a volume ratio of 1:1 between CuI and TMED. The solutions were stirred around three hours before the deposition takes place. The solutions were then deposited onto dye/TiO<sub>2</sub>/FTO glass substrates using drop and spin coating technique. After the deposition process was completed, the cell was annealed at 80°C for 10 minutes. Indium electrodes were deposited on the surface of the cells using thermal evaporator with a voltage of 70 kV for 60 seconds.

The surface morphology of CuI thin film nanostructure with and without TMED

was studied using Field Emission Scanning Electron Microscopic (FESEM), and the differences in electrical potential between two points were determined using two probe solar simulator I-V measurements.

**FIGURE 3.5**  
**Preparation and Deposition Process Flow of CuI Thin Films.**



### 3.5 CHARACTERIZATION METHOD

The properties of the materials are evaluated using a variety of characterization

techniques. The characterization procedure is important in order to analyze and determine the quality of prepared materials. In this thesis, the following characterization has been conducted on the:

1. Structural, optical and electrical properties of CuI thin films with and without the effect of temperature,
2. TMED-chelated CuI thin film with and without the effect of temperature, and
3. Deposited of TiO<sub>2</sub>/dye/CuI with and without the incorporation of TMED as chelating agent.

Before the precursor solution is deposited as thin film, the following parameters were measured of the solution:

1. pH and conductivity using conductivity meter, and
2. Particle size using ZETA NANO PARTICLE SIZER (MALVERN INSTRUMENTS, ZEN 1600).

After the deposition of the precursor solution as thin film, the following studies were conducted on the film:

1. Surface morphology using field emission scanning electron microscopy (FESEM),
2. Crystalline properties using X-ray diffractometer (XRD),
3. Optical properties using UV-Vis-NIR spectrophotometer and photoluminescence (PL) spectrofluorometer, and
4. Electrical properties using two probes current-voltage (I-V) measurement system (solar simulator).

### **3.5.1 Measurements of pH and Conductivity**

After the CuI solution was stirred for three hours, its pH and conductivity were measured in order to study the effects of the different concentrations, hence different pH, of precursor solution on the ion conductivity of the solution. In solid conductors, current is moved and carried by electrons, but in solution, current is carried by ions ((+) cations and (-) anions). The conductivity of a solution is

dependent on the concentration of the ions present; the greater the concentration of the ions, the greater the conductivity of the solution. All of these ions have the electrical unit charges shown by their symbols ( $S/cm^{-1}$ ), but they move at different mobility through the solution, so they contribute differently to the conductivity [109-110]. On the other hand, the pH is a measure of the concentration of the hydrogen ( $H^+$ ) and hydroxyl ( $OH^-$ ) ions present in the solution. For an acidic solution, the lower the pH caused by the higher  $H^+$  concentration contained in the solution, the greater will be its conductivity [111]. In this research, the pH and conductivity meter was used to measure the solutions.

### 3.5.2 Particles Size Measurement

While the precursor solution is still in liquid form, the precursor particle size is measured using ZETA NANO PARTICLE SIZER (MALVERN INSTRUMENTS, ZEN 1600). This measurement is conducted so as to observe any changes or differences in precursor particles with and without TMED chelating agent. This measurement could be considered as the first step of analyzing the size of particles before proceeding to the next stage.

### 3.5.3 Surface Morphology

The surface morphology of CuI thin films have been characterized using field emission scanning electron microscopy (FESEM), or simply SEM, whose image provides information on the thin film morphology as well as the CuI particles size. The FESEM used in the study are the ZEISS Supra 40VP and JEOL JSM 6701F, both equipments located at the Physics Department, Faculty of Applied Sciences, UiTM. The microscope is equipped with an Energy-dispersive X-ray spectroscopy (EDX) for sample composition identification. The EDX analysis was based on point analysis, line scanning and dot-mapping which depends on CuI structure. The samples were prepared with the size of 1 cm x

1cm. For FESEM imaging, the accelerating voltage used was 5kV with built-in lens and secondary electron mode, while the magnification used ranges from 10 to 200,000.

### 3.5.4 Crystalline Properties

X-ray diffraction measurement, an important characterization technique for analyzing the structural properties of materials, is used to identify the materials used in the thin film, characterize its crystal orientation and size, and to study the defects in the crystal. The structure of a crystal structure is defined as a structure in which the atoms are arranged in a regular pattern. When an X-ray beam hit the atoms of a material, the electron around the atoms will oscillate with the same frequency as the incoming beam. The directions of the output beam are governed by the planes inside the crystals. The orientation and inter-planar spacing of these planes are defined by three integer h,k,l indices. If the path difference  $\Delta l$  is a multiple integer of the wavelength, the scattered X-ray beams of each lattice plane interfere constructively with each other. Bragg's law, or Bragg's equation, describes the relation between the interaction of the X-ray beam with the created secondary diffracted beams using the following Equation (3.1) [112-113]:

$$\Delta l = n\lambda = 2d\sin\theta \quad (3.1)$$

where  $n$  is an integer,  $\lambda$  is the wavelength of the X-ray in nm,  $d$  is the inter-planar spacing generating the diffraction in meter, and  $\theta$  is the diffraction angle in degree. Every material will diffract different X-ray patterns because of the different atomic structure characteristic. Therefore, an XRD pattern is like a fingerprint of the substance, thus determining the structural properties of the material.

The XRD analysis in this research were performed using Rigaku (D/MAX-2000) and Bruker (AXS D8 Advance) with monochromatic Cu K $\alpha$

radiation ( $\lambda = 0.154 \text{ nm}$ ) at room temperature. The standard setting for the Bruker XRD was 40 kV at an electron current of 40 mA while for Rigaku XRD was 40 kV at an electron current of 30 mA. All samples were measured in the range of  $10^\circ$  degree to  $60^\circ$  degree. Using data from XRD, crystal or grain size of a material can be calculated using Scherrer's Equation (3.2) [113]:

$$D = \frac{0.9 \lambda}{B \cos \theta} \quad (3.2)$$

where  $D$  is the grain size in meter,  $\lambda$  is the X-ray wavelength of  $1.54 \text{ \AA}$ ,  $B$  is the full-width at half maximum of the plane angle in radians, and  $\theta$  is the Bragg's angle in degrees.

### 3.5.5 Characterizations of Optical Properties

Ultraviolet-Visible-Near Infra Red (UV-Vis-NIR) Spectrophotometer (UV-Vis-NIR) is used to characterize optical properties of a material. Basic optical properties of the material, such as light transmittance, absorbance and reflectance, could be studied using the equipment. In the characterization process, the measurement data could be manipulated or used to define other properties of materials, including the porosity of the thin films, optical band-gap energy, structural disorder properties called Urbach energy, refractive indices and carrier concentration could be obtained from the UV-Vis-NIR spectrophotometer measurement [114].

In this thesis, the UV-Vis-NIR measurements were conducted using Varian Cary 5000 UV-Vis-NIR spectrophotometer. The instrument uses deuterium lamp as a UV light source while tungsten lamp is used as the source for visible and NIR light. Before the optical band-gap energy can be calculated, the absorption coefficient of the thin film must first be determined. The absorption coefficient

could be determined from the results obtained from the measurement of transmittance spectra using Lambert's law as shown in Equation (3.3) [115-116]:

$$\alpha = \frac{1}{t} \ln \left( \frac{1}{T} \right) \quad (3.3)$$

where  $\alpha$  is the absorption coefficient,  $t$  is the film thickness in meter and  $T$  is the transmittance of the film in percentage. The optical band-gap energy  $E_g$  is derived by assuming the direction of transit of the electron between the edges of the valence band and the conduction band, where the absorption coefficient varies with the photon energy from sunlight. The relationship between the direct band-gap energy, the absorption coefficient and photon energy is given by Equation (3.4) [116]:

$$\alpha h\nu = A(h\nu - E_g)^{\frac{1}{2}} \quad (3.4)$$

where  $A$  is constant and  $h\nu$  is the photon energy in electron volt (eV). The direct band-gap of CuI thin films is estimated by plotting  $(\alpha h\nu)^2$  versus  $h\nu$  and extrapolating the linear portion near the onset of absorption edge to the  $h\nu$  axis.

The structural energy, called Urbach energy, of the film can be determined using Equation (3.8) [117]:

$$\alpha = \alpha_0 \exp \left( \frac{h\nu}{E_0} \right) \quad (3.8)$$

where  $\alpha$  is the absorption coefficient,  $\alpha_0$  is a constant,  $h\nu$  is the photon energy in (eV) and  $E_0$  is the Urbach energy in (eV). Hence, the Urbach energy could be determined through the plot of  $\ln[\alpha(\lambda)]$  versus photon energy ( $h\nu$ ) where the value of the Urbach energy is equal with the reciprocal gradient of the linear portion of the plot.

### 3.5.6 Luminescence Properties

When energy of light is greater than the band gap energy of materials, the electrons from valence band will be excited to conduction band, releasing electrons and leaving holes behind. The electrons then will recombine through either radiatively or nonradiatively. Radiative recombination results in light emission; the phenomenon is called photoluminescence (PL) [118].

PL is the measure of radiative recombination when a sample is illuminated in order to excite excess carriers. As light generates excess carriers, their concentrations build up to values that depend on defects, impurities, and other recombination mechanisms in that region. PL measurement uses a light source such as Xenon (Xe) lamp and He-Cd laser to excite electron in the valence band of the materials. The light emitted through radiative recombination will be detected at the associated wavelength. The PL measurement produces results which could be used to study material defect, optical band gap, impurity levels, material quality and material luminescence properties. PL measurement also gives information of the transition energies of the electrons that are occupying the various states, thus the electronic energy level in the materials could be determined [119-121].

Photoluminescence spectrometer used to measure luminescence properties of CuI material in this research is Jobin Yvon Horiba FluoroMax-3. The measurement for CuI thin films were done at excitation wavelength of 325 nm and the emission spectra range from 350~800 nm was recorded.

### 3.5.7 Current-Voltage Measurement

Important electrical properties, such as resistivity, conductivity, and ohmic or Schottky behavior, can be characterized using two-probe system, and the current-voltage (I-V) measurement is conducted on the thin film as its electrical behavior of could be obtained from the measurement. It is essential to determine

the electrical properties of materials used in the fabrication electronic devices as it affects the performance of the device.

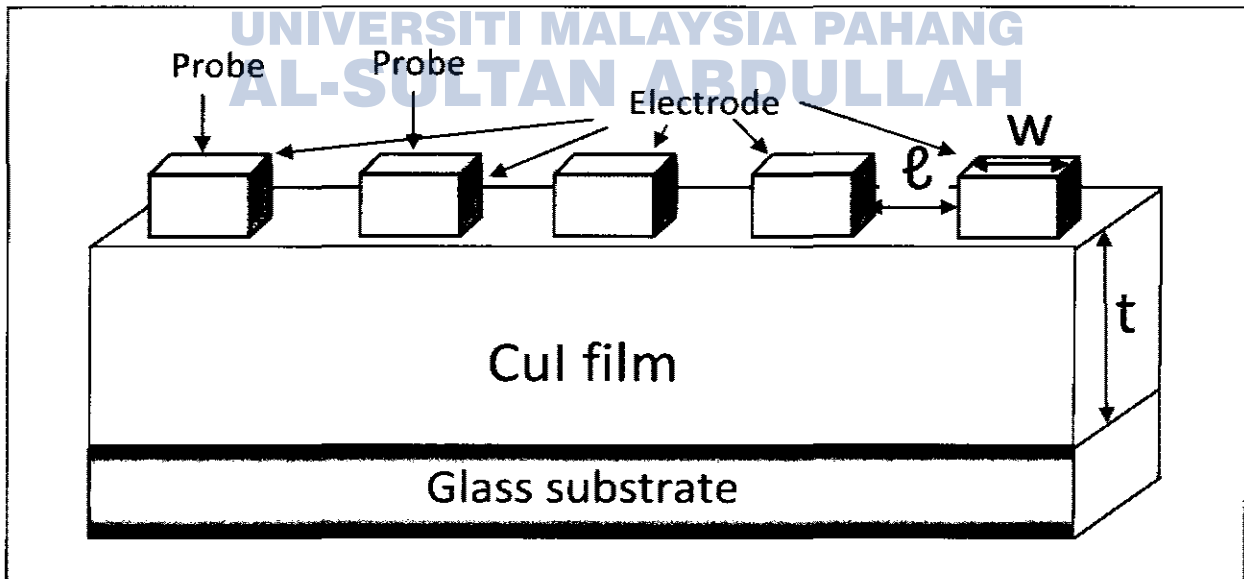
In this study, two electrical properties, namely, resistivity and conductivity, of the thin film were investigated, while photo-current and photo-voltage were measured. I-V measurement of the thin film using a two probe system is carried out as illustrated in Figure 3.5. The resistivity of the thin film,  $\rho$  can be calculated using Equation (3.11) [122]:

$$\rho = \left(\frac{V}{I}\right) \frac{wt}{l} \quad (3.11)$$

where  $V$  is supplied voltage in volt,  $I$  is measured current in ampere,  $t$  is the film's thickness in meter,  $w$  is the electrode width in meter and  $l$  is the length between electrodes in meter. Also, the conductivity  $\sigma$  ( $\text{S.m}^2$ ) can be determined using Equation (3.12) [122]:

$$\sigma = \frac{1}{\rho} \quad (3.12)$$

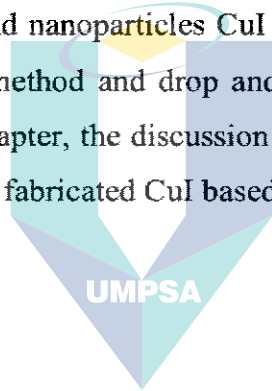
FIGURE 3.6  
Schematic Diagram for I-V Measurement of CuI Thin Films.



The photocurrent properties of CuI thin films were measured using two probe current-voltage (I-V) measurement system (solar simulator) under ultraviolet irradiation ( $\lambda = 365 \text{ nm}$ ,  $4 \text{ W}$ ). The photocurrent measurements were conducted to study the response of prepared CuI thin films or fabricated CuI based solid-state DSSC to UV light.

### 3.6 SUMMARY

In this chapter, the details of the preparation and characterization of CuI thin films and CuI based solid-state DSSC fabrication is given. The preparation parameters of nanoparticles CuI thin films and nanoparticles CuI thin films that incorporate TMED as chelating agent using sol-gel method and drop and spin coating deposition method are presented. At the end of the chapter, the discussion on the characterization techniques of the prepared CuI thin films and fabricated CuI based solid-state DSSC are given.



اونيورسيتي مليسيا قهغ السلطان عبد الله  
UNIVERSITI MALAYSIA PAHANG  
AL-SULTAN ABDULLAH

# CHAPTER FOUR

## CHARACTERIZATION OF NANOPARTICLES COPPER (I) IODIDE (CuI) THIN FILMS

### 4.1 INTRODUCTION

Copper (I) iodide (CuI), also known as cuprous iodide, has become a well-known material and versatile compound and, being inorganic type of semiconductor, is getting a lot of attention in many fields of materials research [123]. Also, its chemistry arrangement and combination with a lot of inorganic and organic ligands makes it possible to chemically adjust to produce other compounds, and making it suitable for applications in electronics and optoelectronics from the perspective of solid-state physics [124].

CuI is a solid that is insoluble in water and has three crystalline phases  $\alpha$ ,  $\beta$  and  $\gamma$ . In this research, the low temperature (below 350 °C) of  $\gamma$ -type CuI was chosen to be a precursor in every experiment conducted. The compound have a cubic structure making it possible to function as a p-type semiconductor with band-gap 3.1 eV which is below the visible spectrum and its conductivity is dependent on the presence of iodine in stoichiometric excess [125]. Furthermore, the  $\gamma$ -CuI semiconductor films are suitable in the fabrication of solar cells device where it is applicable in collecting and transporting holes [53, 126-127]. Moreover, it is also used in others devices, such as light and/or chemical sensor [128], optical display products [129], and in the preparation of conducting transparent films [130]. Their scope of applicability in optoelectronics can be further extended when organic dye molecules are coupled to them. From the perspective of chemistry and biochemistry, it can be applied in catalysis, in which CuI can be used as a catalyst for hydrophosphinylation and arylation [131], and it can also be applied in synthesis with CuI coordination chemistry, including the formation of both inorganic and biochemical supra-molecular compounds [132].

Researchers have fabricated CuI thin film using various techniques, which includes vacuum evaporation [126], radio frequency/direct current (rf-dc) magnetron

sputtering [130], pulsed laser deposition (PLD) [133-134], hybrid electrochemical/chemical synthesis [10, 135], and others [136-137]. However, there is still a need for alternative deposition technique that can reproduce and fabricate better quality films that are independent of the complex procedures, sophisticated equipment or rigid experimental conditions that are currently needed.

Acetonitrile solvent has been found to have good dissolving ability for CuI samples at room temperature, and this has been confirmed by infrared and Raman spectra investigations [138-139].

## **4.2 CHARACTERIZATION AT DIFFERENT MOLAR CONCENTRATION OF CuI SOLUTION**

The effects of molar concentration on CuI thin film properties were studied to understand the film behaviour at different molar concentrations, and the information can be used as guidelines for the fabrication of dye sensitized solar cell. The preparation of the CuI thin films at different molar concentration has been described in Chapter 3.

### **4.2.1 Conductivity and pH**

Conductivity and pH of an aqueous solution are two measurements often made on solution matrices. These are usually categorized as physical tests, though they are strongly dependent on the chemical characteristics of an aqueous solution. In general, pH is a measure of hydrogen ion concentration in water, where there is a one unit change in pH for every tenfold change in hydrogen ion concentration. Conductivity refers to the electrical conductivity of the solution, and it increases as more ions are dissolved in the solution; the ions originate not only from the hydrogen ions but also from other materials present in the solution [111].

Table 4.1 shows the measured pH and conductivity of CuI aqueous solution at different molarities. It shows that the increase in molarities of the CuI

solution, the pH value changed toward alkaline and its conductivity also increases further. Moreover, the conductivity of CuI is very dependent on the presence of iodine in stoichiometric excess [126]. When the molarities of CuI increases, it is assumed that it increases the level of iodine in the solution, hence resulting in higher conductivities.

**TABLE 4.1**  
**Conductivity and Acidity (Ph) Results of CuI Solution at Different Molar Concentration.**

Solution	pH	Conductivity ( $\mu\text{S}/\text{cm}$ )
1.0M CuI	7.79	1545
0.5M CuI	6.57	1413
0.1M CuI	6.49	1319
0.05M CuI	6.34	1310

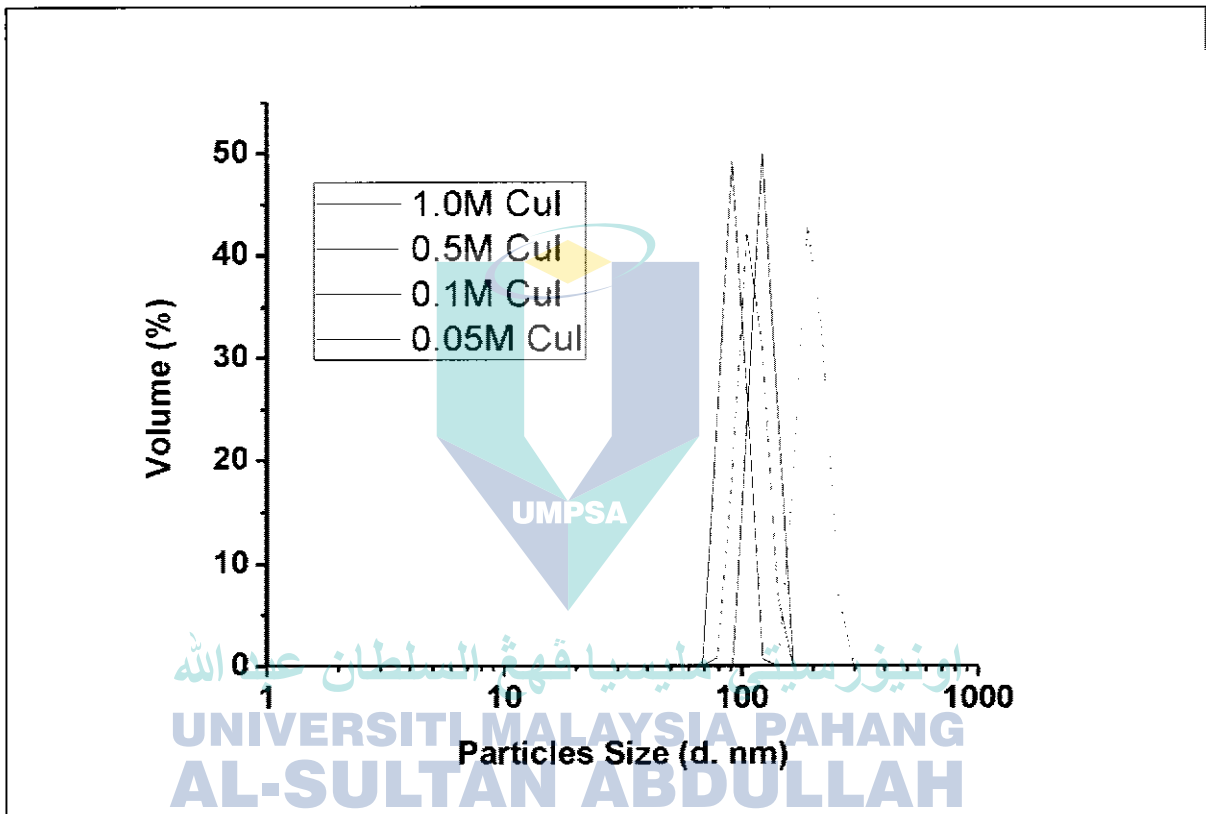
#### 4.2.2 Particles Size Measurement

The particles size distribution (PSD) within a volume of solution could be determined by measuring the size of the particles in the solution. The particle-size distribution of particles dispersed in a liquid is a list of values or a mathematical function that defines the relative amounts of particles present, sorted according to size [140]. The PSD of a material is essential in comprehending its physical and chemical properties as it affects the reactivity of solids involved in the chemical reactions.

Figure 4.1 shows the particles size measurements of CuI solution with different molarities, where it is noted that the size of CuI particles are almost the same for the different molarities, and the size ranges from 90 nm ~ 200 nm in 50% volume of the solution. If compare to the XRD result of CuI thin film as stated in section 4.1.3.2 which the size of particles are around 37.8 nm to 43.2 nm for 0.05M to 1.0 M respectively, the size by particle measurement could consider large. The reason for the large and almost similar particle sizes could be due to the

occurrence of agglomeration among the particles, and this signifies more loosely bound particles occurring during synthesis. Nanoparticles oftentimes accumulate as a result of high ionic strength of environmental and biological fluids, which shields the repulsion due to charges on the nanoparticles [141].

**FIGURE 4.1**  
**Particles Size of CuI Solution in Different Molar Concentration.**



Another reason is if the particles are not well distributed, or in other words it is well connected to each other, that will affect the measurement since the signal reflected from particles is coming from the overall objects. Hence, this will affect the size of the particles in form of solid state when it is deposited as a thin film. This size of particles can be considered as not sufficiently small in nanotechnology engineering, especially when related to making the solar cell devices.

### 4.2.3 Surface Morphology of CuI Thin Film

Images of CuI thin films deposited on glass and ITO substrate were taken using FESEM are shown in Figure 4.2. FESEM images show different density in film morphology among films deposited at different molarities. All the images were taken at 50K magnification. It could be understood that the CuI thin film become denser when higher molarities are used. Though the physical size of the particles of the displayed morphology looks different, the particles are actually of the same size since they were taken using different measuring equipments; the use of the equipments is dependent on the conductivity of the thin film. The quality of the captured images is dependent on how good the electron beam from the measuring equipment is transferred to the thin film. The captured images were taken using different electron flow: 5.0 KV is used for 1.0M and 0.5M, and 2.0 KV is used for 0.1M and 0.05M.

As observed from FESEM images, the average size of CuI grains is in order of micrometer ( $\mu\text{m}$ ) and exhibited a polymorphic characteristic with a wide distribution of the grain size. The CuI grains boundaries is hard to observe even at the maximum possible enlargement power of FESEM, probably due to the formation of ultrafine partials of CuI grains. FESEM images also indicate that the particles become more closed to each other when higher molarities are used. This connection is very important for a continuous transport pathway to develop in the granular film to facilitate movement of electrons or holes.

The chemical composition and the nature of CuI in the deposited thin films are characterised using energy dispersive x-ray (EDX) measurement and it is compared to a sample of a high purity CuI powder (99.99%). The measured EDX spectra of CuI thin films are shown in Figure 4.3. Partial areas of the CuI thin films surface were jointly investigated with SEM and EDX. From the EDX spectra of the backing material, large scattered particles of the radiated x-ray is intensified for copper (Cu) and iodine (I), indicating that these large particles are clusters of copper (I) iodide (CuI). The presence of Cu and I molecules on the

surface is confirmed from the spectrum resulting from the measurement, hence proving that the thin film is CuI compound. Other materials that appeared in the spectrum from the EDX are Tin (Sn) and Oxygen (O), and this is due to the fact that the thin film was deposited on Indium doped SnO (ITO) substrate with oxygen vacancies in the thin films.

**FIGURE 4.2**  
**FESEM Images of CuI Thin Film at Different Molar Concentration (a) 1.0M CuI, (b) 0.5M CuI, (c) 0.1M CuI and (d) 0.05M CuI.**

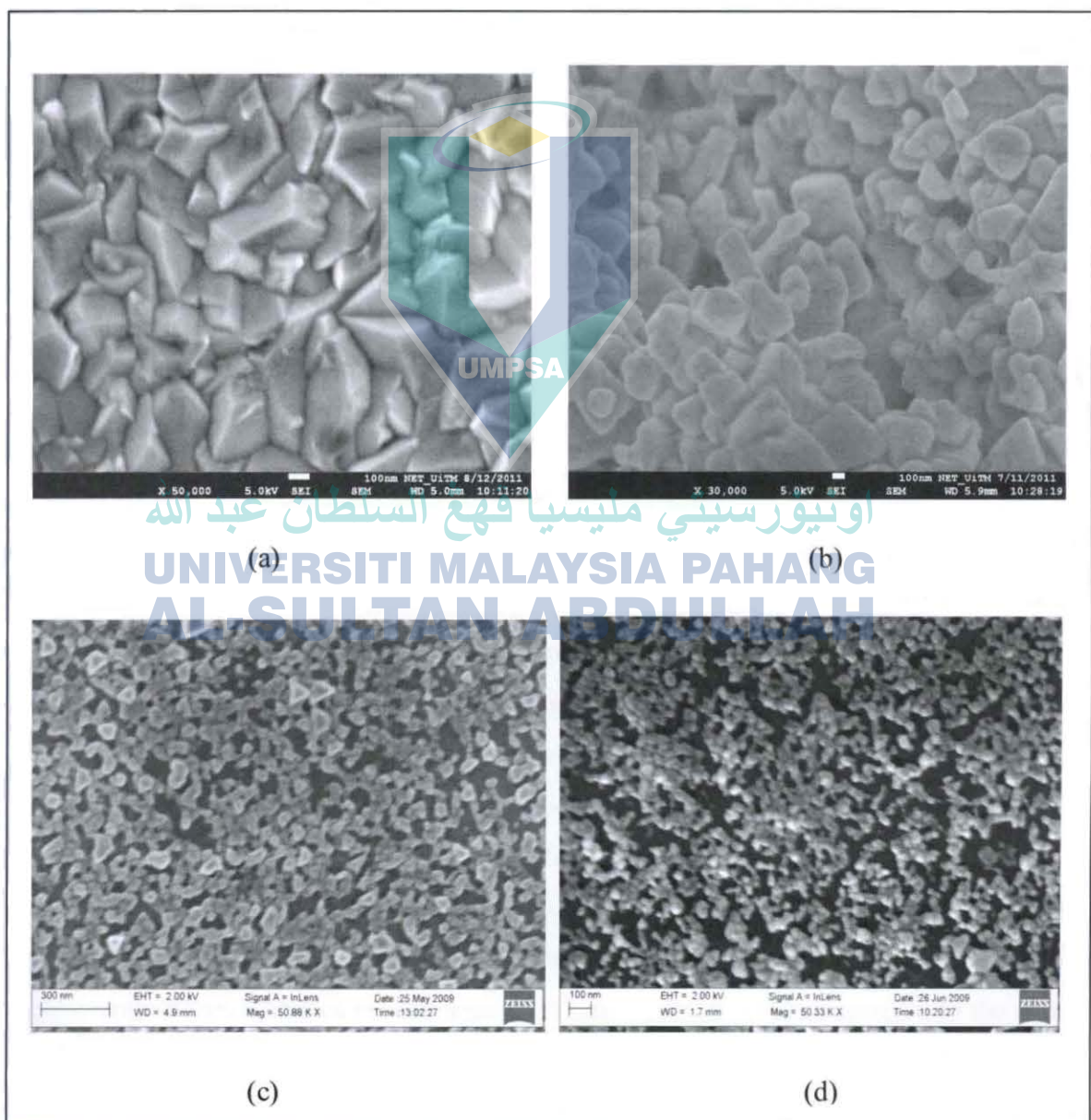
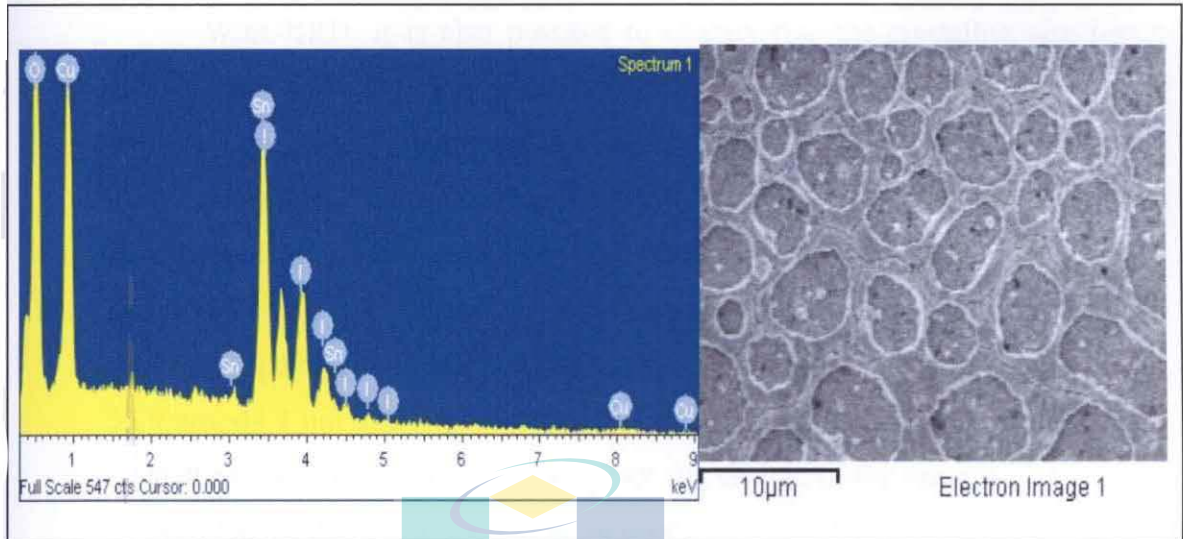


**FIGURE 4.3**  
**EDX Analysis of CuI Thin Film.**



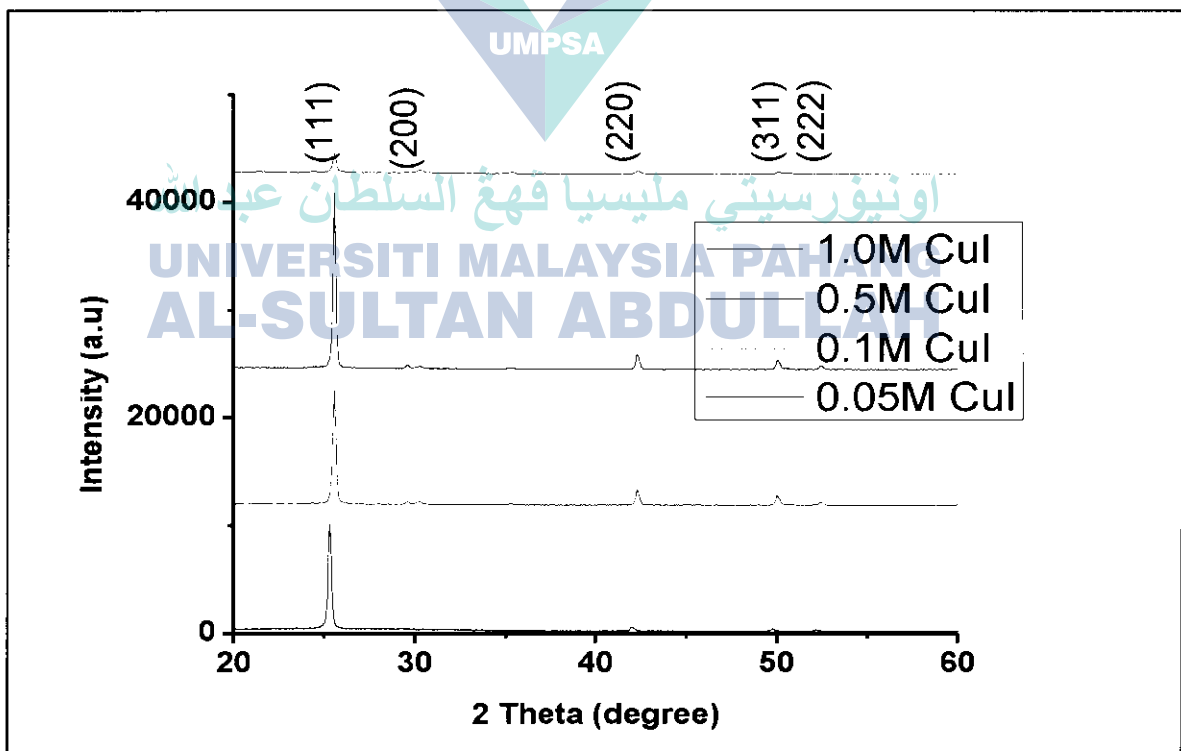
#### 4.2.4 XRD Spectra

In order to study the structural properties of the deposited thin films, the films can be characterized using XRD. Figure 4.4 represent the XRD spectra of CuI thin films with different concentrations prepared using drop and spin coating technique. The XRD spectrum of the as-deposited films as shown in Figure 4.4 exhibits a broad peak in  $2\theta$  range of  $20^\circ\text{C} \sim 60^\circ\text{C}$ . It is noted that all the samples with the different solution concentrations peaks at the point that corresponds to that of the standard CuI (according to JCPDS data 25-390). The observed characteristic peaks at preferred orientation in the X-ray diffractograms indicate that the composed thin films are polycrystalline CuI  $\gamma$ -phase. The spectrum obviously indicate five peaks at preferred orientation of  $25.52^\circ$ ,  $29.55^\circ$ ,  $42.25^\circ$ ,  $49.99^\circ$ , and  $52.37^\circ$  corresponding to the (111), (200), (220), (311) and (222) reflections of the CuI nanocrystals. The thin film prepared using 0.5M concentration shows the strongest diffraction peak at (111) compared to the films prepared using other concentrations indicating that the film is strongly a cubic crystal in structure. Increasing the concentration of the solution up to 1.0M,

however, led to a decrease of (111) and other (200), (220), (311) and (222) orientation growth in the thin film.

With XRD, it is also possible to characterize the crystallite size (grain size) of the materials. The grain size of CuI thin film were estimated using Scherer's equation as mentioned in Chapter 3 [113]. Analyzing the spectra of the samples obtained from the measurements, the full width at half maximum (FWHM) of the samples is  $0.197^\circ$  for 1.0M ,  $0.152^\circ$  for 0.5M,  $0.193^\circ$  for 0.1M, and  $0.265^\circ$  for 0.05M. Using Scherer's equation, the evaluated grain size for the thin film deposited with 1.0M, 0.5M, 0.1M and 0.05M concentrations are 43.2 nm, 55.9 nm, 44.2 nm and 37.8 nm, respectively. Hence, the results indicate that the crystalline size of CuI thin films vary but the change in the particle size is quite independent of the molar concentration used.

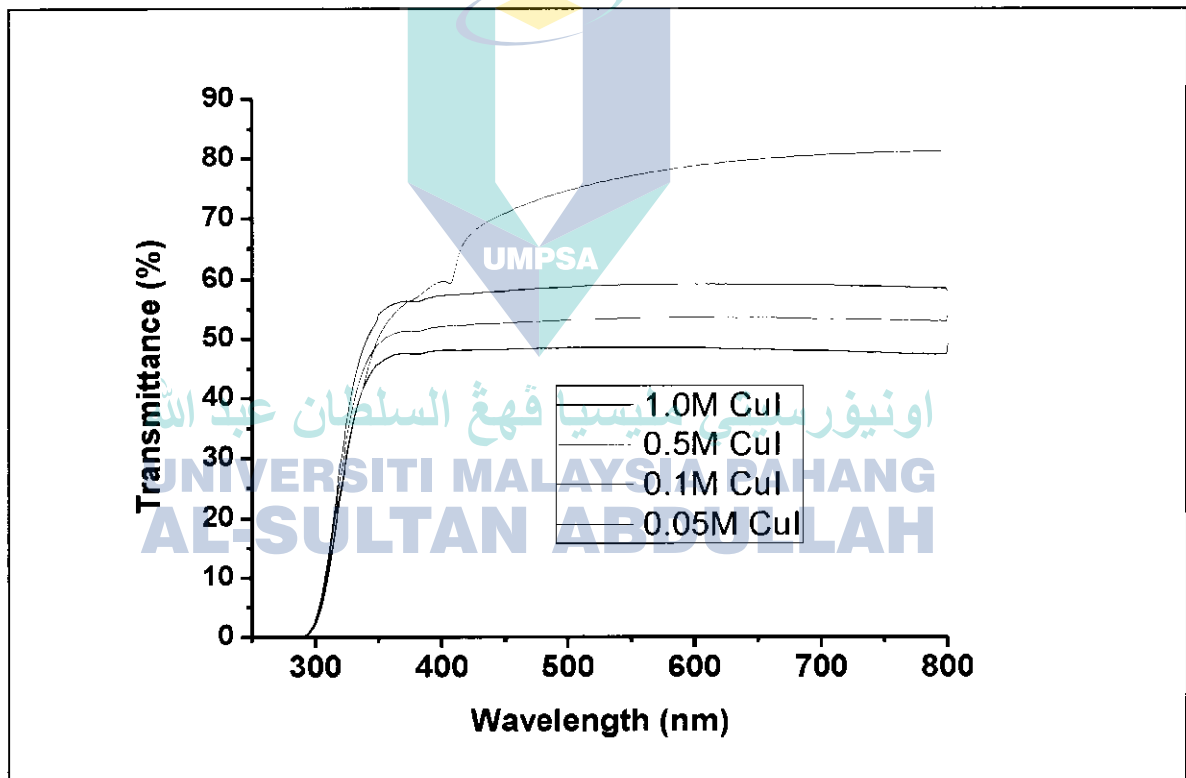
FIGURE 4.4  
XRD Spectra of CuI Thin Film at Different Molar Concentrations.



#### 4.2.5 UV-Vis-NIR Spectra

Figure 4.5 shows the optical transmittance spectra of CuI thin films with the different molar concentrations, whose wavelengths range from 300 nm ~ 900 nm. The results revealed that the concentration of the CuI solution affects the optical properties of the thin films; the highest transmittance is obtained in samples deposited using 0.05M solution, while the lowest transmittance is observed in thin films deposited using 1.0M solution.

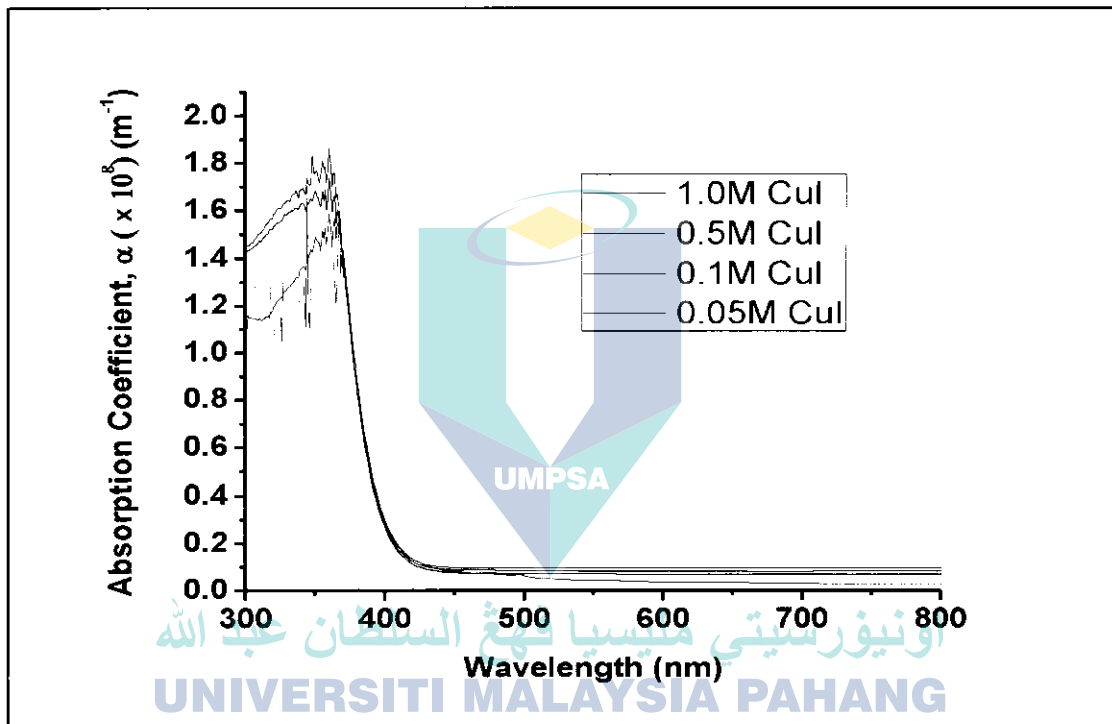
FIGURE 4.5  
Optical Transmittance of CuI Thin Films at Different Molar Concentrations.



The fact that the CuI thin film with 0.05M showed the highest optical transmittance could be understood when looking at the FESEM results as shown in Figure 4.2. The results also exhibited that the transmittance of the films are in the range of 49% to 81%, depending on the concentration of the solution used.

The onset hump in the optical spectra occurred in the range of 400 to 440 nm which corresponds to the band-gap excitation. In this research, the transmittance of the film increases with increasing molar concentration of the solution as the structure of the thin films becomes denser with higher solution concentration.

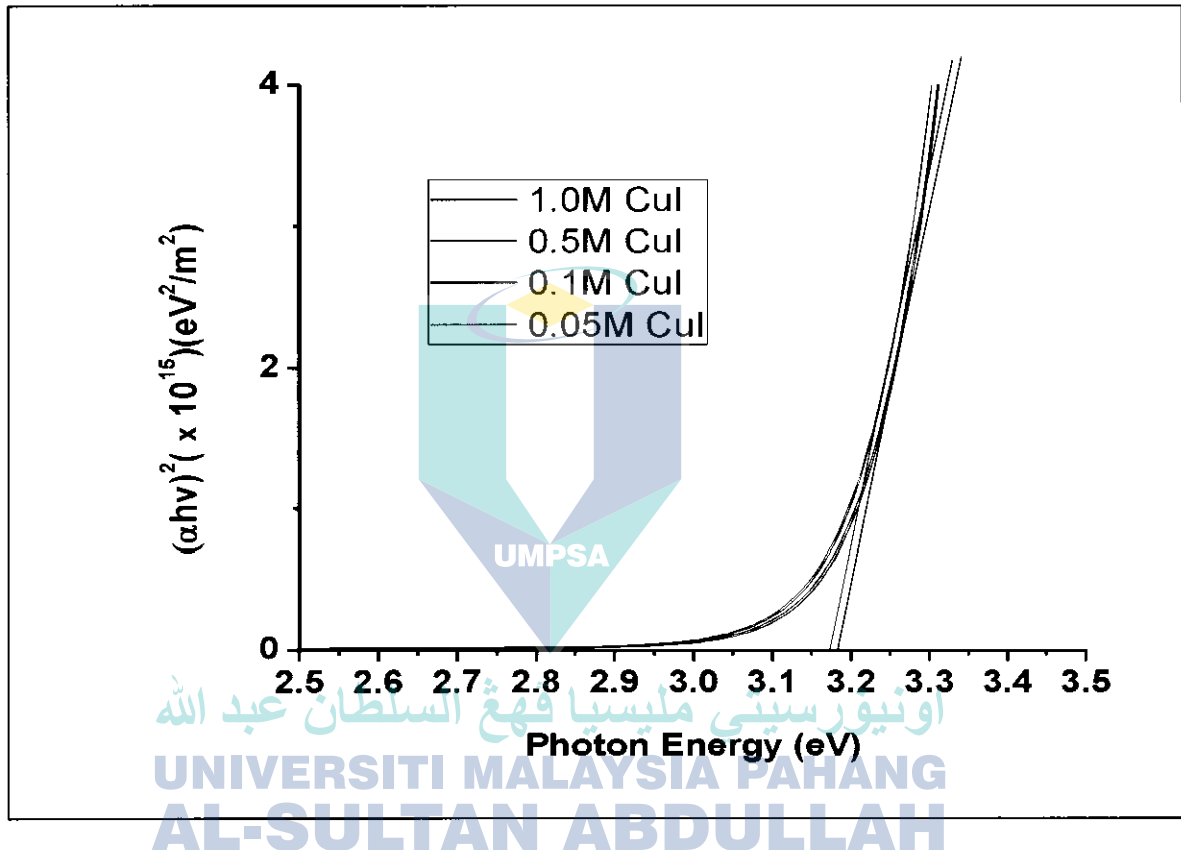
**FIGURE 4.6**  
Absorption Coefficient of CuI Thin Films Prepared With Different Molar Concentration.



The ultra violet (UV) absorption coefficient spectra of CuI thin films prepared by drop and spin coating technique at different molar concentrations are presented in Figure 4.6. Looking at the spectra as shown in the figure, it can be inferred that CuI crystals have sufficient transmission in the entire visible region. It is observed that the onset of the absorption coefficient hump is at 429 nm for 1.0M molar concentration, 430 nm for 0.5M, 432 nm for 0.1M, and 433 nm for 0.05M. Furthermore, the observed hump could be due to the electrons from the sub-bands in the valence band being excited to the conduction band. Hence, the increase and decrease of the absorption coefficient might be due to the effect of

the increase and decrease of the CuI particle size or CuI species with the different molar concentrations.

**FIGURE 4.7**  
**Optical Band-Gap Energy Estimation of CuI Thin Film at Different Molar Concentrations Using Tauc's Plot.**



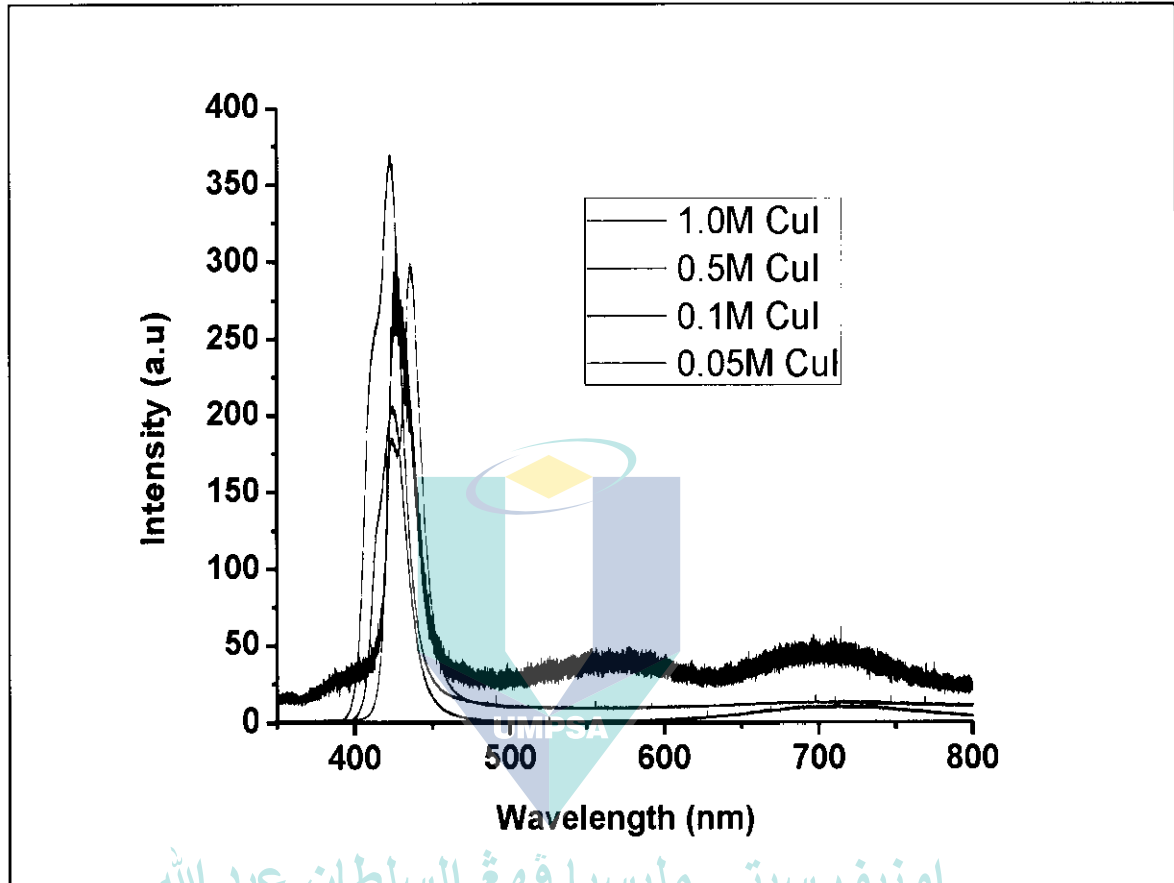
The values of the optical band-gap for the CuI thin films shown in Figure 4.7 were obtained from the transmission measurement by plotting  $(\alpha h\nu)^2$  versus photon energy  $h\nu$ , where  $\alpha$  is the absorption coefficient and  $h\nu$  is the photonic energy as mentioned in Section 3.5.4.1. The evaluated band-gap energies for the different molar concentrations are 3.17 eV for 1.0M and 0.5M CuI concentration, and 3.18 eV for 0.1M and 0.05M CuI concentration, respectively. These values can be considered near, or slightly higher than, the 3.1 eV for polycrystalline  $\gamma$ -phase CuI band-gap value as reported by other researchers [126]. The electron transition is observed to contain higher energy than the band-gap, and this is due

to the splitting of spin-orbital of the upper most valence band ( $\Delta_0 = 50$  meV) and sub-energy levels in the conduction band ( $\Delta_1 = 700$  meV) [142]. Another reason that shifts the band-gap energy to a higher energy could be due to the surface roughness of the films and the wider distribution of the grain formation [143].

#### 4.2.6 Photoluminescence (PL) Spectra

Photoluminescence (PL) spectra of CuI thin films on glass substrate deposited using drop and spin coating technique are shown in Figure 4.8. The spectra shows that all CuI thin films exhibited UV emission originated from the recombination of photon-generated charge carriers from the conduction band into the valence band. As shown in the figure, CuI thin films that are prepared at different molar concentrations exhibited peaks at almost the same wavelength except that of the 0.5M solution which is slightly shifted to the right. The CuI thin films exhibited main emission peaks at 424 nm for 1.0M solution, 436 nm for 0.5M, 422 nm for 0.1M and 423 nm for 0.05M. In each case, the peaking of the main emission is due to the recombination of electrons and holes at  $\text{Cu}^{1+}$  centres. The reasons for the observed shift of emission toward the longer wavelengths are repulsion of ions and quenching of excited luminescence centres [133-134]. This is inferred since the same phenomena was also observed by other researchers who had conducted photoluminescence experiments of materials doped with  $\text{Cu}^{1+}$  and  $\text{Cu}^{2+}$  ions. For example, photoluminescence study on zinc sulphide (ZnS) by Yang et al. had observed two luminescent centres at 450 and 530 nm [144], while Zeolites doped with  $\text{Cu}^{1+}$  ion exhibited luminescent centres at 500 and 540 nm respectively [145]. Emission band due to  $\text{Cu}^{1+}$  ions are associated to electron transition  $3d^{10} \rightarrow 3d^9 4s^1$  [146] resulting in shorter wavelength compared to that of  $\text{Cu}^{2+}$  ions where absorption of  $\text{Cu}^{2+}$  ions is in red region and is associated electron transition in  $3d^9 \rightarrow 4p$  [147].

**FIGURE 4.8**  
**Photoluminescence (PL) Spectra of CuI Thin Film at Different Molar Concentrations**  
**(Excitation Wavelength at 325 Nm).**

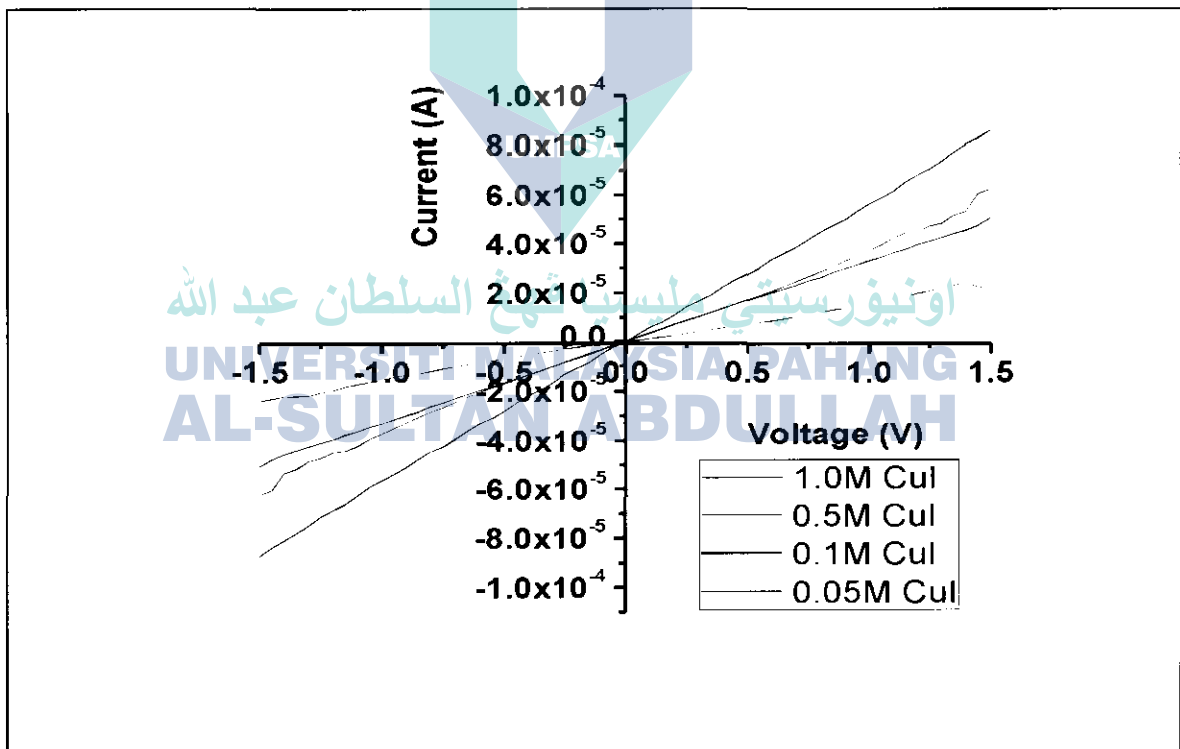


#### 4.2.7 Electrical Properties of CuI Thin Films

The electrical conductivity of CuI thin films was determined by investigating its behaviour between metal and semiconductor junctions (M-S). The Current-Voltage (I-V) of CuI thin films prepared with different molar concentrations has been measured and is as shown in Figure 4.9. It is observed that, using Indium (In) as metal contacts, all the thin films exhibited ohmic behaviour with linear I-V curve. This result revealed the theory of M-S junction, where not all metal-semiconductor junctions will form a rectifying curve [148-149]. To those metal-semiconductor junction that does not rectify current is called an ohmic contact [148-149]. Rectifying properties depend on the metal's work

function, the band gap of the intrinsic semiconductor and the type and concentration of dopants in the semiconductor. If the work function of metal is greater than band gap of semiconductor material and the concentration of semiconductor used is more dopant (especially p-type), a linear ohmic contact will occur [148-149]. In this research, the work function of indium is reported at 4.12 eV [150] while the band gap of CuI is around 3.1 eV. Furthermore, CuI is known as p-type semiconductor and has been used as p-dopant in others research for the study of metal-semiconductor behaviour [151]. Thus, linear I-V curve result that shows in Figure 4.9 could consider good metal-semiconductor junction properties that allow electrons to flow in both directions easily.

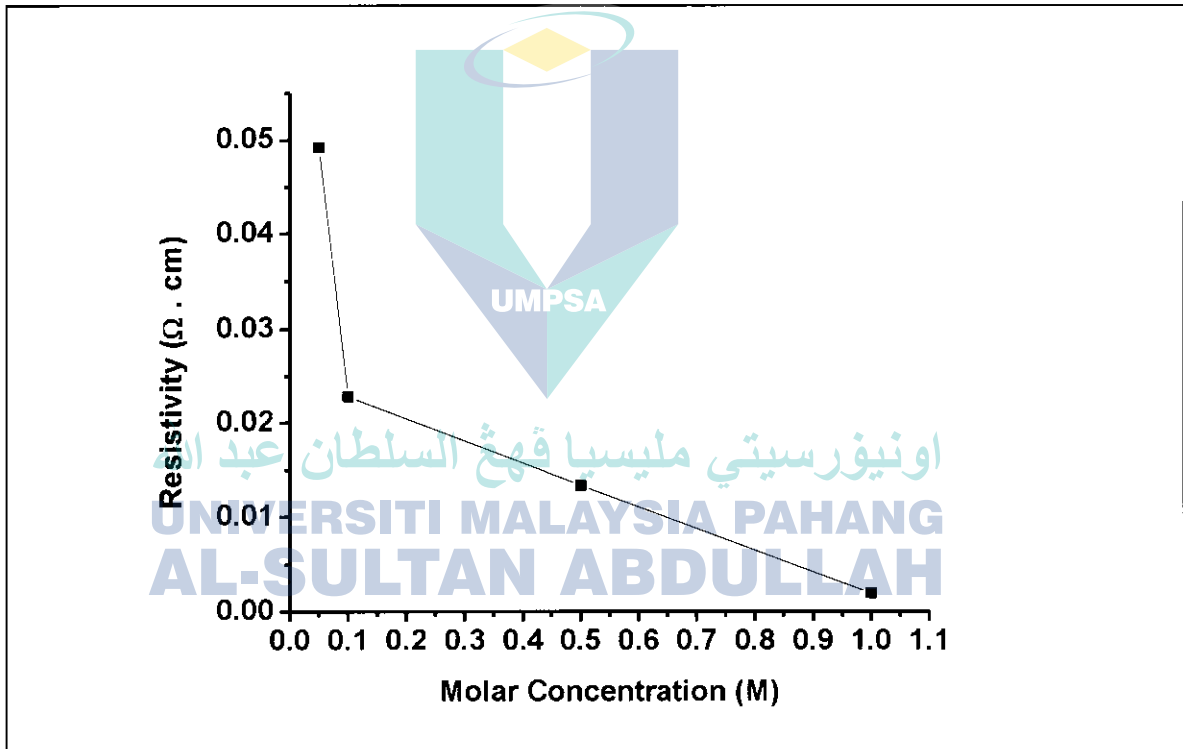
**FIGURE 4.9**  
**Current-Voltage (I-V) Measurement of CuI Thin Film at Different Molar Concentrations.**



Theoretically, in solid state dye sensitized solar cells (SSDSSC), CuI is used as the hole transport layer replacing the redox couple electrolyte for the regeneration of dye. The CuI is in contact with counter electrode where the

electron flows from the counter electrode to CuI. Therefore, the junction between the metal and semiconductor must not having a rectifying curve to avoid barrier between the two junction and thus easy for movement of electron from back electrode to CuI [151]. It also has been found that the values of current at a particular voltage increased linearly with increasing of molar concentration, and this is due to the increase in the electron concentration at higher molar concentration.

**FIGURE 4.10**  
**Resistivity of CuI Thin Film at Different Molar Concentrations.**



The relationship between the resistivity and conductivity of CuI thin films to the different molar concentrations are shown in Figure 4.10. The results show that the resistivity of CuI thin films decreases with the increase in the molar concentration of the solution used in the preparation of the thin film. This is attributed by the increase in the CuI particles with higher molar concentration,

contributing to the higher carrier concentration in the thin films and hence providing smooth connection among the particles. Higher molar concentrations also lead to increased particle size in the thin film which increases the surface contact between particles and improves the packing density in the thin films, as previously discussed related to the results of XRD. This situation will affect the reduction of oxygen adsorption in grain boundaries, thus reducing carrier trapping, thus lowering the resistivity of the thin films.

Trapping of carrier concentration in the thin films could become electrically charged and pose a potential barrier to the CuI particles, preventing a smooth movement of the carrier within the thin films, and thus decreasing the carrier mobility of CuI thin films. However, improvement in the surface contact among particles as a result of the increase in the particle size with increased molar concentration produces better carrier mobility in the thin films, and hence reducing its resistivity.

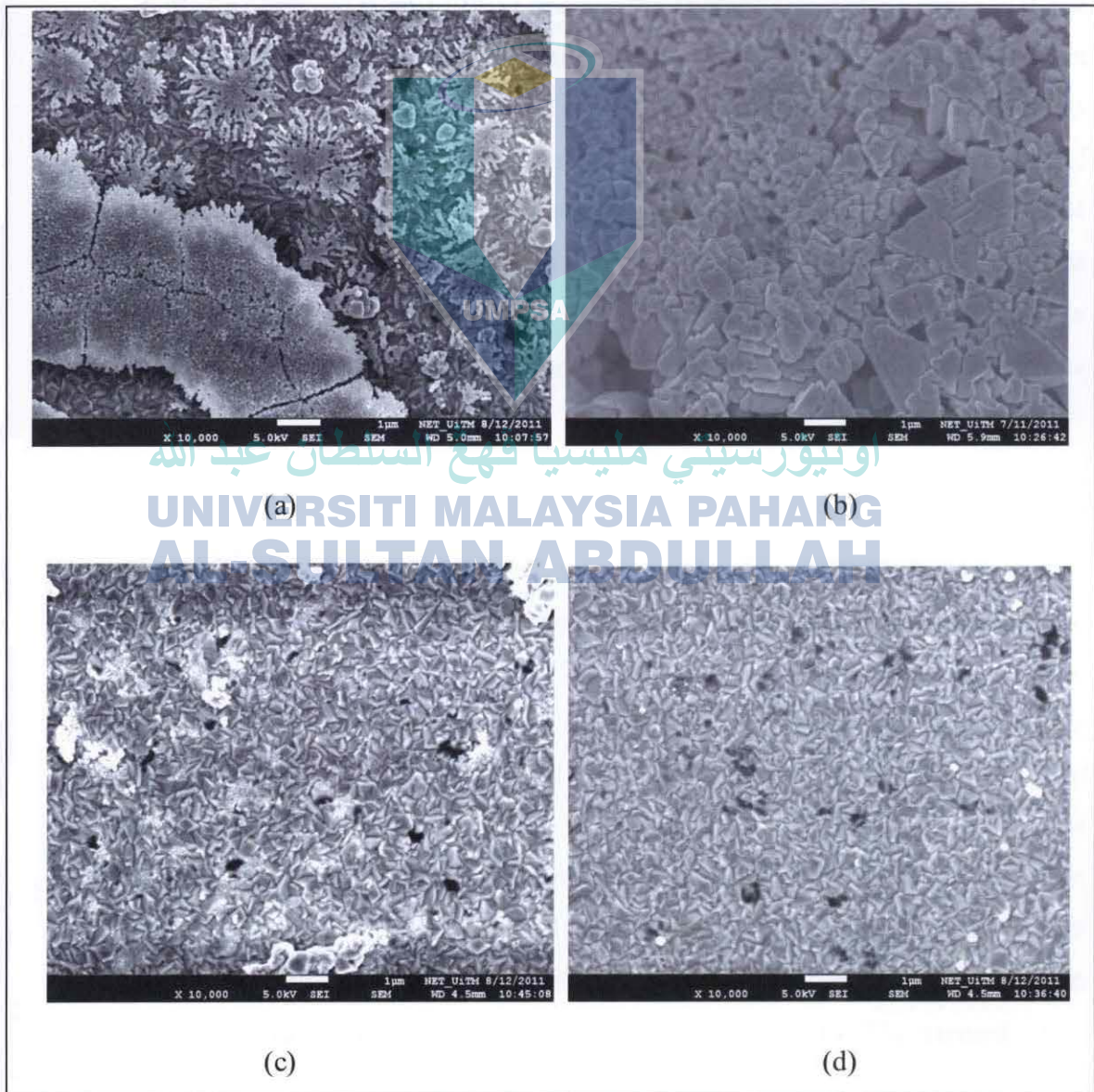
#### **4.3 EFFECT OF ANNEALING TEMPERATURE ON CuI THIN FILMS**

Annealing temperature is one of the factors that could affect the properties of CuI thin film. The process of annealing could be defined as the process of applying energy to a material in order to alter the properties of the material's internal structure. During the annealing process, diffusion of electrons occurs so that the materials progressed into equilibrium state. In this section, a study is conducted on the properties of CuI thin films that are prepared at different annealing temperatures. The aim of the study is to determine the optimum annealing temperature which will yield CuI films having high efficiency and performance that is suitable for applications in various electronic devices. In this study, the preparation and characterizations process of the CuI thin films have been prepared as described in Chapter 3 but using different annealing temperatures.

### 4.3.1 Surface Morphology of Annealed Thin Films

FESEM images of CuI thin films deposited on ITO substrate at as deposited, 50°C, 80°C and 110°C are shown in Figure 4.11. A study of the effect of temperature on CuI thin films were conducted using films that have been prepared using the solution with 1.0M concentration.

**FIGURE 4.11**  
**FESEM Images of 1.0M CuI Thin Films at Different Annealed Temperatures (a) As Deposited, (b) 50°C, (c) 80°C, and (d) 110°C.**



The 1.0M concentration was chosen based on the results of the characterization of copper (I) iodide (CuI) thin film as discussed in the previous section. Physically, the images of the thin films that have been subjected to the different annealing temperature are similar. Also, the surface density of the thin films is similar, and the samples are crystalline in nature.

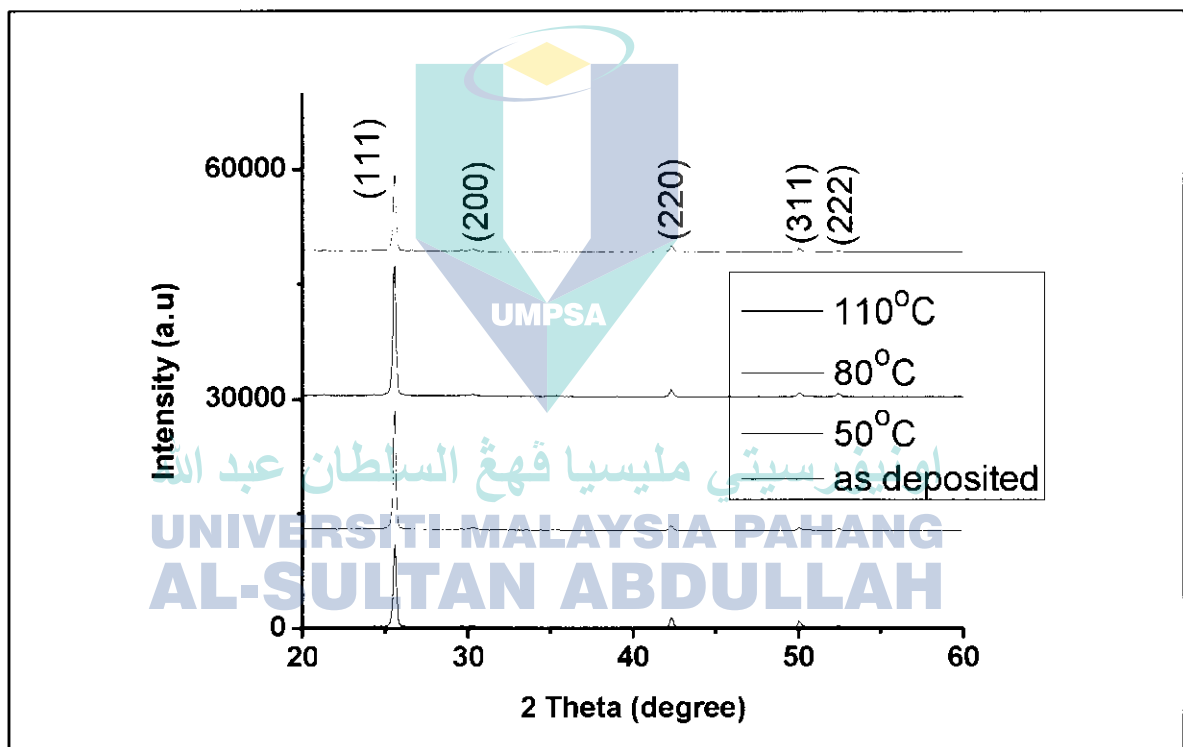
Generally, in wet chemical synthesis process, the primary particles that nucleated from solutions are known to grow by molecular addition or aggregation with small sub-units. The types of solvents can also affect the particle growth after nucleation because the particle interaction potential is different in each solvent. As observed from FESEM images, the average size of CuI grains is in the order of micrometer ( $\mu\text{m}$ ), and the grain also exhibited a polymorphic characteristic with a wide distribution of the grain size. The CuI grains boundaries are hard to observe even at the maximum possible enlargement of FESEM, and this could be due to the formation of ultrafine partials of CuI grains. FESEM images also indicate that the particles are more connected to each other when subjected to annealing temperature. This is very important in developing a continuous transport pathway in the granular film for the movement of electrons or holes.

#### 4.3.2 XRD Spectra

The XRD spectra for CuI thin films that have been annealed at different temperatures are shown in Figure 4.12. The structural properties of the annealed thin film were conducted again using the films that have been prepared using the 1.0M solution, and it is observed that all the CuI thin films exhibited polycrystalline of  $\gamma$ -phase structure belonging to the CuI cubic crystal type (JCPDS data 25-390). The spectra revealed that the grains of all the annealed thin films grow in the direction of their (111) axis. The growth of the film grains arises because of the formation of a commensurate hexagonal atomic lattice of iodine on Cu (111) and ordered lattice which lead to the formation of (111) oriented  $\gamma$ -CuI

nuclei, and is consistent with the findings of other researchers [152]. While the as deposited thin film sample shows a weak intensity indicating poor crystalline structure and could be due to a mix of the film with the amorphous structure, the annealing process improved the CuI crystalline structure as sharp peak and high intensity were observed for all samples. The growth tendency along (111) axis is an important factor in CuI based dye sensitized solar cell application as holes conductor.

**FIGURE 4.12**  
XRD Spectra of 1.0M CuI Thin Films at Different Annealing Temperatures.



The full width at half maximum (FWHM) value of the as deposited thin films and the films annealed at 50°C, 80°C and 110°C are 0.197°, 0.239°, 0.227° and 0.336°, respectively. The calculated crystalline sizes from Scherer's equation for samples at as deposited, 50°C, 80°C and 110°C are 43.2 nm, 35.6 nm, 37.5 nm and 25.3 nm, respectively. The improvement in the crystalline structure of CuI thin films is shown by the increase in FWHM and the decrease in crystal size

value with increasing annealing temperature. Through XRD analysis, that the samples annealed at higher temperature produced much better peak intensity, and simultaneously increased the FWHM and decreased the crystal size indicating that the crystallinity of CuI thin films is improved by sintering. It was also understood that the grain size calculated from Scherer's equation is quite different when visually compared to the images obtained from FESEM (value not shown) as in Figure 4.12. K. Prabakar et al. has reported that the difference between the size measurement obtained using XRD to that obtained using microscope (SEM, TEM, etc) is due to the difference in the measuring method used in the instruments. The grain size image captured by SEM or TEM is measured according to the distance between the visible grain boundaries, while the XRD used more stringent criteria where the grain size is determined by the extend of crystalline regions that diffract the X-ray coherently which give smaller grain size than microscope [153].

#### 4.3.3 UV-Vis-NIR Spectra

Figure 4.13 shows the optical transmittance spectra of the CuI thin films annealed at different temperatures, and note that the wavelength of the transmittance is ranged between 300 nm to 900 nm. All the thin films are found to be transparent (< 60%) in the visible and near infra-red (NIR) range with a sharp absorption edge at wavelength of about 420 nm, which is close to the intrinsic band-gap energy of CuI. The spectra show the optical transmittance of CuI thin films in the visible region (400 nm – 1500 nm) has tendency to increase with increasing annealing temperatures. The highest recorded transmittance is 53% for the thin film sample annealed at 80°C, while the lowest transmittance of 33% obtained for sample annealed at 110°C over the same wavelength.

Figure 4.14 shows the absorption coefficient of CuI thin films with different annealing temperatures as a function of the wavelength. The absorption coefficient was calculated using the measured transmittance data using UV-Vis-NIR spectrophotometer. The value of the absorption coefficient at the

corresponding wavelength is obtained by applying Lambert's law as mentioned in Chapter 3. The result indicates that all the thin film exhibit low absorption in the visible and near infra-red (NIR) range but exhibit high absorption in the ultra-violet (UV) range. The behaviour suggested that the transparency properties of CuI thin films in the visible region are beneficial for solar cell devices application.

**FIGURE 4.13**  
Optical Transmittance of 1.0M CuI Thin Films at Different Annealing Temperatures.

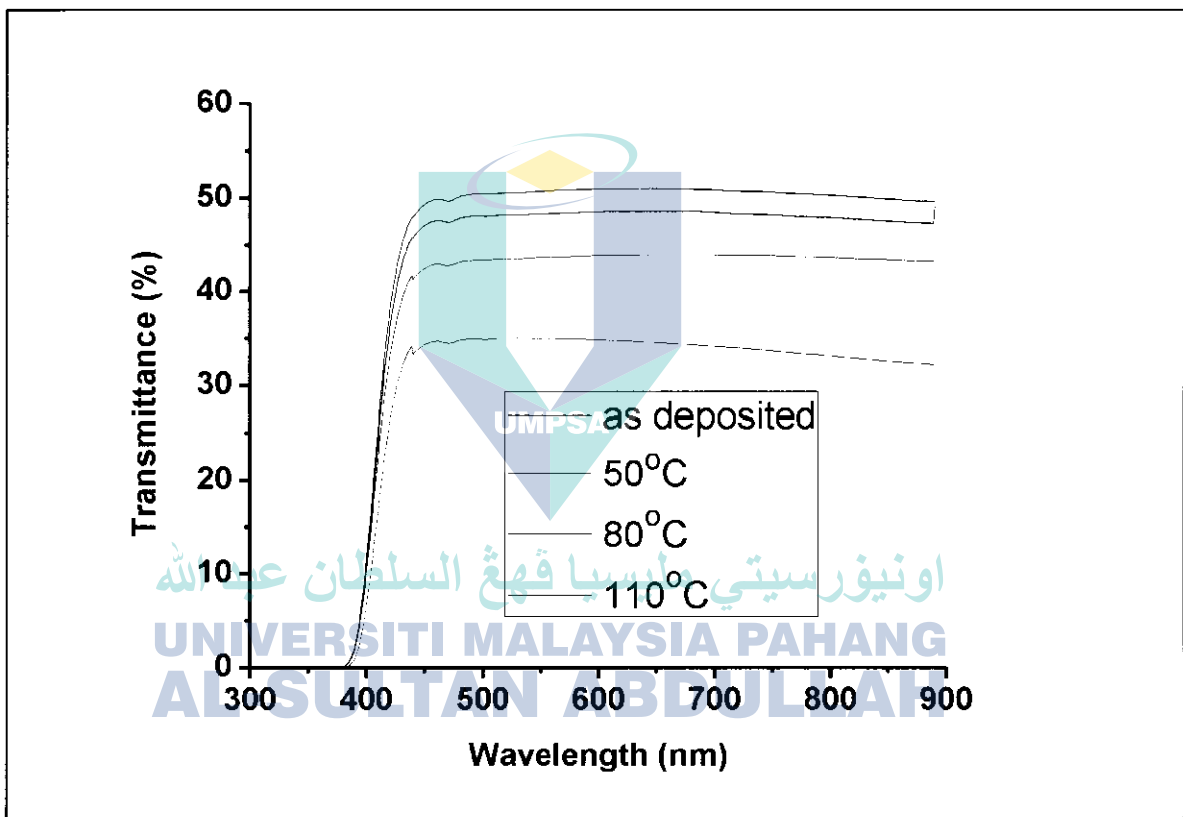
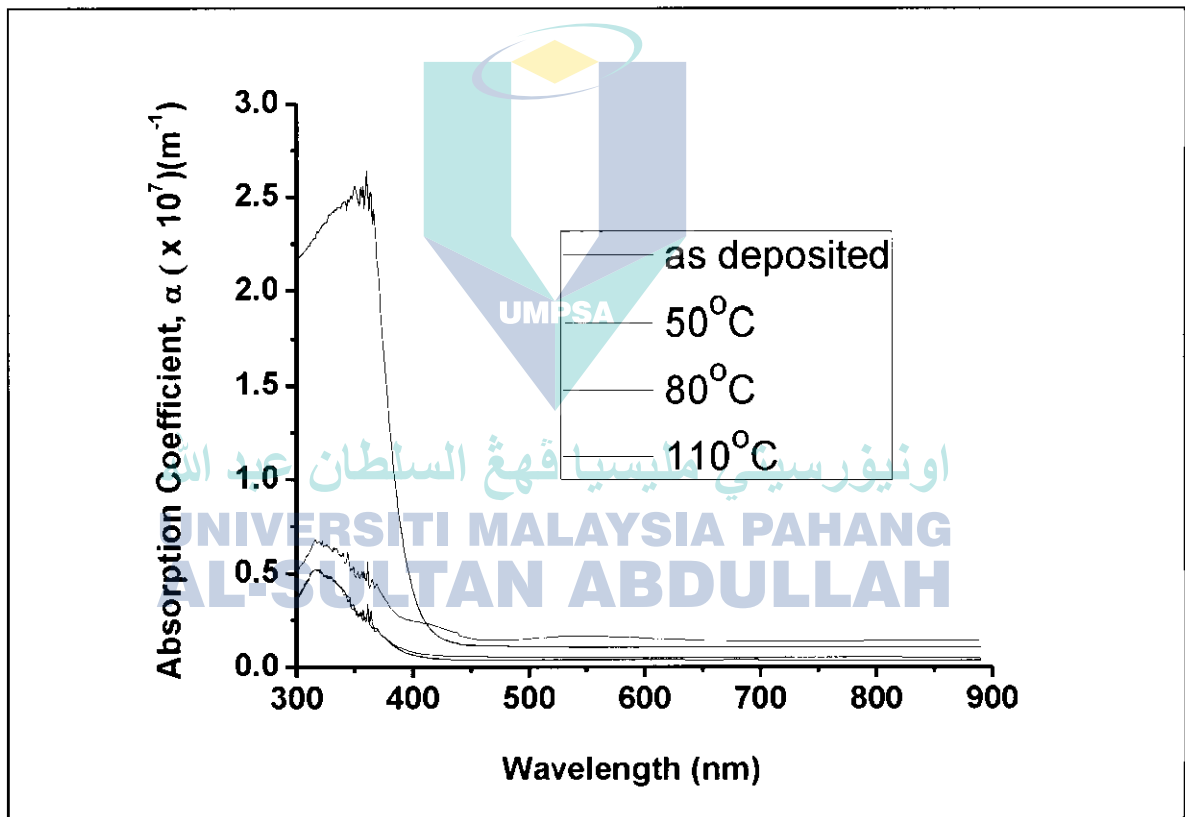


Figure 4.15 shows the optical band-gap estimation of CuI thin films at different annealing temperature using Tauc's plot. The graph was plotted using the equation mentioned in Chapter 3. The optical band-gap calculated from the graph shows a slight shift towards the higher energy with increasing annealing temperature. For the different annealing temperatures, the direct band-gap energies of the films was evaluated at 3.08 eV for 50°C, 3.17 eV for 80°C and

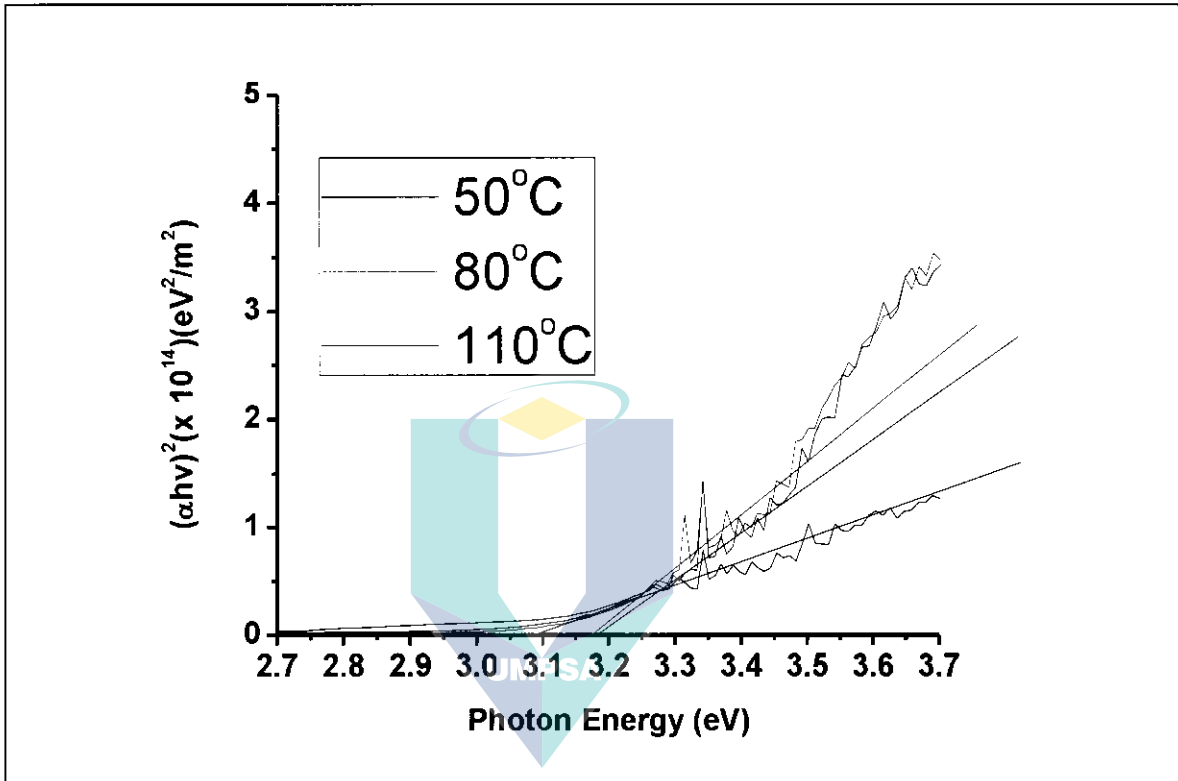
3.19 eV for 110°C. These values can be considered close or slightly higher than the band-gap value reported by other researchers, which is 3.1 eV for polycrystalline  $\gamma$ -phase CuI [126], and this shows that CuI thin film absorbs light efficiently in spite of the different annealing temperatures. The reason the observed electron transition is observed at higher energies than the band-gap is because the splitting of spin-orbital occur at the upper most valence band ( $\Delta_0 = 50$  meV) and sub-energy levels in the conduction band ( $\Delta_1 = 700$  meV) [142].

**FIGURE 4.14**  
Absorption Coefficient of 1.0M CuI Thin Films at Different Annealed Temperatures.



Another reason that makes band-gap energy shifted to the higher energies could be due to the roughness of the surface of films and the formation of grains with a wide distribution [143].

**FIGURE 4.15**  
**Optical Band-Gap Energy Estimation of 1.0M CuI Thin Films at Different Annealing Temperatures**  
**Using Tauc's Plot.**



اونيورسيتي مليسيا قهغ السلطان عبد الله

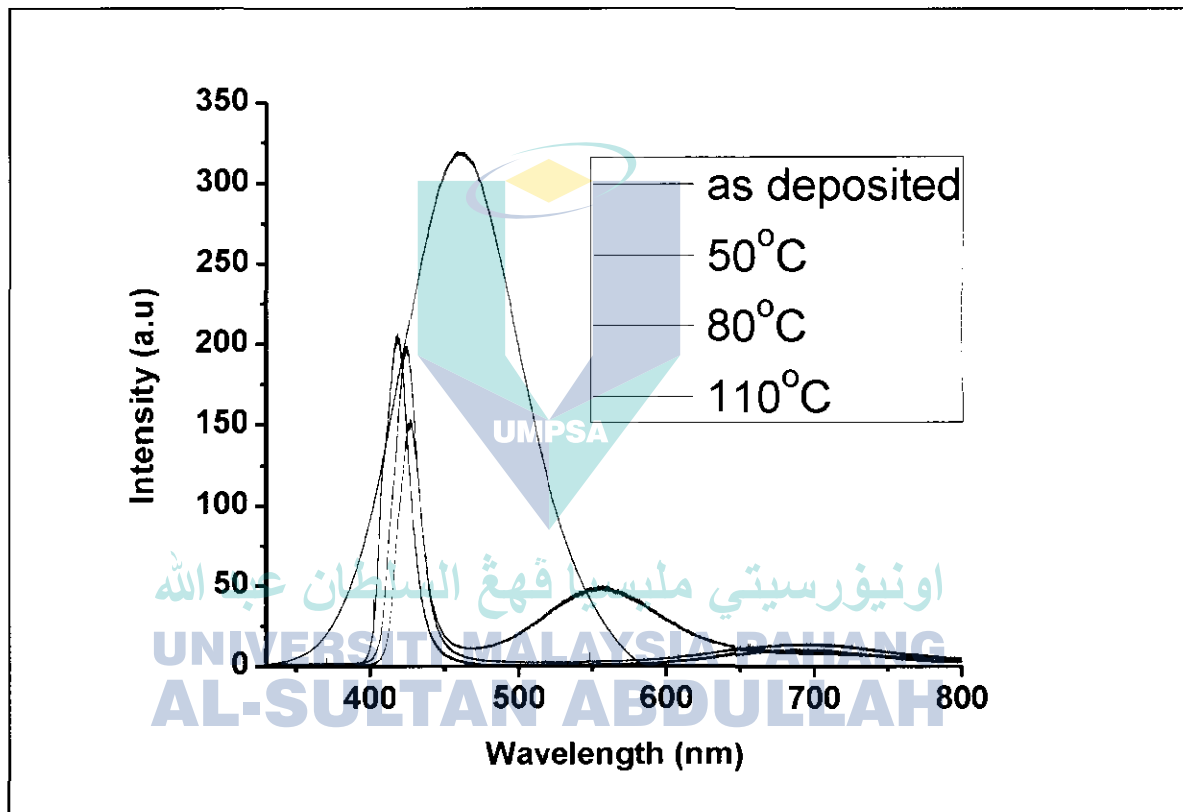
#### 4.3.4 Photoluminescence (PL) Spectra

Photoluminescence (PL) spectra of CuI thin films on glass substrate deposited using drop and spin coating technique are shown in Figure 4.16. The measurement was conducted at room temperature in the range of 330 nm to 800 nm using Xenon (Xe) lamp as a PL light source with excitation at 325 nm. The spectra show significant difference in the optical properties of as deposited thin films with the annealed thin films.

The spectra also show that all CuI thin films exhibited UV emission originated from recombination of photo-generated charge carriers from the conduction band into valence band. As shown in the figure, CuI thin film prepared at different annealing temperature exhibited emission peaks at different

wavelengths. The CuI thin films exhibited centre emission peak at 417 nm for as deposited, 423 nm for 50°C, 457 nm for 80°C and 427 nm for 110°C. It noted that the film annealed at 80°C is shifted to the longer wavelength compared to that of the other films, and its intensity is stronger compared to that of other annealing temperature which indicates the improvement of the film's crystalline structure.

**FIGURE 4.16**  
Photoluminescence (PL) Spectra of 1.0M CuI Thin Films at Different Annealing Temperatures.



The emission of centre peaks of all thin films annealed at different temperatures is due to recombination of electron and holes at  $\text{Cu}^{2+}$  and  $\text{Cu}^{1+}$  centres. In the case of CuI, higher intensity in UV emission might also due to the increase in carrier concentration at certain annealing temperature which increases the recombination reaction [154].

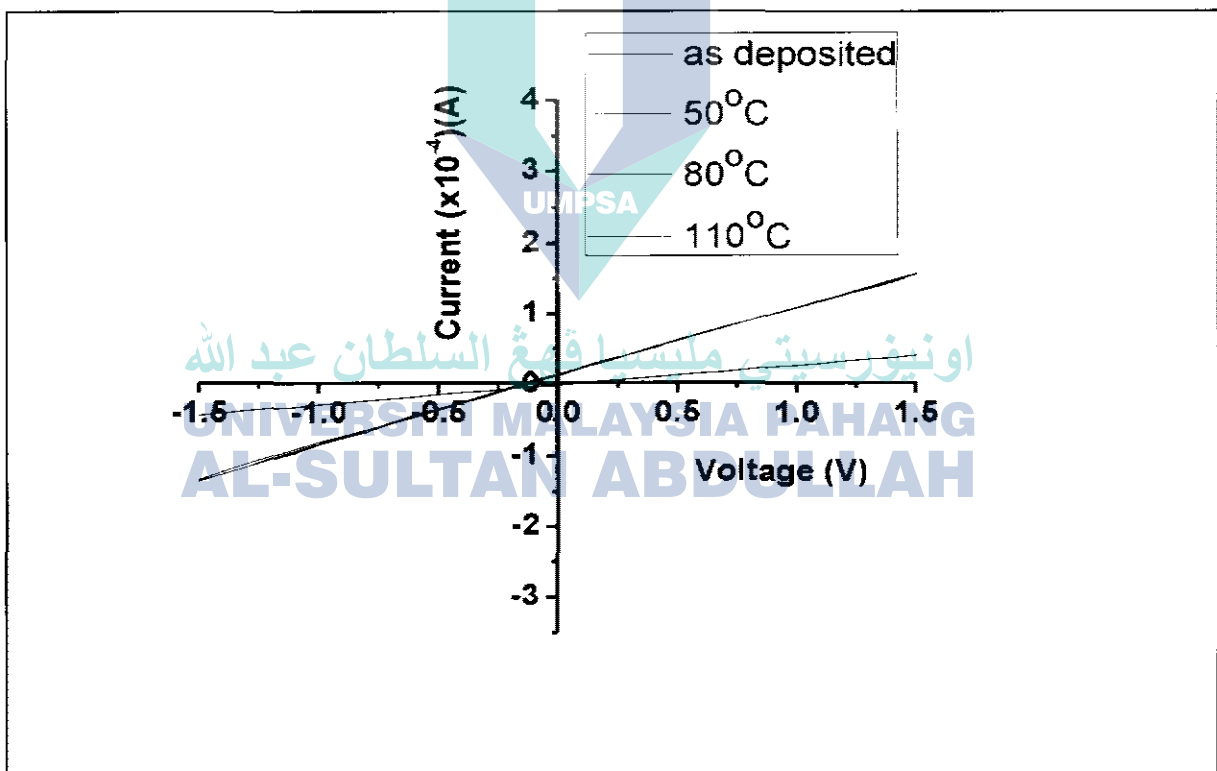
#### 4.3.5 Electrical Properties of Thin Film

The electrical properties of CuI thin films were measured using two-point probe as mentioned in Chapter 3. The results of Current-Voltage (I-V) measurement of 1.0M CuI thin films prepared at different annealing temperatures with 10 minutes of annealing time are shown in Figure 4.17. Indium (In) was used as metal contacts in this measurement. The results show that all the thin films give ohmic contact and exhibited linear I-V curve. The explanations on why it behaves linear ohmic can be found in section 4.1.5. The resistances of the thin films can be obtained from the slope of the curves in Figure 4.17. It could also be seen that current value at respective voltage increased linearly with annealing temperature. Hardly any difference is observed in the I-V behaviour of the thin films annealed at different temperatures, but according to the numerical data (not shown) the thin film that has been annealed at 80°C shows the highest current value and as deposited thin films shows the lowest current value at the corresponding voltages. The results indicate that the electrical properties of CuI thin films improved with increasing annealing temperature. One of the reasons for the behaviour is the improvement of crystal structure of the thin films when the film is annealed.

The resistivity and conductivity of CuI thin films obtained from the I-V curve in Figure 4.17 as the function of different annealing temperatures are shown in Figure 4.18. The values of the resistivity and conductivity are determined from the equation stated in Chapter 3, where the thickness of the thin films was maintained at 0.5  $\mu\text{m}$ . The result shows progressive decrease in resistivity of CuI thin films until the annealing temperature of 80°C is reached while the conductivity progressively increases at the same annealing temperature, which suggest improvement in holes mobility of p-type materials possibly due to the coalescence of crystallites. During the annealing process, atoms rearrange to form fine crystalline structure. The energy supplied during the annealing process influences the diffusion of atoms absorbed on the substrate and accelerates the migration of atoms to the favourable position. Depending on the materials used,

increasing the annealing temperature will increase the supplied energy needed for atom rearrangement. Thus, the annealing process improves the crystalline structure of CuI thin and, at a certain temperature, will enhance holes mobility and concentration. Furthermore, the presence of iodine in stoichiometric excess will affect the conductivity of CuI thin films. However, heating the thin film higher than 80°C for a long time will remove the iodine from the films which will increase the resistance of the thin films. Fracturing and loosening of the film could happen when annealed at higher temperature, probably due to the difference in expansion of CuI particles and glass [126].

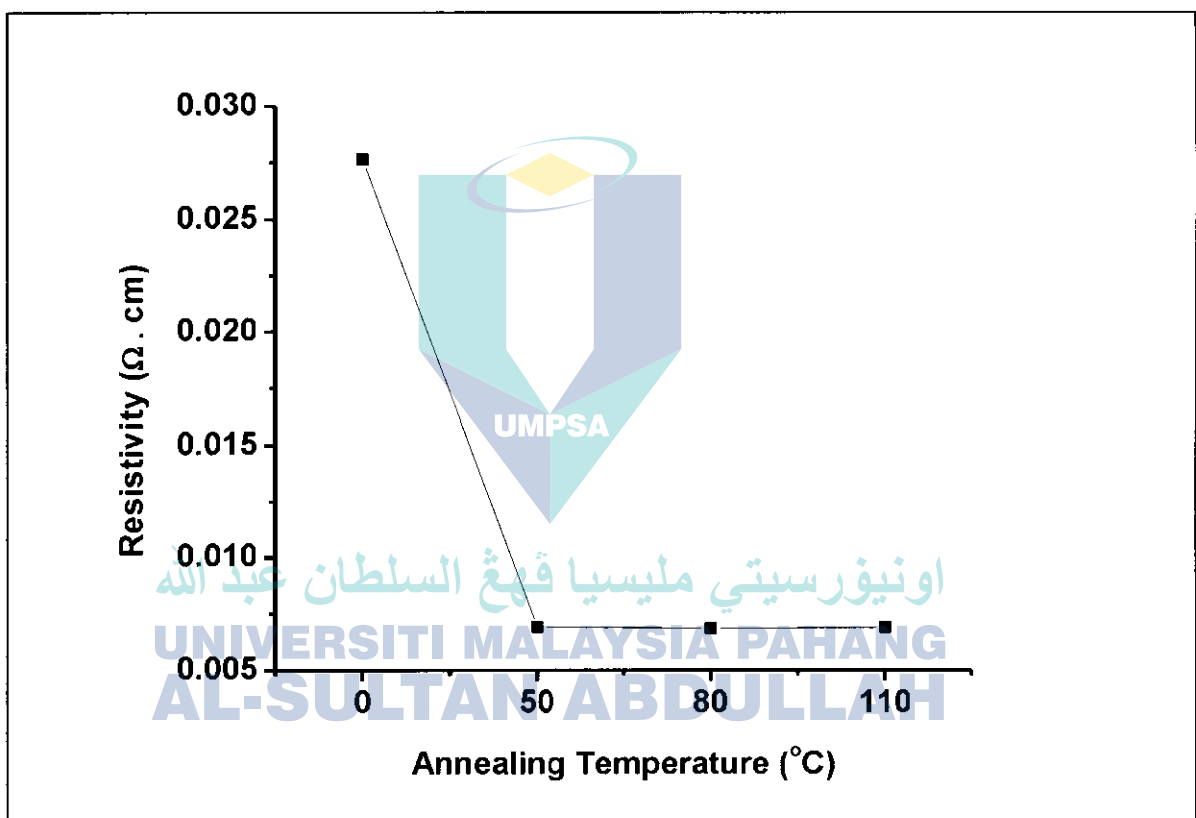
FIGURE 4.17  
Current-Voltage (I-V) Measurement of 1.0M CuI Thin Films at Different Annealing Temperatures.



Moreover, the increasing resistance of CuI thin films at annealing temperature higher than 80°C could be due to the formation of copper oxide inside the thin films [155]. Thermal activations of electrons from the valence band

to acceptor levels results in a hole in the valence band which helps increase the conductivity and decrease the resistivity of the films [155]. Furthermore, improvement on the CuI thin films is significant to circumvent the degradation of CuI films due to excessive iodine in the CuI films that will strongly decreased the photocurrent of the cell [156].

**FIGURE 4.18**  
Resistivity of 1.0M CuI Thin Films at Different Annealed Temperatures.



#### 4.4 SUMMARY

The CuI thin films have successfully been prepared by drop and spin coating technique. The properties of intrinsic CuI thin films deposited on glass and ITO substrates prepared at different molar concentrations and different annealing temperature have been investigated. The study of the effect of molar concentration on CuI thin films properties suggested precursor of 1.0M concentration has shown good quality when

characterization of its electrical properties exhibited good conductivity. Result of I-V measurement using two point probes shows the resistivity of CuI thin films deposited at different molarities increased with increasing CuI molar concentration. The lowest resistivity is at 1.0M with 0.002  $\Omega$ .cm and the highest resistivity is at 0.05M with 0.049  $\Omega$ .cm. Characterization of the optical properties show that CuI thin films tend to produce good optical transmittance with high molar concentration even though the deposited particles on substrate surface is more dense than with lower concentration. The thickness of deposited film is maintained at approximately 0.5  $\mu$ m for all the thin films. The optical band-gap of CuI thin films is observed to be in the range of 3.17 eV and 3.18 eV. The increase in the carrier concentration with precursor's molar concentration as the result of the increased CuI particles in the thin film also contribute to better electrical conductivity as well as UV emission.

In the study of the effects of annealing temperature on the electrical properties of the thin film, the optimum annealing temperature is found to be 80°C as the conductivity of the film is highest when annealed at that temperature. The thin films annealed at 80°C also showed better crystallinity properties compared to other films annealed at other temperature. The optical properties of CuI thin film annealed at 80°C is the best among the other thin films, with the highest transparency properties in the visible and near infra-red (NIR) regions and the highest absorption properties in the UV region. Also, it is found that the UV emission peak intensity by photoluminescence (PL) increases with increasing annealing temperature, and the sample annealed at 80°C produces the highest intensity. Additionally, it is evident from the study that when up to 80°C annealing temperature is used, the annealing process has improved the properties of direct band-gap of the CuI thin films.

**CHAPTER FIVE**  
**CHARACTERIZATION OF NANOPARTICLES COPPER (I)**  
**IODIDE (CuI) THIN FILM THAT INCORPORATES TMED AS**  
**CHELATING AGENT**

**5.1 INTRODUCTION**

In this research, an alternative chelating agent is proposed to be used as the CuI crystal growth inhibitor and as an option to the fabrication of DSSC as previously discussed. However, a novel approach used to obtain a new CuI-related composite film is demonstrated by making use of CuI-acetonitrile solution. The chelating agent is known as tetra-methyl-ethylene-diamine (TMED@TMEDA). The TMED-chelate CuI thin films are then characterized by its structural, optical and electrical properties, and investigation is conducted to improve the performance of the film by incorporating different amount of TMED to the CuI solution. It is found that highly (111) oriented CuI film with improved quality could be easily prepared on glass and ITO substrates. Furthermore, the films exhibit improved band-gap photoluminescence, indicating that TMED@TMEDA is a reagent used in the synthesis of an inorganic material while exhibiting a special function in many metal halides. Currently, no studies on the structural, optical and electrical properties of TMED-chelate CuI thin films have been reported.

**5.2 STUDY ON DIFFERENT VOLUMES OF CHELATING AGENT INTO**  
**TMED-CHELATE CuI SOLUTION**

In this chapter, the effects of different volumes of chelating agent to the main precursor solution of the TMED-chelate CuI thin film properties were studied and discussed. The main objective of this study is to determine the optimum volume, and to understand the behavior of TMED-chelate CuI thin films at different volume ratio of TMED to the CuI solution which could be used as the guidelines for the fabrication of dye sensitized solar cell. Also, the study was conducted to examine the effects of TMED

volume ratio on the structural, optical and electrical properties of the TMED-chelate CuI thin films. The preparation of the films using different volumes of TMED to the CuI solution has been described in Chapter 3.

### 5.2.1 Conductivity and pH

Table 5.1 shows the measured pH and conductivity of TMED-chelate CuI aqueous solution at different volumes of TMED to the CuI solution, where the CuI molar concentration has been fixed at 1.0M concentration. The results show that the higher the TMED volume ratio to the CuI solution the higher is the pH value but the lower is its conductivity. This could be the effect of metal-ligand bonding between CuI and TMED, where the changes in crystallization structure occur due to the environmental factors such as pH, exposure to light or change in temperature [157-158].

**TABLE 5.1**  
**Acidity (Ph) and Conductivity of CuI Solution Incorporated With Different Volumes of TMED.**

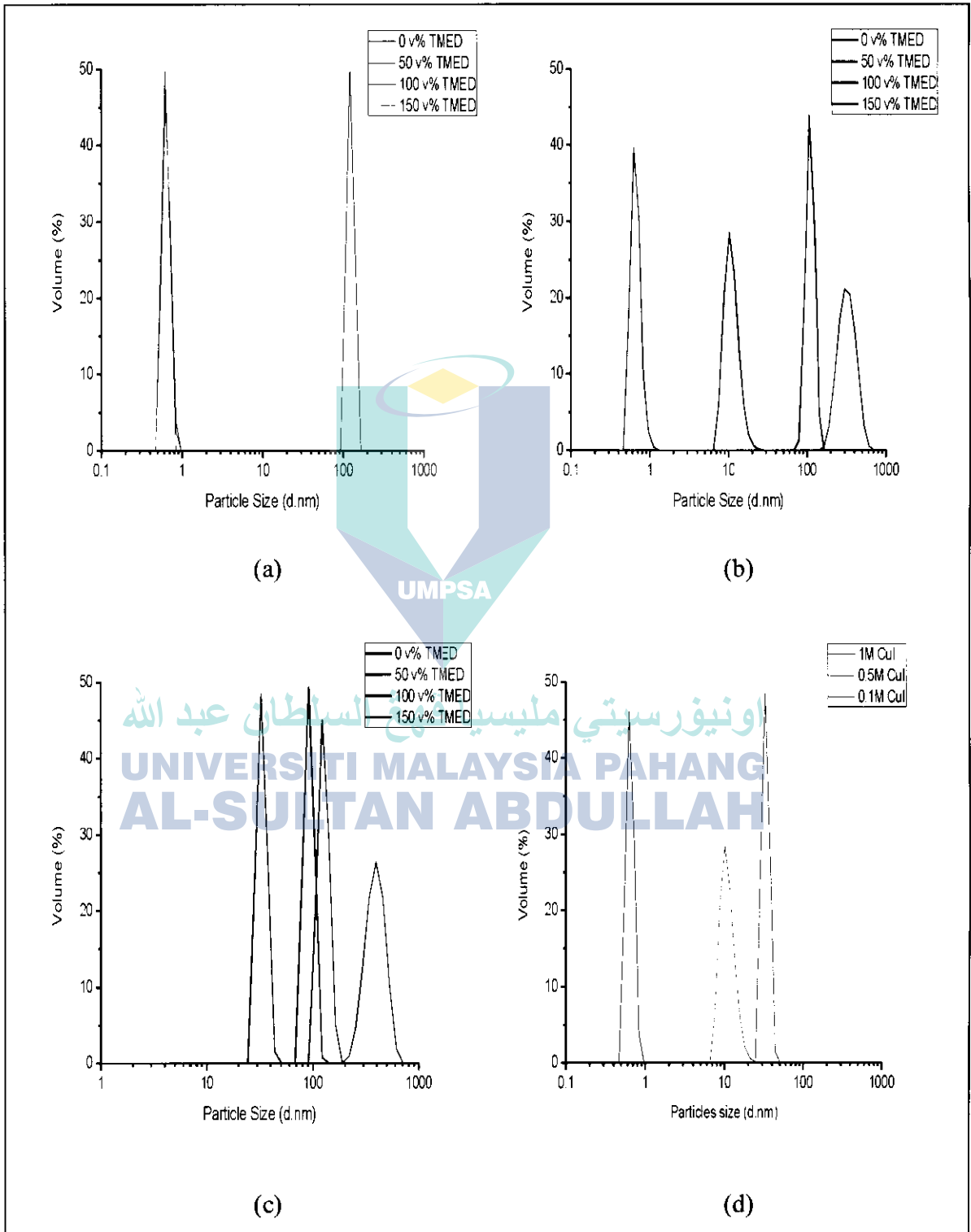
Solution (ratio)	pH	Conductivity ( $\mu\text{S}/\text{cm}$ )
CuI:TMED (1:0)	7.79	1545
CuI:TMED (1:0.5)	9.97	1408
CuI:TMED (1:1)	11.38	1387
CuI:TMED (1:1.5)	11.89	1352

The interaction between the metal d-orbital and the  $\pi^*$  level of the bridging ligand also changes the conductivity of the solution when the metal atom in the centre are aligned and conduction decreases as the atoms go from parallel to perpendicular [159].

### 5.2.2 Particles Size Measurement

To examine the role of TMED in the formation of the TMED-chelate CuI aqueous solution, particles size was measured was carried out after the CuI solution, without and with TMED, was stirred about 3 hours. Figure 5.1 shows the measured particles size of CuI solution with different volume ratios of TMED to the CuI solution. Observing the size distribution of particles, as shown in Figure 5.2 (a), (b) and (c), the CuI solution without TMED chelating agent are composed of large CuI grains with about 43% of the particles having a size of approximately  $0.1 \mu\text{m}$  as the peak is centred around 100 (d.nm). On the other hand, much smaller crystals are produced in the CuI solution which has been mixed with TMED (50 v %, 100 v %, and 150 v %) than those produced in CuI solution without TMED, where 38% to 50% of the volume contributed to the small crystals. The particles size of the various molar concentrations of CuI solution with the different ratios of TMED peaked at approximately at around 0.7 to 300 (d.nm). From Figure 5.1 (a) ~ (c), it is observed that regardless of the ratio of TMED to the CuI solution, the solution with 1.0M molar concentration has the highest peak with particles size at approximately 0.6 nm in diameter (d.nm). Furthermore, it can be seen that the most consistent result is obtained with the 100 v% ratio of TMED to the CuI solution with particles size around 0.6 to 12 nm in diameter (d.nm). The results revealed that the size of CuI particles got smaller or its growth is suppressed when a suitable amount of TMED is added to the solution. Hence, with the addition of TMED, the particles of CuI solution are controllable within nano-size and the particles are well dispersed thus preventing the scaling or precipitating of the particles.

**FIGURE 5.1**  
**Particles Size of CuI Solution at Different Molar Concentrations Without and With TMED as Chelating Agent (a) 1.0M (b) 0.5M (c) 0.1M and (d) 1:1 Of CuI:TMED Ratio.**



### 5.2.3 Surface Morphology of TMED-Chelate CuI Thin Films

Using FESEM, the surface morphology of CuI thin film prepared with 1.0M concentration, incorporating the various ratios of TMED, is shown in Figure 5.2. At ambient conditions, CuI is a mixture of several coexisting phases, that is, zinc blende, wurtzite, and a layered hexagonal structure [160]. As observed from Figure 5.2(a), the shape of the CuI crystals without incorporating TMED is composed of large, isolated and irregularly shaped CuI grains indicating that the crystallization process occurred at a fast pace and is uncontrolled. Also, CuI thin films that are prepared without the addition of any chelating agent exhibited a polymorphic characteristic with grains of different sizes distributed throughout the film, as can be seen from the results of XRD. As observed from FESEM images, the average size of CuI grains is in order of micrometer ( $\mu\text{m}$ ). As of images (b), (c) and (d), it is observed that the size of CuI crystals decreases to the order of nanometer corresponding to the ratio of TMED to CuI solution. A dramatic decrease in the crystals size from the order of micrometer to nanometer could be seen when the pictures are compared. Also, TMED-chelate CuI films are uniformly deposited while its crystals are well distributed. Though CuI solution in the absence of TMED consists of polymorphic character at ambient temperature, the relative percentages of phases present in the film is altered when the chelating agent is incorporated into the solution, as seen from XRD. Also, the film prepared from the solution with a ratio of 1:1 to TMED produce small particles of CuI as shown in Figure 5.2(c), such that the particles is hopefully can be penetrated and filled the voids of the porous  $\text{TiO}_2$  film when fabricating the cells. This shows that the size of the CuI crystals can be controlled and it is better distributed with the addition of TMED.

In Figure 5.2(d), a soft shell (layer) seen on the surface of the CuI crystals is function as to reduces direct contact between the crystals and unconcealed part of the dyed  $\text{TiO}_2$  film resulting in significant decrease in short-circuits between

them [51, 161] and reduces the deterioration of the CuI which consequently improves the lifetime of the solar cell [162].

**FIGURE 5.2**  
**FESEM Images of CuI Thin Film at 1.0M CuI Concentration Without and With TMED as Chelating Agent. (a) CuI without TMED, (b) CuI with 50 V% TMED, (c) CuI with 100 V% TMED, And (d) CuI with 150 V% TMED.**

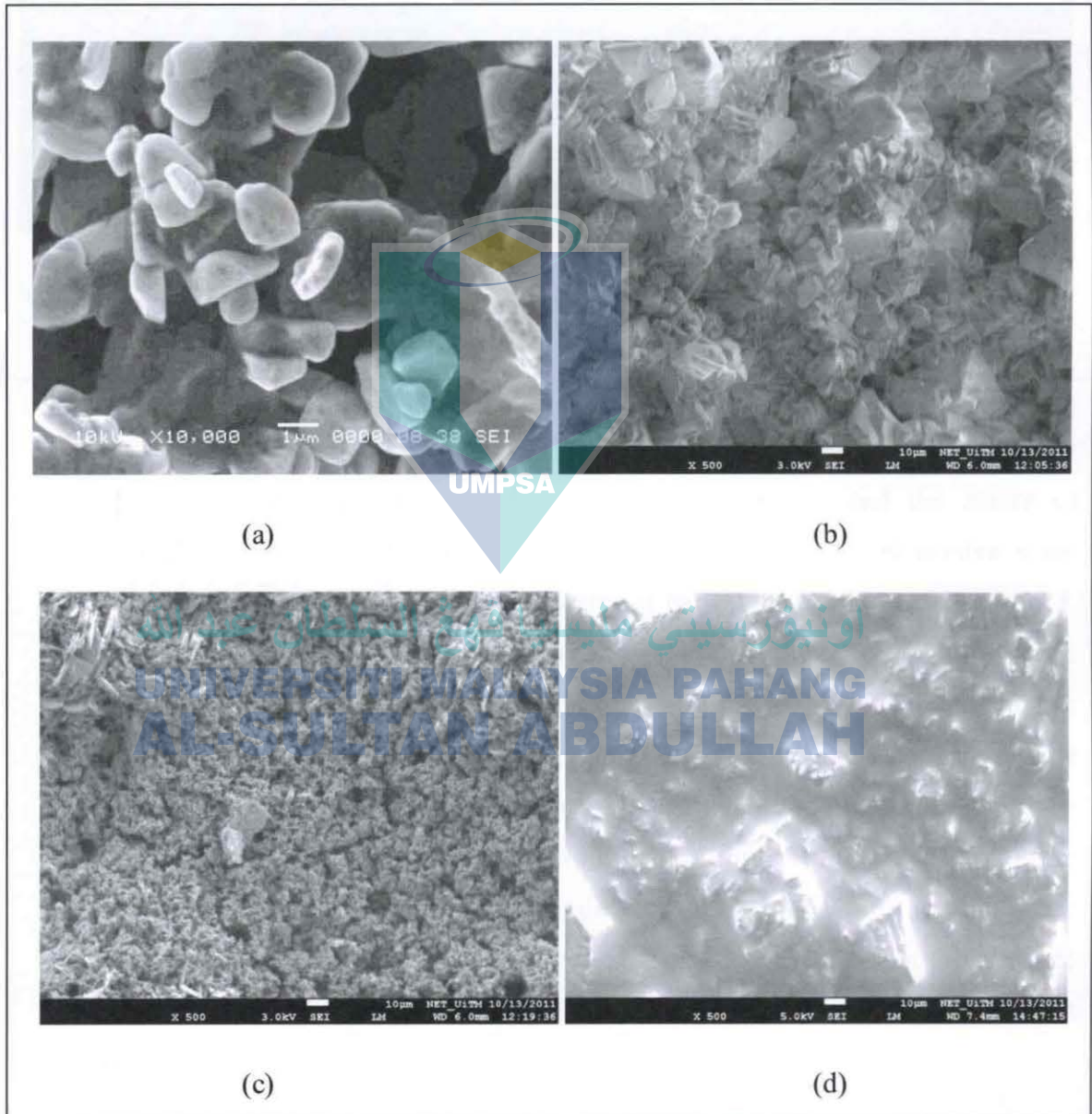
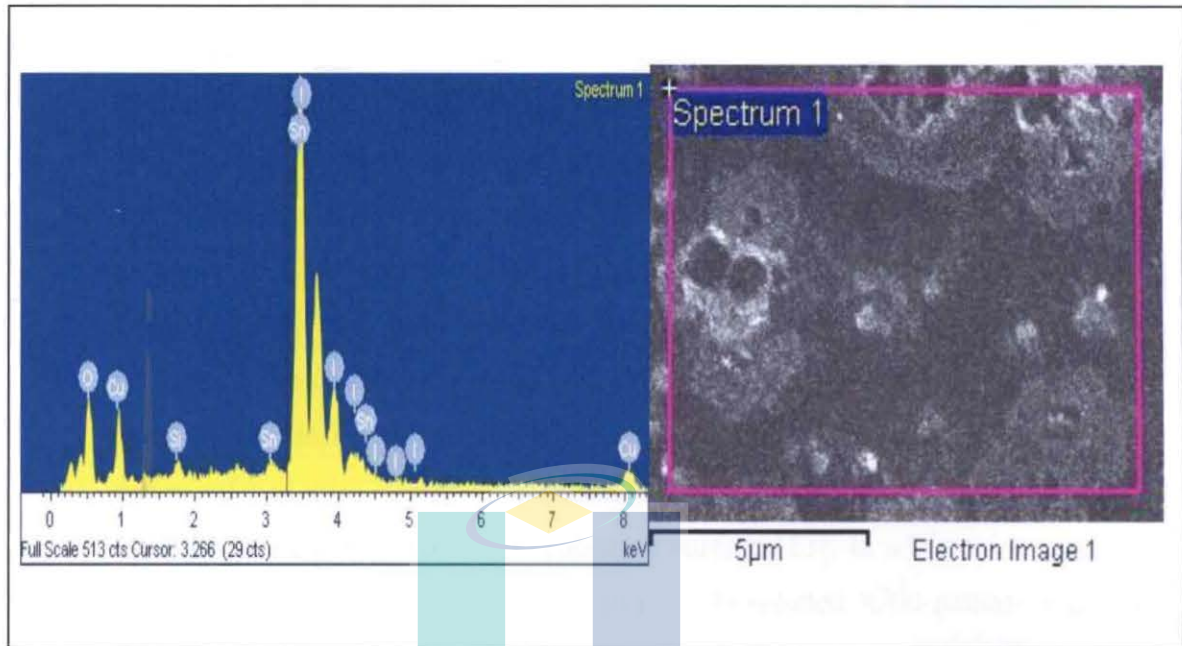


**FIGURE 5.3**  
**EDX Analysis of 1.0 $\mu$ m CuI Thin Film Incorporated With TMED.**



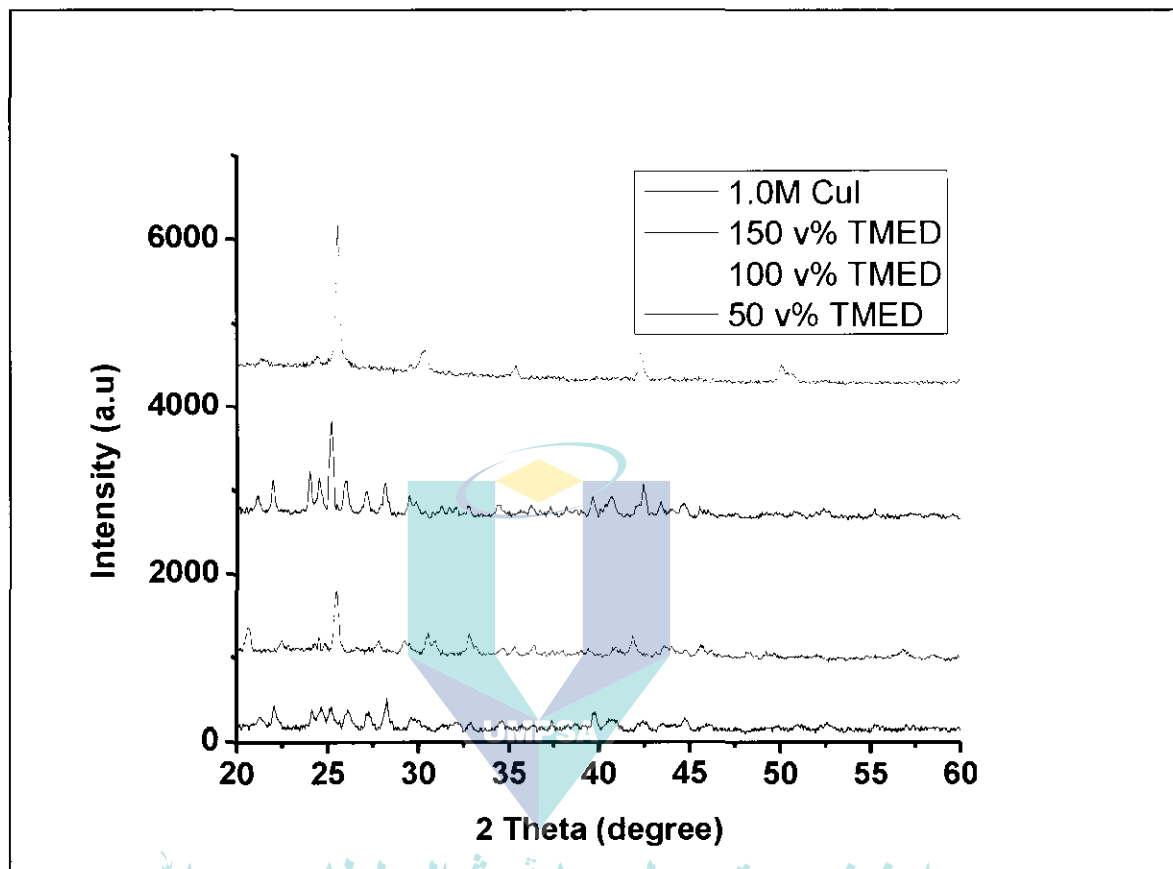
The characterisation of the chemical composition and the nature of TMED-chelate CuI thin films were conducted using energy dispersive x-ray (EDX) measurement, and the EDX spectra of the films are shown in Figure 5.3. In addition, partial areas of the CuI thin films surface were examined using SEM and EDX. From the spectrum, high intensities of x-ray radiation is found only for iodine (I), copper (Cu), tin (Sn) and oxygen (O), indicating that these particles are clusters of copper (I) iodide (CuI) that has been deposited on Indium doped Sn (ITO) substrate with oxygen vacancies inside the films. The EDX spectrum thus confirmed the presence of Cu and I molecules on the surface of the film, hence proving that the thin film is CuI compound. This also revealed that the presence of TMED in CuI solution does not change the chemical compound of CuI thin film.

#### 5.2.4 XRD Spectra

Figure 5.4 shows the XRD spectra of CuI thin films without and with the addition of TMED. The 2 Theta (phase) peaks listed in the table underneath the XRD spectra shows the coordination peaks, both strong and weak, obtained from the TMED-chelate CuI thin films. These peaks also could be assigned to the planes of the face-centered-cubic structure (fcc) of CuI. It is observed that all the TMED-chelate CuI thin films exhibited polycrystalline of  $\gamma$ -phase structure that belongs to the CuI cubic crystal type (JCPDS data 25-390). The very high peak intensity of the (111) and the coexistence of the (200) plane indicate that the deposited CuI film incorporated with TMED is highly oriented along the (111) crystal axis perpendicular to the substrate surface [13]. In addition, owing to the very strong (111) diffraction of CuI film, the broadened XRD pattern originating from the substrate could not be observed. Therefore, the prepared film is highly crystalline even at room temperature. It is noted that in this case the property of the substrate has minor effects on the film orientation. The results above indicate that the growth of highly oriented grain of the deposited CuI films can be assisted with the addition of TMED. The growth of the grain along (111) axis, which acts as holes conductor, is an important factor in CuI based dye sensitized solar cell application.

The full width at half maximum (FWHM) value of TMED-chelate CuI thin films with 0 v% TMED, 50 v% TMED, 100 v% TMED and 150 v% TMED is  $0.197^\circ$ ,  $0.31^\circ$ ,  $0.44^\circ$  and  $0.39^\circ$ , respectively, while the calculated crystalline size (using Scherer's equation) for the samples is 43.2 nm, 27.2 nm, 19.3 nm and 22.0 nm, respectively. The improvement in the crystals of CuI thin films is shown by the increase in the FWHM and the decrease in crystal size when TMED is added to the solution. This indicates that the CuI crystal size is suppressed regardless of the amount of TMED is added to the CuI solution; however, from the analysis of the XRD spectra, it is found that the sample with 1:1 ratio of TMED volume produced much smaller crystals compared to other ratios of the chelating agent.

**FIGURE 5.4**  
**XRD Spectra and Peak List Table of 1.0M CuI Thin Film Incorporated With TMED as Chelating Agent at Different Volume Percentage.**



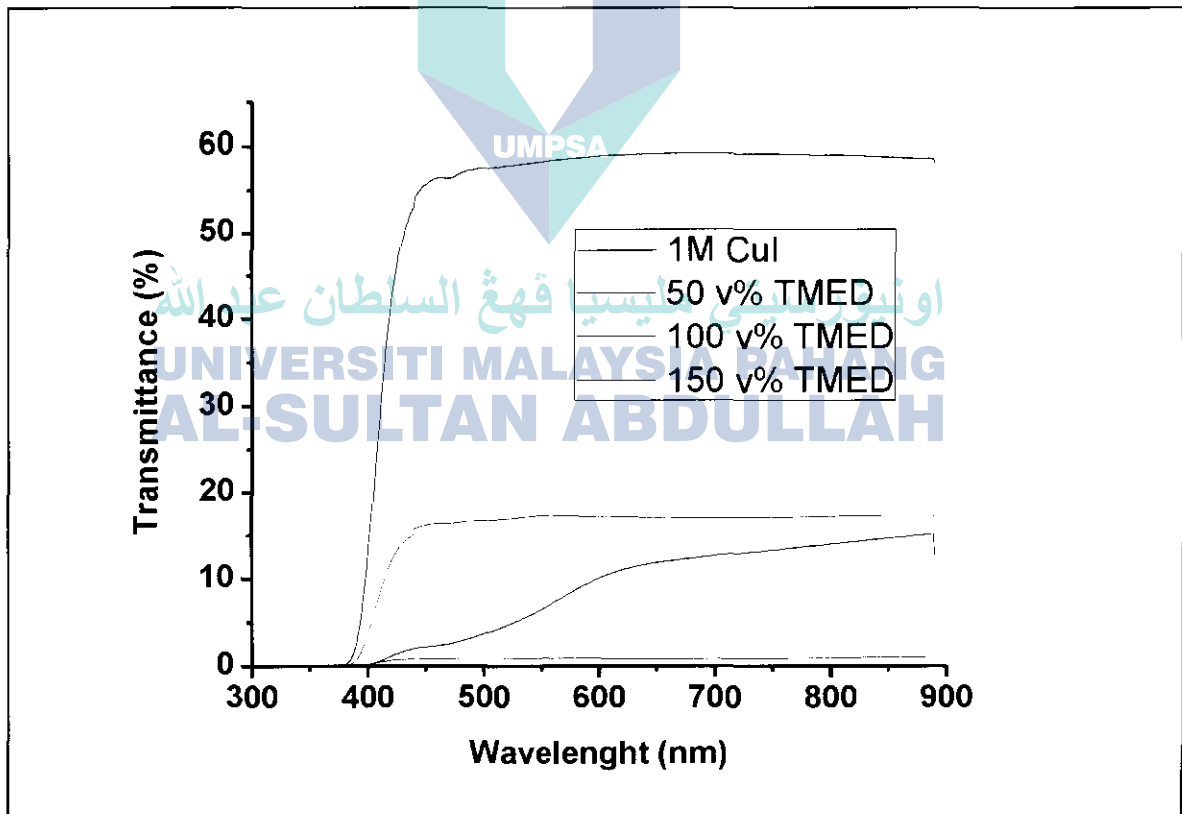
Compound	Peak list 2 Theta (phase)			
1.0M CuI	25.54 (111)	30.30 (200)	42.30 (220)	49.97 (311)
1.0M CuI with 50 v% TMED	25.13 (111)	29.33 (200)	42.60 (220)	Other elements (I, N,C,H)
1.0M CuI with 100 v% TMED	25.55 (111)	29.12 (200)	41.86 (220)	Other elements (I, N,C,H)
1.0M CuI with 150 v% TMED	25.02 (111)	29.38 (200)	42.45 (220)	Other elements (I, N,C,H)

### 5.2.5 UV-Vis-NIR Spectra

Using UV-Vis-NIR spectrophotometer, the optical properties of TMED-chelate CuI thin films were characterized. Three main aspects related to the

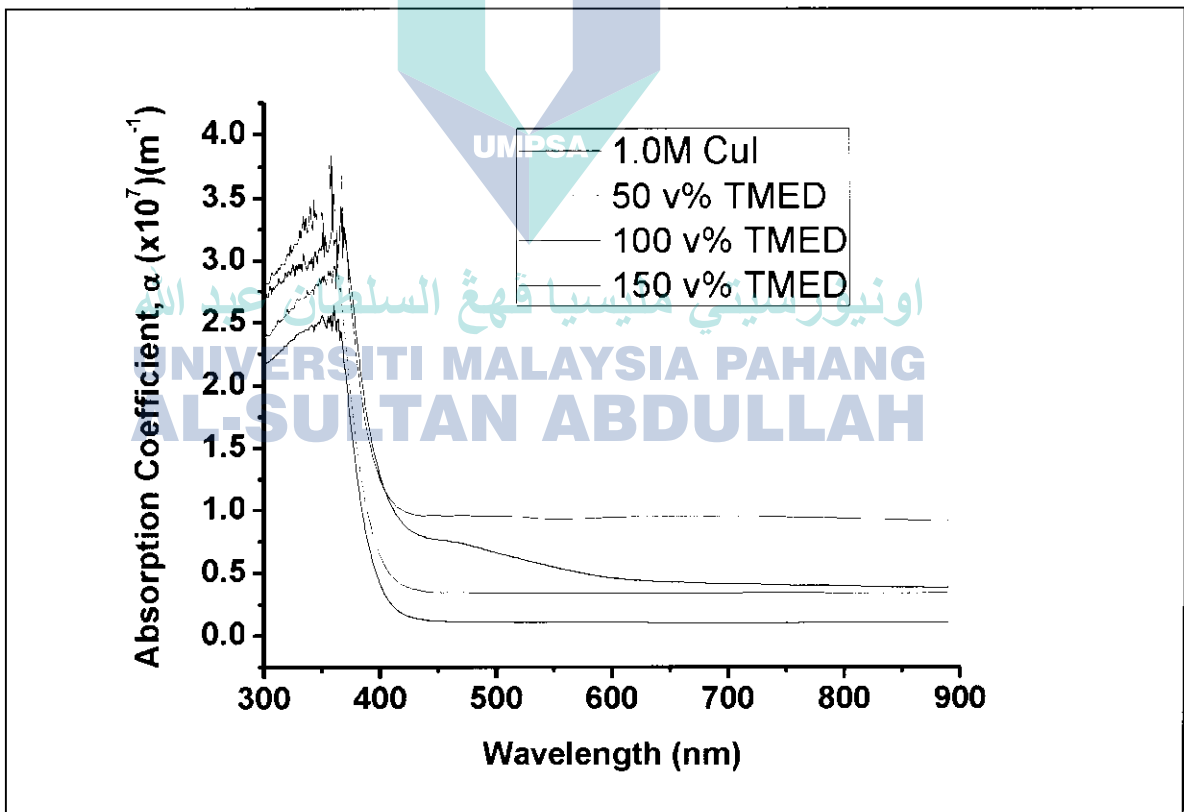
optical properties are transmittance, absorption coefficient and the optical band-gap. Transmittance spectra of the CuI thin films, with and without TMED-chelate, are shown in Figure 5.5. The results showed that all the TMED-chelate CuI thin films exhibit low transparency of below 20% between visible wavelengths of 400 – 800 nm. The low transmittance results could be due to the amorphous structure and porosity that covered most of surface of the substrate which affect the transmitted optical light. These can be seen from the surface morphology as shown in Figure 5.2. On reaching the surface of the film, the incident light may be reflected or absorbed instead of transmitted, and therefore a destructive interference may occur which will lower the transmission of light through the film.

**FIGURE 5.5**  
**Optical Transmittance Of TMED-Chelate CuI Thin Films At Different Volume Of TMED.**



The absorption coefficient properties of TMED-chelate CuI thin films shown in the Figure 5.6 are defined by the transmittance results in Figure 5.5, and the coefficients are calculated using the equation derived in Chapter 3. The absorption coefficient spectra revealed that all the TMED-chelate films exhibit low absorbance in the visible region but high absorbance in the UV range. The transition from low to high absorption coefficient of CuI thin films that were prepared with TMED happens at 430 to 412, while the absorption for CuI thin film prepared without TMED occur near the 402 nm region. The evaluated band-gap energy for the film without TMED is 3.08 eV, while that for the thin film with TMED is between 2.88 eV to 3.01 eV.

**FIGURE 5.6**  
Absorption Coefficient of TMED-Chelate CuI Thin Films at Different Volume of TMED.



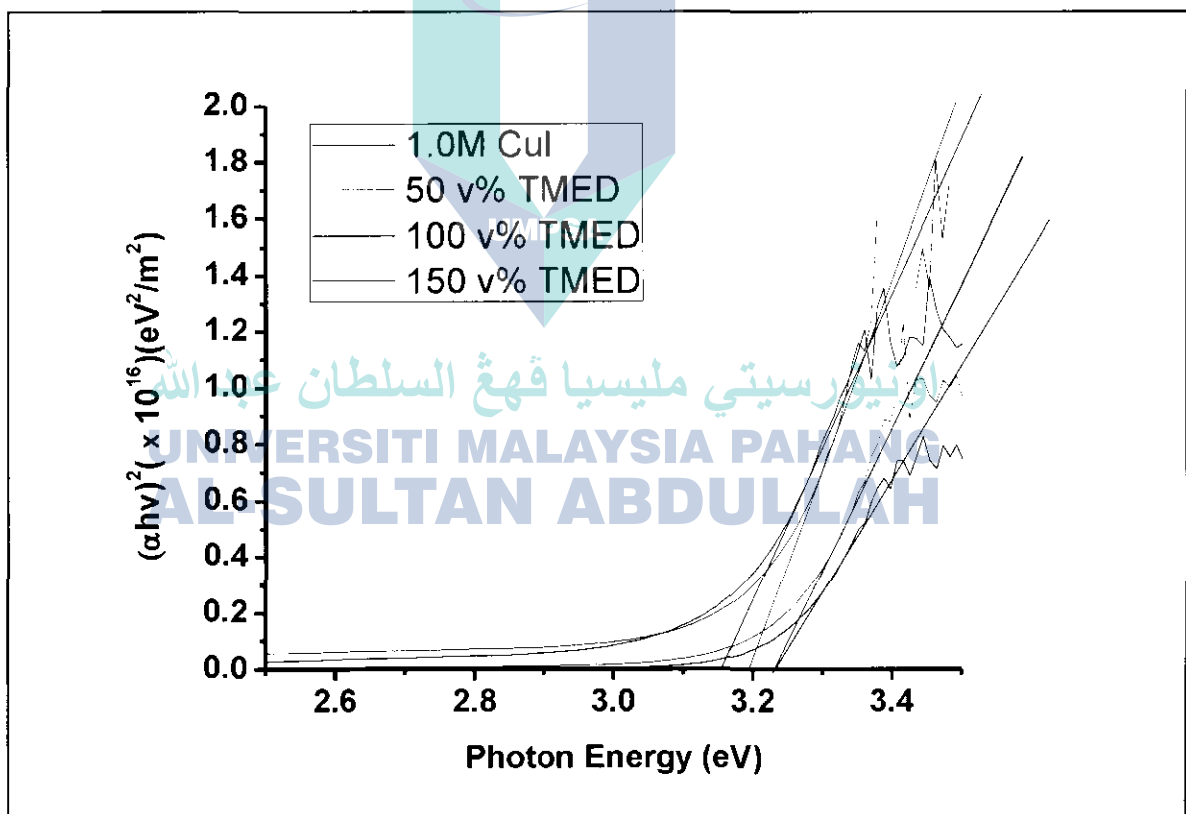
Also, it is observed that for the CuI film with TMED, electrons transition at lower energies than the band-gap (3.1 eV), and this is supported by the optical band-gap estimation of TMED-chelate CuI thin films at different volumes of TMED using Tauc's plot shown in Figure 5.7. The evaluated direct band-gap energies of TMED-chelate CuI thin films is 3.23 eV for 0 v% TMED, 3.19 eV for 50 v% TMED, 3.15 eV for 100 v% TMED, and 3.22 eV for 150 v% TMED. Again, the result shows that optical band-gap is reduced with the existence of TMED in the CuI solution where the lowest band-gap energy transition occurs when the ratio of CuI solution to TMED is 1:1. The reason behind this situation is related to the concentration of the solution. Absorption coefficient and optical band-gap occur at longer wavelength for the solution with 50 v% TMED, 100 v% TMED and 150 v% TMED, but it occurs at a shorter wavelength for the solution with 0 v% [13]. This is due to the effect of metal-ligand bonding in the deposited thin films as all the properties of the film is strongly affected by the resulting complex with/by the arrangement of the d-orbital on the central atom. When the film is deposited from the CuI solution without the addition of TMED, nucleation occurs on the substrate surface in the initial stage of the deposition while the solvent evaporates [163-164], and the smooth surfaces of the film tends to orientate the crystals so as to develop a minimum free energy configuration [164-165]. Hence, the CuI concentration is higher when acetonitrile evaporated from the system and the CuI adducts that exist in the solution will conglomerate into large crystals. At the critical concentration these adducts are apt to aggregate into randomly oriented nuclei as a result of the rapid rate of growth of the crystals and further increasing its size.

On the other hand, the situation is different with the films that were deposited from a mixture of CuI solution and TMED. Since initially the amount of acetonitrile molecules is much more than that of TMED, the bonding of nitrogen in TMED molecules to cuprous ion is partially suppressed. However, acetonitrile serves as a reasonably good solvent for cuprous ion when its concentration is high, but acetonitrile will be first to vaporise during the evaporation process as it has a low boiling point. The decrease in acetonitrile will

improve the coordination interaction between cuprous ions and nitrogen atom from TMED, and in this situation the TMED-related complexes will be the preferential species in this system.

After the evaporation of TMED, the TMED-related complexes species will gradually lose their ligands, and the remaining cuprous and iodine ions will crystallize in-situ into many small CuI nuclei. The nuclei with the (111) plane is parallel to the substrate surface and will have the lowest free energy since the CuI surface with (111) plane has the lowest surface energy.

**FIGURE 5.7**  
Optical Band-Gap Energy Estimation of TMED-Chelate CuI Thin Films at Different Volume of TMED Using Tauc's Plot.



This plane is the original orientation of crystal growth due to nucleation at the film/substrate interface. With TMED-related complexes sequentially decomposed, the nuclei will grow at a faster rate in other planes besides the (111)

plane, either parallel to or inclined to the substrate until they run into with the adjacent growing nuclei. Therefore, the impetus for the nucleation is related to decrease in the interfacial energy due to the transformation of the nuclei from the complex to the equilibrium crystalline state. Such growth will cause the CuI thin films to consist of small crystals, thus making its surface dense and smooth [166-167].

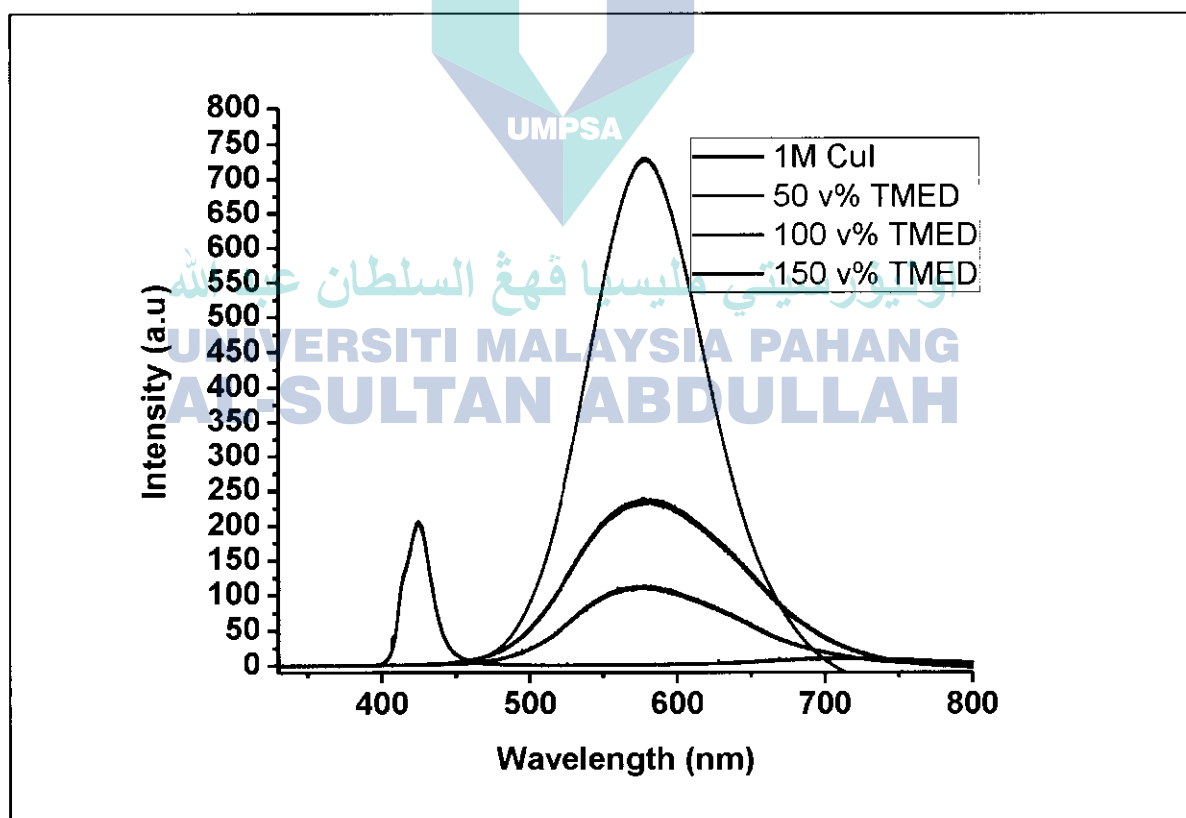
### 5.2.6 Photoluminescence (PL) Spectra

The photoluminescence of TMED-chelate CuI thin films was evaluated as the coordination environments has strong effects on the film emission properties [13], and the photoluminescence spectra of the CuI thin film is shown in Figure 5.8. The emission spectrum of CuI thin film without the addition TMED is observed to peak at approximately 410 nm ( $\sim 3.1$  eV), which can be assumed to be the recombination band-gap of CuI. On the other hand, the emission spectrum of CuI thin film prepared with the addition of TMED exhibited emission peak at approximately 583 nm ( $\sim 2.13$  eV). This energy shift from the blue region to red region could be due to the ligand-to-metal charge transfer process (LMCT) where the excitation energy from the absorbed light is passed on to the metal ions.

According to crystal field theory, the interaction between a ligand and transition metal arises from the attraction between the negative charge on the non-bonding electrons of the ligand and the positively charged metal cations. When a ligand moves closer to the metal ion, the electrons from the ligand will be nearer to some of the d-orbital electrons while others are further away resulting in a loss of degeneracy, and at the same time the d-orbital electrons will repel those in the ligand. Thus, the d-orbital electrons that are further away from the ligand will have a lower energy than those that are closer to the ligand, hence splitting the d-orbital energy. Furthermore, when a photon of visible light is absorbed by the molecules, a transient excited state atom is created as some of the electrons may momentarily jump from the lower energy d-orbital to the higher energy.

The energy of the absorbed photon is equal to the energy difference between the energy of the atom in the excited state and that of the atom in the ground state, and this is inversely related to the wavelength of the light [168]. Hence, the large energy difference as a result of the strong ligand causes light to be absorbed at the shorter the wavelength (400 nm) and emitted at a longer wavelength (560 nm) [22]. Thus, the results of PL for the TMED-chelate CuI thin films obtained in this study can be explained using crystal field theory, where the absorption of light occurred at 410 nm and emission at 580 nm, and this shows that the ligand in use is a strong one. The charge transfer from the ligand to the metal can also be seen by the PL intensity produced.

**FIGURE 5.8**  
Photoluminescence (PL) Spectra of TMED-Chelate 1.0M CuI Thin Films at Different Volumes of TMED.



Also, it is observed that the CuI thin film with the addition of TMED exhibits higher intensity than that of the film without TMED. The low PL intensity of CuI thin film without the addition of TMED is caused by the trapping of holes on CuI surface, which constitute to the major cause of recombination for the film [16]. Thus, the peak of PL intensity of CuI thin film that has been added with TMED is increased compared to that without the addition of TMED, and this is due to the changes to the optical transition efficiency.

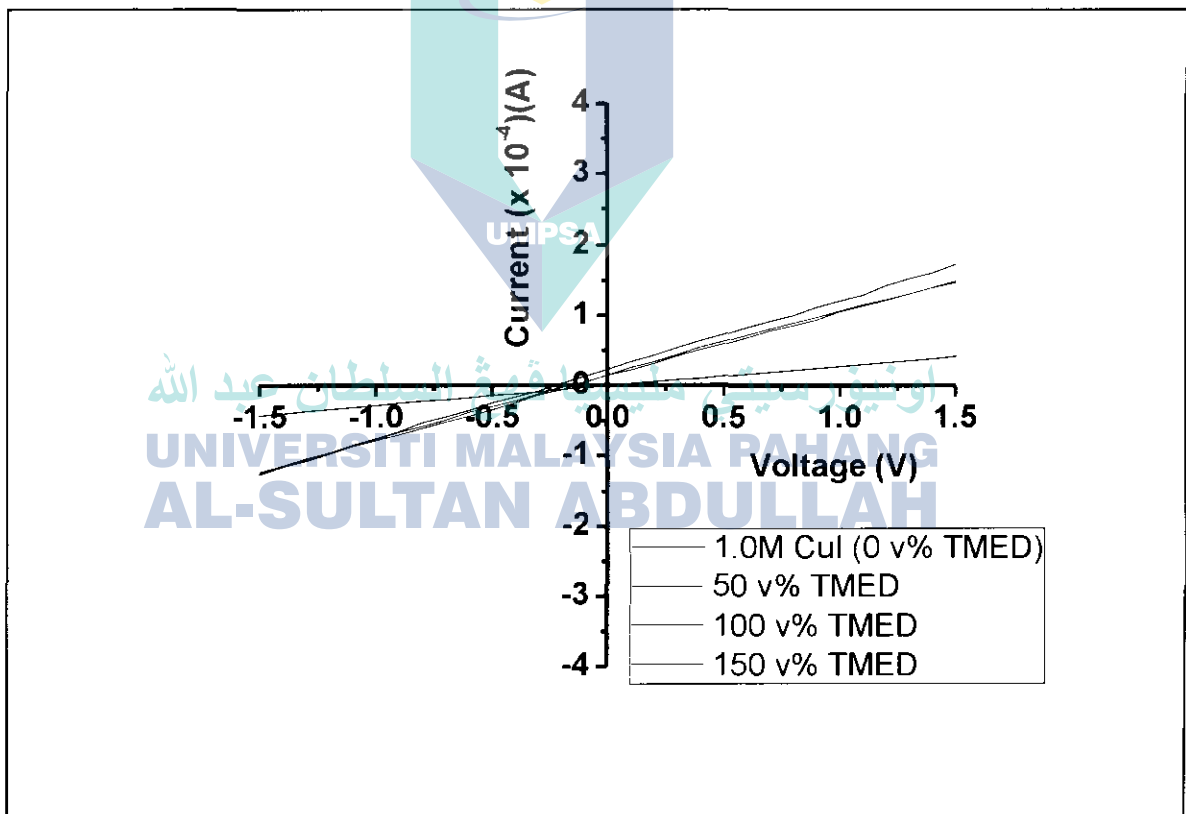
### 5.2.7 Electrical Properties Of TMED-Chelate CuI Thin Films

The electrical properties of a semiconductor material are directly dependent on the concentration of current carriers per unit volume. The current carrier is formed by the release of free electrons when covalent bonds of the precursor atom are broken by the heat energy that is absorbed by the atom. The free electrons, being mobile charged particles, are able to flow through the crystal to create electric current [169-170]. The current flow is dependent on the crystals of the fabricated thin film; the current flow is better and more energy is released if the shape of the crystals is uniform.

Electrical properties, specifically resistivity and contact resistance, of the CuI thin films with different volumes of TMED are shown in Figure 5.9. Two-point probe method with indium-plated contact on top of the films was used to measure the contact resistance at room temperature. The results show that the films produced have ohmic contact resistance where the current is a linearly proportional to the voltage. A result of linear I-V curve is common on metal to semiconductor theory as mentioned in section 4.1.5. The value of the contact resistance is the average of measurements taken at several locations on the surface of the film. It is noted that the addition of TMED does not change the type of semiconductor of CuI which it improves the resistance, and the film with 100 v% TMED gives the highest value of electron flow. The structures of the compound in all the CuI solution that has been added with TMED can have short inorganic

and conjugated organic bridges providing pathways for electrical conduction. The conductivity is due to the interaction between the metal d-orbital and the  $\pi^*$  level of the bridging ligand and its linearity can be due to the uniformity of films structure and coalescence of crystallites. Hence, the use of appropriate volume of TMED should be determined to match the molarities of CuI solution. On the other hand, the presence of iodine determines the conductivity of CuI that was prepared without the addition TMED, and heating the film for a long time will remove iodine from the film, increasing the resistance [171].

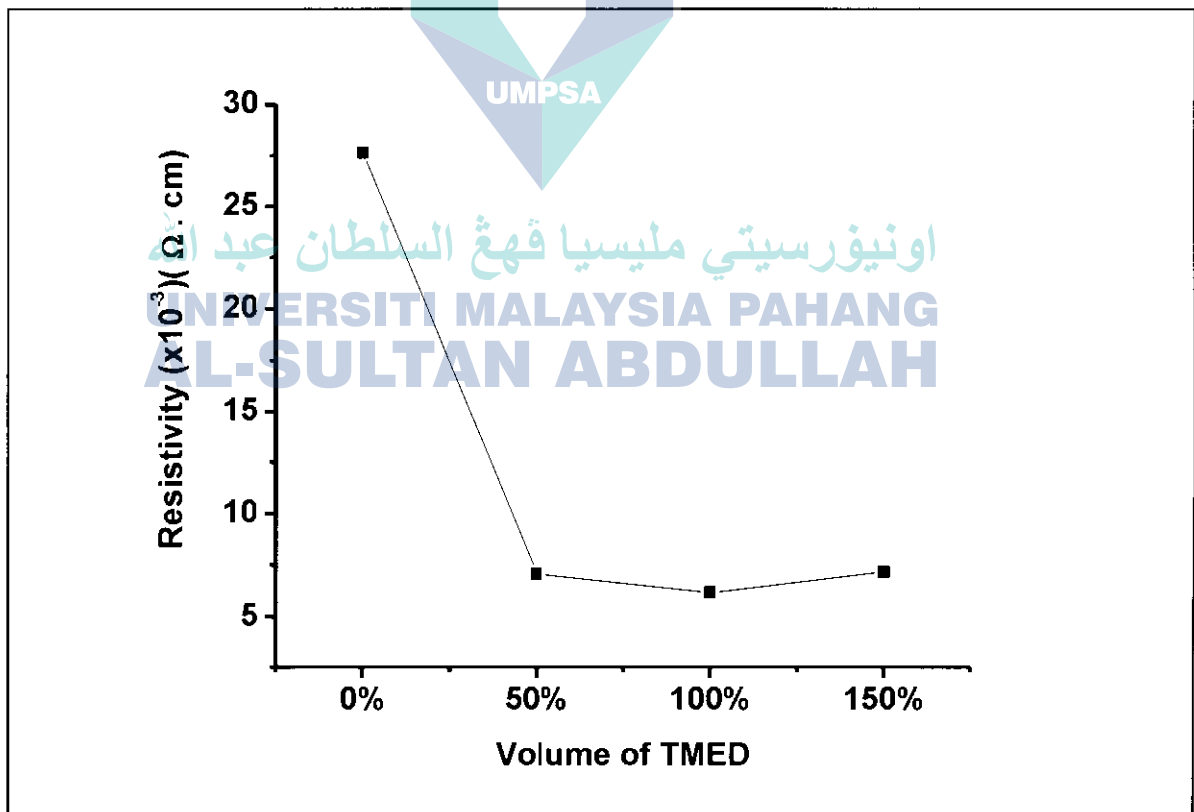
**FIGURE 5.9**  
**Current-Voltage (I-V) Measurement of TMED-Chelate 1.0M CuI Thin Films at Different Volumes of TMED.**



The resistivity and conductivity of TMED-chelate CuI thin films as the function of different volume of TMED are shown in Figure 5.10. The results show that the lowest resistivity and the highest conductivity are obtained from the

100 v% TMED of TMED-chelate CuI thin films, which could be due to the chelating agent enhancing the affinity of chelating ligands for a metal ion. Compared to the concentration of metal-ligand compound in CuI solution without the addition of the chelating agent, the concentration of the compound is higher in CuI solution with added TMED with the ratio of 1:1. Higher concentration of the compound results in higher concentration of current carrier in the thin films, thus providing smooth connection among the particles. In addition, the improvement of packing density and the increase in the surface contact between particles is the result of the higher concentration of the compound. Also, oxygen adsorption in grain boundaries of the thin film is reduced by the situation and results in the lowering its resistivity due to reduced carrier trapping.

**FIGURE 5.10**  
**Resistivity of TMED-Chelate 1.0M CuI Thin Films at Different Volumes of TMED.**



Trapping of current carrier could cause the thin film to be electrically charged making it a potential barrier for the smooth flow of the carrier and decreasing the mobility of the carrier in the film. Furthermore, the increase in the concentration of the metal-ligand compound increases the particles size, enhances the surface contact among the particles, improves the mobility of the current carrier in the thin film, which then reduces its resistivity and increases its conductivity.

### **5.3 EFFECT OF ANNEALING TEMPERATURE ON TMED-CHELATE CuI THIN FILMS**

In this section the study on the effect of annealing temperature on CuI thin films without and with the incorporation of TMED chelating agent are presented. The study were conducted on TMED-chelate CuI thin films prepared from a mixture of CuI solution and TMED with a ratio of 1:1 as detailed in Section 5.2. The objective of this study is to determine the changes in reaction or behavior of the structural, optical and electrical properties of the film when different annealing temperatures are used. The details of the methodology employed are as presented in Chapter 3.

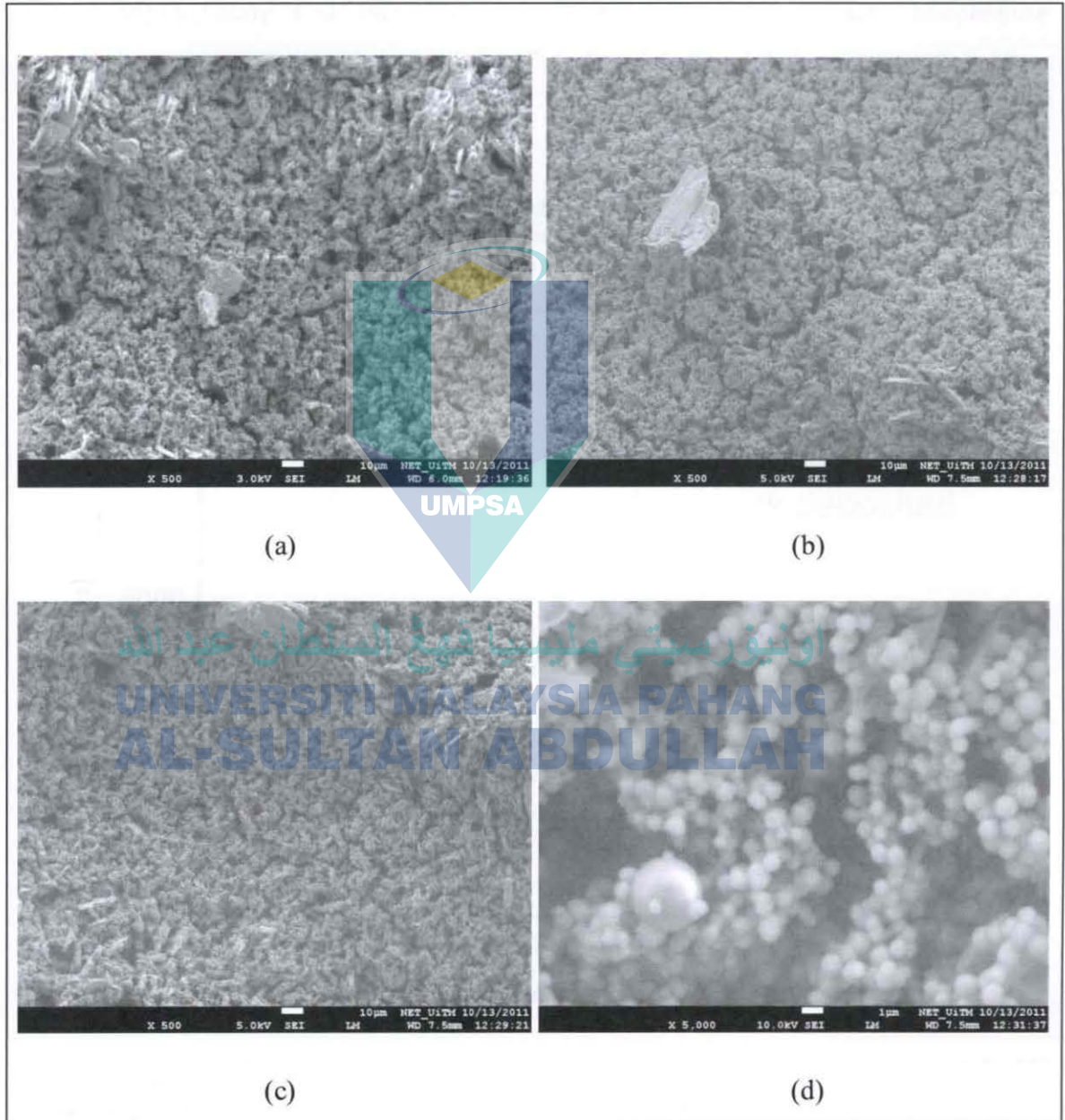
#### **5.3.1 Surface Morphology of Annealed Thin Films**

FESEM images of TMED-chelate CuI thin films deposited on ITO substrate prepared at different annealing temperature are shown in Figure 5.11. The images show that surface morphology of the films is similar and as though it is not affected by the different annealing temperature used in their preparations. The surface is dense and the grains are well connected to each other, as can be seen in Figure 5.11(d), which enhances the conductivity of the film as the contact at the of the grain boundary is improved. The average size of TMED-chelate CuI grains is in order of nanometer (nm), which is the similar to that of the film before undergoing the annealing process. However, by investigating other characteristics

of the CuI thin film, it will be seen that the annealing temperature does improve the crystallinity of the films.

**FIGURE 5.11**

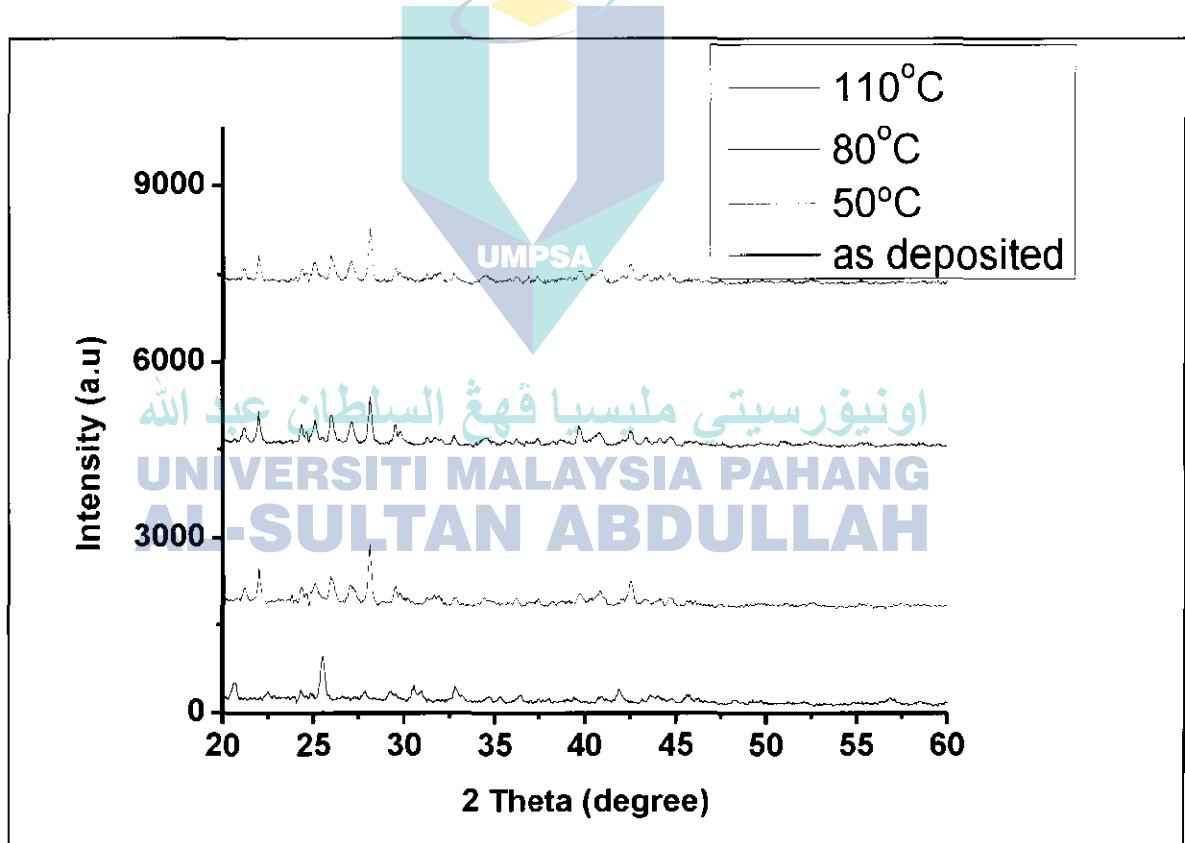
**FESEM Images of 1:1 Volume Ratio of TMED-Chelate CuI Thin Films at Different Annealed Temperatures (a) as Deposited, (b) 50°C, (c) 80°C, and (d) Higher Magnification of 80°C Image.**



### 5.3.2 XRD Spectra

The XRD pattern of CuI thin films without and with the addition of TMED at 1:1 volume ratio under different annealing temperature is shown in Figure 5.12. From the peak list, it is noted that the peaks coordination of the TMED-chelate CuI thin films prepared at different annealed temperature correspond to the polycrystalline of  $\gamma$ -phase structure belonging to CuI cubic crystal type (JCPDS data 25-390).

**FIGURE 5.12**  
XRD Spectra and Peak List Table of 1:1 Volume Ratio of TMED-Chelate CuI Thin Film at Different Annealing Temperatures.



Annealing temperature	Peak list			
	2 Theta (phase)			
as deposited	25.55 (111)	29.12 (200)	41.86 (220)	Others (element of I,N,C,H)
50°C	24.98 (111)	29.39 (200)	42.47 (220)	Others (element of I,N,C,H)

80°C	24.59 (111)	29.43 (200)	42.39 (220)	Others (element of I,N,C,H)
110°C	24.97 (111)	29.40 (200)	41.98 (220)	Others (element of I,N,C,H)

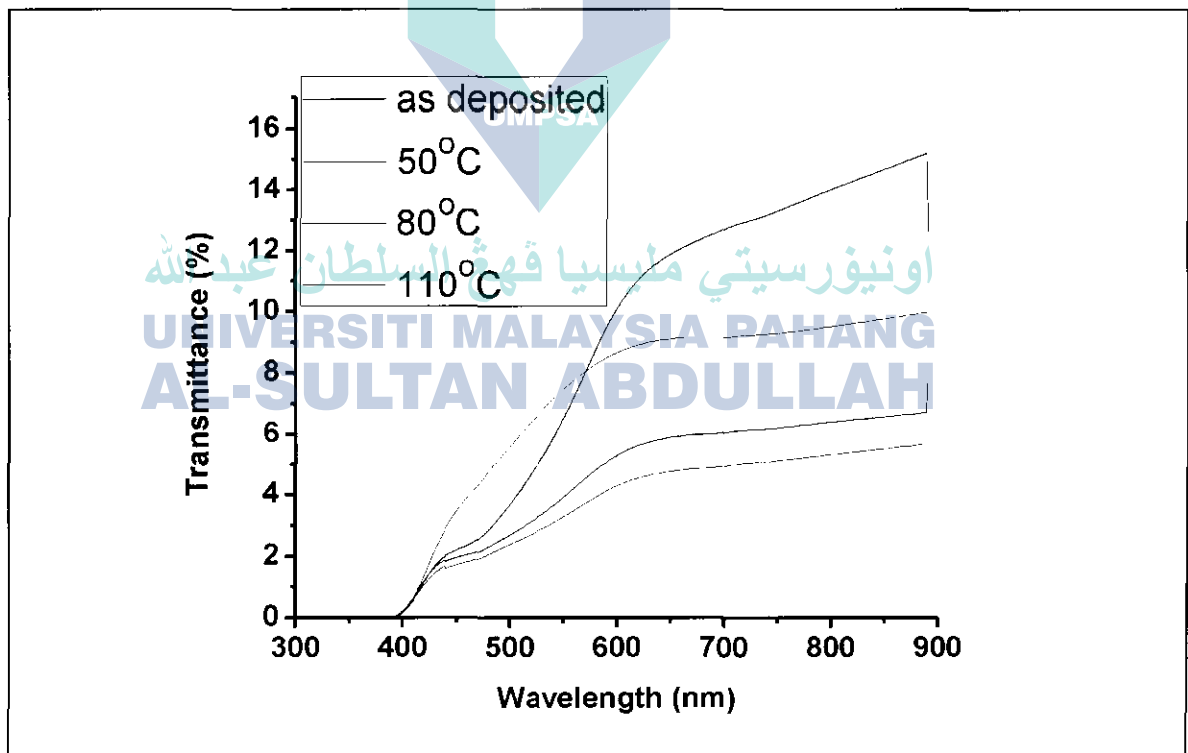
The peaks for CuI are low in intensity while the peaks with the higher intensity indicate the presence of iodine and TMED (N, C, and H). All the films show very weak peak intensity of the (111), regardless of the annealing temperature. The coexistence of the (200) plane which is slightly shifted, compared to that of the film that has not been annealed, indicates that the film structure has been altered due to the effect of the chelating agent, and this could be due to the strong chemical bonding of the TMED-chelate solution to the Cu<sup>+</sup> ion. Moreover, the boiling point of TMED being 120 – 122 °C may promote a higher degree of polymerization. The crystallization process of the film is affected by the different degree of polymerization of TMED, which can be described in terms of nucleation and growth process. The annealing process increases the bonding force of the TMED-chelate CuI solution, and this increases the energy barrier and hinders the crystallisation process as a result of the higher nucleation barrier. Therefore, the crystallization process will be enhanced when the energy attributable to the energy barrier is reduced as this will cause the lattice between the CuI and the substrate to match each other [172], as shown in the data of Figure 5.12. This explains the previous result as to why the CuI films prepared with the addition of TMED have very weak of (111) plane orientation.

The full width at half maximum (FWHM) value of TMED-chelate CuI thin films annealed at as deposited °C, 50 °C, 80 °C and 110 °C is 0.44°, 0.37°, 0.28° and 0.39°, respectively, while the crystalline size calculated using Scherer's equation for all the samples is 19.3 nm, 22.9 nm, 30.3 nm and 29.7 nm, respectively. Note that different annealing temperatures resulted in the small increase of the grain size, and this might be due to the merging of the CuI particles to form denser film.

### 5.3.2 UV-VIS-NIR Spectra

The transmittance spectra of the TMED-chelate CuI thin film that has been annealed at different temperature shown in Figure 5.13. It is observed that the films exhibit low transparency of less than 20% in the 400 – 800 nm wavelengths, and the transmittance edge being at 430 nm indicating that the transparency of the film is in the visible region. The low transmittance could be due to the compact and dense nature of the film's crystalline structure after undergoing the annealing process, making the film thicker and reducing the passage of light through the film.

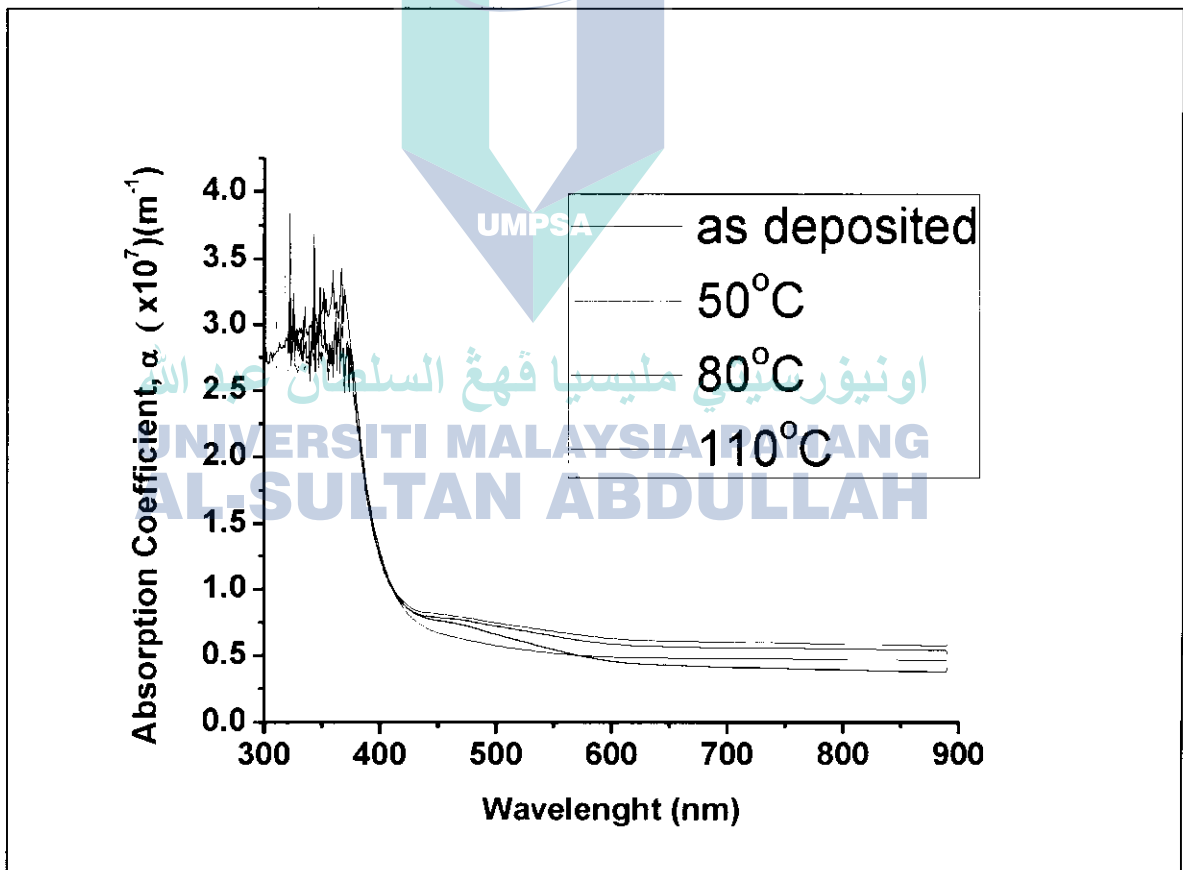
**FIGURE 5.13**  
Optical Transmittance of 1:1 Volume Ratio of TMED-Chelate CuI Thin Films at Different Annealing Temperatures.



The absorption coefficient of 1:1 volume ratio of TMED-chelate CuI thin films, defined by the measured optical transmittance, is shown in the Figure 5.14.

The absorption coefficients spectra revealed that the absorption rate in the visible region improves when the TMED-chelate films underwent the annealed process compared to that of the film that has not undergone the annealing process; however, high absorbance near the UV range is observed in all the films. The absorption edges from low to high absorption of all the films is at 430 nm (2.88 eV), showing that the electron transition occur at lower band-gap energy. This transition is supported by the optical band-gap estimation of annealed TMED-chelate CuI thin films using Tauc's plot as shown in Figure 5.15.

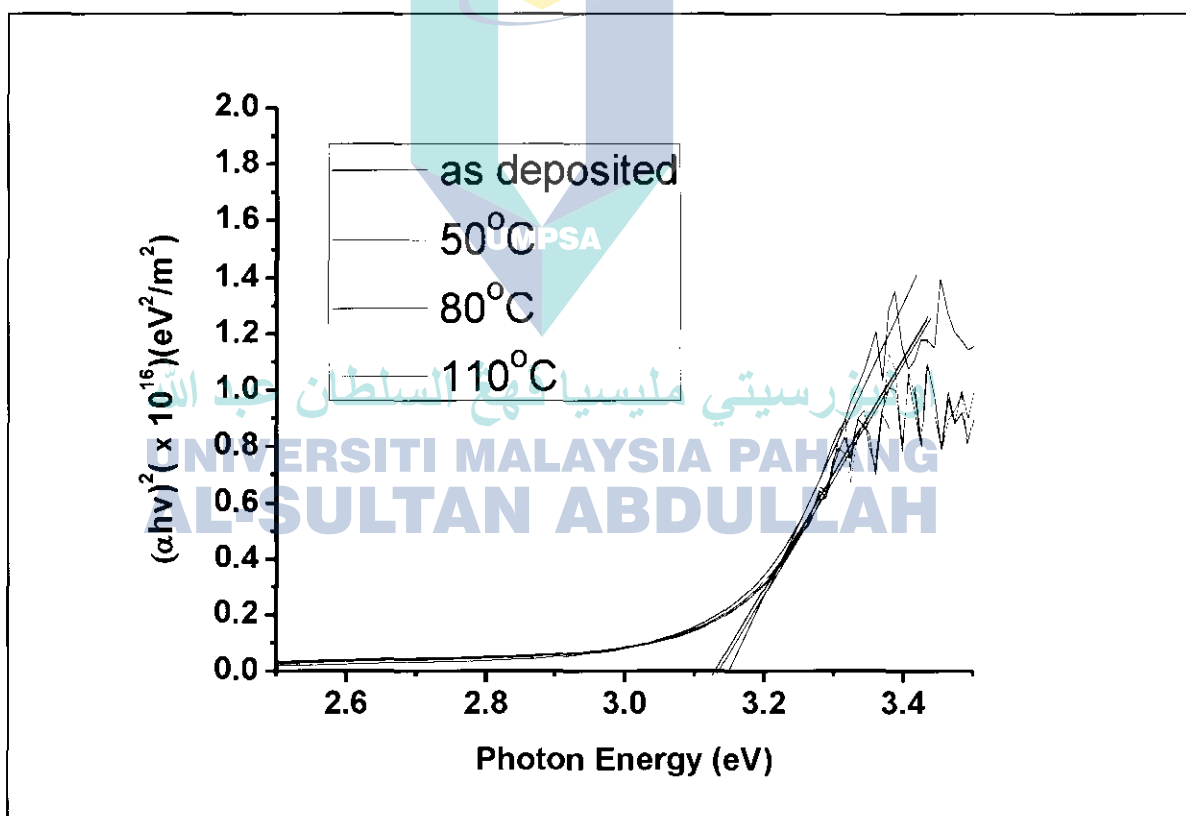
**FIGURE 5.14**  
Absorption Coefficient of 1:1 Volume Ratio of TMED-Chelate CuI Thin Films at Different Annealing Temperatures.



The extrapolation of the graph was plotted using the equation mentioned in Chapter 3 and this gave the evaluated direct band-gap energy of TMED-chelate

CuI thin films at 3.18 eV for as deposited and 3.15 eV for all the annealed films, which shows that the optical band-gap is reduced when TMED is mixed the CuI solution. This can be related to the formation of a metastable species complex in the system, and this transition might be attributed to the charge transfer from cuprous ion to acetonitrile. When TMED is added to CuI-acetonitrile solution, the change is a result of the coordinating ability of TMED to compete with acetonitrile for the metal sites, which might result in the formation of some planar TMED-related complexes with high stability [13].

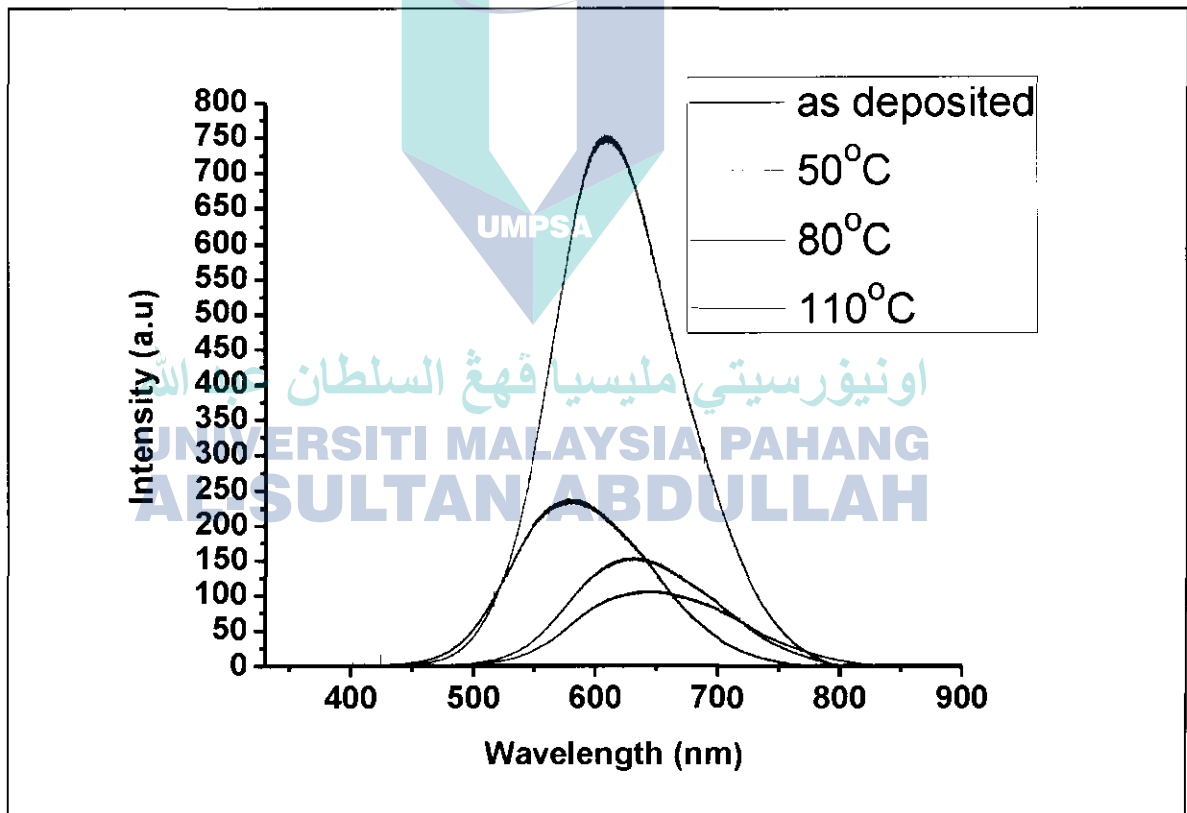
**FIGURE 5.15**  
Optical Band-Gap Energy Estimation of 1:1 Volume Ratio of TMED-Chelate CuI Thin Films at Different Annealing Temperatures Using Tauc's Plot.



### 5.3.4 Photoluminescence (PL) Spectra

One of the characteristics of the optical properties is the bonding behaviour of the chelating agent to the precursor which can be evaluated via photoluminescence (PL) measurement. The broad peak of the PL spectra of the TMED-chelate CuI films show that the wavelength is between 610 nm to 650 nm for the films annealed with temperature between 50°C to 110°C and 580 nm for non-annealed film, as shown in Figure 5.16.

FIGURE 5.16  
Photoluminescence (PL) Spectra of 1:1 Volume Ratio of TMED-Chelate CuI Thin Films at Different Annealing Temperatures.



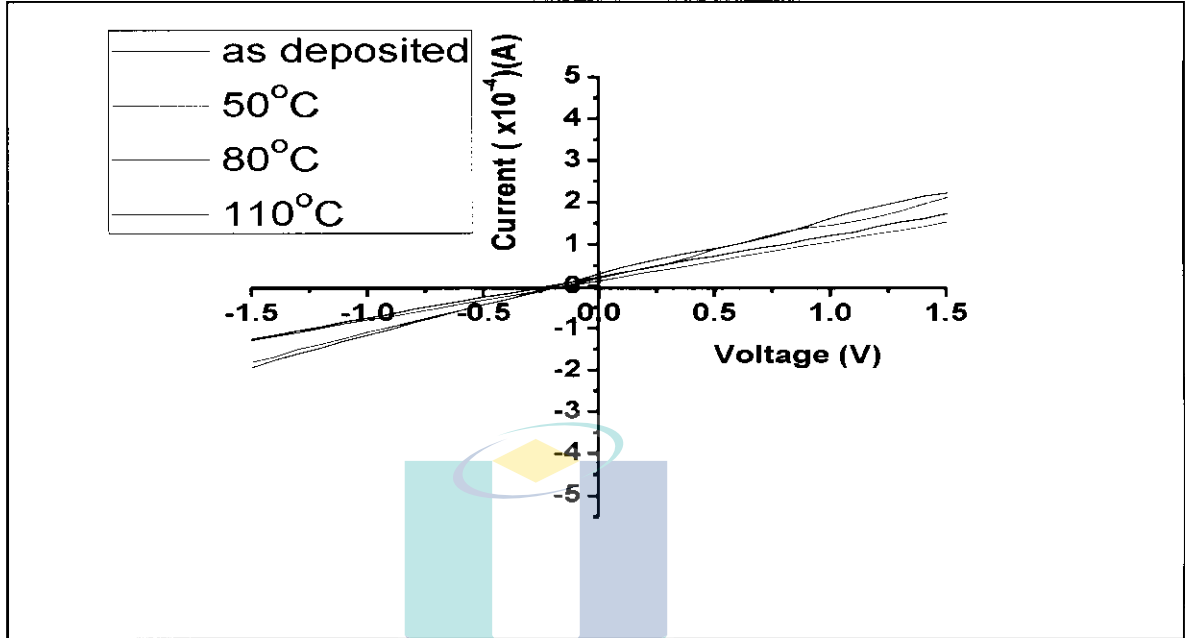
The film annealed at 80°C produces the highest peak intensity which can be related to the evaporation of the solvent and other organic compound, and this could be due to endothermic effect corresponding to the strong bound organic

compound [173] remaining in the precursor. Hence, the loss of weight of the compound during annealing also could give some impact to the peaks appearing at longer wavelength [174]. Thus, the PL results show that the crystallization of CuI films derived from TMED-chelate solution is improved at higher temperature, as long as the temperature is kept below its boiling point (120°C-122°C). The tensile stress in the deposited films is also affected by the annealing temperature, and this is indicated by the shift in the position of the XRD peak as shown in Figure 5.16. The stress might be the result of the lattice mismatch, and the mismatch between the thermal expansion coefficients of the film and the substrate [175].

### 5.3.5 Electrical Properties of Annealed Thin Films

Current-voltage (I-V) measurements of the TMED-chelate CuI thin film annealed at different temperature are shown in Figure 5.17. Two-point probe method is used to measure this characteristic at room temperature with indium-plated contact placed on top of the films. The results show a linear I-V ohmic behaviour for all the annealed TMED-chelate CuI thin films, but the current increases only up to a certain temperature. As previously mentioned, the ohmic characteristic of metal-semiconductor junction is thoroughly depending on 3 main points as describe in section 4.1.5. Moreover, the electrical properties in a semiconductor is dependent on current carrier per unit volume, and more carriers will be formed when the endothermic of the precursor atom released electron (hole) carrying away the energy and flowing through the crystal creating electric current. From the measurements, the formed crystals are in good shape and more energy is released from the better current flow as a result of the annealing process.

**FIGURE 5.17**  
**Current-Voltage (I-V) Measurement of 1:1 Volume Ratio of TMED-Chelate CuI Thin Films at Different Annealing Temperatures.**

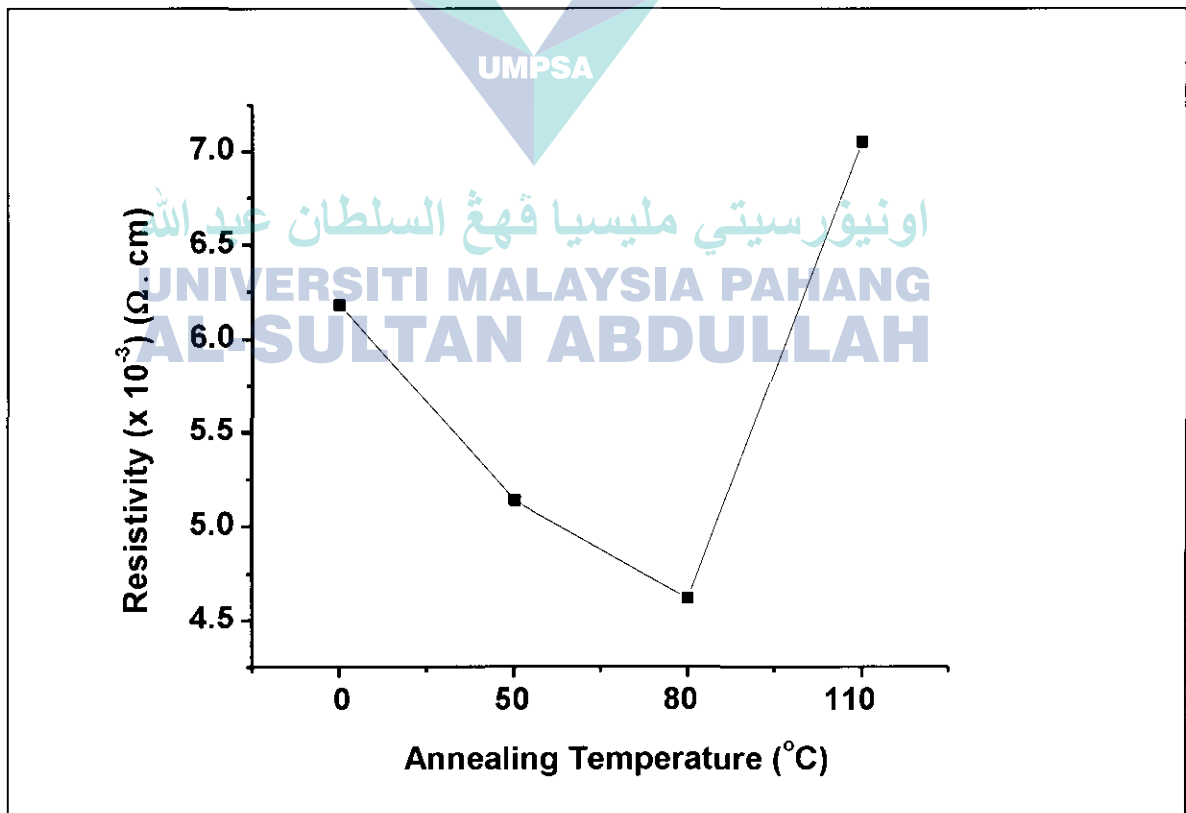


The resistivity and conductivity of the annealed TMED-chelate CuI thin films is shown in Figure 5.18. Compared to the other TMED-chelate CuI thin films, the 100 v% TMED thin film produced the lowest resistivity and the highest conductivity. This could be due to the effect of temperature on the chelating agent as according to van't Hoff equation [176], increasing the temperature will increase the concentration of ligand-metal solution. Thus, temperature effect subsequently will increase the chelate effect to the ligand-metal deposited thin films where the affinity of chelating ligands for a metal ion is further enhanced, thus improving the crystalline structure of the films which contributed to the reduction of electrical resistivity to a certain degree. Besides, the increase of the carrier concentration with increasing annealing temperature due to ionization of oxygen vacancies also contributed to the improvement of electrical conductivity [177]; film densification process will occur with the increase in the annealing temperature resulting in merging of particles which reduces oxygen adsorption on the grain boundaries [178]. This condition decreases carrier trapping

phenomenon in the thin film and increases the conductivity of TMED-chelate thin film. In polycrystalline structure, the crystalline order is limited to small regions called grains and the grain boundary is the area or region between adjacent grains. At the boundary, the atomic arrangement is less ordered than inside the grain and foreign atoms tend to accumulate.

In the presence of oxygen atoms, the conduction electrons near the grain boundary are attracted towards and trapped in the grain boundaries. The condition creates depletion regions close to the grain boundaries which act as barriers to the electron flow from one grain to another. The oxygen desorption in the grain boundaries is an important factor which enhances electrons (holes) mobility in the films hence increasing its conductivity.

**FIGURE 5.18**  
Resistivity of 1:1 Volume Ratio of TMED-Chelate CuI Thin Films at Different Annealing Temperatures.



## 5.4 SUMMARY

The CuI thin films incorporated with TMED as chelating agent have been successfully deposited using drop and spin coating technique and its structural, optical and electrical properties have been characterised. The intrinsic properties of TMED-chelate CuI thin films deposited on glass and ITO substrates prepared with different volume ratios of TMED and different annealing temperatures have been investigated and compared with the CuI thin films without the addition of TMED and without undergoing the annealing process. From the study, it is observed that the properties of the TMED-chelate CuI thin films with the 1:1 ratio of CuI:TMED at 1.0M CuI concentration exhibited good conductivity with low resistivity. The results of the I-V measurement using two point probes shows the resistivity of TMED-chelate CuI thin films deposited using different volumes of TMED decreases with increasing TMED volume percentage. However, the optimum TMED volume percentage is when the ratio to the CuI solution at 1:1. The lowest resistivity of 5.6  $\Omega\cdot\text{cm}$  and highest conductivity of 165  $\text{S}/\text{cm}^2$  is obtained with 100 v% of TMED; the highest resistivity of 28  $\Omega\cdot\text{cm}$  and lowest conductivity of 38  $\text{S}/\text{cm}^2$  is obtained for CuI thin film without the addition of TMED. Characterization of the optical properties also shows that CuI thin films with 1:1 ratio to TMED volume percentage produce good optical absorption. The results matched the findings of some researchers that the ethylenediamine type of ligand is optimum when the volume concentration is the same with the precursor solution [179]. With the thickness of all the deposited thin films maintained at approximately 0.5  $\mu\text{m}$ , the optical band-gap of TMED-chelate CuI thin films is observed to be in the range of 3.15 eV and 3.22 eV. The increase in the carrier concentration with optimum volume ratio as the result of the increased CuI particles in the thin film also contribute to better electrical conductivity as well as electron emission by photoluminescence.

In the study on the effects of annealing temperature on the electrical properties of the thin film, 80°C is found to be the optimum annealing temperature for the film as it produces not only the highest conductivity but also shows better crystalline properties compared to films annealed at other temperatures. However, the structural properties of

the films annealed at any temperature shows very weak peak intensity at (111) and the coexistence of the (200) plane, where both peaks are slightly shifted compared to the films that has not undergone the annealing process. This indicates that the chelating agent, as a consequent of the annealing process, has changed the structure of the films. The optical properties of TMED-chelate CuI thin film annealed at 80°C is better compared to the other thin films as its absorption properties is improved in the visible region and near the UV region. With the absorption energy nearly the same as the original band-gap, it shows that the crystallisation process is improved due to the effect of the chelating agent and the annealing process. Additionally, it is evident from the study that when up to 80°C annealing temperature is used, the annealing process has improved the properties of direct band-gap of the CuI thin films. Also, it is found that the shifting of energy in electron emission towards the longer wavelength, as indicated by the PL spectra, shows that the chelating agent used is a strong type of ligand where photons is absorbed at a shorter wavelength and emitted at longer wavelength. The peak intensity by photoluminescence increases with increasing annealing temperature, where the peak is shifted towards the longer wavelength, and the sample annealed at 80°C produces the highest intensity. The shifting of electron emission to longer wavelength (low energy) is necessary in order to support the dye with an electron, extending the lifetime of the electron once the electrons are excited to TiO<sub>2</sub> of the DSSC device during the fabrication of the DSSC solar cell.

## CHAPTER 6

# PERFORMANCE OF n-TiO<sub>2</sub>/dye/p-CuI INCORPORATED WITH NEW CHELATING AGENT FOR SOLID STATE DYE SENSITIZED SOLAR CELL

### 6.1 INTRODUCTION

To date, one well-known approach that most researchers was to employ in the fabrication of DSSC is to use CuI as holes conductor probably because it is not water-soluble, however, CuI is soluble in acetonitrile at room temperature. Its solubility in acetonitrile is attributed to the formation of weak CuI-acetonitrile adducts whose coordination originates from a significant  $\pi$  back-bonding from cuprous ion to nitrogen, as confirmed by infrared and Raman spectra investigations [180-181]. The formed CuI-acetonitrile adducts are metastable and can easily revert to CuI materials with a ligand missing, but the CuI deposited from acetonitrile solution usually consists of large cubic crystallites resulting in a film with a rough surface. Such a structure cannot form stable and firm contact with other functional materials, hence limiting its application in many optoelectronic devices [89]. Besides, CuI films prepared by evaporating the solution when exposed to light will emit radiation with higher energy than CuI band-gap causing CuI to photo-decompose and iodine is liberated; this photo-decomposition will strongly affect the stability of optical and electronic properties of the film. One example of this emission is when there is variation in the amount of iodine adsorbed on the surface the CuI film resulting in instability of the film.

In this thesis, a novel approach to produce a new CuI-related composite film is demonstrated. This paper introduced an alternative organic chelating agent, called tetramethylethylenediamine (TMED@TMEDA), to be used as CuI crystal growth inhibitor and as an alternative to the previously used chelating agents in the fabrication of DSSCs. Investigation was conducted on the use of the proposed chelating agent in conjunction with eco-friendly p-type materials in the preparation of dye-sensitized solar cells. It is found that highly (111) oriented CuI film with improved quality could be easily

prepared on FTO glass substrate using TMED. Furthermore, the TMED-chelate CuI film exhibit improved band-gap photoluminescence, indicating that TMED is a kind of reagent in inorganic synthesis that is more effective than using either MEISCN or THT. So far, the use of TMED in CuI solution in the fabricating of solid-state DSSC has not yet been reported.

Subsequently an n-TiO<sub>2</sub>/dye/p-CuI solid-state DSSC cell was fabricated and characterized. The chelating agent or ligand that was introduced not only controls the CuI crystal growth and acts as a protective coating for CuI nanocrystals but improves the electrical contact between Titanium dioxide (TiO<sub>2</sub>) particles thus improving the cell performance. Current-voltage characteristics highlighted a larger conversion efficiency of fabricated samples.

## 6.2 EXPERIMENTAL PROCEDURE

Preparation and deposition procedure of TiO<sub>2</sub> thin films has been explained in Section 3.4. The apparatus used for blending the materials and the process used to deposit the films has also been briefed in Section 3.4. After the TiO<sub>2</sub> films have been prepared, the films are soaked for 24 hours in Rhodamine B dye. The preparation and deposition procedure of CuI thin films and TMED-chelate CuI thin films onto dye/TiO<sub>2</sub>/FTO glass substrates using drop and spin coating technique has been explained in Section 3.5.

## 6.3 RESULTS AND DISCUSSION

### 6.3.1 Surface Morphology of N-TiO<sub>2</sub>/Dye/P-CuI

As previously stated there are a number of processes involved in the fabrication of the proposed DSSC cells. In this study the morphology of the deposited films produced after each process was investigated, including that of the TiO<sub>2</sub> film, and this is shown in Figure 6.1. Figure 6.1 (A) shows the morphology of TiO<sub>2</sub> using squeegee method; it is observed that large pores are formed on the

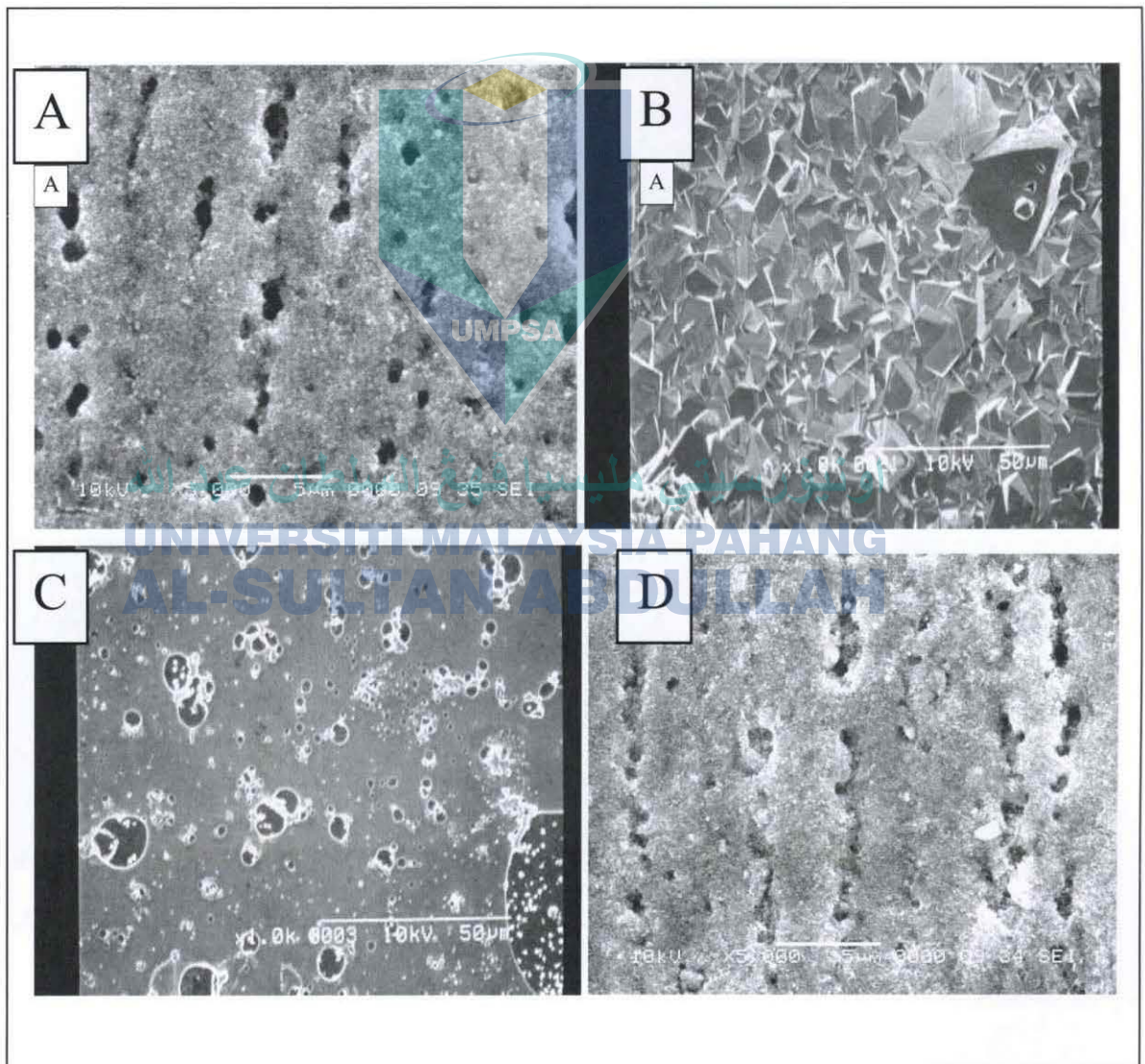
surface of the film and the pores are assumed to also exist inside the film. When these pores are filled with p-type materials, the contact between the dye and p-type materials would be improved [33, 182]. The deposition method employed produces films with a rough surface and the roughness of the surface influences the amount of light that is absorbed, hence affecting the efficiency of energy conversion [183]. The pores and surface roughness of TiO<sub>2</sub> films produces in this study is very much dependent on the volume of polyethylene glycol (PEG) and triton X used, and an appropriate amount of both materials is necessary to prevent the formation of heavy cracks.

The morphology of CuI film prepared without the addition of TMED is presented in Figure 6.1 (B), and large CuI crystals are observed scattered on the deposited film indicating that the crystallization process happened very fast and is uncontrolled [184]. However, the CuI films morphology prepared with the addition of TMED, as shown in Figure 6.1 (C), shows significant reduction in the CuI particles compared to that prepared without the use of TMED showing that TMED can control the crystallization of CuI by acting as a surfactant. From the result, the smaller CuI crystals can better fill the TiO<sub>2</sub> pores, hence improving the contact with the dye monolayer.

Another phenomenon observed in Figure 6.1 (C) is a fine layer covering the CuI crystal surface; the layer serves to reduce immediate contact between the unexposed dyed TiO<sub>2</sub> particles to the CuI crystals, thus reducing the probability of short-circuiting between them. Also, this layer helps decrease degeneration of the CuI due to aging, hence increasing the lifetime of the solar cell [184]. Figure 6.1 (D) shows the morphology of the CuI thin film with the addition of TMED deposited on dye/TiO<sub>2</sub>/FTO substrate. The film is a very thin layer and its surface difference can be seen compared to the TiO<sub>2</sub> only film shown in Figure 6.1 (A), because the reduced CuI crystals size has penetrated deeper into the TiO<sub>2</sub> film, other than covering the surface of the film. One reason for the phenomenon is that the smaller CuI crystals penetrated the pores in the TiO<sub>2</sub> film gradually from surface down into the film, and finally cover the top of the film. Since the

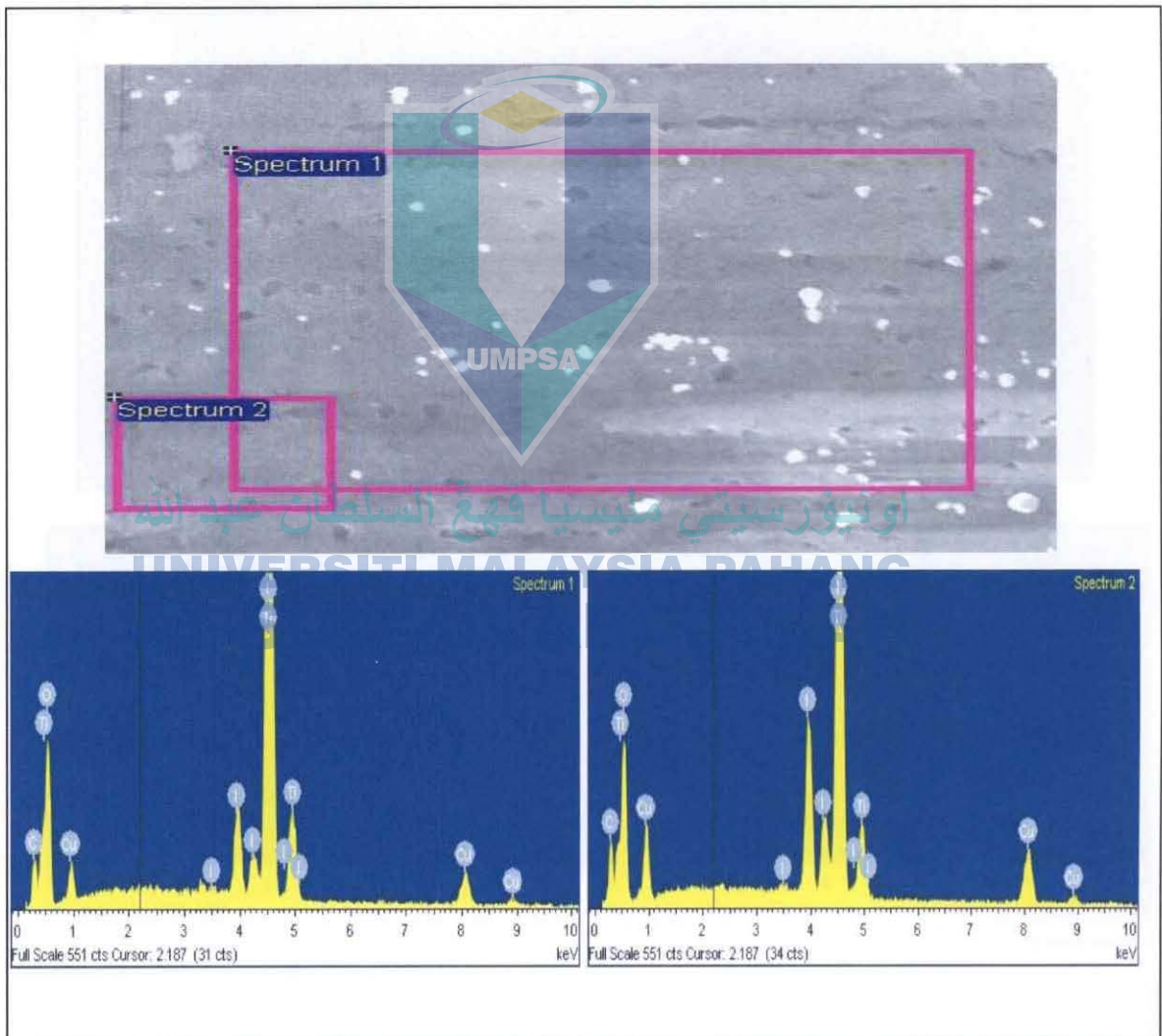
adsorption of TMED in CuI film results in smaller crystals, its average size is determined by the monolayer covering the film. Again, the optimum TMED concentration required was found to be the same order of magnitude as the amount of TMED needed for monolayer coverage of  $\mu\text{m}$  CuI crystallites. TMED being a ligand, its residue, formed at the grain boundaries after evaporation of the solvent, spread into a thin film around the surfaces.

**FIGURE 6.1**  
**The Morphology of Fabricated DSSC Cells (A)  $\text{TiO}_2$  Film, (B) CuI Film without TMED, (C) CuI Film with TMED, (D)  $\text{TiO}_2$ /Dye/CuI (TMED) Film.**



EDX has been performed to verify that the film is composed only of  $\text{TiO}_2$  and  $\text{CuI}$ , and this found to be so as can be seen in spectrum 1 and spectrum 2 shown in Figures 6.2. The EDX revealed that the composite film has only  $\text{TiO}_2$  and  $\text{CuI}$  except that carbon dioxide is also detected which could be from the unresolved TMED element when the film is annealed or due to contamination from the surrounding environment.

**FIGURE 6.2**  
**EDX Measurements on Top of  $\text{TiO}_2/\text{Dye}/\text{CuI}(\text{TMED})$  Film Surface.**



Furthermore, since the  $\text{CuI}$  film is prepared from saturated solutions, all

the particles will not be completely reduced. The particles that underwent incomplete process as growth inhibitor will be left on top of the film as can see in the area of spectrum 1 while the completely reduced particles will gradually penetrate into the pores of  $\text{TiO}_2$  as in spectrum 2.

**FIGURE 6.3**  
EDX Measurement on the Cross-Section of  $\text{TiO}_2$ /Dye/CuI (TMED) Film.

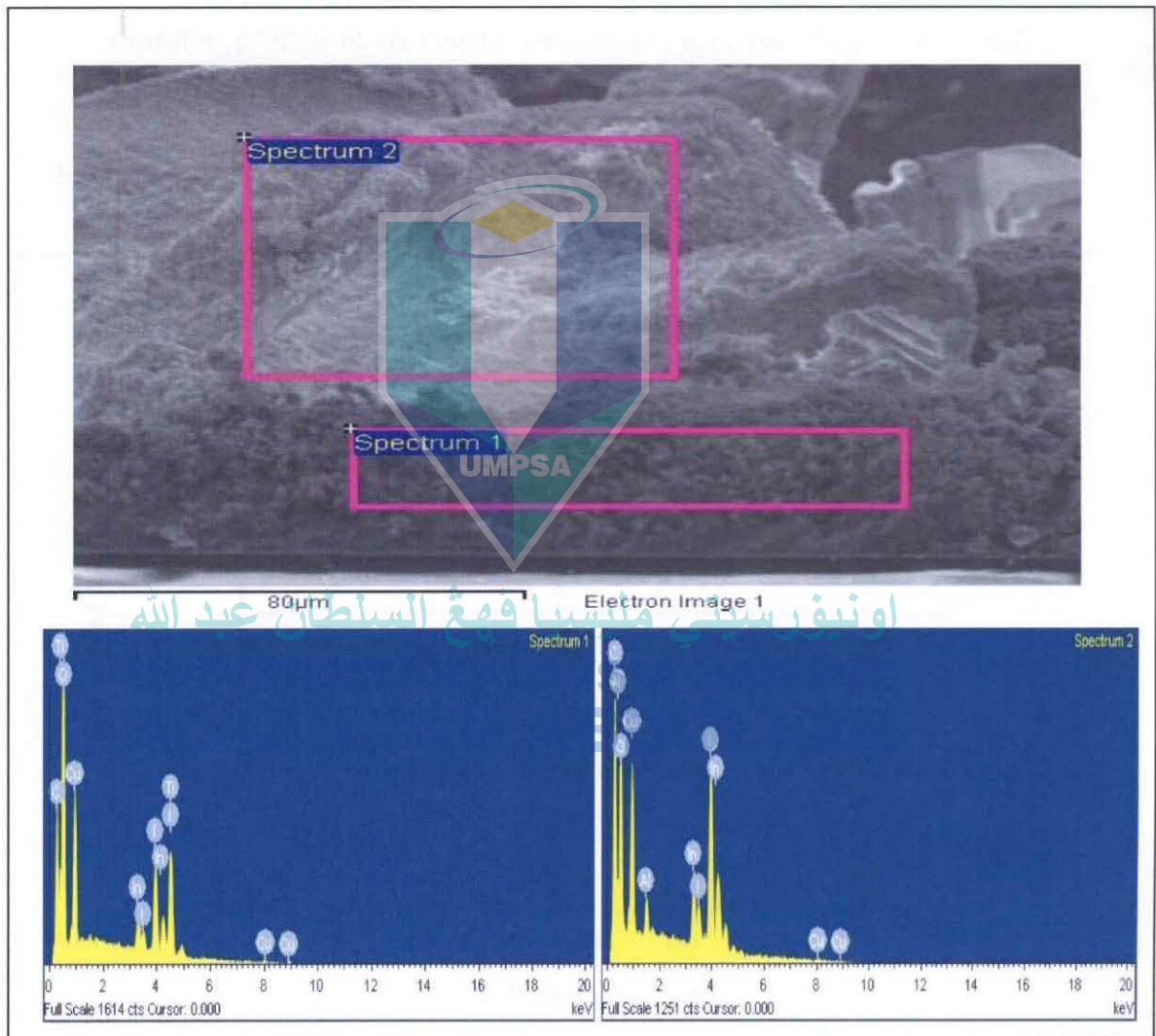


Figure 6.3 shows the EDX measurement, simultaneously represents the SEM images, and of the cross-section of the fabricated films and it is observed

that pore-filling in the TMED-chelate CuI thin films is more advanced. The large opaque areas found in cross-sectional SEM images of the TiO<sub>2</sub> layer signify good pore-filling in those areas, and the EDX measurements proved the covered area is a composite of TiO<sub>2</sub> and CuI film. Other elements that appear in the spectrum, like indium (In), are because the cross-sectional images was taken after the metal contact is deposited on top of the films. Elements like carbon dioxide and aluminum (Al) originate from unresolved TMED element after undergoing the annealing process or are contaminants from the surrounding environment.

**FIGURE 6.4**  
X-Ray Diffraction (XRD) Spectra of the FTO Substrate, TiO<sub>2</sub>/Dye/CuI (TMED) Film, TMED-Chelate CuI Film, and TiO<sub>2</sub> Film.

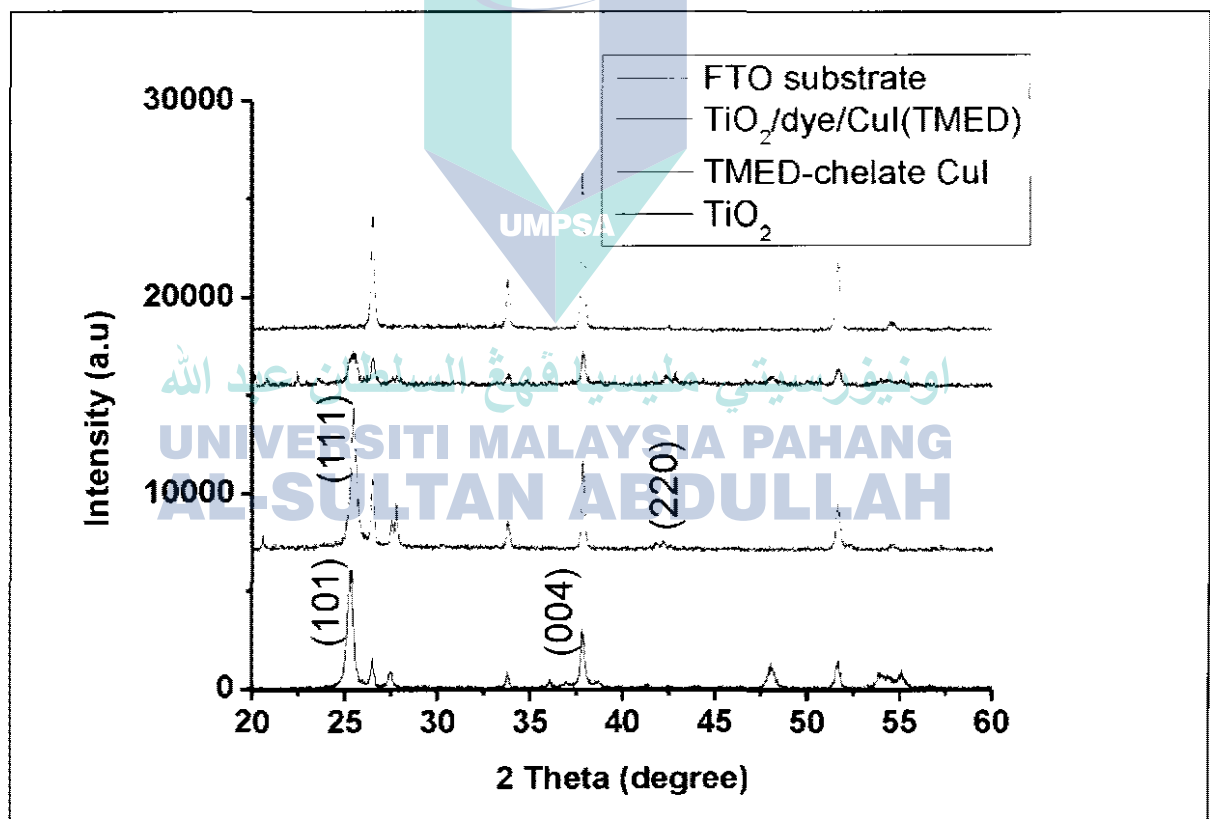


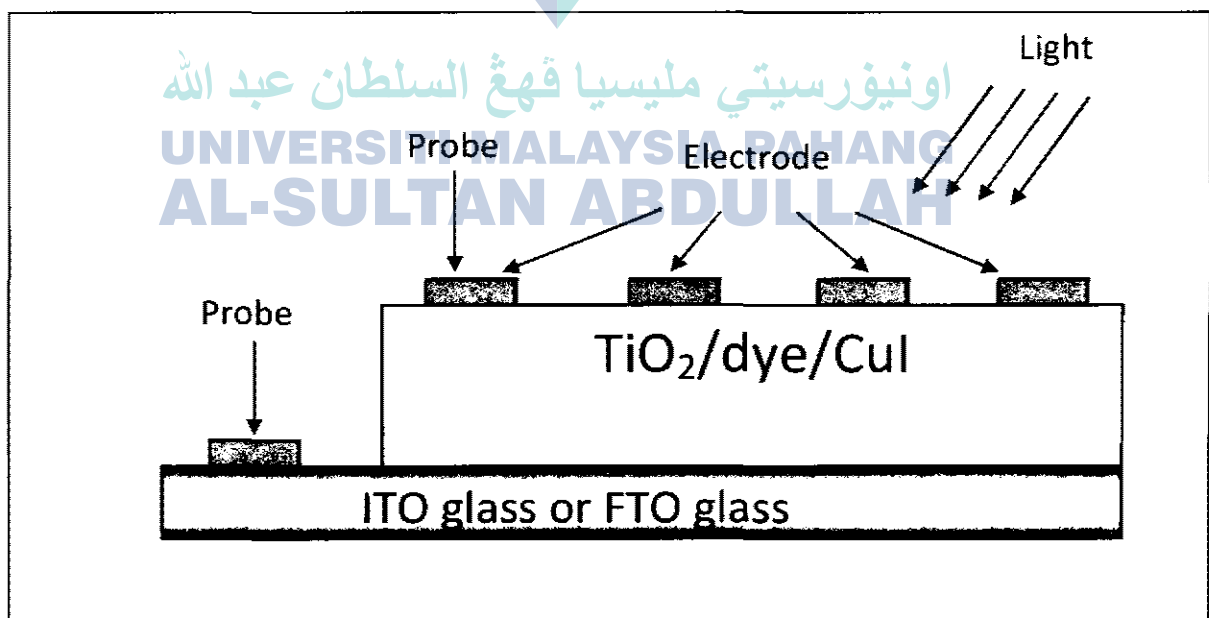
Figure 6.4 shows X-ray diffraction spectra (XRD) for the TiO<sub>2</sub> film, TMED-chelate CuI film, TiO<sub>2</sub>/dye/CuI (TMED) composite film and FTO

substrate. The peaks noted in the  $\text{TiO}_2$  film spectra can be assigned to the  $\text{TiO}_2$  anatase structure and the peaks noted in the TMED-chelate CuI film spectra can be assigned to the CuI polycrystalline  $\gamma$ -phase structure. In the case of  $\text{TiO}_2/\text{dye}/\text{CuI}$  film spectra, other than the  $\text{TiO}_2$  peaks, CuI peaks are also observed. A very strong  $\text{TiO}_2$  (101) and TMED-chelate CuI (111) peaks at  $2\theta$  value around  $25.5^\circ$  can be seen in the composite film proving that it is  $\text{TiO}_2/\text{dye}/\text{CuI}$  film.

### 6.3.2 Electrical Properties of N- $\text{TiO}_2/\text{Dye}/\text{P-CuI}$

The Current-Voltage (I-V) characteristics of the fabricated cells were examined using two-probe solar simulator (BUNKOH KEIKI-CEP2000) where all procedure and measurements are performed under room temperature. An array of indium (In) spots, each 1-mm in diameter, was evaporated on top of composite film as metal contact as shown in Figure 6.5.

**U FIGURE 6.5**  
An Array of Electrodes for the I-V Measurement.



Also shown in the figure is the incident light, maintained at Air Mass (AM) 1.5 (100mW/cm<sup>2</sup>) that illuminated the p-type material during the measurement.

The following equation is used to calculate the efficiency of overall conversion energy,  $\eta_e$  of the photovoltaic cell.

$$\eta_e = (V_{oc} \times I_{sc} \times FF) / P_{inc}$$

where  $V_{oc}$  and  $I_{sc}$  is open-circuit voltage and short-circuit current, respectively, while  $FF$  is the fill factor and  $P_{inc}$  is light sources. Short-circuit current is the current produced at zero voltage while  $V_{oc}$  is the voltage when no current flows. The fill factor  $FF$  is the ratio of maximum obtainable power by calculating the rectangular area under the I-V curve to the product of the open-circuit voltage and short-circuit current. Therefore, the fill factor is given by

$$FF = (V_{max} \times I_{max}) / (V_{oc} \times I_{sc})$$

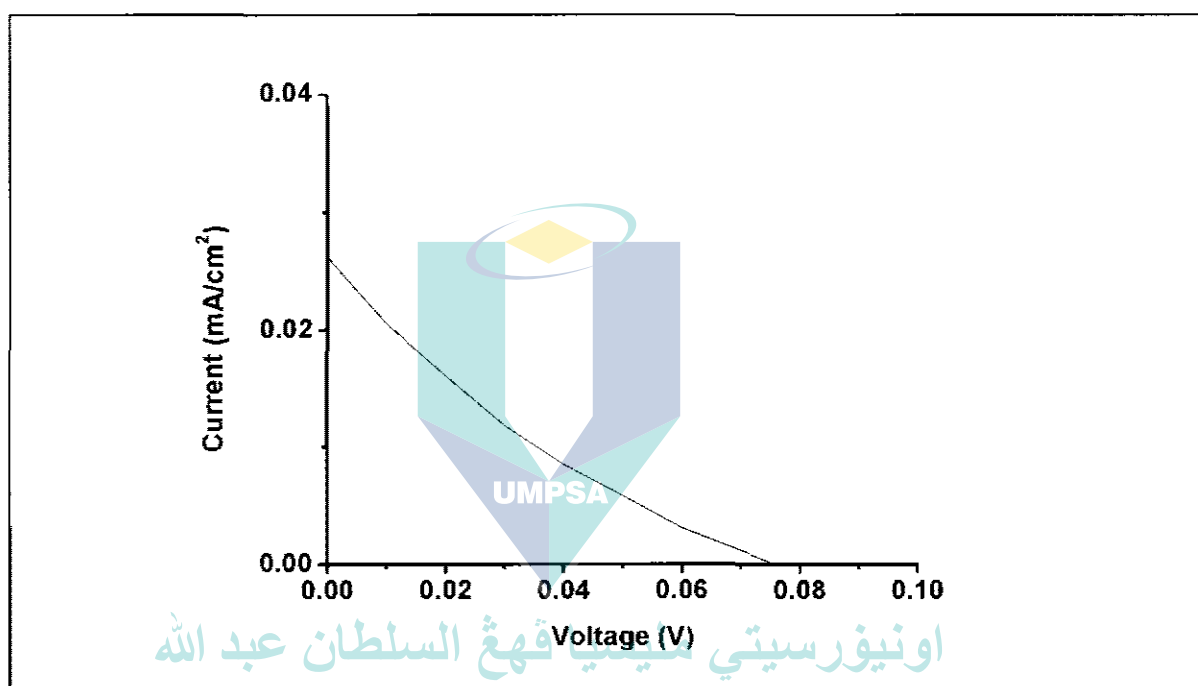
where  $V_{max}$  and  $I_{max}$  are the voltage and current to determine the maximum power point, the point that maximizes  $V \times I$ ; that is, the load for which the cell can deliver maximum electrical power at that level of irradiation.

Figure 6.6 is the investigated photovoltaic performance of TiO<sub>2</sub>/dye/CuI cell prepared without TMED. The characteristic values of the cell are  $V_{oc} = 0.076V$ ,  $I_{sc} = 0.026 \text{ mA/cm}^2$ , a fill factor  $FF = 0.178$  so that the resulting energy conversion efficiency is  $3.54 \times 10^{-4} \%$ . For comparison purposes, the performance of TiO<sub>2</sub>/dye/CuI (TMED) solid-state device DSSC was conducted, and is shown in Figure 6.7. The characteristic values of the cell is as follows:  $V_{oc} = 0.536V$ ,  $I_{sc} = 10.12 \text{ mA/cm}^2$ , a fill factor  $FF = 0.7156$ , and the resulting conversion efficiency of the cell is 3.88%.

All the devices under study were annealed at 80°C of temperature. In the case of CuI films without TMED, it is suggested that the CuI crystals large size results in poor electrical contact between the TiO<sub>2</sub> porous surface and the CuI

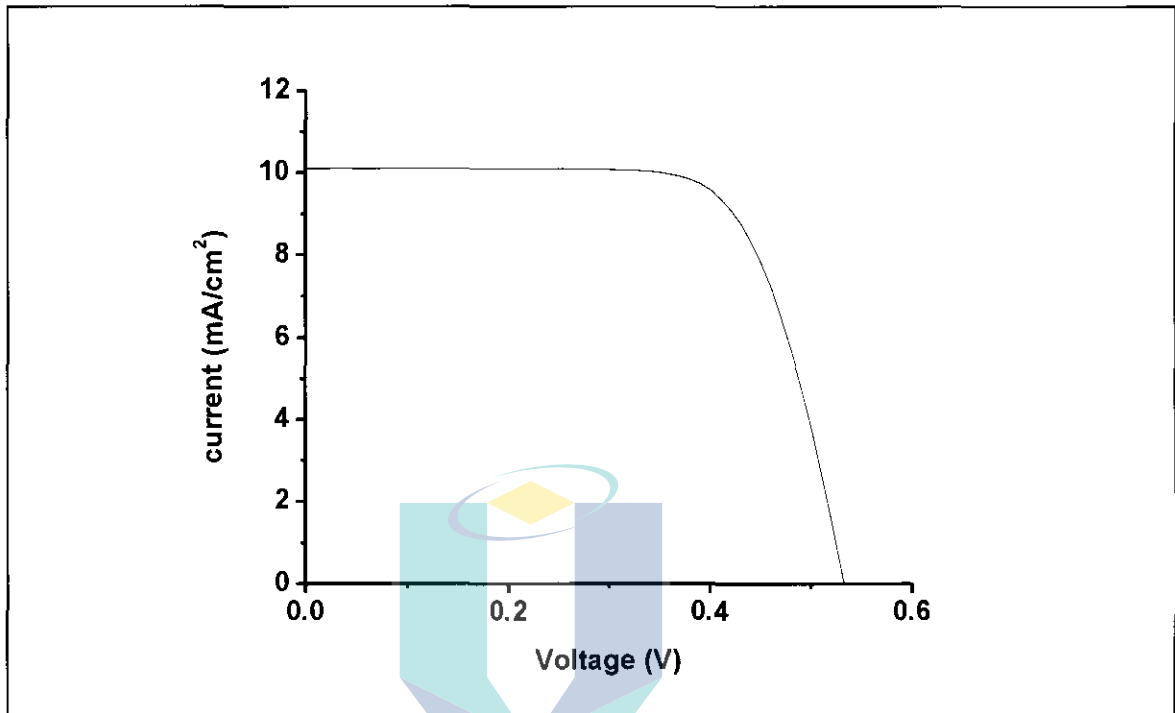
crystal, and improper filling of the pores. The very poor electrical contact decreases the transfer of holes from the dye molecules to the CuI crystal. The uneven pore-filling of the films' void causes a lack in holes transportation in the CuI layer thus decreasing the overall efficiency of the solid-state DSSC [84].

**FIGURE 6.6**  
**I-V Characteristic of TiO<sub>2</sub>/Dye/CuI Film without TMED.**



In the case of CuI films with TMED, the CuI crystals small size together with an almost complete absence of voids in the CuI layer permits good contact between the dyed TiO<sub>2</sub> porous surface and the CuI crystals. Thus, as indicated by the increase in the short-circuit current, the device performance is affected by the pore-filling of the TiO<sub>2</sub> by the p-CuI (TMED) crystals together with the effect of heat energy from the annealing process. This increase indicates an intensification of the charge carriers mobility which create strong electric field inside the cell and is further supported by the complete filling of the pores between the nanoparticles by the transparent holes conductor [84].

**FIGURE 6.7**  
**I-V Characteristic of TiO<sub>2</sub>/Dye/CuI Film with TMED.**



#### 6.4 CONCLUSIONS

This research has demonstrated the operation of CuI solution cells without and with the incorporation of TMED using the drop and spin coating technique to deposit the films onto dye/TiO<sub>2</sub>/FTO substrate, while squeegee method was applied to fabricate the TiO<sub>2</sub> films. Rhodamine B is used as dye in the cells for the purpose of absorbing photon. Indium was evaporated on top of the films in order to characterise the cell's electrical properties. In conclusion, highly efficient solid-state DSSC (TiO<sub>2</sub>/dye/CuI) with improved efficiency was fabricated by controlling the pore-filling of the dyed porous TiO<sub>2</sub> layer with chelating agent capped nanosized CuI crystals. The chelating agent controls the CuI crystal size and protects the CuI crystals from degeneration. Looking at the electrical characteristics of the cells, a very good electrical rectification and photovoltaic efficiency is noted and this shows that the performance of solid-state solar cells is very much dependent on the role of p-type materials pore-filling into TiO<sub>2</sub>. With

incomplete pore-filling, the cell's resistivity is increased causing the degradation of current densities and resulting in poor energy conversion efficiency of the cell under sunlight.

This thesis has shown that TMED-chelate CuI film is a very promising new hole-conductor that can be implemented in solid-state DSSC as it produces relatively high energy conversion efficiency, and it is found photocurrent can be increased with the use of thicker TiO<sub>2</sub> film. The dye used in this study is not necessarily the best absorber to be implemented in solid-state DSSC but the results show that, when interfaced with TiO<sub>2</sub>/dye/CuI, Rhodamine B can produce significant photocurrents.

However, optimization of the various stages of the CuI film's fabrication have yet to be conducted which include parameters such as reproducibility and stability of the cell. An efficient deposition technique should be improved to produce better penetration and distribution of the p-type materials into the TiO<sub>2</sub> pores. Although good penetration and pore-filling is observed, while high energy conversion efficiency has been achieved, there is still room for further improvement in pore-filling, especially down at the lower levels of TiO<sub>2</sub> film. Also, other factors such as electrical contact between the dye and hole conductor, and filling of the TiO<sub>2</sub> pores by p-type materials need further investigation as it gives significant influence on the performance of DSSC cells. As for future work, studies should be carried out to find new techniques that can facilitate more efficient and better distribution of CuI crystals to improve the energy conversion efficiency of DSSC cells.

## CHAPTER 7

### CONCLUSION AND FUTURE WORK

#### 7.1 CONCLUSION

There have been numerous studies conducted by researchers in the field of solid-state DSSC, and it is noted that many of the researchers have used CuI and others p-type materials as holes conductor. However, they have encountered two main problems that have restricted the cell from achieving high energy conversion efficiency. The first problem is the incomplete pore-filling of the nanoporous TiO<sub>2</sub> layer by the holes conductor, and the second problem is the interfacial recombination leading to the degradation of the cell. Several techniques to overcome the problems have been put forward by various researchers, such as using an insulating layer to suppress interfacial recombination, using ALCVD method for thin film preparation, using organic dye with a greater extinction coefficient, using multilayer dye to enhance optical absorption in the IR region, using semiconductor quantum dot to increase absorption in the visible and IR regions, and using better optical design of DSSC. Also, new fabrication techniques are being investigated to improve the efficiency of the cell.

Hence, using CuI as the main precursor, this research has proposed to provide an alternative approach to overcome the weaknesses and disadvantages of solid-state DSSCs by introducing a new chelating agent, or stabilizer, which functions as a ligand in the synthesis of CuI solution for DSSC. This new chelating agent is used to suppress the growth of CuI crystals while simultaneously act as an electron bridge. The function of the proposed chelating agent is similar to THT used by Tennakone, et al. in the preparation of CuI solution, but the proposed chelating agent does not require the complicated chromatography process. The proposed chelating agent used in this research is called tetramethylethylenediamine (TMED @ TMEDA). The main objective of this research is to use CuI as main precursor for holes conductor in solid-state DSSS application and to characterize the structural, optical and electrical properties of nanostructure CuI thin film with and without the addition of TMED into CuI solution. Another objective of the study

is to fabricate n-TiO<sub>2</sub>/dye/p-CuI solid-state DSSC device with and without the addition of TMED in CuI solution, and to characterize their energy conversion efficiency.

In this study, the CuI thin films without and with the addition of TMED have been successfully deposited on glass and ITO substrates using drop and spin coating technique and the thickness of all the fabricated films were maintained at approximately 0.5 μm. The films have been prepared from CuI solutions with different molar concentrations and underwent different annealing temperatures. Increasing the precursor's molar concentration is found to increase the carrier concentration as there are more CuI particles in the thin films and this condition also contribute to better electrical conductivity and UV emission. From the investigating of the effects of molar concentration on the intrinsic properties of the CuI thin films, a precursor of 1.0M concentration is found to exhibit good conductivity and 80°C is found to be the optimum annealing temperature for the thin films. From the results of I-V measurement using two-point probes, the resistivity of CuI thin films increases with increasing CuI molar concentration, where the lowest resistivity is 0.002 Ω.cm at 1.0M concentration and the highest resistivity is 0.049 Ω.cm at 0.05M concentration. Also, it is observed that the optical band-gap of the thin films is in the range of 3.17 eV and 3.18 eV, its optical transmittance improves with increasing CuI molar concentration and the deposited particles on the surface of the substrates is denser.

As for TMED-chelate CuI thin films, the films prepared with different ratios of CuI:TMED and using different annealing temperatures have been successfully deposited on glass and ITO substrates also using drop and spin coating technique. The structural, optical and electrical properties of the film have been characterized and compared to that of CuI thin films without the addition of TMED and without undergoing the annealing process. It is observed that the optimum CuI:TMED ratio is 1:1 with 1.0M CuI molar concentration as the films' electrical properties exhibited highest conductivity and lowest resistivity. Readings from I-V measurement using two point probes indicate that the resistivity of TMED-chelate CuI thin films decreases with increasing CuI:TMED ratio. At the optimum ratio, a low resistivity of 5.6 Ω.cm and a good conductivity of 165 S/cm<sup>2</sup> is measured compared to a high resistivity of 28 Ω.cm and a low conductivity of 38

S/cm<sup>2</sup> is obtained from the CuI thin film prepared without TMED. Also, at the optimum ratio, the films produce good optical absorption and the optical band-gap of the TMED-chelate thin films is observed to be in the range of 3.15 eV and 3.22 eV. This is in agreement with the findings of other researchers who stated that the optimum ratio for ethylenediamine type of ligand is when its volume is the same with that of the precursor solution [179].

As for the effects of annealing temperature on the CuI thin films without the use of TMED, it is found that the optimum annealing temperature is 80°C as the conductivity of the film is highest when annealed at that temperature and its crystalline properties is better compared to films annealed at other temperature. Also, the thin film's optical properties show the highest transparency in the visible and near infra-red (NIR) regions, and the highest absorption in the UV region. Additionally, through photoluminescence (PL), it is found that that the peak intensity of UV emission increases with increasing annealing temperature, and the sample annealed at 80°C produces the highest intensity. Furthermore, it is evident from the study that the properties of direct band-gap of the CuI thin films are improved.

In the case of TMED-chelate CuI thin films, the structure of the films have been altered due to effect of the chelating agent and the annealing temperature as indicated by the very weak peak intensity at the (111) plane and the coexistence of the (200) plane. While the peak intensity by photoluminescence increases with increasing annealing temperature, the films annealed at 80°C produces the highest intensity. However, the optical properties of the films annealed at 80°C is enhanced as absorption is improved in the visible region and near the UV region compared to the thin films that have been annealed at other temperature. Also, the annealing process improves the properties of direct band-gap of the TMED-chelate CuI thin films as the absorption energy is close to the original band-gap. Also, PL shows that there is an energy shift in the electron emission towards the longer wavelength; this shows that the chelating agent used in the study is a strong ligand since photon absorption occurs at shorter wavelength but electron emission occurs at longer wavelength (low energy). The shift in electron emission is

necessary so as to extend the lifetime of the dye once its electron is excited to  $\text{TiO}_2$  of DSSC device during the fabrication of the DSSC solar cell.

Also included in this study is the performance of CuI cells, with and without the addition of TMED, where the films are deposited using drop and dry technique on dye/ $\text{TiO}_2$ /FTO substrates while the  $\text{TiO}_2$  films were prepared using the squeegee method. Rhodamine B was used as dye for absorbing photons, and Indium was evaporated on top of the cells in order to obtain the cell's I-V characteristic. As a result, a solid state DSSC ( $\text{TiO}_2$ /dye/CuI) with improved energy conversion efficiency was successfully fabricated, achieved by controlling the pore-filling of the porous  $\text{TiO}_2$  layer dyed with the chelating agent capped with nanosized CuI crystals. The chelating agent not only controls the crystal size but also protects the CuI crystals from deterioration. Looking at the I-V characterization, the solid-state solar cells showed very good electrical rectification and photovoltaic effects and its performance is very much dependent on the degree of pore-filling of p-type materials into  $\text{TiO}_2$ . If pore-filling is incomplete, the cell's resistivity increases resulting in lower current densities and a poor performance when the cell subjected to sunlight.

This thesis has shown that TMED-chelate CuI thin film is a very promising holes-conductor that can be used in the fabrication of solid state DSSC as the film exhibits high energy conversion efficiency. Also, the photocurrent from the device can be increased with the use of thicker  $\text{TiO}_2$  film, and it has been found that Rhodamine B can produce significant photocurrents in the  $\text{TiO}_2$ /dye/CuI interface.

## 7.2 FUTURE WORK

The findings from this study, though small, but are a significant contribution to the research currently being conducted in the fields of solid-state DSSC. However, there are other aspects related to the fabrication of the device that needs further investigation and optimisation in seeking higher energy conversion efficiency than currently achieved. Such aspects include homogeneity of the deposited holes conductor on dye/ $\text{TiO}_2$  films and the stability of the fabricated cells under continuous illumination.

In spite of the high energy conversion efficiency that has been achieved so far, the pore-filling process should be further investigated so as to better deposit and distribute the p-type particles in the  $\text{TiO}_2$  pores, especially at the lower levels.

Homogeneity across the surface of the cells can be tested by evaporating an array of metal contacts spot as back contact which should output the same efficiency when the I-V probe is attached to any of the spot. However, as observed in this study, this is not the case as there are variations in the homogeneity of the deposited of CuI crystals between the different fabricated cells. Hence, further research should be carried out not only on the deposition and drying processes but also on the nature of the electrical contacts used in the characterisation of the cell.

Further studies should also be carried out on the stability of  $\text{TiO}_2/\text{dye}/\text{CuI}$  cells under illumination, either sealed or exposed to air. Also, the stability seems to be effected by the drying history of the cell, such as under vacuum or argon atmosphere storage. For example, cells tested before vacuum treatment typically show very high series resistance and short-circuit photocurrents but performance of the cell improves after several days of drying.

Finally, it should be possible to use inorganic absorbers with very high absorption coefficient such as lead (II) sulphide (PbS) which have been shown to sensitize  $\text{TiO}_2$  but which are not stable in the electrolyte cells [185]. On the other hand, it remains to be seen if the fill factors in these cells can be brought up to acceptable levels.

## REFERENCES

- [1] S. R.J, "Review of silicon solar cells for high concentrations," *Solar Cells*, vol. 6, pp. 17-38, 1982.
- [2] Images Scientific Instruments (SI), "Photovoltaic Cells - Generating electricity," [www.imagesco.com](http://www.imagesco.com), 2007.
- [3] S. Ranjan, S. Balaji, R. A. Panella, and B. E. Ydstie, "Silicon solar cell production," *Computers & Chemical Engineering*, vol. 35, pp. 1439-1453, 2011.
- [4] D. M. Chapin, , Fuller, C. S. and G. L. Pearson, ,, "A new silicon p-n junction photocell for converting solar radiation into electrical power [3]," *Journal of Applied Physics*, vol. 25, pp. 676-677, 1954.
- [5] K. R. Catchpole, M. J. McCann, K. J. Weber, and A. W. Blakers, "A review of thin-film crystalline silicon for solar cell applications. Part 2: Foreign substrates," *Solar Energy Materials and Solar Cells*, vol. 68, pp. 173-215, 2001.
- [6] C. D. Grant, , Schwartzberg, A. M., Smestad, G. P., Kowalik, J., Tolbert, L. M., and J. Z. Zhang, ,, "Characterization of nanocrystalline and thin film TiO<sub>2</sub> solar cells with poly(3-undecyl-2,2'-bithiophene) as a sensitizer and hole conductor," *Journal of Electroanalytical Chemistry*, vol. 522, pp. 40-48, 2002.
- [7] B. O'Regan, and Grätzel, M., "A low-cost, high efficiency solar cell based on dye-sensitized colloidal TiO<sub>2</sub>films," *Nature Materials*, vol. 353, pp. 737-740, 1991.
- [8] M. Grätzel, "Photoelectrochemical cells," *Nature*, vol. 414, pp. 338-344, 2001.
- [9] M. K. Nazeeruddin, , Kay, A., Rodicio, I., Humphry-Baker, R., Müller, E., Liska, P., Vlachopoulos, N., and M. Grätzel, ,, "Conversion of light to electricity by cis-X<sub>2</sub>bis(2,2'-bipyridyl-4,4'-dicarboxylate)ruthenium(II) charge-transfer sensitizers (X = Cl-, Br-, I-, CN-, and SCN-) on nanocrystalline TiO<sub>2</sub> electrodes," *Journal of the American Chemical Society*, vol. 115, pp. 6382-6390, 1993.
- [10] W. C. Sinke and M. M. Wienk, "Photochemistry: Solid-state organic solar cells," *Nature*, vol. 395, pp. 544-545, 1998.
- [11] M. Matsumoto, , Wada, Y., Kitamura, T., Shigaki, K., Inoue, T., Ikeda, M., and S. Yanagida, ,, "Fabrication of solid-state dye-sensitized TiO<sub>2</sub> solar cell using polymer electrolyte," *Bulletin of the Chemical Society of Japan*, vol. 74, pp. 387-393, 2001.
- [12] T. Taguchi, Zhang, X. T., Sutanto, I., Tokuhiko, K., Tata. N. R., Watanabe, H., Nakamori, H., Uragami, M., and Fujishima, A., "Improving the performance of solid-state dye-sensitized solar cell using MgO-coated TiO<sub>2</sub> nanoporous film," *CHEM. COMMUN.*, vol. 19, pp. 2480-2481, 2003.
- [13] Q. Yang and Gao, "Growth and Photoluminescence Characterization of Highly Oriented CuI/ $\beta$ -Cyclodextrin Hybrid Composite Film," *Langmuir*, vol. 21, pp. 6866-6871, 2005.
- [14] K. Tennakone, Kumara GRRA., Kumara-singhe AR, Wijayantha KGU, and Sirimanne PM., "A dye-sensitized nano-porous solid-state photovoltaic cell," *Semicond. Sci. Technol.*, vol. 10, pp. 1689-1693, 1995.

- [15] G. P. Smestad, , Spiekermann, S., Kowalik, J., Grant, C. D., Schwartzberg, A. M., Zhang, J., Tolbert, L. M., and E. Moons, ,, "A technique to compare polythiophene solid-state dye sensitized TiO<sub>2</sub> solar cells to liquid junction devices," *Solar Energy Materials and Solar Cells*, vol. 76, pp. 85-105, 2003.
- [16] G. R. R. A. Kumara, , Konno, A., Senadeera, G. K. R., Jayaweera, P. V. V., De Silva, D. B. R. A., and K. Tennakone, ,, "Dye-sensitized solar cell with the hole collector p-CuSCN deposited from a solution in n-propyl sulphide," *Solar Energy Materials and Solar Cells*, vol. 69, pp. 195-199, 2001.
- [17] B. O'Regan and D. T. Schwartz, "Large Enhancement in Photocurrent Efficiency Caused by UV Illumination of the Dye-Sensitized Heterojunction TiO<sub>2</sub>/RuLL'NCS/CuSCN: Initiation and Potential Mechanisms," *Chemistry of Materials*, vol. 10, pp. 1501-1509, 1998.
- [18] K. Tennakone, , Kumarasinghe, A.R., Sirimanne, P.M., and G. R. R. A. Kumara, ,, "Chlorophyll-sensitized microporous cuprous iodide photocathode," *Journal of Photochemistry and Photobiology A: Chemistry*, vol. 91, pp. 59-61, 1995.
- [19] K. Tennakone, , Kumara, G. R. R. A., Kottegoda, I. R. M., Wijayantha, K. G. U., and V. P. S. Perera, ,, "A solid-state photovoltaic cell sensitized with a ruthenium bipyridyl complex," *Journal of Physics D: Applied Physics*, vol. 31, pp. 1492-1496, 1998.
- [20] K. Tennakone, , Perera, V. P. S., Kottegoda, I. R. M., and G. R. R. A. Kumara, ,, "Dye-sensitized solid state photovoltaic cell based on composite zinc oxide/tin (IV) oxide films," *Journal of Physics D: Applied Physics*, vol. 32, pp. 374-379, 1999.
- [21] A. K. Shukla, "Turning Sunlight into Electricity: Inorganic Solar Cells and Beyond," *GENERAL ARTICLE RESONANCE*, pp. 42-50, 2006.
- [22] L. Bin, W. Liduo, K. Bonan, W. Peng, and Q. Yong, "Review of recent progress in solid-state dye-sensitized solar cells " *Solar Energy Materials and Solar Cells*, vol. 90, pp. 549-573 2006.
- [23] S. J. Appleyard, "Simple photovoltaic cells for exploring solar energy concepts," *IOP Publishing Ltd*, vol. 41, pp. 409-419, 2006.
- [24] U. Bach, , Lupo, D., Comte, P., Moser, J. E., Weissortel, F., Salbeck, J., Spreitzer, H. and M. Gratzel, ,, "Solid-state dye-sensitized mesoporous TiO<sub>2</sub> solar cells with high photon-to-electron conversion efficiencies," *Nature*, vol. 395, pp. 583-585, 1998.
- [25] Y. Bai, , Cao, Y., Zhang, J., Wang, M., Li, R., Wang, P., Zakeeruddin, S. M. and M. Grätzel, ,, "High-performance dye-sensitized solar cells based on solvent-free electrolytes produced from eutectic melts," *Nature Materials* vol. 7, pp. 626 - 630 2008.
- [26] J. Bandara, , and H. C. Weerasinghe, ,, "Enhancement of photovoltage of dye-sensitized solid-state solar cells by introducing high-band-gap oxide layers," *Solar Energy Materials & Solar Cells*, vol. 88, pp. 341-350, 2005.
- [27] J. Bandara, , and H. Weerasinghe, ,, "Solid-state dye-sensitized solar cell with p-type NiO as a hole collector," *Solar Energy Materials & Solar Cells*, vol. 85, pp. 385-390, 2005.

- [28] K. M. P. Bandaranayake, , Indika Senevirathna, M. K., Prasad Weligamuwa, P. M. G. M. and K. Tennakone, ,, "Dye-sensitized solar cells made from nanocrystalline TiO<sub>2</sub> films coated with outer layers of different oxide materials," *Coordination Chemistry Reviews*, vol. 248, pp. 1277-1281, 2004.
- [29] S. K. Deb, "Dye-sensitized TiO<sub>2</sub> thin-film solar cell research at the National Renewable Energy Laboratory (NREL)," *Solar Energy Materials & Solar Cells*, vol. 88, pp. 1-10, 2005.
- [30] T. Dittrich, , Belaidi, A. and A. Ennaoui, ,, "Concepts of inorganic solid-state nanostructured solar cells," *Solar Energy Materials and Solar Cells*, vol. 95, pp. 1527-1536, 2011.
- [31] D. Gebeyehu, "A SOLID-STATE HYBRID DYE-SENSITIZED TiO<sub>2</sub> SOLAR CELLS USING NOVEL HOLE TRANSPORTING POLY (3-HEXYLTHIOPHENE WITH A CONVERSION EFFICIENCY OF 3%," *African Journal of Science and Technology*, vol. 10, pp. 34 - 41, 2009.
- [32] A. Goetzberger, J. Luther, and G. Willeke, "Solar cells: past, present, future," *Solar Energy Materials & Solar Cells*, vol. 74, pp. 1-11, 2002.
- [33] Fujishima A and Zhang X T., "Solid-state dye-sensitized solar cells," *Proc. Japan Acad.*, vol. 81, pp. 33-42, 2005.
- [34] K. R. Millington, "PHOTOELECTROCHEMICAL CELLS | Dye-Sensitized Cells," in *Encyclopedia of Electrochemical Power Sources*, G. Editor-in-Chief: Jürgen, Ed., ed Amsterdam: Elsevier, 2009, pp. 10-21.
- [35] D.-W. Kim, , Jeong, Yeon-Bok, Kim, Sang-Hern, Lee, Dong-Yoon and J.-S. Song, ,, "Photovoltaic performance of dye-sensitized solar cell assembled with gel polymer electrolyte," *Journal of Power Sources*, vol. 149, pp. 112-116, 2005.
- [36] N. Monishka Rita, "Review: Dye sensitized solar cells based on natural photosensitizers," *Renewable and Sustainable Energy Reviews*, vol. 16, pp. 208-215, 2012.
- [37] Nazeeruddin, Md K., Baranoff, Etienne, and Grätzel Michael, "Dye-sensitized solar cells: A brief overview," *Solar Energy*, vol. 85, pp. 1172-1178, 2011.
- [38] G. C. Vougioukalakis, , Philippopoulos, Athanassios I., Stergiopoulos, Thomas, and P. Falaras, ,, "Contributions to the development of ruthenium-based sensitizers for dye-sensitized solar cells," *Coordination Chemistry Reviews*, vol. 255, pp. 2602-2621, 2011.
- [39] D. Kuang, , Comte, Pascal, Zakeeruddin, Shaik M., Hagberg, Daniel P., Karlsson, Karl Martin, Sun, Licheng, Nazeeruddin, Md K., and M. Grätzel, ,, "Stable dye-sensitized solar cells based on organic chromophores and ionic liquid electrolyte," *Solar Energy*, vol. 85, pp. 1189-1194, 2011.
- [40] M. K. Nazeeruddin and M. Grätzel, "Conversion and Storage of Solar Energy using Dye-sensitized Nanocrystalline TiO<sub>2</sub> Cells," in *Comprehensive Coordination Chemistry II*, J. A. M. Editors-in-Chief: and T. J. Meyer, Eds., ed Oxford: Pergamon, 2003, pp. 719-758.
- [41] M. K. Nazeeruddin, C. Klein, P. Liska, and M. Grätzel, "Synthesis of novel ruthenium sensitizers and their application in dye-sensitized solar cells," *Coordination Chemistry Reviews*, vol. 249, pp. 1460-1467, 2005.

- [42] K. K. Rao, , Hall, D. O., Vlachopoulos, N., Grätzel, M., Evans, M. C. W., and M. Seibert, ,, "Photoelectrochemical responses of photosystem II particles immobilized on dye-derivatized TiO<sub>2</sub> films," *Journal of Photochemistry and Photobiology B: Biology*, vol. 5, pp. 379-389, 1990.
- [43] Fujishima A and Honda K., "Electrochemical photolysis of water at a semiconductor electrode," *Nature*, vol. 238, pp. 37-38, 1972.
- [44] H. Tributsch, "REACTION OF EXCITED CHLOROPHYLL MOLECULES AT ELECTRODES AND IN PHOTOSYNTHESIS\*," *Photochemistry and Photobiology*, vol. 16, pp. 261-269, 1972.
- [45] H. Tsubomura, , Matsumura, M., Nomura, Y., and T. Amamiya, ,, "Dye sensitised zinc oxide: aqueous electrolyte: platinum photocell," *Nature*, vol. 261, pp. 402-403, 1976.
- [46] M. Matsumura, , Matsudaira, Shigeyuki, Tsubomura, Hiroshi, Takata, Masasuke, and H. Yanagida, ,, "Dye Sensitization and Surface Structures of Semiconductor Electrodes," *Industrial & Engineering Chemistry Product Research and Development*, vol. 19, pp. 415-421, 1980/09/01 1980.
- [47] M. Grätzel, "Dye-sensitized solar cells," *Journal of Photochemistry and Photobiology C*, vol. 4, pp. 145-153, 2003.
- [48] A. Fujishima, , Zhang, Xintong, and D. A. Tryk, ,, "TiO<sub>2</sub> photocatalysis and related surface phenomena," *Surface Science Reports*, vol. 63, pp. 515-582, 2008.
- [49] J. J. Lagref, , Nazeeruddin, Md K. and M. Grätzel, ,, "Artificial photosynthesis based on dye-sensitized nanocrystalline TiO<sub>2</sub> solar cells," *Inorganica Chimica Acta*, vol. 361, pp. 735-745, 2008.
- [50] P. Wang, , Zakeeruddin, Shaik M., Moser, Jacques E., Nazeeruddin, Mohammad K., Sekiguchi, Takashi and M. Gratzel, ,, "A stable quasi-solid-state dye-sensitized solar cell with an amphiphilic ruthenium sensitizer and polymer gel electrolyte," *Nat Mater*, vol. 2, pp. 402-407, 2003.
- [51] A. Konno, , Kumara, G. R. A. and K. Tennakone, ,, "Synthesis of thiocyanate molten salts and its application to the solid-state dye-sensitized photovoltaic cells," 2008, p. 575.
- [52] A. Konno, , Kitagawa, T., Kida, H., Kumara, G. R. A. and K. Tennakone, ,, "The effect of particle size and conductivity of CuI layer on the performance of solid-state dye-sensitized photovoltaic cells," *Current Applied Physics*, vol. 5, pp. 149-151, 2005.
- [53] B. Mahrov, , Boschloo, Gerrit, Hagfeldt, Anders, Siegbahn, Hans, and H. Rensmo, ,, "Photoelectron Spectroscopy Studies of Ru(dcbpyH<sub>2</sub>)<sub>2</sub>(NCS)<sub>2</sub>/CuI and Ru(dcbpyH<sub>2</sub>)<sub>2</sub>(NCS)<sub>2</sub>/CuSCN Interfaces for Solar Cell Applications," *The Journal of Physical Chemistry B*, vol. 108, pp. 11604-11610, 2004/08/01 2004.
- [54] B. C. O'Regan and F. Lenzmann, "Charge Transport and Recombination in a Nanoscale Interpenetrating Network of n-Type and p-Type Semiconductors: Transient Photocurrent and Photovoltage Studies of TiO<sub>2</sub>/Dye/CuSCN Photovoltaic Cells," *The Journal of Physical Chemistry B*, vol. 108, pp. 4342-4350, 2004/04/01 2004.
- [55] G. Boschloo, , Marinado, T., Nonomura, K., Edvinsson, T., Agrios, A. G., Hagberg, D. P., Sun, L., Quintana, M., Karthikeyan, C. S., Thelakkat, M. and A.

- Hagfeldt, ,, "A comparative study of a polyene-diphenylaniline dye and Ru(dcbpy)<sub>2</sub>(NCS)<sub>2</sub> in electrolyte-based and solid-state dye-sensitized solar cells," *Thin Solid Films*, vol. 516, pp. 7214-7217, 2008.
- [56] I. K. Ding, , Melas-Kyriazi, John, Cevey-Ha, Ngoc-Le, Chittibabu, Kethinni G., Zakeeruddin, Shaik M., Grätzel, Michael and M. D. McGehee, ,, "Deposition of hole-transport materials in solid-state dye-sensitized solar cells by doctor-blading," *Organic Electronics*, vol. 11, pp. 1217-1222, 2010.
- [57] J. García-Cañadas, Fabregat-Santiago, Francisco, Bolink, Henk J., Palomares, Emilio, Garcia-Belmonte, Germà and J. Bisquert, ,, "Determination of electron and hole energy levels in mesoporous nanocrystalline TiO<sub>2</sub> solid-state dye solar cell," *Synthetic Metals*, vol. 156, pp. 944-948, 2006.
- [58] G. C. Vougioukalakis, A. I. Philippopoulos, T. Stergiopoulos, and P. Falaras, "Contributions to the development of ruthenium-based sensitizers for dye-sensitized solar cells," *Coordination Chemistry Reviews*, vol. 255, pp. 2602-2621, 2011.
- [59] U. Bach, Tachibana, Y., Moser, J. E., Saif, A.H., James R. D., Graätzel, M. and David R. K., "Charge Separation in Solid-State Dye-Sensitized Heterojunction Solar Cells," *J. Am. Chem. Soc.*, vol. 121, pp. 7445-7446, 1999.
- [60] D. I. Kang, , Nicolas T, Je´re´mie B, Brian EH., Eva HS, Samuel JR, Fre´de´ric SE, Grätzel M. and Michael DM, "Pore-Filling of Spiro-OMeTAD in Solid-State Dye Sensitized Solar Cells: Quantification, Mechanism, and Consequences for Device Performance," *Adv. Func. Mat.*, vol. 19, pp. 1-6, 2009.
- [61] X.-t. Zhang, , Sutanto, Irwan, Taguchi, Taketo, Tokuhiro, Kenichi, Meng, Qingbo, Rao, Tata N., Fujishima, Akira, Watanabe, Hiroko, Nakamori, Toshie and M. Uragami, ,, "Al<sub>2</sub>O<sub>3</sub>-coated nanoporous TiO<sub>2</sub> electrode for solid-state dye-sensitized solar cell," *Solar Energy Materials and Solar Cells*, vol. 80, pp. 315-326, 2003.
- [62] C.-C. Yang, , Zhang, Huan Qing and Y. R. Zheng, ,, "DSSC with a novel Pt counter electrodes using pulsed electroplating techniques," *Current Applied Physics*, vol. 11, pp. S147-S153, 2011.
- [63] Y.-H. Chen, , Huang, Kuan-Chieh Chen, Jian-Ging Vittal, R.Ho and Kuo-Chuan, "Titanium flexible photoanode consisting of an array of TiO<sub>2</sub> nanotubes filled with a nanocomposite of TiO<sub>2</sub> and graphite for dye-sensitized solar cells," *Electrochimica Acta*, vol. 56, pp. 7999-8004, 2011.
- [64] X. Hu, , Huang, Kelong, Fang, Dong, and S. Liu, ,, "Enhanced performances of dye-sensitized solar cells based on graphite-TiO<sub>2</sub> composites," *Materials Science and Engineering: B*, vol. 176, pp. 431-435, 2011.
- [65] Z. Huang, , Liu, Xizhe, Li, Kexin, Li, Dongmei, Luo, Yanhong, Li, Hong, Song, Wenbo, Chen, LiQuan, and Q. Meng, ,, "Application of carbon materials as counter electrodes of dye-sensitized solar cells," *Electrochemistry Communications*, vol. 9, pp. 596-598, 2007.
- [66] P. Li, , Wu, Jihuai, Lin, Jianming, Huang, Miaoliang, Huang, Yunfang, and Q. Li, ,, "High-performance and low platinum loading Pt/Carbon black counter electrode for dye-sensitized solar cells," *Solar Energy*, vol. 83, pp. 845-849, 2009.

- [67] Y.-S. Wei, , Jin, Qian-Qian and T.-Z. Ren, ,, "Expanded graphite/pencil-lead as counter electrode for dye-sensitized solar cells," *Solid-State Electronics*, vol. 63, pp. 76-82, 2011.
- [68] B. O'Regan and M. Gratzel, "A low-cost, high-efficiency solar cell based on dye-sensitized colloidal TiO<sub>2</sub> films," *Nature Publishing Group*, vol. 353, pp. 737 - 740, 1991.
- [69] H. Liu, , Avrutin, V., Izyumskaya, N., Özgür, Ü and H. Morkoç, ,, "Transparent conducting oxides for electrode applications in light emitting and absorbing devices," *Superlattices and Microstructures*, vol. 48, pp. 458-484, 2010.
- [70] d. R. Aldo Vieira, "Chapter 14 - Photovoltaic Converters," in *Fundamentals of Renewable Energy Processes (Second Edition)*, ed Boston: Academic Press, 2009, pp. 625-720.
- [71] D. M. Mosher, , Boese, R. E. and R. J. Soukup, ,, "The advantages of Sun tracking for planar silicon solar cells," *Solar Energy*, vol. 19, pp. 91-97, 1977.
- [72] R. Stangl, , Haschke, J., Bivour, M., Korte, L., Schmidt, M., Lips, K. and B. Rech, ,, "Planar rear emitter back contact silicon heterojunction solar cells," *Solar Energy Materials and Solar Cells*, vol. 93, pp. 1900-1903, 2009.
- [73] K. Winz, , Fortmann, C. M., Eickhoff, Th, Beneking, C., Wagner, H., Fujiwara, H. and I. Shimizu, ,, "Novel light-trapping schemes involving planar junctions and diffuse rear reflectors for thin-film silicon-based solar cells," *Solar Energy Materials and Solar Cells*, vol. 49, pp. 195-203, 1997.
- [74] L. Yang, Y. Xuan, Y. Han, and J. Tan, "Investigation on the performance enhancement of silicon solar cells with an assembly grating structure," *Energy Conversion and Management*, vol. 54, pp. 30-37, 2012.
- [75] J. Bisquert and V. S. Vikhrenko, "Interpretation of the Time Constants Measured by Kinetic Techniques in Nanostructured Semiconductor Electrodes and Dye-Sensitized Solar Cells," *The Journal of Physical Chemistry B*, vol. 108, pp. 2313-2322, 2004/02/01 2004.
- [76] K. Tennakone, , Kumara, G. R. R. A., Kottegoda, I. R. M., Perera, V. P. S., and P. S. R. S. Weerasundara, ,, "Sensitization of nano-porous films of TiO<sub>2</sub> with santalin (red sandalwood pigment) and construction of dye-sensitized solid-state photovoltaic cells," *Journal of Photochemistry and Photobiology A: Chemistry*, vol. 117, pp. 137-142, 1998.
- [77] H. Michael A, "A surface science perspective on photocatalysis," *Surface Science Reports*, vol. 66, pp. 185-297, 2011.
- [78] Q. Sun, G. Dong, H. Zhao, J. Qiao, X. Liu, L. Duan, L. Wang, and Y. Qiu, "Modulated intermolecular electrostatic interaction and morphology transition in squarylium dyes based organic field-effect transistors," *Organic Electronics*, vol. 12, pp. 1674-1682, 2011.
- [79] J. Bisquert, A. Zaban, M. Greenshtein, and I. Mora-Seró, "Determination of Rate Constants for Charge Transfer and the Distribution of Semiconductor and Electrolyte Electronic Energy Levels in Dye-Sensitized Solar Cells by Open-Circuit Photovoltage Decay Method," *Journal of the American Chemical Society*, vol. 126, pp. 13550-13559, 2004/10/01 2004.

- [80] S. Wu, H. Han, Q. Tai, J. Zhang, S. Xu, C. Zhou, Y. Yang, H. Hu, B. Chen, and X.-z. Zhao, "Improvement in dye-sensitized solar cells employing TiO<sub>2</sub> electrodes coated with Al<sub>2</sub>O<sub>3</sub> by reactive direct current magnetron sputtering," *Journal of Power Sources*, vol. 182, pp. 119-123, 2008.
- [81] J. R. Durrant, J. N. Clifford, S. A. Haque, T. L. and, and E. Palomares, "Slow charge recombination in dye-sensitized solar cells (DSSC) using Al<sub>2</sub>O<sub>3</sub> coated nanoporous TiO<sub>2</sub> films," *CHEM. COMMUN*, pp. 1464-1465, 2002.
- [82] X.-T. Zhang, H.-W. Liu, T. Taguchi, Q.-B. Meng, O. Sato, and A. Fujishima, "Slow interfacial charge recombination in solid-state dye-sensitized solar cell using Al<sub>2</sub>O<sub>3</sub>-coated nanoporous TiO<sub>2</sub> films," *Solar Energy Materials and Solar Cells*, vol. 81, pp. 197-203, 2004.
- [83] M. Shanmugam, , Baroughi, Mahdi Farrokh and D. Galipeau, ,, "Effect of atomic layer deposited ultra thin HfO<sub>2</sub> and Al<sub>2</sub>O<sub>3</sub> interfacial layers on the performance of dye sensitized solar cells," *Thin Solid Films*, vol. 518, pp. 2678-2682, 2010.
- [84] Q. B. Meng, Takahashi, K., Zhang, X. T., Sutanto, I., Rao, T. N., Sato, O., Fujishima, A., "Fabrication of an Efficient Solid-State Dye-Sensitized Solar Cell," *Langmuir*, vol. 19, pp. 3572-3574, 2003.
- [85] Y. Liu, X. Sun, Q. Tai, H. Hu, B. Chen, N. Huang, B. Sebo, and X.-Z. Zhao, "Influences on photovoltage performance by interfacial modification of FTO/mesoporous TiO<sub>2</sub> using ZnO and TiO<sub>2</sub> as the compact film," *Journal of Alloys and Compounds*, vol. 509, pp. 9264-9270, 2011.
- [86] C. O. Avellaneda, , Gonçalves, Agnaldo D., Benedetti, João E., and A. F. Nogueira, ,, "Preparation and characterization of core-shell electrodes for application in gel electrolyte-based dye-sensitized solar cells," *Electrochimica Acta*, vol. 55, pp. 1468-1474, 2010.
- [87] J. Bandara and U. W. Pradeep, "Tuning of the flat-band potentials of nanocrystalline TiO<sub>2</sub> and SnO<sub>2</sub> particles with an outer-shell MgO layer," *Thin Solid Films*, vol. 517, pp. 952-956, 2008.
- [88] G. Michael, "Dye-sensitized solar cells," *Journal of Photochemistry and Photobiology C: Photochemistry Reviews*, vol. 4, pp. 145-153, 2003.
- [89] G. R. A. Kumara, , Konno, A., Shiratsuchi, K., Tsukahara, J. and K. Tennakone, ,, "Dye-Sensitized Solid-State Solar Cells: Use of Crystal Growth Inhibitors for Deposition of the Hole Collector," *American Chemical Society*, vol. 14, pp. 954-955, 2002.
- [90] G. R. A. Kumara, Kaneko S, Okuya M, Tennakone K., "Fabrication of Dye-Sensitized Solar Cells Using Triethylamine Hydrothiocyanate as a CuI Crystal Growth Inhibitor," *Langmuir*, vol. 18 pp. 10493-10495, 2002.
- [91] R. K. Haynes and S. C. Vonwiller, "N,N,N',N'-Tetramethylethylenediamine," *J. Wiley & Sons, New York*, vol. Encyclopedia of Reagents for Organic Synthesis (Ed: L. Paquette), 2004.
- [92] P. M. Morse and G. S. Girolami, "Are d<sup>0</sup> ML<sub>6</sub> Complexes Always Octahedral? The X-ray Structure of Trigonal Prismatic [Li(tmed)]<sub>2</sub>[ZrMe<sub>6</sub>]," *J. Am. Chem. Soc.*, vol. 111, pp. 4114-5, 1989.

- [93] S. Spiering, A. Eicke, D. Hariskos, M. Powalla, N. Naghavi, and D. Lincot, "Large-area Cd-free CIGS solar modules with In<sub>2</sub>S<sub>3</sub> buffer layer deposited by ALCVD," *Thin Solid Films*, vol. 451-452, pp. 562-566, 2004.
- [94] S. Spiering, D. Hariskos, M. Powalla, N. Naghavi, and D. Lincot, "CD-free Cu(In,Ga)Se<sub>2</sub> thin-film solar modules with In<sub>2</sub>S<sub>3</sub> buffer layer by ALCVD," *Thin Solid Films*, vol. 431-432, pp. 359-363, 2003.
- [95] C.-Y. Hsu, K.-M. Lee, J.-H. Huang, K. R. Justin Thomas, J. T. Lin, and K.-C. Ho, "A novel photoelectrochromic device with dual application based on poly(3,4-alkylenedioxythiophene) thin film and an organic dye," *Journal of Power Sources*, vol. 185, pp. 1505-1508, 2008.
- [96] K. Srinivas, C. R. Kumar, M. A. Reddy, K. Bhanuprakash, V. J. Rao, and L. Giribabu, "D- $\pi$ -A organic dyes with carbazole as donor for dye-sensitized solar cells," *Synthetic Metals*, vol. 161, pp. 96-105, 2011.
- [97] S. Kajiyama, Y. Uemura, H. Miura, K. Hara, and N. Koumura, "Organic dyes with oligo-n-hexylthiophene for dye-sensitized solar cells: Relation between chemical structure of donor and photovoltaic performance," *Dyes and Pigments*, vol. 92, pp. 1250-1256, 2012.
- [98] P. Shen, Y. Liu, X. Huang, B. Zhao, N. Xiang, J. Fei, L. Liu, X. Wang, H. Huang, and S. Tan, "Efficient triphenylamine dyes for solar cells: Effects of alkyl-substituents and  $\pi$ -conjugated thiophene unit," *Dyes and Pigments*, vol. 83, pp. 187-197, 2009.
- [99] Z. Tian, M. Huang, B. Zhao, H. Huang, X. Feng, Y. Nie, P. Shen, and S. Tan, "Low-cost dyes based on methylthiophene for high-performance dye-sensitized solar cells," *Dyes and Pigments*, vol. 87, pp. 181-187, 2010.
- [100] P. K. D. Duleepa P. Pitigala, M. K. Indika Senevirathna, V. P. Susira Perera, and K. Tennakone, "Dye-multilayer semiconductor nanostructures," *Comptes Rendus Chimie*, vol. 9, pp. 605-610.
- [101] R. Sirohi, D. H. Kim, S.-C. Yu, and S. H. Lee, "Novel di-anchoring dye for DSSC by bridging of two mono anchoring dye molecules: A conformational approach to reduce aggregation," *Dyes and Pigments*, vol. 92, pp. 1132-1137, 2012.
- [102] C. S. Karthikeyan, M. Thelakkat, and M. Willert-Porada, "Different mesoporous titania films for solid-state dye sensitised solar cells," *Thin Solid Films*, vol. 511-512, pp. 187-194, 2006.
- [103] Y. Lee and M. Kang, "The optical properties of nanoporous structured titanium dioxide and the photovoltaic efficiency on DSSC," *Materials Chemistry and Physics*, vol. 122, pp. 284-289, 2010.
- [104] P. Sudhagar, R. Sathyamoorthy, and S. Chandramohan, "Influence of porous morphology on optical dispersion properties of template free mesoporous titanium dioxide (TiO<sub>2</sub>) films," *Applied Surface Science*, vol. 254, pp. 1919-1928, 2008.
- [105] S. Li, Y. Liu, G. Zhang, X. Zhao, and J. Yin, "The role of the TiO<sub>2</sub> nanotube array morphologies in the dye-sensitized solar cells," *Thin Solid Films*, vol. 520, pp. 689-693, 2011.
- [106] J. Liu, Y. Wang, and D. Sun, "Enhancing the performance of dye-sensitized solar cells by benzoic acid modified TiO<sub>2</sub> nanorod electrode," *Renewable Energy*, vol. 38, pp. 214-218, 2012.

- [107] L. Meng, T. Ren, and C. Li, "The control of the diameter of the nanorods prepared by dc reactive magnetron sputtering and the applications for DSSC," *Applied Surface Science*, vol. 256, pp. 3676-3682, 2010.
- [108] B. O'Regan, F. Lenzmann, R. Muis, and J. Wienke, "A Solid-State Dye-Sensitized Solar Cell Fabricated with Pressure-Treated P25-TiO<sub>2</sub> and CuSCN: Analysis of Pore Filling," *Chem. Mater.*, vol. 14, pp. 5023-5029, December 16, 2000 2002.
- [109] J. R. Gray, "Conductivity Analyzers and Their Application," *Wiley*, pp. 491-510, 2004.
- [110] M. Bester-Rogac, and Dusan, Habe,, "Modern Advances in Electrical Conductivity Measurements of Solutions," *Acta Chim.*, vol. 53, pp. 391-395, 2006.
- [111] R. P. Buck, S. Rondinini, A. K. Covington, and F. G. K. Baucke, "The measurement of pH- Definition, Standard and Procedures," *Report of the Working Party on pH, IUPAC Provisional Recommendation*, 2001.
- [112] W. H. Bragg, and Bragg, W. L., "X-ray Crystal Structure Analysis in Manchester: from W L Bragg to the Present Day," *Proc. Roy. Soc. London (A)*, vol. 88, p. 428 1913.
- [113] H. P. Klug, and Alexaander, L. E., "X-ray Diffraction Procedure for Crystalline and Amorphous Materials," *Wiley*, p. 662, 1974.
- [114] R. Kartha, Trotier, F., Kreuz, A., and Huber, A., "Spectrophotometer Quantification of Nano-and Standard-Volume Samples," *American Biotechnology Laboratory*, vol. 26, pp. 14-16, 2008.
- [115] E. Ziegler, A., Heinrich, H., Oppermann, and G., Stover,, "Electrical properties and non-stoichiometry in ZnO single crystal," *Phys. Stat. Sol. A.*, vol. 66, p. 63, 1981.
- [116] W. A. Harrison, "Electronic Structure and the Properties of Solids," *Dover Publications*, 1989.
- [117] F. Urbach, "The Long-Wavelength Edge of Photographic Sensitivity and of the Electronic Absorption of Solids," *Phys. Rev.*, vol. 92, p. 1324, 1953.
- [118] S. Johnston, "Photoluminescence and Electroluminescence Imaging Workstation," *NATIONAL RENEWABLE ENERGY LABORATORY*, August 31 2011.
- [119] H. T. Gfroerer and R. A. Meyers, "Photoluminescence in Analysis of Surfaces and Interfaces. In Encyclopaedia of Analytical Chemistry," *John Wiley and Sons Ltd.: Chichester*, pp. 9209-9231, 2000.
- [120] Y. Fedoryshyn, P Ma, P Strasser, M Golling, F Robin, and H Jäckel, , "MBE-growth of thin InGaAs/AlAsSb coupled double quantum wells combined with a vertical waveguiding structure," *14th Europ. MBE Workshop*, March 5-7 2007.
- [121] Donald A. McQuarrie and J. D. Simon, "Physical Chemistry, a molecular approach," *University Science Books*, 1997.
- [122] Y. Pauleau and P. B. Barna, "Protective coatings and thin films: synthesis, characterization, and applications," *Springer*, p. 215, 1997.
- [123] G. B. Kauffman and L. Y. Fang, "Purification of Copper(I) Iodide," *Inorganic Syntheses* vol. 22, pp. 101-103, 1983.

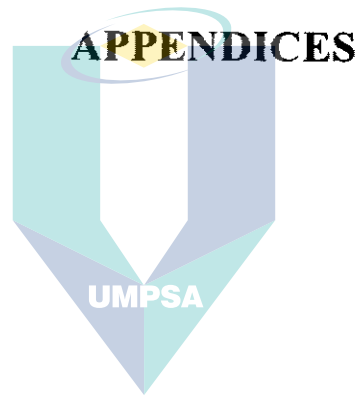
- [124] A. F. Holleman and E. Wiberg, "Inorganic Chemistry," *Academic Press: San Diego*, 2001.
- [125] A. F. Wells, "Structural Inorganic Chemistry," *Oxford University Press, Oxford*, vol. 5th ed., pp. 410-444, 1984.
- [126] K. Tennakone, Kumara, G.R.R.A., Kottegoda, I.R.M., Perera, V.P.S., Aponso, G.M.L.P., and K. G. U. Wijayantha, "Deposition of thin conducting films of CuI on glass," *Solar Energy Materials and Solar Cells*, vol. 55, pp. 283-289, 1998.
- [127] P. M. Sirimanne, and Tributsch, H., "Parameters determining efficiency and degradation of TiO<sub>2</sub>|dye|CuI solar cells," *Journal of Solid State Chemistry*, vol. 177, pp. 1789-1795, 2004.
- [128] J. X. M. Zheng-Johansson and R. L. McGreevy, "A molecular dynamics study of ionic conduction in CuI. II. Local ionic motion and conduction mechanisms," *Solid State Ionics*, vol. 83, pp. 35-48, 1996.
- [129] M. Certier, M. Soltani, O. Pages, A. Zaoui, W. Sekkal, and H. Aourag, "Exciton-polariton reflectance in CuI single crystals," *Materials Science and Engineering*, vol. B58, pp. 234-237, 1999.
- [130] T. Tanaka, K. Kawabata, and M. Hirose, "Transparent, conductive CuI films prepared by rf-dc coupled magnetron sputtering," *Thin Solid Films*, vol. 281-282, pp. 179-181, 1996.
- [131] A. Klapars and S. L. Buchwald, "Copper-Catalyzed Halogen Exchange in Aryl Halides: an Aromatic Finkelstein Reaction," *J. Am. Chem. Soc.*, vol. 124, p. 14845, 2002.
- [132] H. W. Richardson, "Copper Compounds," *Ullmann's Encyclopedia of Industrial Chemistry, Wiley-VCH, Weinheim*, 2005.
- [133] P. M. Sirimanne, T. Soga, and T. Jimbo, "Identification of various luminescence centers in CuI films by cathodoluminescence technique," *Journal of Luminescence*, vol. 105, pp. 105-109, 2003.
- [134] P. M. Sirimanne, M. Rusop, T. Shirata, T. Soga, and T. Jimbo, "Characterization of transparent conducting CuI thin films prepared by pulse laser deposition technique," *Chemical Physics Letters*, vol. 366, pp. 485-489, 2002.
- [135] R. Gana, M. Figueroa, V. Arancibia, and M. Baeza, "Electrochemical production of cuprous iodide using the anode-support system," *Hydrometallurgy*, vol. 51, pp. 87-95, 1999.
- [136] A. Moller, R. Kall, V. Till, G. Wortberg, and G. Adomeit, "Experimental and theoretical investigations of low-pressure CVD of Cu using CuI as precursor," *Journal of Crystal Growth*, vol. 174, p. 837-844, 1997.
- [137] B. R. Sankapal, A. Ennanoui, T. Guminskaya, T. Dittrich, W. Bohne, J. Rohrich, E. Strub, and M. C. Lux-Steiner, "Characterization of p-CuI prepared by the SILAR technique on Cu-tape/n-CuInS<sub>2</sub> for solar cells," *Thin Solid Films*, vol. 480-481, pp. 142-146, 2005.
- [138] M. Gu, P. Gao, X.-L. Liu, S.-M. Huang, B. Liu, C. Ni, R.-K. Xu, and J.-m. Ning, "Crystal growth and characterization of CuI single crystals by solvent evaporation technique," *Materials Research Bulletin*, vol. 45, pp. 636-639, 2010.

- [139] Y.-h. Yan, Y.-c. Liu, L. Fang, Z.-c. Lu, Z.-b. Li, and S.-x. Zhou, "Growth of CuI buffer layer prepared by spraying method," *Transactions of Nonferrous Metals Society of China*, vol. 21, pp. 359-363, 2011.
- [140] A. Jillavenkatesa, S. J. Dapkunas, and L.-S. Lum, "Particle Size Characterization," *NIST Special Publication*, vol. 960-1, 2001.
- [141] Z. Justin, "Stable nanoparticle aggregates/agglomerates of different sizes and the effect of their size on hemolytic cytotoxicity," *Nanotoxicology*, pp. 1-14, 2011.
- [142] I. Landolt-Bornstein, : W. Martienssen (Ed.), "Numerical Data and Functional Relationships in Science and Technology, Group III " *Springer, Berlin*, vol. 41.
- [143] M. Ashokkumar, A. Kudo, and T. Sakata, "Synthesis and characterization of RuS<sub>2</sub> nanocrystallites," *Journal of Materials Science*, vol. 30, pp. 2759-2764, 1995.
- [144] P. Yang, C. Song, M. Lü, G. Zhou, Z. Yang, D. Xu, and D. Yuan, "Photoluminescence of Cu<sup>+</sup>-doped and Cu<sup>2+</sup>-doped ZnS nanocrystallites," *Journal of Physics and Chemistry of Solids*, vol. 63, pp. 639-643, 2002.
- [145] J. Dědeček, B. Wichterlová, and P. Kubát, "Siting of the Cu<sup>+</sup> ions in dehydrated ion exchanged synthetic and natural chabasites: a Cu<sup>+</sup> photoluminescence study," *Microporous and Mesoporous Materials*, vol. 32, pp. 63-74, 1999.
- [146] M. Godlewski, W. E. Lamb, and B. C. Cavenett, "ODMR investigations of IR photoluminescence in ZnS:Cu " *J. Phys. C: Solid State Phys.* , vol. 15, p. 3925, 1982.
- [147] G. Steiner, R. Salzer, and W. Reichelt, "Temperature dependence of the optical properties of CuMoO<sub>4</sub>," *Fresenius' Journal of Analytical Chemistry*, vol. 370, pp. 731-734, 2001.
- [148] Nandita Dasgupta Amitava Dasgupta, "Semiconductor Devices: Modelling And Technology," *Phi Learning*, 2004.
- [149] Chih-Tang Sah, "Fundamentals of Solid-State Electronics," *World Scientific*, 1991.
- [150] C. R. Hammond, "CRC Handbook of Chemistry and Physics," 1913-1995.
- [151] J. H. Lee, D. S. Leem, H. J. Kim, and J. J. Kim, "Effectiveness of p -dopants in an organic hole transporting material," *Applied Physics Letters*, vol. 94, 2009.
- [152] Z. Zheng, A. Liu, S. Wang, B. Huang, K. W. Wong, X. Zhang, S. K. Hark, and W. M. Lau, "Growth of highly oriented (110) [gamma]-CuI film with sharp exciton band," *Journal of Materials Chemistry*, vol. 18, pp. 852-854, 2008.
- [153] K. Prabakar, C. Kim, and C. Lee, "UV, violet and blue-green luminescence from RF sputter deposited ZnO:Al thin films," *Crystal Research and Technology*, vol. 40, pp. 1150-1154, 2005.
- [154] H. S. Kang, G. H. Kim, S. H. Lim, H. W. Chang, J. H. Kim, and S. Y. Lee, "Relationship between ultraviolet emission and electron concentration of ZnO thin films," *Thin Solid Films*, vol. 516, pp. 3147-3151, 2008.
- [155] P. M. Sirimanne, M. Rusop, T. Shirata, T. Soga, and T. Jimbo, "Characterization of CuI thin films prepared by different techniques," *Materials Chemistry and Physics*, vol. 80, pp. 461-465, 2003.
- [156] M. Rusop, T. Shirata, P. M. Sirimanne, T. Soga, T. Jimbo, and M. Umeno, "Study on the properties and charge generation in dye-sensitized n-TiO<sub>2</sub>|dye|p-CuI solid

- state photovoltaic solar cells," *Applied Surface Science*, vol. 252, pp. 7389-7396, 2006.
- [157] Z. Zhou, "pH- and mol-ratio dependent formation of zinc(II) coordination polymers with iminodiacetic acid: Synthesis, spectroscopic, crystal structure and thermal studies," *J. Of Sol. Stat. Chem.*, vol. 182, pp. 2698-2706, 2009.
- [158] S. Ng, "Supramolecular Isomerism in Cadmium Hydroxide Phases. Temperature-Dependent Synthesis and Structure of Photoluminescent Coordination Polymers of  $\alpha$ - and  $\beta$ -Cd<sub>2</sub>(OH)<sub>2</sub>(2,4-pyda)," *Cryst. Grow. & Des.*, vol. 5, pp. 837-839, 2005.
- [159] S. R. Batten, "Coordination Polymers: Design, Analysis and Application," *RSC Publishing*, pp. 297-307, 396-407, 2008.
- [160] J. X. M. Zheng-Johansson and R. L. McGreevy, "A molecular dynamics study of ionic conduction in CuI. II. Local ionic motion and conduction mechanisms," *Solid State Ionics*, vol. 83, pp. 35-48, 1996.
- [161] P. M. Sirimanne and H. Tributsch, "Thiocyanate ligands as crucial elements for regeneration and photo-degradation in TiO<sub>2</sub>|dye|CuI solar cells," *Materials Chemistry and Physics*, vol. 99, pp. 5-9, 2006.
- [162] A. Konno, , Kumara, G. R. A., Hata, R. and K. Tennakone, ,, "Effect of imidazolium salts on the performance of solid-state dyesensitized photovoltaic cell using copper iodide as a hole collector," *Electrochemistry*, vol. 70, pp. 432-434, 2002.
- [163] E. I. Givargizov, A. B. Limanov, L. A. Zadorozhnaya, M. A. Lazarenko, and I. G. Lukina, "Artificial epitaxy (graphoepitaxy) of semiconductors," *Journal of Crystal Growth*, vol. 65, pp. 339-342, 1983.
- [164] A. B. Limanov and E. I. Givargizov, "Control of the structure in zone-melted silicon films on amorphous substrates," *Materials Letters*, vol. 2, pp. 93-96, 1983.
- [165] M. Izaki, "Light-assisted chemical deposition of highly (0001) oriented zinc oxide film," *Chemical Communications*, pp. 476-477, 2002.
- [166] N. Brabez, R. M. Lynch, L. Xu, R. J. Gillies, G. Chassaing, S. Lavielle, and V. J. Hruby, "Design, Synthesis, and Biological Studies of Efficient Multivalent Melanotropin Ligands: Tools toward Melanoma Diagnosis and Treatment," *Journal of Medicinal Chemistry*, vol. 54, pp. 7375-7384, 2011/10/27 2011.
- [167] Z. A. Li, W. Wu, G. Qiu, G. Yu, Y. Liu, C. Ye, J. Qin, and Z. Li, "New series of AB<sub>2</sub>-type hyperbranched polytriazoles derived from the same polymeric intermediate: Different endcapping spacers with adjustable bulk and convenient syntheses via click chemistry under copper(I) catalysis," *Journal of Polymer Science Part A: Polymer Chemistry*, vol. 49, pp. 1977-1987, 2011.
- [168] S. M. Silberberg, "Chemistry: The Molecular Nature of Matter and Change (4th ed.)," *New York: McGraw Hill Company*, 2006.
- [169] A. P. Alivisatos, "Semiconductor Clusters, Nanocrystals, and Quantum Dots," *Science*, vol. 271, pp. 933-937, February 16, 1996 1996.
- [170] A. P. Alivisatos, "Perspectives on the Physical Chemistry of Semiconductor Nanocrystals," *The Journal of Physical Chemistry*, vol. 100, pp. 13226-13239, 1996/01/01 1996.

- [171] V. P. S. Perera, M. K. I. Senevirathna, P. K. D. D. P. Pitigala, and K. Tennakone, "Doping CuSCN films for enhancement of conductivity: Application in dye-sensitized solid-state solar cells," *Solar Energy Materials and Solar Cells*, vol. 86, pp. 443-450, 2005.
- [172] S. H. Yoon and D.-J. Kim, "Effect of substrate on the preferred orientation of ZnO films by chemical solution deposition," *Journal of Crystal Growth*, vol. 303, pp. 568-573, 2007.
- [173] S. H. Yoon, D. Liu, D. Shen, M. Park, and D. J. Kim, "Effect of chelating agents on the preferred orientation of ZnO films by sol-gel process," *J Mater Sci*, vol. 43, pp. 6177-6181, 2008.
- [174] H. Guo, M. Yin, N. Dong, M. Xu, L. Lou, and W. Zhang, "Effect of heat-treatment temperature on the luminescent properties of Lu<sub>2</sub>O<sub>3</sub>:Eu film prepared by Pechini sol-gel method," *Applied Surface Science*, vol. 243, pp. 245-250, 2005.
- [175] Y. Huang, M. Liu, Z. Li, Y. Zeng, and S. Liu, "Raman spectroscopy study of ZnO-based ceramic films fabricated by novel sol-gel process," *Materials Science and Engineering: B*, vol. 97, pp. 111-116, 2003.
- [176] P. Atkins and J. De Paula, "Physical Chemistry (8th ed.)," *W.H. Freeman and Company*, p. 212, 2006.
- [177] J.-K. Yang, W. S. Kim, and H.-H. Park, "The effect of excess Pb content on the crystallization and electrical properties in sol-gel derived Pb (Zr<sub>0.4</sub>Ti<sub>0.6</sub>)O<sub>3</sub> thin films," *Thin Solid Films*, vol. 377-378, pp. 739-744, 2000.
- [178] H. Liu, J. Li, Z. Zhang, Z. Gong, and Y. Yang, "The effects of sintering temperature and time on the structure and electrochemical performance of LiNi & cathode materials derived from sol-gel method," *Journal of Solid State Electrochemistry*, vol. 7, pp. 456-462, 2003.
- [179] N. Greenwood Norman and E. Alan, "Chemistry of the Elements (2nd ed.)," *Oxford: Butterworth-Heinemann*, p. 910, 1997.
- [180] J. Zarembowitch and R. Maleki, "Copper(I) halide adducts with acetonitrile: an infrared and Raman investigation," *Spectrochimica Acta Part A: Molecular Spectroscopy*, vol. 39, pp. 43-46, 1983.
- [181] A. Bell, R. A. Walton, D. A. Edwards, and M. A. Poulter, "Cationic copper(I) isocyanide complexes, [Cu(CNR)<sub>4</sub>]<sup>+</sup> (R = CH<sub>3</sub>, C(CH<sub>3</sub>)<sub>3</sub> and 2,6-(CH<sub>3</sub>)<sub>2</sub>C<sub>6</sub>H<sub>3</sub>): Preparations, spectroscopic properties and reactions with neutral ligands. A comparison of the vibrational spectra of [Cu(CNCH<sub>3</sub>)<sub>4</sub>]<sup>+</sup>, [Cu(NCCH<sub>3</sub>)<sub>4</sub>]<sup>+</sup> and [Cu(NCCD<sub>3</sub>)<sub>4</sub>]<sup>+</sup>," *Inorganica Chimica Acta*, vol. 104, pp. 171-178, 1985.
- [182] Schmidt-Mende L. and Grätzel M., "TiO<sub>2</sub> pore-filling and its effect on the efficiency of solid-state dye-sensitized solar cells," *Thin Solid Films*, vol. 500, pp. 296-301, 2006.
- [183] A. Fujishima and X.-T. Zhang, "Chapter 9 - Solid-State Dye-Sensitized Solar Cells," in *Nanostructured Materials for Solar Energy Conversion*, S. Tetsuo, Ed., ed Amsterdam: Elsevier, 2006, pp. 255-273.
- [184] A. R. Zainun, S. Tomoya, U. Mohd Noor, M. Rusop, and I. Masaya, "New approach for generating Cu<sub>2</sub>O/TiO<sub>2</sub> composite films for solar cell applications," *Materials Letters*, vol. 66, pp. 254-256, 2012.

- [185] R. Vogel, P. Hoyer, and H. Weller, "Quantum-Sized PbS, CdS, Ag<sub>2</sub>S, Sb<sub>2</sub>S<sub>3</sub> and Bi<sub>2</sub>S<sub>3</sub> particles as Sensitizers for Various Nanoporous Wide-Bandgap Semiconductors," *J. Phys. Chem.*, vol. 98, pp. 3183-3188, 1994.
- [186] I. Kaiser, K. Ernst, C. H. Fischer, R. Könenkamp, C. Rost, I. Sieber, and M. C. Lux-Steiner, "Eta-solar cell with CuInS<sub>2</sub>: A photovoltaic cell concept using an extremely thin absorber (eta)," *Solar Energy Materials and Solar Cells*, vol. 67, pp. 89-96, 2001.
- [187] A. J. Nozik, "Quantum dot solar cells," *Physica E: Low-dimensional Systems and Nanostructures*, vol. 14, pp. 115-120, 2002.
- [188] H. Tsukigase, Y. Suzuki, M.-H. Berger, T. Sagawa, and S. Yoshikawa, "Synthesis of SnS Nanoparticles by SILAR Method for Quantum Dot-Sensitized Solar Cells," *J. Nanosci. Nanotech.*, vol. 11, pp. 1914-1922, 2011.
- [189] K. Ernst, Belaidi A, and Könenkamp R., "Solar cell with extremely thin absorber on highly structured substrate," *Semicond. Sci. Technol.*, vol. 18, pp. 475-479, 2003.
- [190] M. Nanu, J. Schoonman, and A. Goossens, "Solar-energy conversion in TiO<sub>2</sub>/CuInS<sub>2</sub> nanocomposites," *Adv. Func. Mat.*, vol. 15, pp. 95-100, 2005.
- [191] Yu Wang, Hao Gong, Benhu Fan, and Guangxia Hu, "Photovoltaic Behavior of Nanocrystalline SnS/TiO<sub>2</sub>," *J. Phys. Chem.*, vol. 114, pp. 3256-3259, 2010.
- [192] M. Izaki, T. Shinagawa, K. T. Mizuno, Y. Ida, M. Inaba, and A. Tasaka, "Electrochemically constructed p-Cu<sub>2</sub>O/n-ZnO heterojunction diode for photovoltaic effect," *J. Phys. D: Appl. Phys.*, vol. 40, pp. 3326-3329, 2007.
- [193] J. Cui and Gibson UJ, "A Simple Two-Step Electrodeposition of Cu<sub>2</sub>O/ZnO Nanopillar," *Solar Cells. J. Phys. Chem. C*, vol. 114, pp. 6408-6412, 2010.
- [194] E. W. McFarland, W. Siripala, A. Ivanovskaya, T. F. Jaramillo, and S. H. Baeck, "A Cu<sub>2</sub>O/TiO<sub>2</sub> heterojunction thin film cathode for photoelectrocatalysis," *Solar Energy Materials & Solar Cells*, vol. 77 pp. 229-237, 2003.
- [195] D. Li, C.-J. Chien, S. Deora, P.-C. Chang, E. Moulin, and J. G. Lu, "Prototype of a scalable core-shell Cu<sub>2</sub>O/TiO<sub>2</sub> solar cell," *Chemical Physics Letters*, vol. 501, pp. 446-450, 2011.
- [196] B. Zhou, L. Zhiguo, W. Hongxia, Y. Yanqiang, and S. Wenhui, "Experimental Study on Photocatalytic Activity of Cu<sub>2</sub>O/Cu Nanocomposites Under Visible Light," *Catal. Lett.*, vol. 132, pp. 75-80, 2009.



اونيورسيتي مليسيا قهغ السلطان عبد الله  
**UNIVERSITI MALAYSIA PAHANG**  
**AL-SULTAN ABDULLAH**

## APPENDIX A:

### Fabricating Cu<sub>2</sub>O/TiO<sub>2</sub> Composite Film for Solar Cell Applications

#### 1.1 Introduction

TiO<sub>2</sub>, an n-type semiconductor having band-gap energy of 3.2 eV, was founded by Akira Fujimura and has become the semiconductor of choice for use as mesoporous electrode in the Gratzel cell where it act as quite an efficient solar energy convertor. Originally, Fujimura et al. experimented TiO<sub>2</sub> as a photo-function in the photo-electrochemical water splitting, but other researchers have shown that it has many advantages in the fields of sensitized photochemistry and photo-electrochemistry [43, 48]. It is inexpensive in cost, abundantly available and non-toxic. TiO<sub>2</sub> is highly stable in electrolytic solution, has almost an ideal energy band positions for the PEC, and has become the dominant material for environmental photo-catalysis. In the case of Gratzel cell, under normal sunlight, the ruthenium dye can maintain 10<sup>8</sup> redox cycles without perceptible loss of performance, and is assumed to withstand up to 20 years of continuous operation [47, 49].

The problems related to solid-state DSSCs could be overcome by employing extremely thin absorber (ETA) solar cells or quantum dot (QD) sensitized solar cells, which are conceptually similar to solid-state DSSCs [33, 186-188]. In these solar cells, a small band-gap p-type semiconductor, such as CuInS<sub>2</sub>, CdTe and SnS, is used in place of the molecular dye normally used in DSSC acting as a photon absorber in the cells [189-191]. The p-type semiconductor typically is spread over the surface of the n-type semiconductor film, which is usually TiO<sub>2</sub>. The structure of the ETA and QD solar cells is such that light absorption is enhanced due to surface enlargement and multiple scattering [33, 187]. Nanu et al. [190] generated TiO<sub>2</sub>/CuInS<sub>2</sub> solar cells using an atomic layer chemical vapour deposition method (ALCVD) with 4% solar energy conversion efficiency. Also, the TiO<sub>2</sub>/CdTe cells fabricated by Ernst et al. [189] exhibited an open-circuit voltage of 0.67V and a short-circuit current of 8.9mA cm<sup>-2</sup> under 100 mW cm<sup>-2</sup> of simulated sunlight.

Based on these reviews, the use of cuprous oxide ( $\text{Cu}_2\text{O}$ ), a p-type solar cell material, is proposed for use as a photon absorber in conjunction with  $\text{TiO}_2$  for solar cell applications [184].  $\text{Cu}_2\text{O}$ , with a direct band-gap of 2.1 eV, is regarded as a suitable material for high-efficiency solar cells [192-193], and McFarland et al. observed a photo response in a photo electrochemical cell when they created a  $\text{Cu}_2\text{O}/\text{TiO}_2$  heterojunction thin film [194]. Meanwhile Li et al. has successfully prepared a core shell  $\text{Cu}_2\text{O}/\text{TiO}_2$  solar cell with an efficiency  $\sim 0.01\%$  [195]. Hence, it may be concluded that the combination of  $\text{Cu}_2\text{O}$  and  $\text{TiO}_2$  could contribute to efficient photoelectric conversion. In this research,  $\text{Cu}_2\text{O}/\text{TiO}_2$  composite thin films were generated through a combination of squeegee and electrochemical deposition (ECD) methods, and a cell was fabricated by attaching metal electrodes on the film. The structural and optical properties of the fabricated films were characterized, and the photo response of the cell was measured [184].

## 1.2 Experimental Procedures

$\text{TiO}_2$  films with thickness around  $16\mu\text{m}$  were prepared by squeegee method using 0.8g/ml  $\text{TiO}_2$  paste of  $\text{TiO}_2$  powders (P25, Aerosol Japan). 0.5ml acetyl acetone was added into the powder and stirred by hand until light yellow color appeared. 5mL of water was divided into two parts which is 2mL + 3 mL and was added to paste and stirred again by hand in 5 minutes of time for each step. The mixed materials were then blended by mortar at 20 minutes. After that, 0.4g polyethylene glycol and 2.5ml triton X were added and blended again around 5min in each process. Then the  $\text{TiO}_2$  paste was deposited on FTO substrate and annealed at  $100^\circ\text{C}$  and  $400^\circ\text{C}$  for 30 minutes each at room temperature. The substrate used was F-doped  $\text{SnO}_2$  (FTO) coated glass. The apparatus and the process of depositing the thin films are shown in Figure 3.4 of chapter 3 and the process flow of the preparation and deposition of the thin film is summarized as in Figure 3.5 in the same chapter.

On the other hand, the deposition of  $\text{Cu}_2\text{O}$  on  $\text{TiO}_2/\text{FTO}$  substrate by ECD was conducted using three electrode cells with a saturated calomel electrode (SCE) as the

reference electrode. FTO/TiO<sub>2</sub> nanoporous electrode was used as the working electrode and a platinum sheet was used as the counter electrode. An aqueous solution containing 0.5 mol copper (II) sulphate (CuSO<sub>4</sub>) is dissolved in 20ml of pure water where a blue color of solution is appeared. 6ml lactic acid was added in to form copper lactate complex. The solution pH was then adjusted until the pH of solution around 12.5 with KOH. At this point, the physical color of the solution changes to dark blue. The electrochemical deposition on the FTO/TiO<sub>2</sub> substrate by galvano static was carried out at current density -1 mA/cm<sup>2</sup> and the deposition time was 10 minutes unless otherwise stated. After the experiment ended, the deposited film were washed in pure water and naturally dried in air. The method used for deposition of Cu<sub>2</sub>O is shown in Figure 1.1. The preparation of the thin films can be summarized in Figure 1.2 of process flow diagram.

**FIGURE 1.1**  
Schematic Diagram of Electrochemical Deposition (ECD) Method.

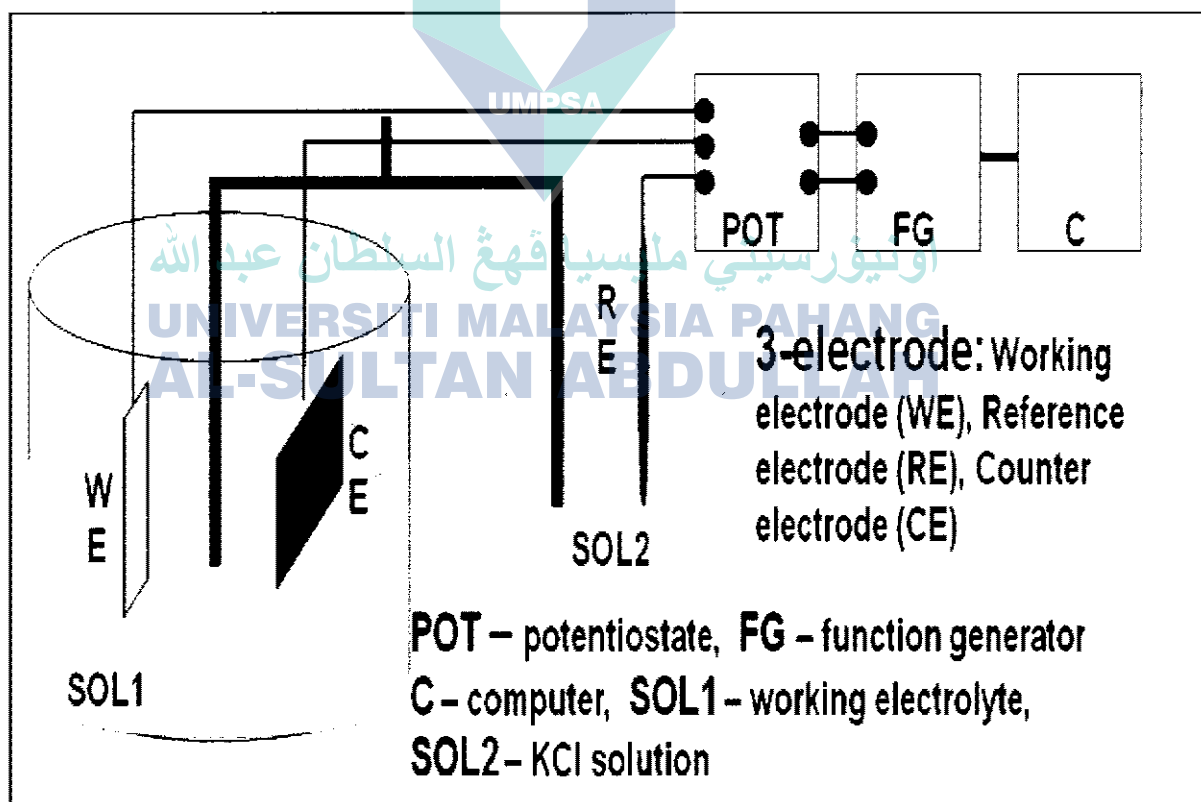
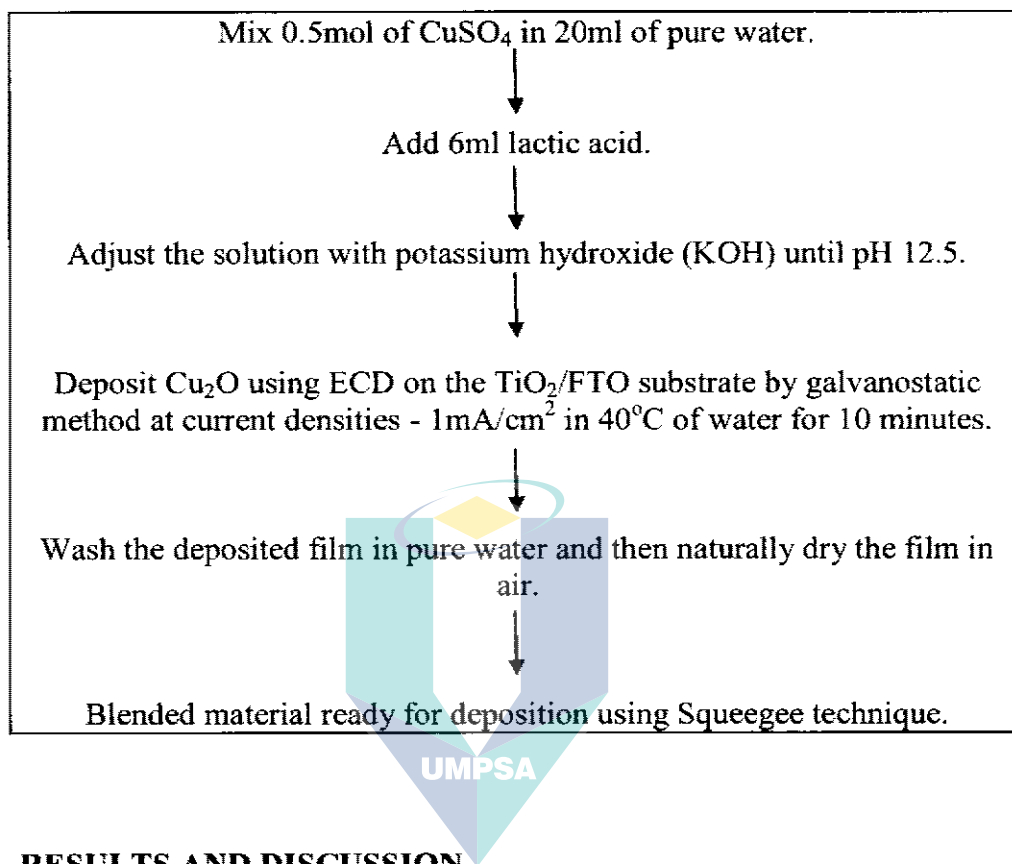


**FIGURE 1.2**  
**Process Flow Diagram for Preparation and Deposition of Cu<sub>2</sub>O Thin Films.**



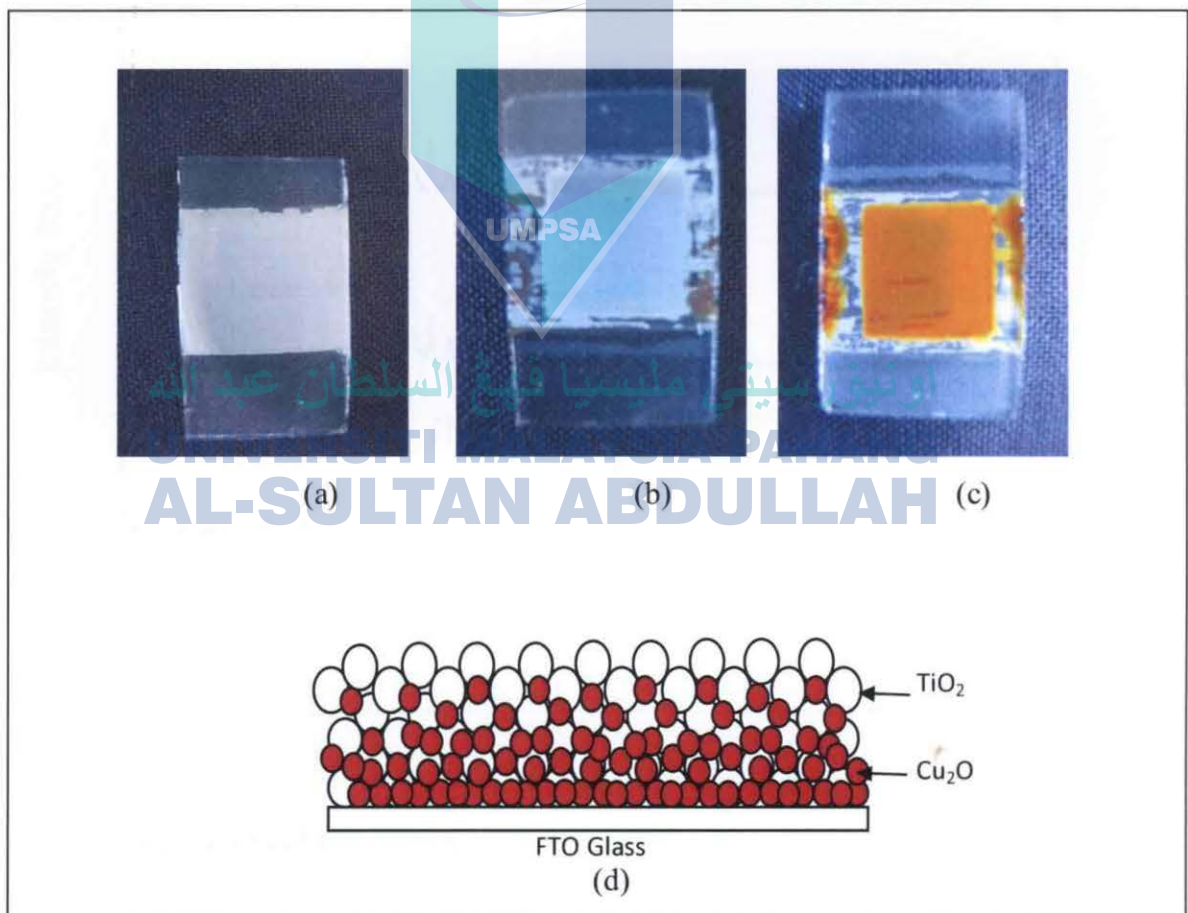
### 1.3 RESULTS AND DISCUSSION

#### 1.3.1 Structural Properties

The physical morphologies of the films are shown in Figure 7.3 (a), (b) and (c). After the deposition process using the squeegee method, the TiO<sub>2</sub> film is white in colour as in Figure 7.3 (a). The Cu<sub>2</sub>O deposited on top of TiO<sub>2</sub>/FTO substrate using electrochemical deposition (ECD) technique is light blue in colour as in Figure 7.3 (b), the colour could be effected by the Cu<sub>2</sub>O solution during deposition process, while the bottom view of the substrate, as shown in Figure 7.3 (c), is orange which is the colour of Cu<sub>2</sub>O. The Cu<sub>2</sub>O appeared to penetrate the TiO<sub>2</sub> film and was primarily deposited near the TiO<sub>2</sub>/FTO interface, most likely because the Cu<sub>2</sub>O gradually filled the porous matrix of TiO<sub>2</sub> from the bottom to the top of the film, as shown in Figure 7.3 (d).

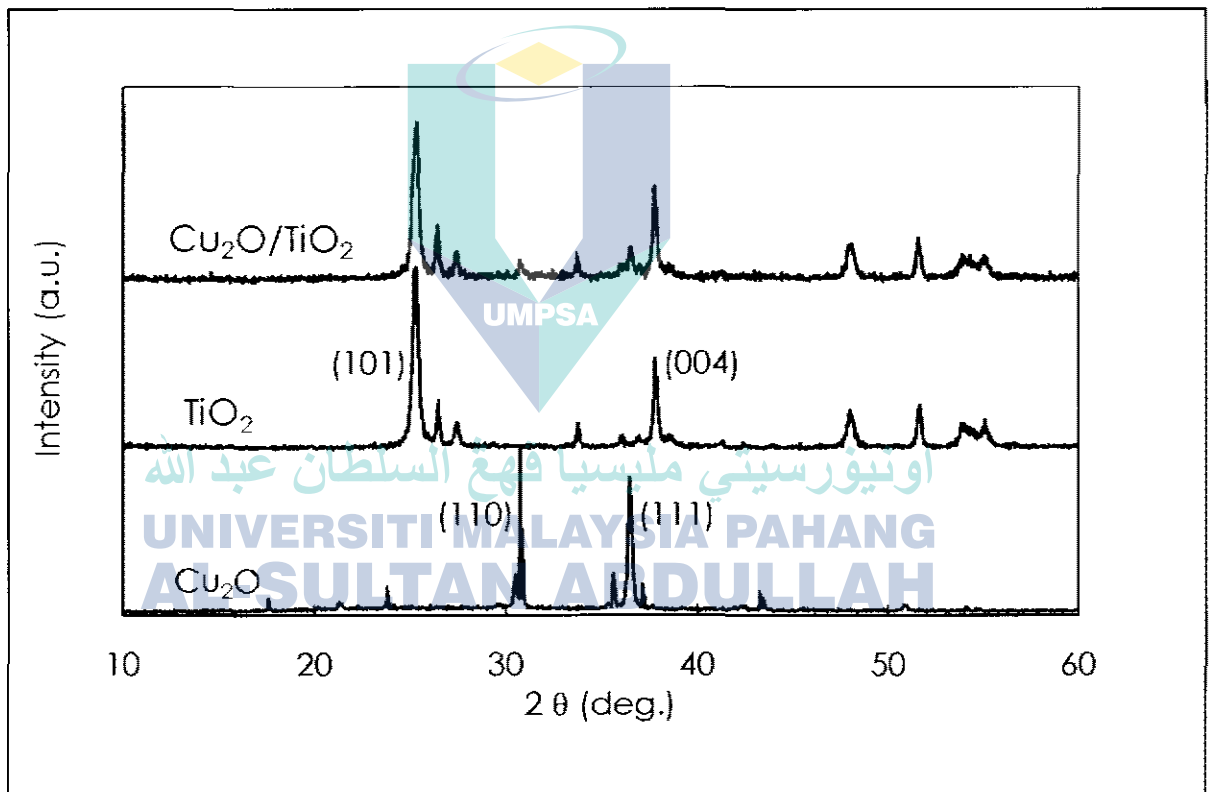
When first deposited, the  $\text{Cu}_2\text{O}$  solution easily penetrated the  $\text{TiO}_2$  film; however, for  $\text{Cu}_2\text{O}$  to deposit on the top surface of the  $\text{TiO}_2$  film, electric current is required for the  $\text{Cu}_2\text{O}$  solution to flow through the  $\text{TiO}_2$  matrix. However, the  $\text{TiO}_2$  particles are resistive, and therefore, it is possible that the current preferentially flowed from the film/substrate interface into the solution being deposited. Thus  $\text{Cu}_2\text{O}$  was preferentially deposited near the interface rather than on the top surface [184].

**FIGURE 1.3**  
**(a) Physical Appearance Of The  $\text{TiO}_2$  Film; (b) and (c) Top View And Bottom View Images Of Deposited  $\text{Cu}_2\text{O}$  On  $\text{TiO}_2$ , and (d) Model Of The  $\text{Cu}_2\text{O}/\text{TiO}_2$  Film Structure.**



The X-ray diffraction pattern for the  $\text{Cu}_2\text{O}$ ,  $\text{TiO}_2$  and  $\text{Cu}_2\text{O}/\text{TiO}_2$  composite films are shown in Figure 7.4. All of the identified peaks observed for  $\text{Cu}_2\text{O}$  can be attributed to the  $\text{Cu}_2\text{O}$  cubic structure, while the peaks observed for  $\text{TiO}_2$  can be attributed to the  $\text{TiO}_2$  anatase structure. The  $\text{Cu}_2\text{O}$  film showed a (111) and (110) preferred orientation, while the  $\text{TiO}_2$  film showed an excellent (101) and (004) [196]. For the composite film,  $\text{Cu}_2\text{O}$  peaks were also observed in addition to the  $\text{TiO}_2$  peaks.

**FIGURE 1.4**  
X-Ray Diffraction Spectra of  $\text{Cu}_2\text{O}$ ,  $\text{TiO}_2$ , and  $\text{Cu}_2\text{O}/\text{TiO}_2$  Composite Films.

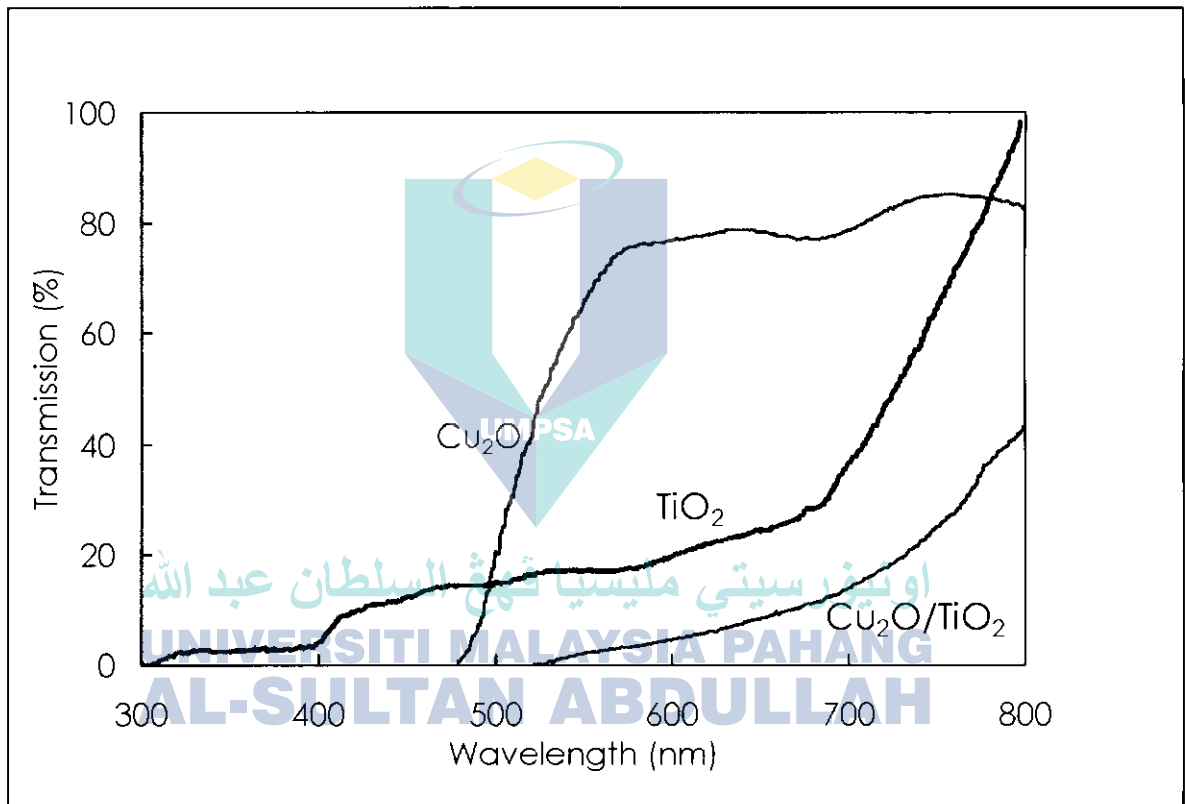


### 1.3.2 Optical Properties

The optical transmission spectra of the  $\text{TiO}_2$ ,  $\text{Cu}_2\text{O}$ , and  $\text{Cu}_2\text{O}/\text{TiO}_2$  composite films are shown in Figure 7.5. The  $\text{Cu}_2\text{O}$  film has an absorption edge

around 570 nm, which corresponds to its band-gap of 2.1 eV. Since the TiO<sub>2</sub> film is porous, its transmission is low in the visible range due to scattering and the absorption edge is observed near 400 nm. For the composite films, the transmission was minimal for wavelengths shorter than 520 nm due to absorption by Cu<sub>2</sub>O.

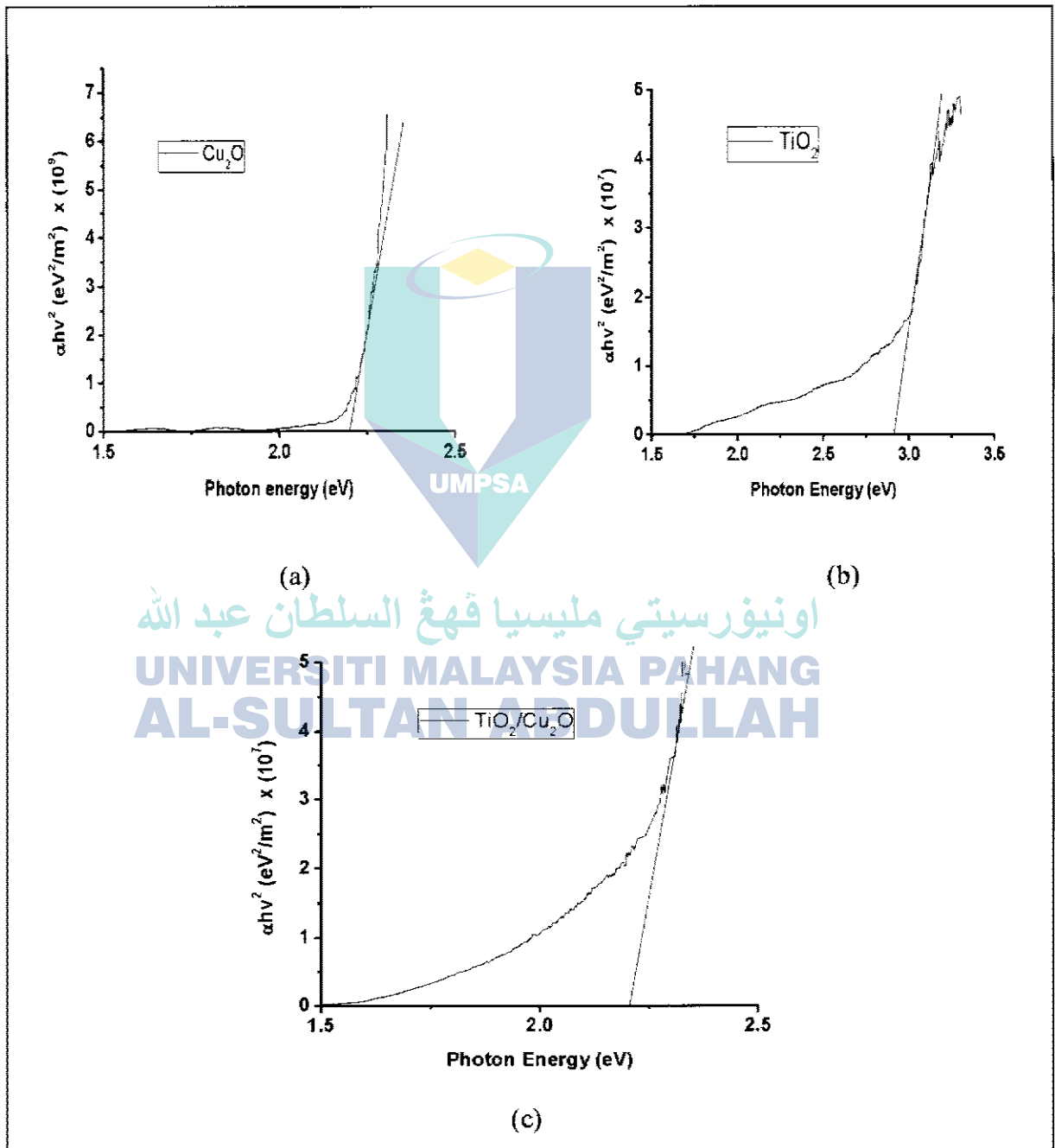
**FIGURE 1.5**  
Transmission Spectra Of Cu<sub>2</sub>O, TiO<sub>2</sub>, and Cu<sub>2</sub>O/TiO<sub>2</sub> Composite Films.



The optical band-gap energy  $E_g$  is calculated from the classical relation for direct band-gap optical absorption. It is observed that the absorption coefficients of Cu<sub>2</sub>O, TiO<sub>2</sub> and Cu<sub>2</sub>O/TiO<sub>2</sub> composite films are dependent on photon energy as shown in Figure 7.6. The band-gap energy of the Cu<sub>2</sub>O and TiO<sub>2</sub> can be seen at about 2.2 eV and 2.9 eV, respectively, while that of Cu<sub>2</sub>O/TiO<sub>2</sub> composite film can be observed around 2.2 eV. The lower value of band-gap energy of composite

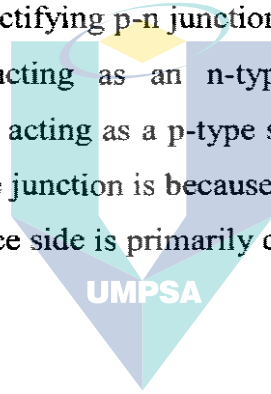
film may be due to the effect of the random atom arrangement of  $\text{Cu}_2\text{O}$  inside the  $\text{TiO}_2$  particles [193].

**FIGURE 1.6:**  
The Dependence of Absorption Coefficient to Photon Energy of (a)  $\text{Cu}_2\text{O}$ , (b)  $\text{TiO}_2$ , and (c)  $\text{Cu}_2\text{O}/\text{TiO}_2$  Composite Film.



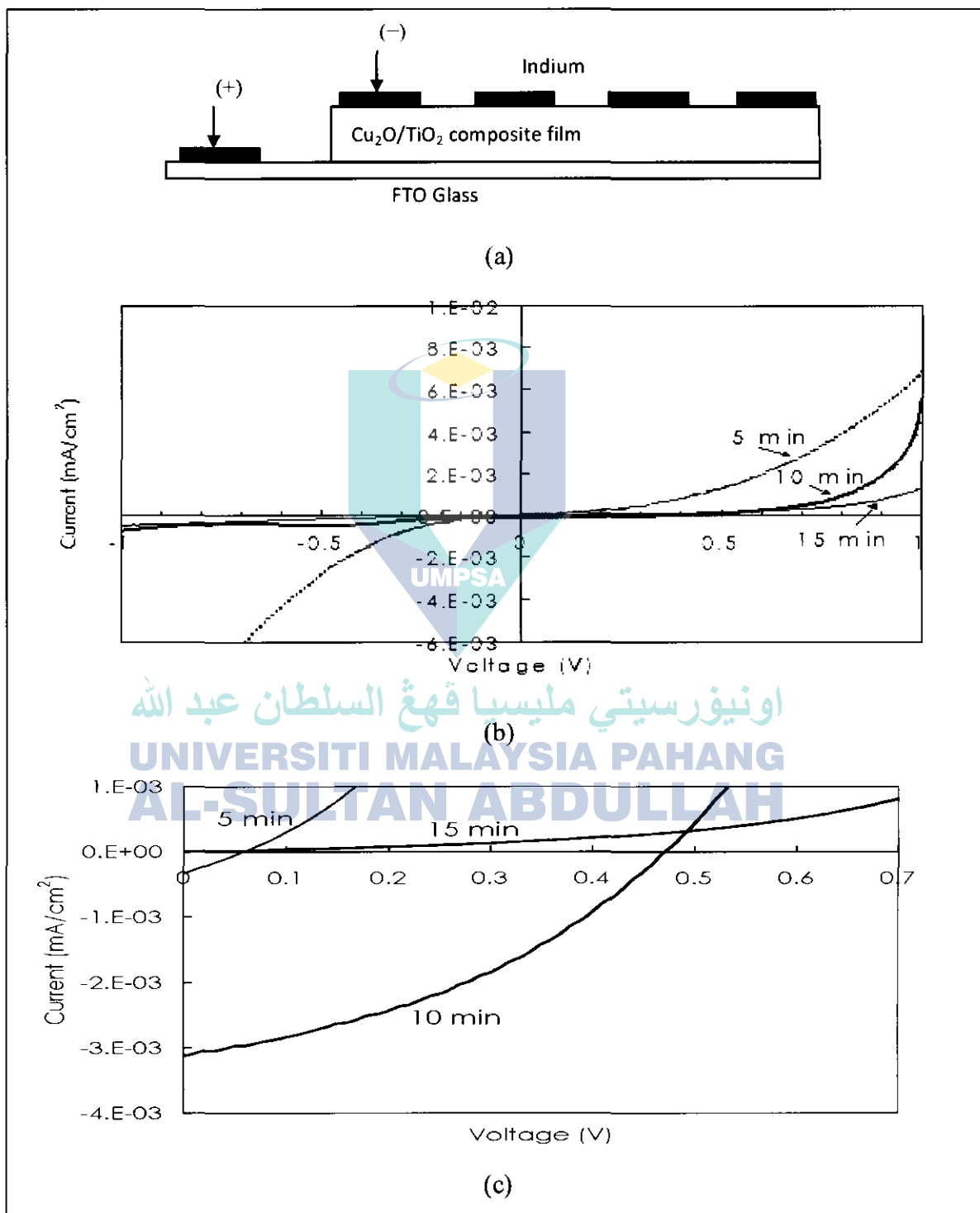
### 1.3.3 Electrical Properties

For the I-V characterization, indium contacts were evaporated on the thin film as shown in Figure 7.7 (a). Figure 7.7 (b) shows the photovoltaic behaviour of the Cu<sub>2</sub>O/TiO<sub>2</sub> composite films measured while being illuminated through the FTO glass substrate. Three samples with different Cu<sub>2</sub>O deposition times (5 minutes, 10 minutes and 15 minutes) were prepared and measured while AM1.5 light intensity was maintained at 100mW/cm<sup>2</sup> for all of the measurements. For the sample that underwent 10 minutes of deposition, the short-circuit current is measured at 0.0031 mA/cm<sup>2</sup>, the open-circuit voltage at 0.47 V, and the efficiency is 5x10<sup>-3</sup> %. Thus, a rectifying p-n junction is established, with the top surface of the composite film acting as an n-type semiconductor while the bottom film/substrate interface acting as a p-type semiconductor. The most likely reason for the formation of the junction is because the top surface is primarily comprised of TiO<sub>2</sub> and the interface side is primarily comprised of Cu<sub>2</sub>O, as shown in Figure 7.3.



اونيورسيتي مليسيا قهغ السلطان عبد الله  
UNIVERSITI MALAYSIA PAHANG  
AL-SULTAN ABDULLAH

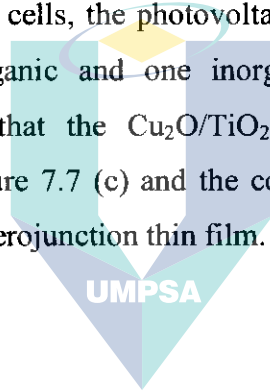
**FIGURE 1.7**  
**(a) Position of The Electrodes For The I-V Measurement, (b) I-V Curves For  $\text{Cu}_2\text{O}/\text{TiO}_2$  Composite Films With Different  $\text{Cu}_2\text{O}$  Deposition Times, and (c) Photo-Response Behaviour From I-V Characterization of The  $\text{Cu}_2\text{O}/\text{TiO}_2$  Composite Films Under an Illumination of  $100\text{mw}/\text{cm}^2$ .**



## 1.4 CONCLUSIONS

$\text{Cu}_2\text{O}$  films were deposited utilising ECD onto  $\text{TiO}_2$  films that have been prepared using the squeegee method, and a cell is generated by evaporating indium contacts on the film. When characterised, the cell showed electrical rectification and photovoltaic effects, hence demonstrating that an inorganic bulk heterojunction solar cell can be created using approach the ECD and squeegee methods, even without optimising the overall performance of the cell.

A solar cell based on a mixture of n-type and p-type semiconductors is commonly called a blend solar cell or a bulk-heterojunction solar cell. In almost all previous studies on bulk-heterojunction solar cells, the photovoltaic blend film consisted of two organic semiconductors or one organic and one inorganic semiconductor. This study has successfully demonstrated that the  $\text{Cu}_2\text{O}/\text{TiO}_2$  composite film shows photovoltaic behaviour, as shown in Figure 7.7 (c) and the composite film can be considered as an inorganic-inorganic bulk-heterojunction thin film.



اونيورسيتي مليسيا قهغ السلطان عبد الله  
UNIVERSITI MALAYSIA PAHANG  
AL-SULTAN ABDULLAH

## APPENDIX B:

### Publication during the period of candidature:

#### Academic Journals:

- [1] **Ayib Rosdi Zainun**, Sakamoto Tomoya, Uzer Mohd Noor, Mohamad Rusop, Ichimura Masaya, "New approach for generating  $\text{Cu}_2\text{O}/\text{TiO}_2$  composite films for solar cell applications." *Materials Letters, Volume 66, Issue 1, 1 January 2012, Pages 254-25.*
- [2] **A.R. Zainun**, M. Rusop, U.M. Noor, "Electrical and Optical Properties of Nanostructured Copper (I) Iodide (CuI) Incorporate with Ligand Agent for Dye Sensitized Solar Cell Applications." *International Journal of the Physical Sciences, volume 6(16), 18<sup>th</sup> August 2011, pp. 3993-3998.*
- [3] **A. R. Zainun**, M. H. Mamat, U. M. Noor and M Rusop, "Particles Size and Conductivity Study of P-Type Copper (I) Iodide (CuI) Thin Film for Solid State Dye-Sensitized Solar Cells." 2011 *IOP Conf. Ser.: Mater. Sci. Eng.* 17, Issue 1 (2011) 012009.

اونيورسيتي مليسيا قهغ السلطان عبد الله

#### Proceeding: UNIVERSITI MALAYSIA PAHANG AL-SULTAN ABDULLAH

- [4] **Ayib Rosdi Zainun**, Sakamoto, Uzer Mohd Noor, Mohamad Rusop, Masaya Ichimura, "FABRICATION AND CHARACTERIZATION OF  $\text{Cu}_2\text{O}/\text{TiO}_2$  COMPOSITE FILMS FOR SOLAR CELL APPLICATIONS." International Conference on Composites or Nano Engineering, ICCE-19, July 2011, Shanghai, China, *World Journal of Engineering (WJOE)*, [www.wjoe.hebeu.edu.cn](http://www.wjoe.hebeu.edu.cn).
- [5] Amalina, M.N., **Zainun, A.R.**, Rusop, M., "Photoconductivity of Copper (I) Iodide (CuI) thin films for dye-sensitized solar cells." Electrical and Computer Engineering (ICECE), IEEE 2010 International Conference, Dhaka, pp. 757-760.

- [6] **Zainun, A.R.**, Rusop, M., Noor, U.Z., "Photoluminescence characterization of nanostructured copper (I) iodide (CuI) incorporate with bidentate ligand." *Electronic Devices, Systems and Applications (ICEDSA), IEEE 2010 Intl. Conf., Kuala Lumpur, pp. 427 - 430.*
- [7] **A. R. Zainun**, M. H. Mamat, and M. Rusop, "Structural Properties of  $\Gamma$ -Phase Copper (I) Iodide Nano-Structured Thin Films Prepared by Sol Gel Method." *AIP Conf. Proc. 1136, pp. 845-849.*
- [8] **A. R. Zainun**, M. H. Mamat, and M. Rusop, "Crystalline Size Effect on the Electrical Properties of Zinc Oxide Nano-Structured Thin Films for Solar Cell Applications." *AIP Conf. Proc. 1136, pp. 855-860.*

**Presentation:**

- [1] **Ayib Rosdi Zainun**, Ichimura Masaya, "STUDY ON Cu<sub>2</sub>O/TiO<sub>2</sub> COMPOSITE FILMS FOR SOLAR CELL APPLICATIONS." Presented at 10<sup>th</sup> Conference of Japan Surface Science on 18<sup>th</sup> December 2010, Nagoya Institute of Technology (NIT).
- [2] **A.R. ZAINUN**, U. M. NOOR, M. RUSOP, "STUDY ON CuI + TMED FOR DSSC." Presented at Nagoya Institute of Technology (NIT) under **Exchange Program For Fostering Young Researcher Capable of Reducing Environmental Risk In Asia By Using Nanomaterials**, Nagoya, Japan, 5 - 20 December 2009.

**Award:**

- [1] **A. R. Zainun**, M.H. Mamat, U. M. Noor and M. Rusop, "Fabricating of Dye-Sensitized Solar Cells Using New but Commercially Available Chelating Agent", **Bronze Medal** at IID-FKE UiTM Shah Alam, 23-24 November 2009.

- [2] **Ayib Rosdi Zainun**, Uzer Mohd Noor, Muhamad Rusop Mahmud, “Dye-Sensitized Solar Cell (DSSC): Eco-Friendly Solar Cell”, **Gold Medal** at 7<sup>th</sup> IID organized by UiTM, Shah Alam, 12-14 January 2010.
- [3] **A. R. Zainun**, M.H. Mamat, U. M. Noor and M. Rusop, “Fabricating of Dye-Sensitized Solar Cells Using New but Commercially Available Chelating Agent”, Participated in Malaysia Technology Expo 2010 (MTE 2010), organized by MARS, Kuala Lumpur, 4-6 February 2010.
- [4] **Ayib Rosdi Zainun**, Uzer Mohd Noor, Muhamad Rusop Mahmud, “Dye-Sensitized Solar Cell (DSSC): Eco-Friendly Solar Cell”, **Bronze Medal** at MTE 2011 organized by Malaysian Association of Research Scientists (MARS), Kuala Lumpur, 15-17 February 2011.



اونيورسيتي مليسيا قهغ السلطان عبد الله  
**UNIVERSITI MALAYSIA PAHANG  
AL-SULTAN ABDULLAH**